LCH Laboratoire de Constructions Hydrauliques
Laboratory of Hydraulic Constructions

ÉCOLE POLYTECHNIQUE
FÉDÉRALE DE LAUSANNE

Communication 45

Sediment evacuation from reservoirs through intakes by jet induced flow

Jolanda Jenzer Althaus

Editeur : Prof. Dr A. Schleiss

Lausanne, 2011

Communications du Laboratoire de Constructions Hydrauliques ISSN 1661-1179
Ecole Polytechnique Fédérale de Lausanne
Editeur: Prof. Dr A. Schleiss

PREFACE

Today's worldwide yearly mean loss of storage capacity due to sedimentation is already higher than the increase of capacity by the construction of new reservoirs for irrigation, drinking water and hydropower. In Asia for example 80% of the useful storage capacity for hydropower production will be lost in 2035.

In Alpine regions the loss rate in reservoir capacity is significantly below world average. The main process in narrow reservoirs is the formation of turbidity currents, which transport the fine sediments regularly near the dam, where they can increase sediment levels up to 1 m per year. The outlet devices such as intakes and bottom outlets are therefore in many reservoirs after 40 to 50 years of operation already affected. The effects of climate change will in future increase the sediment yield entering the reservoirs. Turbidity currents may be stopped and forced to settle down by obstacles situated in the upper part of the reservoir in order to keep the outlet structures free of sediments.

Another new idea is to whirl up the fine sediments near the dam and intakes and keep them all the time in suspension, which allows a continuous release through the turbines. Mrs. Dr. Jolanda Jenzer Althaus studied this new idea for the first time with systematic hydraulic model tests combined with numerical simulations.

Special water jet arrangements were developed which can be installed near the dam in front of the intake in order to generate an optimum circulation needed to maintain the fine sediments in suspension. In such a way a significant amount of sediment can be released continuously during powerhouse operation.

In order to understand the involved physical processes in detail, systematic hydraulic model tests were carried out in a rectangular tank equipped at its front wall with an intake. First a configuration of four jets arranged in a circle on a horizontal plane in front of the intake was tested. For comparison in a second step also a linear jet configuration located parallel to the front wall with the intake was studied. Detailed measurements of flow velocity and sediment release helped to find the optimum combination of the parameters defining the circular jet arrangement. Finally, numerical simulations could reproduce the flow patterns.

We would like to thank Dr. Johannes Bühler (IfU-ETH Zurich) for his continuous support and guidance during the project as well as his valuable comments for the final thesis report. We thank also the members of the jury Prof. Robert Boes (VAW-ETH Zurich), Prof. Rollin Hotchkiss (Brigham Young University, USA) and Ass. Prof. Dr. Helmut Knoblauch (TU Graz, Austria) for their helpful suggestions. Finally we also thank gratefully Swisselectric Research for their financial support.

Prof. Dr. Anton Schleiss Dr. Giovanni De Cesare

Contents

Abstract

Reservoir sedimentation is worldwide a significant long term problem and requires in view of the current mitigation measures an alternative and more sustainable solution. This challenge motivated the present study with the purpose to develop an alternative efficient method to release sediment out of a reservoir. The concept is based on the release of sediment through the headrace tunnel and turbines whereby a special focus was set on the fine sediment in the area in front of the power intakes. Specific jet arrangements should provide the energy and generate the optimum circulation needed to maintain the sediment in suspension and enhance its entrainment into the power intakes during turbining sequences.

This new idea was experimentally tested in a rectangular laboratory tank with the following dimensions: 2 m wide, 1.5 m high and 4 m long. Two jet configurations were systematically investigated: a configuration of four jets arranged in a circle on a horizontal plane and a linear jet configuration located parallel to the front wall. The influence of the jet characteristics (nozzle diameter d_j, jet velocity v_j, jet discharge Q_j, and jet angle θ) and the geometrical configuration parameters on the sediment release was investigated.

As initial condition an almost homogeneous sediment concentration distribution was induced by air bubbles. This condition simulated a muddy layer like in front of the dam by the fading of a turbidity current. The water level during all the experiments was held constant by releasing the same discharge through the water intake as was introduced by the jets (experiments with jets) or through the back wall (experiments without jets), respectively. Turbidity measurements combined with flow velocity measurements gave information about the sediment release efficiency.

The sediment release (evacuated sediment ratio, ESR) is defined as the evacuated sediment weight P_{out} divided by the sediment weight initially supplied P_{in} and represents the normalized temporal integral of the released sediment amount: $ESR = P_{out}/P_{in}$. Analogously, the settled sediment ratio is the settled sediment divided by the sediment weight initially supplied P_{in}.

Experiments without jets as reference configuration showed an almost linear relation between the sediment release and the discharge within the tested range: the higher the discharge, the higher the evacuated sediment ratio. For a constant discharge the ultimate sediment release as well as the settled sediment ratio was easily estimated by a simple physical approach taking into account the settling velocity and the flow field generated by the discharge through the water intake and the back wall. For the tested discharge range the sediment release was between 0.09 and 0.37 for reference configuration.

Jets are effectively mixing: after roughly half an hour the standard deviation of the suspended sediment concentration was approximately 5 %, what in chemistry is considered as homogeneous. Consequently, less sediment was settled and, hence, the sediment release was

higher than without jets and reached for the highest tested discharge (ΣQ_j = 4050 *l/h*) *ESR* = 0.73.

Moreover, contrary to the experiments without jets, with jets resuspension of settled sediment was observed. Resuspension started once steady state conditions for the circulation were reached. It has been detected for discharges higher than an experimentally determined threshold. The observed evolution of the resuspension rate suggests that for a final stage all of the initially supplied sediment can be evacuated.

The circular jet arrangement was identified as the most efficient configuration regarding sediment release. Additionally, the normalized optimal geometrical parameter combination was determined as follows: off-bottom clearance of the jet arrangement C/B = 0.175, water intake height h_i/B = 0.25, distance of the jet arrangement to the front wall d_{axis}/B = 0.525, distance between two neighbouring jets l_j/B = 0.15, jet angle θ = 0° and water height in the tank h/B = 0.6. Under optimum conditions and with the highest tested jet discharge (ΣQ_j = 4050 *l/h*) after four hours a sediment release of *ESR* = 0.73 was achieved. Without jets and with the same discharge through the water intake the sediment release reached *ESR* = 0.37.

The corresponding flow pattern in the transversal plane was similar to an axial mixer, which in the literature is reported as favourable for suspension. In the longitudinal flow patterns resulting from higher discharges, a single rotor was found between jets and water intake, whereas for smaller discharges the flow pattern was similar to a radial mixer.

A variation of a single geometrical parameter within the tested range (i.e. 60 to 200 % of the optimum value) caused a sediment release reduction of up to 40 %, depending on the parameter and the duration.

The linear jet arrangement was found to be much less favourable in view of sediment release. Its results were in the same magnitude as for the experiments without jets (*ESR* between 0.37 and 0.45). This is due to the direction of the induced rotation which is unfavourable regarding sediment suspension: the sediment is drawn to the bottom where it is settled and difficult to be put in suspension again.

The efficiency of the jets was established by comparing the sediment release obtained under different conditions: once when jets were employed, once without jets. The predicted efficiency based on time and discharge independent empirical relationships is around 1.7 for the optimum jet configuration. Using the measured data the efficiency depends on discharge and increases with time. At the end of the transient phase and when resuspension started the efficiency was approximately 1.5. With the highest tested discharge the efficiency reached after four hours almost 2 (ΣQ_j = 4050 *l/h*).

Due to the fine grain size used in the experiments (mean diameter of 60 μm) the application focuses on large reservoirs where the sediment is well sized along the thalweg and only fine particles are expected in front of the dam as it is the case for sediments transported by turbidity currents.

In the case study of Mauvoisin with a 520 *m* long dam crest creating a large reservoir in Switzerland, a first attempt was made to up-scale the research results. Based on the available discharge and head of the existing water transfer tunnel a preliminary optimal circular jet arrangement was suggested. However, the width of the reservoir was estimated at approximately three times as large as optimal experimental conditions. Nevertheless, with a circular jet arrangement could definitely more sediment be evacuated than without jets.

Moreover, the region near the outlet devices could be maintained free of sediment and their clogging could be avoided.

An economic study revealed that a jet arrangement is a low cost installation which, based on the performed experiments, is essential when aiming for high sediment release and fighting against reservoir sedimentation.

Key words: Reservoir sedimentation, suspended sediment, sediment release, resuspension, circular jet arrangement, UVP-measurements, turbidity measurements, axial mixer-like flow pattern, radial mixer-like flow pattern, jet mixing, numerical simulation, physical experiments, hydro-power plants, turbidity current.

Résumé

Evacuation de sédiments d'un réservoir à travers la prise d'eau à l'aide de jets

La sédimentation dans les réservoirs est un problème à long terme, important et mondial. Elle requiert une alternative plus durable que les mesures actuellement utilisées. La présente étude a été initiée pour relever ce défi. Elle a pour objectif de développer une méthode alternative et efficace d'évacuation des sédiments d'un réservoir. Le concept est d'évacuer les sédiments à travers la conduite forcée et les turbines, en se focalisant spécialement sur les sédiments fins qui se trouvent dans la zone de la prise d'eau. Des dispositifs spécifiques à jets devraient fournir l'énergie nécessaire et générer un écoulement optimal, permettant de maintenir les sédiments en suspension et d'engendrer leur entrainement dans la prise d'eau pendant les heures de turbinage.

Cette nouvelle idée a été testée expérimentalement dans un réservoir rectangulaire du laboratoire avec les dimensions suivantes : 2 *m* de large, 1.5 *m* de haut et 4 *m* de long. Deux configurations à jets ont été testées systématiquement: une configuration à quatre jets disposés en cercle sur un plan horizontal et une configuration à quatre jets alignés, située parallèlement à la paroi frontale. L'influence des caractéristiques du jet (diamètre du jet d_j, vitesse du jet v_j, débit du jet Q_j et angle d'inclinaison du jet θ), et celle des paramètres géométriques de la configuration sur l'évacuation des sédiments ont été testées.

Afin de fixer la condition initiale, une distribution pratiquement homogène de la concentration de sédiments a été établie grâce à des bulles d'air,. Cette condition simulait une couche d'eau chargée en sédiments comparable à celles qui restent au front des barrages après le passage d'un courant de turbidité. Le niveau d'eau a été maintenu constant pendant toutes les expériences en relâchant par la prise d'eau, la quantité qui avait été introduite, soit par les jets (expériences avec jets) soit par la paroi arrière (expériences sans jets). Les mesures de turbidité combinées aux mesures de vitesse d'écoulement, ont permi de déterminer l'efficacité d'évacuation des sédiments.

L'évacuation de sédiments (*ESR* pour Evacuated Sediment Ratio) est définie par le rapport entre le poids de sédiments évacués P_{out} et le poids de sédiments initialement ajoutés P_{in}. Ce rapport représente l'intégrale temporelle normalisée de la quantité de sédiments évacués : $ESR = P_{out}/P_{in}$. Par analogie, la proportion de sédiments déposés est la quantité de sédiments déposés divisée par le poids de sédiments initialement ajoutés P_{in}.

Les expériences sans jets ont servi de configurations de référence et ont montré, sur l'ensemble des tests, une relation pratiquement linéaire entre la proportion de sédiments évacués et le

débit : plus le débit était élevé, plus la proportion de sédiments évacués était grande. Pour un débit constant, les proportions finales de sédiments évacués et de sédiments déposés ont été estimées par une approche mathématique simple qui tient compte de la vitesse de décantation et du champ de vitesse engendré par le débit à travers la prise d'eau d'une part, et par la vitesse à travers la paroi arrière d'autre part. Pour l'ensemble des débits testés, la proportion de sédiments évacués était comprise entre 0.09 et 0.37 dans la configuration de référence.

Les jets sont des mélangeurs efficaces : après une demi-heure environ, l'écart-type de la concentration de sédiments en suspension était d'environ 5 %, ce qui, en chimie, est considéré comme homogène. Par conséquent, moins de sédiments étaient décantés et la proportion de sédiments évacués était plus élevée que sans les jets, jusqu'à atteindre une valeur ESR = 0.73 pour le débit le plus grand testé (ΣQ_j = 4050 l/h).

D'autre part, contrairement aux expériences sans jets, les sédiments ont été remis en suspension avec les jets. La remise en suspension commençait quand la circulation avait atteint des conditions d'équilibre. Elle a été détectée pour des débits supérieurs à une valeur limite déterminée expérimentalement. L'évolution temporelle de la vitesse de remise en suspension, suggère que tous les sédiments initialement ajoutés pourraient être finalement évacués.

La configuration circulaire des jets a été identifiée comme étant la plus efficace pour l'évacuation des sédiments. La combinaison optimale des paramètres géométriques normalisés par rapport à la largeur du bassin B a été déterminée comme suit : hauteur de la position des jets C/B = 0.175, hauteur de la prise d'eau h_i/B = 0.25, distance à la paroi frontale du centre de l'arrangement circulaire des jets d_{axis}/B = 0.525, distance entre deux jets voisins l_j/B = 0.15, angle du jet θ = 0°, hauteur d'eau dans le réservoir h/B = 0.6. Avec ces conditions optimales et le plus grand débit de jet testé (ΣQ_j = 4050 l/h), le taux de sédiments évacués ESR = 0.73 a été atteint après quatre heures. Sans jets et avec le même débit à travers la prise d'eau, la proportion de sédiments évacués a atteint ESR = 0.37.

Transversalement, le champ d'écoulement correspondant était semblable à celui d'un mélangeur axial, qui selon la littérature, est favorable à une mise en suspension. Longitudinalement, en cas de forts débits, une seule cellule de rotation s'est formée entre les jets et la prise d'eau, tandis que pour des débits plus faibles, le champ d'écoulement était similaire à celui d'un mélangeur radial.

La variation d'un seul paramètre géométrique dans la gamme testée (soit de 60 à 200 % de la valeur maximale) a provoqué une réduction de la proportion de sédiments évacués atteignant 40 %, selon le paramètre et la durée.

La configuration à jets alignés s'est révélée beaucoup moins favorable à l'évacuation des sédiments. Les résultats obtenus dans ces conditions étaient comparables à ceux des expériences sans jets (ESR entre 0.37 et 0.45). Ceci est dû à l'orientation de la rotation qui est défavorable à la suspension des sédiments : les sédiments sont attirés vers le fond où ils décantent et sont difficilement remis en suspension.

L'efficacité des jets a été établie en comparant la proportion des sédiments évacués obtenue dans différentes conditions : une fois avec jets, une fois sans jets. L'efficacité prédite, en se basant sur des relations empiriques et indépendantes du temps et du débit, est d'environ 1.7 pour la configuration optimale. En utilisant les valeurs mesurées, l'efficacité dépend du débit et augmente en fonction du temps. En fin de phase non stationnaire et quand la remise en

suspension commence, l'efficacité était d'environ 1.5. Avec le plus grand débit testé (ΣQ_j = 4050 *l/h*) et après quatre heures l'efficacité était presque de 2.

Au vue de la granulométrie fine des sédiments expérimentalement testés (diamètre moyen de 60 μm), l'application s'est focalisée sur les grands réservoirs où les sédiments sont bien triés le long du thalweg et où seules les particules fines sont attendues devant le barrage, comme c'est le cas pour les sédiments transportés par des courants de turbidité.

Une première application à l'échelle prototype des résultats de laboratoire a été effectuée au grand réservoir de Mauvoisin créé par le barrage du même nom, dont la couronne mesure 520 *m* de longueur. En se basant sur le débit et la chute de l'adduction existante, une disposition préliminaire circulaire de jets a été proposée. Cependant, la largeur du réservoir a été estimée être environ trois fois plus grande que celle des conditions optimales des essais. Malgré tout, une configuration circulaire des jets devrait certainement permettre d'évacuer davantage de sédiments que sans les jets. En plus, la zone proche de la prise d'eau pourrait être maintenue libre de sédiments et les obstructions devraient ainsi être évitées.

Une étude économique montre qu'un arrangement de jets est une installation peu onéreuse, qui, selon les essais, est essentielle lorsqu'une bonne évacuation de sédiments est recherchée et dans la lutte contre la sédimentation des réservoirs.

Mots-clés : sédimentation des réservoirs, sédiments en suspension, évacuation des sédiments, re-suspension, arrangement circulaire de jets, mesures UVP, mesures de turbidité, champs de vitesse de type mélangeur axial, champs de vitesse de type mélangeur radial, mélanges de jets, simulation numérique, expériences physiques, aménagements hydrauliques, courants de turbidité

Zusammenfassung

Entlandung von Stauseen über Triebwasserfassungen durch Aufwirbeln der Feinsedimente mit Wasserstrahlen

Die Stauraumverlandung ist weltweit ein relevantes und bis dato nicht abschliessend gelöstes Langzeitproblem von Talsperren. Angesichts der aktuell angewandten Gegenmassnahmen, welche oft eine eingeschränkte Wirkung aufweisen, sind nachhaltigere Lösungsansätze gefragt. Die vorliegende Studie hat daher zum Ziel, eine alternative Methode zum Austrag von Feinsedimenten aus betroffenen Stauseen zu entwickeln. Das Konzept umfasst einen Austrag der Sedimente durch den Triebwasserstollen, mit einem Fokus auf Feinsedimente im Bereich der Wasserfassung. Eine gezielte Anwendung optimierter Wasserstrahlen nahe der Fassung soll durch eine Zirkulationsströmung die Sedimentsuspension unterstützen, und dadurch den Sedimenteintrag in die Wasserfassung während den Turbinierzeiten steigern.

Das vorgestellte Konzept wurde experimentell in einem Labortank mit 4 *m* Länge, 2 *m* Breite und 1.5 *m* Höhe untersucht und optimiert. Zwei Wasserstrahlanordnungen wurden getestet: (1) eine kreisförmige Konfiguration mit vier horizontal und exzentrisch angeordneten Wasserstrahlen, und (2) eine lineare Konfiguration, bei der die Wasserstrahlen auf einer Linie angeordnet sind. Der Einfluss der Wasserstrahleigenschaften (Düsendurchmesser d_j, Wasserstrahlgeschwindigkeit v_j, Wasserstrahlabfluss Q_j und Wasserstrahlwinkel θ) und der geometrischen Konfiguration auf den Sedimentaustrag wurde systematisch untersucht.

Als Anfangsbedingung wurde eine annähernd homogene Sedimentkonzentrationsverteilung mittels Luftblasenschleier erzeugt. Diese Bedingung simulierte einen „Muddy layer“, wie er nach einem Trübestrom vor einer Talsperre auftritt. Der Wasserspiegel wurde während der Experimente konstant gehalten, indem der Abfluss durch die Wasserfassung mittels der Wasserstrahlen (bei Wasserstrahlexperimenten) oder mittels eines Zuflusses bei der Rückwand des Tanks (Experimente ohne Wasserstrahlen) kompensiert wurde. Trübemessungen gaben Aufschluss über die Effizienz der Massnahme bezüglich des angestrebten Sedimentaustrags.

Der Sedimentaustrag (Evacuated Sediment Ratio *ESR*) ist definiert als das normierte zeitliche Integral der entleerten Sedimentmasse P_{out}, normiert mit der anfänglich zugegebenen Sedimentmasse P_{in}. Analog dazu ist der abgesetzte Sedimentanteil gleich der abgesetzten Sedimentmasse verglichen mit der anfänglich zugegebenen Sedimentmasse P_{in}.

Experimente ohne Wasserstrahlen dienten als Referenzkonfigurationen und wiesen ein beinahe lineares Verhältnis zwischen dem *ESR* und dem Abfluss auf: Je grösser der Abfluss ist, desto höher die Sedimententleerung. Für einen konstanten Abfluss konnte der endgültige Sedimentaustrag sowie der endgültig abgesetzte Sedimentanteil mittels einer physikalischen

Näherung abgeschätzt werden. Diese berücksichtigt die Absetzgeschwindigkeit und das Strömungsfeld, welches durch den Nutzwasserfassungsabfluss und durch jenen bei der Rückwand des Tanks erzeugt wurde. Für den Bereich der untersuchten Abflüsse war der Sedimentaustrag zwischen 0.09 und 0.37 für die Referenzkonfiguration.

Die Wasserstrahlen mischen das Wasser und das Sediment effizient. Nach ungefähr einer halben Stunde Mischzeit war die Standardabweichung der suspendierten Sedimentkonzentration ca. 5%. Dies wird in der Chemie als homogene Mischung bezeichnet. Es werden dann entsprechend weniger Sedimente abgesetzt, weshalb der Sedimentaustrag beim maximal untersuchten Abfluss (ΣQ_j = 4050 l/h) mit ESR = 0.73 höher war als ohne Wasserstrahlen.

Zudem wurde, im Gegensatz zu den Experimenten ohne Wasserstrahlen, mit Wasserstrahlen eine Re-suspension von abgesetzten Sedimenten beobachtet. Re-suspension setzte ein, sobald stationäre Strömungsbedingungen im Wassertank erreicht waren, und wurde für Abflüsse beobachtet, welche grösser als ein experimentell ermittelter Schwellenwert sind. Die beobachtete zeitliche Entwicklung der Re-suspensionrate lässt vermuten, dass schliesslich alle anfänglich zugegebenen Sedimente ausgetragen werden.

Die kreisförmige Konfiguration (1) der Wasserstrahlen wurde als am effizientesten hinsichtlich des Sedimentaustrags identifiziert. Zusätzlich wurde eine optimale normierte Kombination der geometrischen Parameter bestimmt, gültig im Rahmen der untersuchten Modellgeometrie:

- Abstand der Wasserstrahlen zum Tankboden C/B = 0.175,
- Höhe der Wasserfassung h_i/B = 0.25,
- Abstand des Konfigurationskreiszentrums zur Frontwand des Tanks d_{axis}/B = 0.525,
- Abstand zwischen zwei benachbarten Wasserstrahlen l_j/B = 0.15,
- Wasserstrahlneigungswinkel θ = 0°, und
- Wasserhöhe im Tank h/B = 0.6.

Unter optimalen Bedingungen und mit dem maximalen geprüften Abfluss (ΣQ_j = 4050 l/h) wurde nach vier Stunden Betrieb ein Sedimentaustrag von ESR = 0.73 erreicht. Ohne Wasserstrahlen und mit demselben Abfluss durch die Wasserfassung war der Sedimentaustrag bloss ESR = 0.37.

Das zugehörige Strömungsbild in der Querebene war ähnlich wie das eines axialen Mixers, welches gemäss Literatur günstig für Suspension sein soll. In der Längsebene wurde für grosse Abflüsse eine einzelne Zirkulationszelle zwischen Wasserstrahlen und Wasserfassung gemessen, während für kleinere Abflüsse das Strömungsbild ähnlich dem eines radialen Mixers war.

Eine Abweichung eines einzelnen Parameters in der geprüften Spannweite (i.e. 60 bis 200 % des optimalen Wertes) verursachte eine Reduktion des Sedimentaustrages von bis zu 40 %, in Abhängigkeit des Parameters und der Versuchsdauer.

Die lineare Wasserstrahlanordnung (2) stellte sich als weniger günstig für den Sedimentaustrag heraus. Die Austragsraten waren im Bereich jener ohne Wasserstrahlen ($0.09 \leq ESR \leq 0.37$). Dies kann mit dem Drehsinn der Rotationszellen erklärt werden, welche sich ungünstig auf die Suspension auswirkt: Die Sedimente werden zum Tankboden gelenkt, wo sie sich absetzen und kaum mehr in Schwebe gelangen.

Die Effizienz der Wasserstrahlen wurde mittels eines Vergleichs zwischen den jeweiligen Sedimentaustragsraten bestimmt, die mit und ohne Wasserstrahlen gemessen wurden.

Die Effizienz als Funktion von zeit- und abflussunabhängigen Verhältnissen wurde für die optimale Wasserstrahlkonfiguration auf 1.7 prognostiziert. Falls die Effizienz mittels gemessener Daten errechnet wird, ist sie zeit- und abflussabhängig. Am Ende der instationären Phase, d.h. sobald Re-suspension einsetzt, war die Effizienz ca. 1.5. Mit dem maximal getesteten Abfluss (ΣQ_j = 4050 l/h) wurde nach vier Stunden Versuchsdauer eine Effizienz von beinahe 2 erreicht.

Aufgrund der in den Experimenten verwendeten feinen Korngrösse (mittlerer Durchmesser 60 μm) eignet sich diese Anwendung vor allem für grosse Stauräume, bei denen die Sedimente entlang des Talwegs der Grösse nach sortiert werden und nur feine Fraktionen vor der Sperre zu erwarten sind, wie bei Trübeströmen typisch.

Im Rahmen einer Fallstudie wurde bei Mauvoisin, einem Schweizer Stausee mit einer 250 m hohen Bogenmauer, ein erster Versuch unternommen, die Resultate der physikalischen Experimente im Prototyp anzuwenden. Basierend auf dem Abfluss und der Fallhöhe eines Seitenzuflusses wurde eine erste kreisförmige Konfiguration (1) der Wasserstrahlen vorgeschlagen. Obwohl das Reservoir etwa 3 mal breiter ist als das Modell, könnten dennoch mit der kreisförmigen Wasserstrahlanordnung mehr Sedimente ausgetragen werden als ohne Wasserstrahlen. Dieser Sedimentaustrag verringert zudem die Wahrscheinlichkeit einer Verlandung der Nutzwasserfassung.

Eine Wirtschaftlichkeitsanalyse weist zudem darauf hin, dass die Wasserstrahlanordnung insbesondere dann preisgünstig ist, wenn ein hoher Sedimentaustrag erzielt werden soll.

Stichwörter: Verlandung von Stauhaltungen, Feststoffe in Schwebe, Sedimentaustrag, Re-suspension, kreisförmige Wasserstrahlanordnung, UVP-Messungen, Trübemessungen, axiales Strömungsbild, radiales Strömungsbild, Mixer mit Wasserstrahlen, numerische Simulation, physikalische Experimente, Stauanlagen, Trübeströme.

List of symbols

Roman symbols

A_j	nozzle opening surface
a_s, b_s, c_s	diameters of a non-round particles, with c_s the value of the shortest axis
b	transverse distance of jet
B	inner width of experimental basin
B_i	interaction width
B_0	wetted transverse tank section
$b_{1/2}$	jet half-width, defined as the transverse distance r for axial velocity v(r) to fall to one half of the centreline value, v_{CL}
$b_{0.37}$	jet width where the excess velocity is $e^{-1} = 0.37$ of v_{CL}
C	off-bottom clearance of jet arrangement
c_{US}	velocity of ultrasound
c	instantaneous concentration at a given location
$\bar{c}$	suspended sediment concentration in case of perfect mixing
C_1	a proportionality constant for the jet velocity
C_2	a proportionality constant relating $b_{1/2}$ and s
C_3	constant
c_D	drag coefficient
$c_{s,init}$	initial suspended sediment concentration
$c_{s,instant}$	instantaneous suspended sediment concentration at a given location
c_{s1}	SSC after one time step of Δt
c_{s2}	SSC after two time steps of Δt
c_{si}	SSC after i time steps of Δt
C_R	storage capacity of the reservoir
D	mass diffusivity
D^*	dimensionless nominal diameter of sediment particle
d_{60}	sediment particle diameter with 60 % finer by weight
d_{30}	sediment particle diameter with 30 % finer by weight

d_{10}	sediment particle diameter with 10 % finer by weight
d_{axis}	distance between the jet circle centre and the front wall (circular jet arrangement)
ΔGL	annual mean relative change of the length of the glacier
$D_{impeller}$	impeller diameter
d_j	nozzle opening diameter
d_{line}	the distance between the jets and the front wall (aligned jet arrangement)
d_m	median sediment particle diameter
D_n	nominal particle diameter
d_s	sediment particle diameter
$d(s)$	jet diameter at distance s
D_{tank}	diameter of cylindrical tank
EB	percentage of surfaces covered with easily eroded soil
ESR	evacuated sediment ratio ($ESR = P_{out}/P_{in}$)
ESR_{ideal}	evacuated sediment ratio in idealized conditions (no settling, perfectly homogeneous sediment concentration)
ESR_{jet}	evacuated sediment ratio with jets
$ESR_{no\ jets}$	evacuated sediment ratio without jets
F_D	fluid drag force
Fr_j	densimetric Froude number
f_0	ultrasound frequency
g'	reduced graviational acceleration
G	gravity force
h	water height in tank
H_{avg}	mean head
h_i	height of water intake
H_{sommer}	mean rainfall height in the summer term (June to September)
I	mean annual discharge
i	nteration step number
L	tank length
L_{cf}	concentration fluctuations
L_{axial}	axial jet length
l_j	distance between two neighbouring jets (circular jet arrangement)
M_j	jet momentum flux
n	exponent in mixing time correlations
OV	percentage of surfaces without vegetation
P_{in}	sediment weight initially added to the basin
P_{out}	evacuated sediment weight
P_{out1}	sediment weight evacuated during the first time step
P_{out2}	sediment weight evacuated during the second time step

$Q(s)$	total volume flux at distance s from nozzle
Q_e	volumetric flow rate of the bulk liquid entrained by the jet
Q_{50d}	discharge likely to be equal or exceeded during 50 days of the year
Q_j	jet discharge at one nozzle
Q_{out}	discharge released through the water intake
Q_p	propeller flow rate
Q^*	flow-rate ratio $Q^* = Q_p/Q_{out}$
r	radial coordinate in jet
R	radius of bubble plume
r_i	radial distance between the sediment particle and the water intake
Re	Reynolds number
Re_i	Reynolds number at the water intake
Re_j	jet Reynolds number
Re_s	sediment particle Reynolds number
r_j	nozzle opening radius
RR	resuspension rate
s	axial coordinate of the jet
SF	shape factor of particle
SSC	suspended sediment concentration
SSC_{calc}	estimated SSC using the laboratory-driven calibration equation
SSC_{known}	known SSC using the known sediment weight and water volume
SSR	settled sediment ratio
SSR_{max}	maximal settled sediment ratio
T	temperature
t	time
Δt	time step duration
t^*	dimensionless time defined by the real time devided by the residence time
t_c	mean circulation time
TE	trap efficiency
t_m	mixing time
U_{max}	maximum detectable velocity using UDVP
u_{*cr}	critical shear velocity
V	water volume (in experimental basin or reservoir)
$v\ (r)$	axial jet velocity at radius r
VA	annual erosion volume per unit surface
v_a	flow velocity at a distance r_i in front of the water intake
v_b	average flow velocity through the back wall
v_{CL}	centreline jet velocity at distance s from nozzle
v_j	jet velocity at nozzle

V_{10}	estimated water volume expected to contribute sediment particles of the grain size spectrum d_{10} to d_{30}, corresponding to a portion of 20 %
V_{30}	estimated water volume expected to contribute sediment particles of the grain size spectrum d_{30} to d_{60}, corresponding to a portion of 30 %
V_{60}	estimated water volume expected to contribute sediment particles of the grain size spectrum d_{60} to d_{100}, corresponding to an estimated portion of 90 %
V_s	volume of sediment particle
W^*	dimensionless nominal settling velocity
w_s	settling velocity (particle fall velocity in a clear fluid)
$w_{s,m}$	particle fall velocity in fluid with suspended material
x	longitudinal (horizontal) coordinate with the origin at the front wall
x_1	length of the initial region of jets
t_{rs}	time at which resuspension starts
t_{re}	time at which resuspension ends
y	transversal coordinate
z	vertical coordinate

Greek symbols

α_{jet}	a constant (0.055)
β	angle between the line connecting the particle position with the water intake, and the horizontal
δ	jet expansion angle
ε	dissipation rate of turbulent kinetic energy
ν	kinematic viscosity
λ_S	turbulent Schmidt number
λ	model scale factor
λ_L	length scale
λ_Q	discharge scale
λ_{ws}	settling velocity scale
ρ_s	sediment density
ρ_w	density of water
σ_g	standard deviation of grain size distribution
$\Sigma c_{s,i}$	sum of suspended sediment concentration measurements recorded in time intervals of Δt
τ_m	mean residence time V/Q_{out}
τ_s	mean settling time h/w_s
θ	jet angle to the horizontal

List of Tables

List of Figures

1 Introduction

1.1 Problem of reservoir sedimentation

1.1.1 Long term problem

Reservoir sedimentation is a problem with increasing significance and impact in the decades to come. All kinds of water bodies are affected, fresh waters as well as estuaries.

In most natural river reaches sediment inflow and outflow are approximately balanced. Dam construction dramatically alters this balance leading to transformations in the fluvial process and creating a reservoir characterized by extremely low flow velocities and efficient sediment trapping. The continuity of sediment transport is interrupted and the sediments are captured in the reservoir in front of the dam.

Each reservoir created on natural rivers, independent of its use (water supply, irrigation, energy or flood control), can have its capacity decreased due to deposition over the years. In an extreme case, this may result in the reservoir becoming filled up with sediments, and the river flowing over land again. Figure 1.1 shows the example of the reservoir Forni in Italy, where flushing and dredging were not allowed during many years. In this example the filling material was mainly cobbles, gravels and sand and the reservoir is located immediately downstream a retreating glacier.

Figure 1.1 The reservoir Forni (Italy) almost filled up to the dam crest (source: CESI)

A reservoir, like a natural lake, silts up more or less rapidly. In actual fact, reservoirs may be completely filled up with sediments even within just a few decades, whereas natural lakes e.g.

in Alpine foreland, may remain as stable features of the landscape for as much as 10'000 or 20'000 years after they were formed during the last Ice Age.

As the accumulating sediments successively reduce the water storage capacity, at long-term the reservoir operates only at reduced functional efficiency. Declining storage volume reduces and eventually eliminates the capacity for flow regulation and therefore all benefits of water supply, energy and flood control (Graf 1984, International Committee on Large Dams (ICOLD) 1989). This process can even lead to a disturbed water intake operation and to sediment entrainment in waterway systems and hydropower schemes. Depending on the degree of sediment accumulation, the outlet works may be clogged by the sediments. A clogged bottom outlet device is also a severe security problem (Boillat and Delley 1992, Schleiss et al. 1996, De Cesare 1998).

Reservoir sedimentation reduces the value of or even nullifies the investment for dam construction. The use for which a reservoir was built can be sustainable or represent a renewable source of energy only where sedimentation is controlled by adequate management, for which suitable measures should be devised. Even if hydropower in general is a sustainable energy reservoir sedimentation can threaten the sustainable use of storage power plants (Schleiss et al. 2009). Lasting use of reservoirs in terms of water resources management involves the need for desiltation.

Until today there have been several methods practised to prevent the sedimentation problem in reservoirs. Most of them do not guarantee a life-time use for the entire design life of the reservoir, what might be defined as goal of sustainability regarding reservoirs (Lafitte and De Cesare 2005).

The reservoir sedimentation problem calls for a sustainable innovation. Based on the above described fact the most efficient method consists in nearly restoring the sediment balance by creating a sediment transfer through the reservoir. Concerning fine sediment, this is best realised by a transfer through the headrace tunnel and the turbines during operation time, when water is released anyway.

1.1.2 Statistics and historical evolution

The worldwide average annual sedimentation rate of all the reservoirs, and consequently the annual loss of storage capacity due to sedimentation are estimated to be 1 to 2 % of the storage capacity (Jacobsen 1999, Mahmood 1987, Basson 2009). A detailed collection of sedimentation rates in regions all over the world can be found in Batuca and Jordaan (2000) and in Basson 2009. Knoblauch et al. (2005) report that the Alps together with the Himalaya, the Andes and the mountains at the Pacific coast of America are the regions with the highest erosion rate. The evolution over the last century and the predicted future development of the volumes of water storage capacity lost due to reservoir sedimentation and the volumes of installed water storage capacity in the world are presented in Figure 1.2 (Oehy 2003). Bearing in mind that the annual increase of storage volume due to the construction of new reservoirs is close to 1 %, the problem of sustainability becomes apparent (Oehy et al. 2000). If there are no effective measures undertaken, the major part of the worldwide useful volume will be lost by the end of the 21st century. The sedimentation rate in each particular reservoir is highly variable, depending more particularly on the climatic situation, the geomorphology and the conception of the reservoir, including its outlet works. Beyer Portner (1998) showed that on average in Switzerland approximately 0.2 % of the storage capacity is lost annually due to

sedimentation (Figure 1.2). The lower sedimentation rate in the Alps is due to the geologic characteristics, mainly rocky mountains, of the catchment areas at high altitudes (Oehy 2003). From the point of view of loss of storage volume, the Swiss Alpine reservoirs are more sustainable. Nevertheless after 40 to 60 years of operation the sedimentation process becomes a real threat for safe operation due to the turbidity currents (De Cesare 1998).

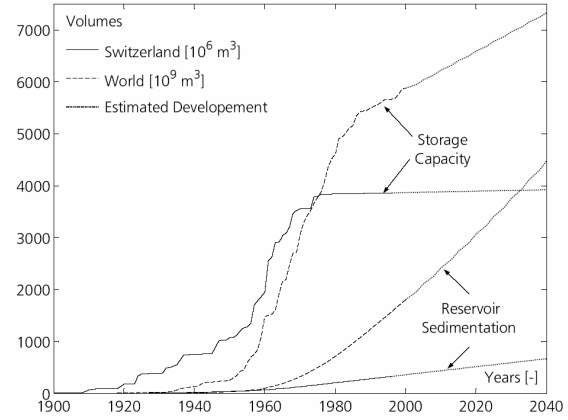

Figure 1.2 Increase of the reservoir capacity by the construction of new dams and storage volume loss by sedimentation worldwide and in Switzerland, after Oehy (2003)

1.1.3 Trap efficiency – problem quantification

The trap efficiency of a reservoir can be defined as the percentage of the total inflowing sediment that is retained in the reservoir. Factors influencing the trap efficiency are hydraulic characteristics of the reservoir and sediment characteristics of the inflowing sediment. Hydraulic characteristics include:

- The ratio between storage capacity and annual inflow volume
- Reservoir geometry
- Type of outlets
- Reservoir operation

The capacity-inflow ratio indicates the retention time. The greater the retention time, the lower is the average transit velocity and associated turbulence, and the greater is the rate of deposition. The geometry of the reservoir determines the effective retention time and could cause "short circuiting" in which the effective time becomes much less than the retention time as determined by the capacity-inflow ratio. This means that, because of the shape of the reservoir, in some areas of it there is no flow. Bottom outlets placed deep enough can reduce trap efficiency of fine sediments, particularly if they are periodically opened to pass turbidity currents. Lowering of the reservoir elevation decreases the retention time which subsequently

decreases the trap efficiency. This can be very effective if done during periods of higher flows with its high sediment concentrations.

Sediment characteristics affecting the trap efficiency are

- particle size distribution of the inflowing sediment load
- particle shape
- behaviour of fine sediments under varying temperatures, concentration, water chemical composition, secondary currents and turbulence
- particle density

Grain size distribution and particle shape determine particle fall velocities, and in conjunction with water depth and detention time, determine the percentage of the sediment that deposit or remain in suspension. Fine sediments (clay and silt sizes) are usually the only ones that remain in suspension long enough to reach the outlets. Temperature, concentration, and chemical composition of the water affect the aggregation properties of these fines (U.S. Army Corps of Engineers 1995) which likely influence the resuspension of deposited sediments and the transport capability of the fines.

Brune (1953) as well as Brown (1950) and Churchill (1948) developed empirical relationships to define trap efficiency. The following prediction equation draws the Brune's median curve:

$$TE = 100 \cdot 0.97^{0.19^{\log(C_R/I)}} \qquad (Eq.\ 1.1)$$

With C_R: storage capacity of the reservoir [m^3]

I: mean annual discharge [m^3]

TE: Trap efficiency

Some alpine reservoirs are classified and plotted on Brune's curve in Figure 1.3. A higher trap efficiency TE indicates a higher amount of sediments retained in the reservoir. Because no measures had been taken over a very long time, the Reservoir Forni (Italy) has already been filled up with sediments (Figure 1.1).

Walling (1997) analyses the records of annual suspended sediment yield for the River Isar at Munich, Germany, for the period 1930-1990, showing a significant reduction that reflects the development of hydropower stations and associated storage reservoirs on this river. More particularly, since the commissioning of the Sylvenstein dam in 1959 sediment yields have decreased to about 20 % of their former level over this period, and the trend shows that the reduction has intensified in recent years.

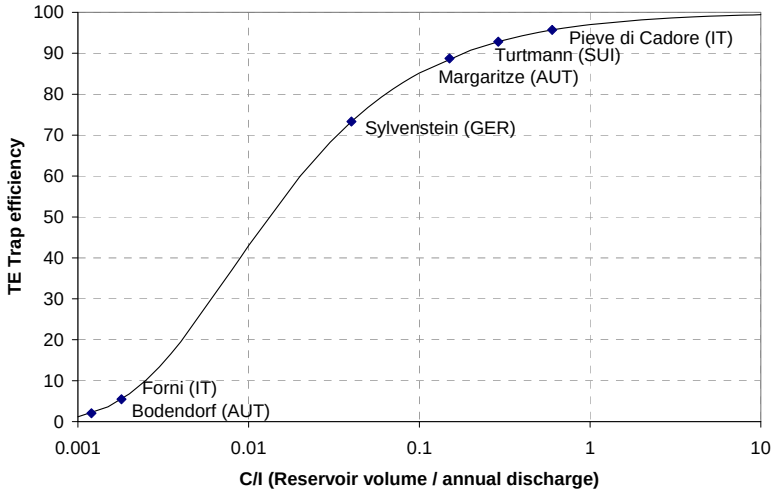

Figure 1.3 Retention factor (trap efficiency TE) after Brune (1953). Comparison of the pilot actions (case study projects) in the framework of the project Interreg IIIB-ALPRESERV

1.1.4 Origin of the sediments

The sediment load of a river is due to erosion in its catchment. Bechteler (2008) states that there are exogenous processes like wind, rainfall, temperature, glaciers and vegetation acting on the crust of the earth and leading to weathering, loosening, diminishing and transporting of the soil materials. This process starts in the high mountainous regions, and continues in the highlands and plains and ends in the lakes or in the sea respectively where - due to the decreasing flow velocity – sedimentation occurs. The transported material originates from erosion, landslides, riverside erosion as well as from erosion in the riverbed. As a consequence of these processes there will be a flattening of the mountainous relief and a filling up of the concave zones.

Beyer Portner (1998) described the annual erosion volume per surface by an empirical equation. This equation has been elaborated based on the analysis of sedimentation data of 19 Swiss reservoirs. A valuable general connection between the analysed reservoirs depends on the following parameters (see also Schleiss and Oehy 2002):

- H_{Sommer}: Mean rainfall in the summer (June to September) [mm]
- OV: Percentage of the surfaces without vegetation [%]
- EB: Percentage of the surface covered by easily eroded soil [%]
- ΔGL: Annual mean relative change of the length of the glacier [%]

$$V_A = 0.2112 \cdot 1.10683^{OV} - 5.684 \cdot OV + 0.2112 \cdot \left(H_{Sommer} \cdot \Delta GL + OV \cdot EB\right) + 11 \frac{m^3}{km^2\ a} \qquad (Eq.\ 1.2)$$

Depending upon the sediment supply and the flow intensity in terms of velocity and turbulence, rivers usually carry sediment particles within a wide range of sizes. Bed load consists of the coarser components which are transported near the river bed. The suspended sediments are generated by superficial erosion as well as by smashing and abrasion of coarser components.

During flood events the fraction of sediments smaller than sand reaches 80 to 90 % of the total sediment carried by many rivers (Alam 1999, Sinniger et al. 1999), and the total sediment discharge is usually significant. Due to larger erosive forces and transport capacities with increasing discharge, the sediment concentration in a river is especially high. If the sediment concentration is high enough it may lead to turbidity currents in reservoirs.

1.1.5 Turbidity currents

Schleiss and Oehy (2002) already proposed to mix the fine sediments transported by the turbidity currents with the surrounding water and to maintain them in suspension and to evacuate them through the turbines. Since this idea is resumed in the present study, the main characteristics of the turbidity current are outlined as follows.

In large Alpine reservoirs, turbidity currents are often the governing process in reservoir sedimentation by transporting fine materials in high concentrations. They are flows of water laden with sediment that move downslope in otherwise still waters like oceans, lakes and reservoirs. Their driving force is gained from the suspended matter (fine solid material), which makes the flowing turbid water heavier than the clear water above it. This phenomenon takes place sporadically during yearly floods.

When a river flows into a reservoir, the coarser particles deposit gradually and form a delta in the headwater area of the reservoir that extends further into the reservoir as deposition continues. Finer particles, being suspended, flow through the delta and pass its lip point. If after the lip point of the delta, the difference in density between the lake water and inflowing water is large enough, it may cause the flow to plunge and a turbidity current can be induced. During the passage through the reservoir, the turbidity current may unload or even resuspend granular material. Subsequently the sediments are deposited along the path due to a decrease in flow velocity caused by the increased cross-sectional area. Fine sediments (clay and silt sizes) are usually the only sediments that remain suspended long enough to reach the outlets (Figure 1.4).

When the turbidity current reaches a barrier, such as the dam, its kinetic energy is converted into potential energy as the current head rises up against the face of the dam and subsequently falls back down, initiating the formation of a muddy layer. After some time the fine sediment deposits cover the bottom (Oehy 2003). The sediment concentration within turbidity currents was measured during several turbidity currents events. De Cesare (1998) summarizes values found in the literature and states that they are usually in the range of 0.2 to 70 *g/l* (0.0075 to 2.6 *vol.-%*).

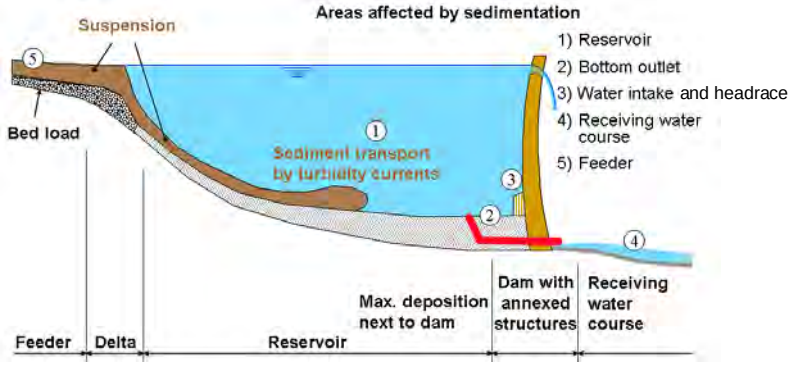

Figure 1.4 Areas affected by sedimentation in and downstream of a reservoir (De Cesare 1998)

1.2 Measures against reservoir sedimentation

1.2.1 General

Over the years several measures against reservoir sedimentation have been proposed (Schleiss and Oehy 2002), but not all of them are sustainable, efficient and affordable. For example the heightening of dams and outlet works doesn't provide a long term solution (Boillat and Delley 1992).

There is a strong need to limit sediment accumulation in reservoirs in order to ensure their sustainable use. Management of sedimentation in Alpine reservoirs cannot be performed by a standard generalized rule or procedure. Furthermore, sediment management is not limited to the reservoir itself. It begins in the catchment areas and extends to the downstream river. Every situation has to be analysed for itself in order to determine the best combination of solutions to be applied. It happens that the simultaneous implementation of several alternatives is necessary in order to stabilize reservoir sedimentation. Possible measures are summarized in Figure 1.5 and grouped according to the areas where they can be applied: catchment area, reservoir and at the dam.

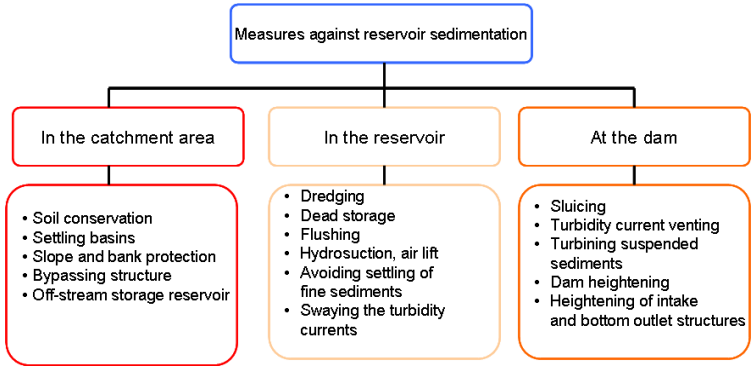

Figure 1.5 Inventory of possible measures for sediment management (Schleiss and Oehy 2002)

An integrated approach to sediment management that includes all feasible strategies is required to balance the sediment budget across reservoirs (Morris 1995). Integrated sediment management includes analysis of the complete the sediment problem and application of the range of sediment strategies as appropriate for the site. It implies that the dam and the impoundment are operated in a manner consistent with the preservation of sustainable long-term benefits, rather than the present strategy of developing and operating a reservoir as a non-sustainable source of water supply (Morris 1996).

A sustainable sediment strategy should also include the downstream reaches; therefore monitoring data should also include downstream impacts as well as sedimentation processes in the reservoir (Morris and Fan 1997).

In the following the actually known measures subdivided as in Figure 1.5 are described.

1.2.2 Measures in the catchment area

A major cause of increase in reservoir sedimentation is related to damage of the vegetal cover in the watershed. This can have its origin in human activities like skiing or in natural events like wind or storm causing deforestation or melting of glaciers and permafrost. This erosion increases soil instability and water runoff.

A reduction of sediment yield by soil conservation in the catchment area can be very effective, and can solve the reservoir sedimentation problem in a sustainable way. Where the climatic conditions allow for vegetation, the soil can be protected from erosion by afforestation or vegetation screens. However, these measures are very complex and often related to different agricultural techniques than the ones used in the area. Erosion protection can only be achieved with engineering measures such as gully control, as well as slope and bank protection works on rivers (Oehy 2003).

Settling basins are often constructed in the catchment area to limit gully erosion. The small size dams trap only the coarser sediment particles and the sediment load quickly builds up again downstream. Therefore, this measure has rarely a major impact on the sediment yield. The construction of such debris trap dams in the upper catchment areas may be a solution; but

without proper regular maintenance, these will fill up by bed load transport very quickly and in the long term they serve no purpose. A further problem with upstream sediment trap dams is finding a place for continuous, long-term disposal of the incoming sediments, which accumulate indefinitely. Often the settling basins are also too small to significantly affect the sediment flux into the reservoir.

It is well known that the sediment yield is closely related to the characteristics of the catchment area. Walling (1997) cites a series of studies analysing the influence of land use change, the impact of forest clearance and gold mining activity, the expansion of agriculture and construction activities associated with rapid and extensive urban and suburban development within the catchment area. Reservoirs which have a small catchment area or which are off-stream may be supplied by conveying channels from neighbouring catchment areas on condition that the intake structures of the waterways systems have sediment traps. For rivers transporting large volumes of coarse materials, from cobbles to coarse sands, it is possible to extract the materials regularly or continuously from the delta near the upstream end of the reservoir. Such extracted materials can often be used as construction materials (Schleiss and Oehy 2002).

While erosion control is an essential management activity, it alone cannot establish a sediment balance across the impounded reach and preserve long-term capacity (Morris 1995). Walling (1997) cites experiments documenting the impact of soil conservation and related practices aiming the reduction of suspended sediment yields. He presents the results obtained from studies of four small catchments in the highly eroded loess region of the Middle Yellow River aimed at evaluating the success of soil conservation measures such as tree planting and construction of terraces and check dams in reducing sediment yields. In these cases sediment yields have been reduced by approx. 90 % or more.

Worldwide only a limited number of sediment bypass tunnels has been constructed because of adverse topographical, hydrological or economical conditions. Bypass tunnels, however, have many advantages. They can be constructed even for existing dams, and avoid a loss of stored reservoir water caused by the lowering of the reservoir water level. They are also considered to have a relatively small impact on the environment downstream because inflow discharge can be passed through tunnels very naturally during flood time (Sumi 2004). Vischer et al. (1997) studied several bypass tunnels in Alpine reservoirs and found that they are successfully deviating coarse sediments.

1.2.3 Control of sedimentation within the reservoir

1.2.3.1 Dead storage

The most common method to conserve the storage capacity is to oversize reservoirs, i.e. to keep some of the impoundment available for sedimentation. In case this volume is not available for reservoir operation, it is called dead storage (Schleiss and Oehy 2002).

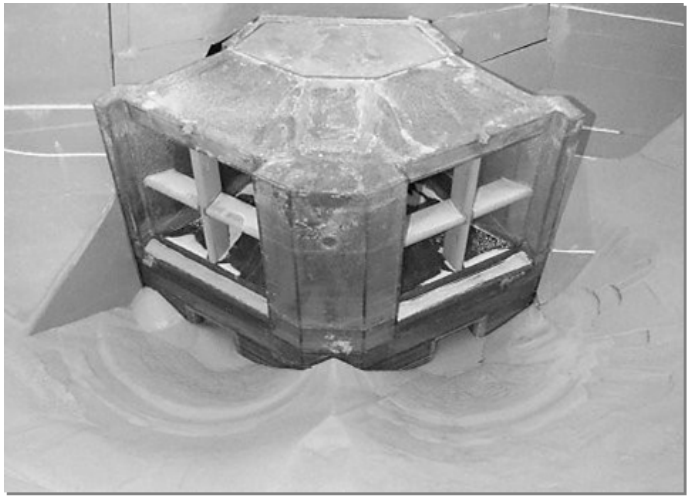

Figure 1.6 Construction of the water intake at a higher level, with bottom outlets directly placed below the water intake (source: LCH-EPFL)

Accepted practice has been to design and operate reservoirs which fill up with sediment while generating benefits from the remaining storage volume over a finite period of time. The consequences of sedimentation and project abandonment are left to the future. These consequences can be summarized as: sediments reaching intakes and greatly accelerating abrasion of hydraulic machinery, decreasing their efficiency and increasing maintenance costs; blockage of intake and bottom outlet structures or damage to gates that are not designed for sediment passage (Boillat and Delley 1992), etc. This 'future' has already arrived for many existing reservoirs and most others will eventually experience a similar fate, thereby imposing substantial costs on society (Palmiere et al. 2001).

1.2.3.2 Obstacles, screens, water jets and bubble curtains for controlling turbidity currents

To control the sedimentation within the reservoir, Oehy (2003) investigated the effects of obstacles, screens, water jets and bubble curtains on the turbidity current by means of physical experiments and numerical simulations. From these investigations, some recommendations could be drawn as rules of thumb, and some measures to control reservoir sedimentation due to turbidity currents were proposed. In a case study one the Grimsel reservoir, the possibility of influencing the turbidity current with submerged dams was evaluated with numerical models (Oehy 2003). The result showed that due to the blocking effect of the dam, the sediments can be retained efficiently and sediment deposits in the area of the intake and bottom outlet structures can be prevented.

1.2.3.3 Flushing

Hydraulic flushing has been used for a long time. The oldest known method of flushing, practised in Spain in the 16th century, was referred to by D'Rohan (1911, ref. Brown 1943).

Since that time there have been discussions about whether flushing is more suitable for large or small reservoirs. Flushing is not possible when fish are killed (Salih 1994) or the released sediments are heavily polluted (Scheuerlein 1995, Huwyler 2002).

Sediment flushing is a technique whereby previously accumulated and deposited sediments in a reservoir are hydraulically eroded and removed by accelerated flows generated by opening the bottom outlets of the dam. Flushing can be classified into flushing under pressure and free-flow flushing or draw-down. During flushing under pressure water is released through the bottom outlets while the water level in the reservoir is kept high. For free-flow flushing the reservoir is emptied and the inflowing water is routed through the reservoir, resembling natural riverine conditions. If flushing is carried out under pressure, only a very limited area in the reservoir is cleared (Schoklitsch 1935, ref. Brown 1943). Free-flow flushing can transport a much greater sediment load (sometimes even consolidated sediments) than flushing under pressurized conditions.

Figure 1.7 Flushing with bottom outlets at Jiroft Dam, Iran (Picture: Soleyman Emami)

If the water level is drawn down during flushing, the sediment removal occurs in several phases (Figure 1.7). Flushing is most effective during the first hours. A free-flow phase then begins with high rates of sediment removal in the first few days or weeks, but when the stream has re-established approximately its original gradient through the reservoir basin, the amount of sediment picked up and transported will greatly decrease (Brown 1943) and the turbidity remains stable. The timing of flushing is important, both for economical and ecological reasons. In regions with pronounced flood seasons flushing has to be performed before the beginning of the yearly food. Where the prime purpose of a dam is irrigation water storage, flushing is done at the end of the irrigation season, because this is the period of least water demand. Kereselidze et al. (1986) recommended that flushing should be performed immediately before fish spawn and after they rear the fry. Shen and Lai (1996) pointed out that flushing should be done regularly especially for cohesive clay deposits, before deposits consolidate.

Flushing becomes more effective the longer it lasts, the narrower, straighter and shorter the reservoir is, the greater the discharge of the flushing stream is, the greater the dimensions and the lower the location of the flushing outlet are, the finer and the rounder the particles in the sediment are, the younger and the less consolidated the sediments are and the steeper the original stream gradient through the reservoir is (Orth 1934, cited by Brown 1943).

Flushing is often associated with a host of adverse environmental impacts. Generally, flushing methods must be chosen with the aim of limiting the impact of the downstream reaches of the river (OFEFP 1994). Moreover, legal requirements may restrict or prohibit the practice of removing sediments from surface waters and reintroducing them into the flow at a later time (Suter 1998; Boillat and Pougatsch 2000).

1.2.3.4 Hydrosuction

Different systems of fixed pipes to route the sediment through or around the dam, have been suggested for a long time. Hotchkiss and Huang (1995) stated that the shock to the downstream reach associated with flushing can be avoided by using a hydrosuction sediment-removal system, because it is continuous and of longer duration. These techniques try to return the system to more natural pre-dam conditions by releasing sediments in accordance with the downstream transport capacity.

Hydrosuction systems remove deposited sediments by using the available energy head due to the difference between water levels upstream and downstream of a dam. Hotchkiss and Huang (1995) describe the design of such a system and presented some field tests. The pumping device is equipped with a drill head in order to facilitate the disintegration of the deposits. The volume of the pumped mixture will normally be conducted into decantation basins. It can also be diverted into the downstream river. This type of operation was performed in the Luzzone Reservoir (Switzerland) in order to clear the water intake opening. An extraction of 17'000 m^3 of sediments in 1983 and of 25'000 m^3 was achieved in 1984 (Boillat and Pougatsch 2000).

The main problem with a gravity suction system is that the approach flow velocities drop quickly as the radial distance from the suction point increases, and sediments are no longer entrained into the suction pipe. To be efficient, the suction end of the pipe would have to be repositioned almost continuously. But with a long pipe length and high sediment volume, the head loss may increase dramatically, choking the pipeline (Alam 1999). A special suction system was presented by Jacobsen (1998) and consists of a slotted pipe which is laid on the reservoir bottom. The sediments are then evacuated by suction either through the bottom outlets or over the spillway. Huwyler (2002) presented some preliminary tests for a new approach in resuspension of fine sediments by an air-lift system and by evacuating sediments within an acceptable range of concentrations through the intake structures.

Vigl and Pürer (1996) report about a hydrosuction system applied in the reservoir Bolgenach dredging continuously fine sediment out of the dead storage and transferring it by airlift through the water intake downstream. In order to avoid high sediment concentrations downstream of the reservoir clear turbining water and turbining water with supplied dredged fine sediment are alternatively released. The downstream concentration is continuously monitored.

1.2.3.5 Dredging

One obvious alternative to flushing or routing sediments through a reservoir is underwater dredging or dry excavation of the deposited material (Figure 1.8). The drawback of dredging is the high cost for sediment removal, but as reservoir level drawdown for flushing and sluicing may not solve all sediment-related problems, the impounded reach will need to be dredged due to continued accumulation of gravels (Morris and Fan 1997). Underwater dredging requires a lesser drawdown of the reservoir water level than sluicing.

Figure 1.8 Left: Dredging in Margaritze (Aut). Right: Analysis of the composition of the sediments in Pieve di Cadore (It). (Hauenstein 2005)

Another concern is the deposal of the sediments after dredging. Depending on the legal framework, disposal of the sediments stored over years in the reservoir is not permitted or shouldn't be done because of ecological reasons. Returning them into the downstream part of the river is delicate. Polluted sediments are not appropriate for an ecological system, and the concentration is still difficult to control. Furthermore, muddy lake deposits mainly composed of silt and clay are not easy to remove or use because of their high organic matter and water contents. Deposition of the fines is delicate because the wind takes them easily away. Depending on the reservoir, the sediment quantity to be extracted and transported to another place is large and requires lots of truck rides. From an ecological point of view and regarding the access roads of the reservoirs, this might be an unfortunate solution.

1.2.4 Measures at the dam

1.2.4.1 Sluicing

During sluicing operations, the water level in the reservoir is drawn down to allow for the sediment-laden inflow to pass through the reservoir with a minimum of deposition. Typical of sluicing in a flood-detention reservoir is that during a rising water level of a flood the outflowing sediment discharge is always smaller than that of the inflow. During the drawdown of the water level, the outflowing sediment load is greater than the inflowing one, due to erosion in the reservoir (Fan 1985). Since inflowing sediment concentration during a flood tends to be highest during the rising limb of the hydrograph, the reservoir can be filled with less turbid water following the flood peak (Fan and Morris 1992). Sluicing operations should

be timed to accommodate the higher sediment concentrations brought in by flood flows. By opening bottom gates fast enough, the rate of increase of the outflow can be made equal to the rate of increase of an incoming flood. The detention effect of the hydrograph of the sediment is then minimized. The sediment outflow thus approaches the natural flow condition. Sluicing is successful if the capacity of the outflow structures is adequate, the operation is done judiciously, the river is transporting mainly suspended sediments and the flow hydrograph is predictable with confidence at the dam site (Basson and Rooseboom 1997).

1.2.4.2 Turbidity current venting

Venting of density currents means that the incoming sediment-laden flow is routed under the stored water and through the bottom outlets in the dam. Since the reservoir may stay impounded during the release of density currents, this method is widely used in arid regions where water is in shortage. Fan and Morris (1992) suggested that density-current venting may be well suited at large reservoirs with multiyear storage capacity where drawdown is unwanted. Venting operations have much better chance of accomplishing their purpose when they are timed to intercept gravity underflows as they reach the dam. The correct timing of opening and closing gate is very important. A late start of sluice operation or a too small outflow will result in a smaller amount of sediment removed from the reservoir. Conversely, if the gate is opened too early or the opening is too large, a loss of valuable water occurs (Chen and Zhao 1992). The capacity of the bottom outlets has to be high enough to allow turbidity current venting, i.e. at least in the range of the incoming flow.

An early application of this method, where submerged dykes were used to confine the turbidity current to a narrow channel, was presented by Schaad (1979). Schneider et al. (2007) demonstrated by measurements in Grosssölk that during floods turbidity currents follow the thalweg until they reach the dam, although the turbine was in operation and the bottom outlet was closed. This is very promising for the venting method to work.

1.2.4.3 Heightening of dam, intake and bottom outlet structures

An increase of the dam height and raising its outlet structures is an alternative to reducing the loss of reservoir capacity due to sedimentation. Although it might be cost effective in the mid term, dam heightening does not provide a sustainable solution of the sedimentation problem. Construction of new dams to solve the sedimentation problem in the future leads to the same problems. Finally, by raising the intake and bottom outlet structures, the dead storage volume is increased and sediment entrainment into the intakes can be prevented for some time.

1.2.5 Concluding remarks

The conventional methods of sediment evacuation all have drawbacks. Some of them are too expensive, in others the loss of precious water and energy is considerable, and some are simply not efficient enough. Others produce ecological problems by exceeding the acceptable concentration or present unsolved problems in producing tons of sediments which have to be transported and stored somewhere. No good and economically interesting solution has been found for the use of fine sediments yet. Furthermore the sediments captured over a certain time in a reservoir may be polluted and need a special treatment before they can be recycled or given back to nature.

1.3 The innovation, its concept and functional principle

1.3.1 Basic concept of the innovation

As mentioned above, the balance between sediment inflow and outflow of a natural river is altered by dam construction. Therefore, the most efficient method of restoring the balance is to permit a sediment transfer through the reservoir. Thus, the concept of the study focuses on a transfer of fine sediment through the headrace tunnel and the turbines. The ultimate goal would be to come close to the natural pre-dam conditions. The present study focuses on the fine sediments right in front of the power intake. Evacuating the sediments in this area avoids clogging of the outlet works and guarantees their safe operation. Most of the fine sediments reach this area when they are transported by turbidity currents.

In order to evacuate the sediments through power intakes and headrace tunnels during turbining sequences, they need to be in suspension in front of the water intake. Therefore, a way maintaining the sediments in suspension needs to be developed and sediment settling has to be avoided.

The energy needed for keeping the sediments in suspension is available from the drop height of the water transferred from neighbouring catchments. This method has a good chance of working in large reservoirs, where the sediment in front of the water intake is generally fine and has a small settling velocity.

1.3.2 Functional principle

Water collected in neighbouring catchments and transferred in water tunnels to the reservoir under consideration is caught and led into a pressure pipe and led to the bottom of the reservoir. On the bottom it is distributed by well arranged jets. The available water discharge and head feeding these jets supply the energy to establish a circulation and artificial turbulence (Figure 1.9).

This circulation maintains the fine sediments remaining after a flood in the muddy layer (see section 1.1.5) in suspension and lifts them to the height of the water intake from where they are evacuated during operating hours.

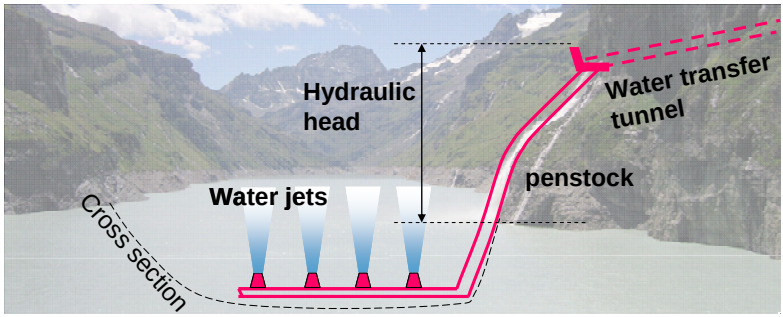

Figure 1.9 Schematic view of jets fed by water transfer tunnels from neighboring watersheds (background of Mauvoisin, source: Wikipedia.org, author: Goudzovski)

1.3.3 Processes not or only implicitly considered in the experimental study

The following problems may hamper the evacuation of sediments.

- The sediments that are deposited in front of the dam are, due to the sedimentation process, usually very fine and cohesion might be a problem.
- Sediments which have been deposited close to the dam a long time ago could have undergone a consolidation process. Hence, the required shear-stress for resuspension process is considerable (Shresta et al. 2004).
- The more stratified the water is (because of temperature or suspended sediment) the more forces are needed to overcome the density differences and to mix the water volume providing a lift for the sediments.

Since fine sediments are used, the present experimental study does implicitly consider the effects due to cohesion and consolidation. But their effect is not quantified. Stratification, eventual woody debris and armouring are not considered.

1.4 General requirements for successful desilting

1.4.1 Type of reservoirs concerned

Depending on the conditions in different catchment areas, the range of grain sizes varies from one reservoir to another. Because of decreasing flow velocities along the thalweg a grain sorting process occurs such that close to the dam the deposition of the finest particles takes place (section 1.1.5). This means that the larger a reservoir is, the finer are the sediments encountered in front of the dam, and the narrower is their grain size distribution. In small reservoirs 70 to 90 % of the sediments consist of clay and silt, whereas in large reservoirs it is 90 to 100 %. The application of the proposed jets is best in large reservoirs where the exclusivity of very fine sediments near the dam is guaranteed. In small reservoirs the grain size needs to be assessed first.

1.4.2 Economic aspects

The loss of storage volume in reservoirs reduces energy production, or limits their retention capacity for drinking or irrigation water, or floods. Furthermore the sedimentation process can block the bottom outlet device as well as the intake structures. A blocked bottom outlet can lead to severe safety problems. This lack of functionality can be expressed in monetary values and give an idea of the economic importance of the problem.

Conventional methods of dredging or sucking are very expensive. Seasonal water level changes make dredging even more complicated or even impossible. The accessibility of alpine reservoir sites is often poor. Therefore, sediment transport by truck is often not feasible and from an ecological point of view disproportional. The deposition of fine sediments and their recycling are difficult due to lack of disposal sites. Exceptionally, sediments may be released by flushing, under the condition that no damage be caused to the environment, or when sediments are needed for a particular purpose. The usually high water content in fine sediments is a problem on both process steps, dredging and deposing.

With the continuous release of sediments through the turbines the abrasion of the turbine wheels and the control devices become more important. This implies that the maintenance of

the hydro-mechanical equipment has to be done more frequently. The resulting costs have to be added to the investment for the desiltation method in case of an economic analysis.

If a reservoir is filled up by sediments also the investment is lost. Therefore it is worth to invest in a profitable measure which is effective in long term and which is considering the ecological needs. It appears obvious that there is the necessity to develop a method which is economical and sustainable at the same time. Without any intervention over the years the whole hydraulic structure is lost due to reservoir sedimentation. Carrying the comparison to the extremes, the major cost that may be accepted for an investment in a new desiltation method is the construction cost of a new hydraulic scheme.

1.4.3 Maximum outflow concentration

1.4.3.1 General

Most of the Alpine reservoirs are designed for hydropower. Consequently, most of the water intakes are power intakes and the water is turbined. If the water was stored for drinking or irrigation purposes the maximum outflow concentration would be subject to different water quality requirements than for the hydropower production or need a supplementary treatment. The case for drinking and irrigation water supply was not subject of the present study.

It seems obvious that because of ecological aspects and because of hydraulic machinery abrasion due to the increased sediments impact, the outflowing sediment concentration has to be regularly monitored and controlled, and an upper limit needs to be defined.

If a complete balance of incoming and outflowing fine sediments was aimed, the evacuated sediment concentration would match that of the sediment supply of the watershed. Assuming that the total useful volume of seasonal reservoirs is filled and emptied once a year and that all the fine sediments inflowing during one year are evacuated at a constant concentration, sediment concentrations for three analyzed Swiss Alpine reservoirs (Grimsel, Mauvoisin and Tourtemagne) can be expected in the range of 900 to 2000 *mg/l*. This estimate is performed neither considering the turbined discharge nor the operation hours. The average yearly inflowing sediment quantity is simply compared with the total reservoir capacity, excluding dead storage volume.

Scheuerlein (1995) suggested that the sediment concentration due to flushing actions should not exceed the upper limit measured already during historical natural-flood events in a river. Formerly, the downstream ecosystem was accustomed to this occasional impact. This extremely high concentration should, however, rarely be repeated and only last for a few hours or days. The federal network for suspended sediment monitoring (in 1999 consisting of 13 stations) measured at two stations maximal sediment concentrations of around 30'000 *mg/l* (Landquart and Arve). The 95-percentile including all 13 stations was between 89 and 2600 *mg/l* (Bucher 2002). The differences between the reaches are significant and underline the necessity of elaborating appropriate maximum values for each separate case.

There are four main aspects limiting the admissible sediment concentration: the agricultural land irrigated with tailwater, the clogging of filter systems of cooling and control systems in powerhouses, the transport capacity in penstocks or headrace tunnels, the ecosystem of the downstream water course and the abrasion of the turbines and control devices (Schleiss et al. 1996). The three latter are more thoroughly discussed hereafter.

1.4.3.2 Ecological aspects

Eckholm (cited by Walling 1997) showed in 1976, that suspended sediments are the largest human made water pollution in the world. The effects of high sediment concentration are versatile and of physical, chemical and biological nature. There are hardly any studies investigating the response of the biocoenosis as a whole (Ryan 1991). However, enough information is now available to show that, for example, the ecological consequences must receive greater consideration (Petts 1987, cited by Bucher 2002). To forecast effects on the biota, knowledge about the physical processes concerned is required. The topic of downstream effects during and after flushing operations has received much less attention than flushing procedures themselves (Morris and Fan 1997).

At the time there aren't any federal guidelines in Switzerland regarding maximum released sediment concentration. The only rules apply to flushing procedures, which can't be compared with a continuous release of sediments. In Switzerland the values of 5'000 to 10'000 *mg/l* (dry weight per litre, Staub 2000) are the maximum limit to be respected in the case of flushing. For flushing the ordinance of the Canton of Valais has fixed an admissible concentration as a function of time whereas the concentration values can vary from a watershed to another. Not only the high concentration peak but also the fast sediment concentration increase at the beginning of flushing is very stressful for aquatic fauna (Bucher 2002).

In order to define the upper concentration limit for the hydrologic and the morphologic conditions as well as for the present biocoenosis, the particular tailrace needs to be analyzed first. This provides the required overview of the ecosystem and gives an idea of the expected impact. Fish species react differently to sediment impact, so do invertebrates and aquatic flora. Their response depends on the life history stage too.

According to the U.S. Environmental Protection Agency and to the Swiss Federal Institute of Aquatic Science and Technology (EAWAG, Bucher 2002) suspended sediment in high concentrations irritates the gills of fish, and can cause death. Sediment can destroy the protective mucous covering the eyes and scales of fish, making them more susceptible to infection and disease. The severity of damage appears to be related to the dose of exposure as well as the size and angularity of the particles involved. Furthermore, settling sediment can bury and suffocate fish eggs, and bury the gravel nests they rest in. Fine grained sands, silts and clays can cover up coarser sediments and the spaces between rocks and cobbles that provide habitats for aquatic life. Suspended sediment in high concentrations can dislodge plants, invertebrates, and insects on the stream bed. This affects the food source of fish, and can result in smaller and fewer fish. Suspended sediment decreases the penetration of light into the water. This deprives the plants of light needed for photosynthesis, affects fish feeding and schooling practices, and can lead to reduced survival. Sediment particles absorb warmth from the sun and thus increase water temperature. This can stress some species of fish. Severity of effect caused by suspended sediments is a function of many factors, which, in addition to sediment concentration, duration, particle size, and life history stage, may include temperature, physical and chemical characteristics of the particles, associated toxicants, acclimatization, other stressors, and interactions of these factors.

By releasing the sediments through the turbines we can influence both the sediment concentration and the exposure time and to a certain extent the particle size. Newcombe and McDonald (1991) and Newcombe and Jensen (1996) define the product of concentration multiplied by exposure duration as a parameter indicating survival probability. Bucher (2002)

cites experiments conducted by different authors using different particles and fish species. The mortality probability attributed to the exposure time and suspended sediment concentration are shown in Figure 1.10.

The composition of the sediments has great influence on the impact on fish. Alabaster (1980) discovered that at a suspended sediment concentration of 1000 *mg/l* and more due to snowmelt during several months, populations were observed in the investigated reaches, even if not in a big number.

Bucher (2002) summarizes several studies mentioning the critical sediment concentration to be 80 *mg/l* for permanent exposure. Only few effects on fish are observed. Bucher points out that a sediment concentration higher than 400 *mg/l* leads to substantial damage to the fish population. According to Griffiths and Walton (1978), the upper tolerance level for suspended sediment in North America is between 80-100 *mg/l* for fish, and as low as 10-15 *mg/l* for bottom invertebrates. Bucher (2002) emphasises that both the rate of sediment concentration increase and the relative increase in concentration are factors describing the effect on fish.

A guideline from the USA (the standards vary from state to state, Ryan 1991) is geared to the natural conditions in the river flows and requires an increase of less than 10 % relative to the background concentration, depending on the season and the water level (flood or low flow period). Clear water bodies should have a stronger protection than already turbid rivers. In Canada a guideline recommends that the suspended sediment concentration shouldn't be increased by more than 10 *mg/l* in case the natural load is smaller than 100 *mg/l*. In rivers with higher loads the increase shouldn't exceed 10 % (Ryan 1991).

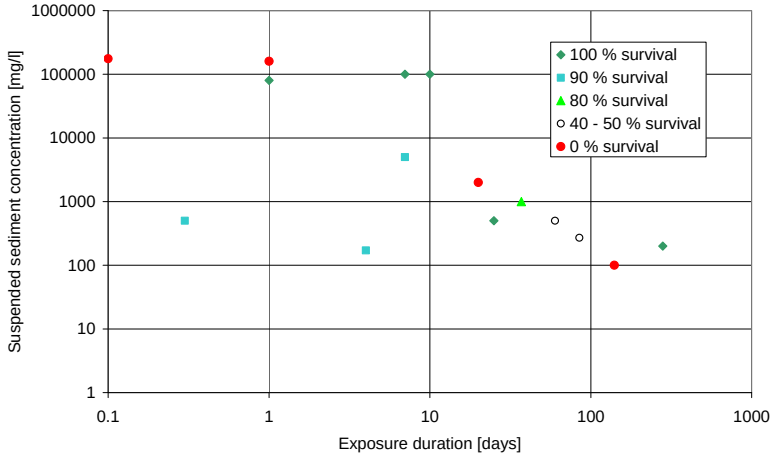

Figure 1.10 *Overview of the influence of the sediment concentration and the exposure duration on the mortality of fish. In the studies cited by Bucher (2002) several different particles and different fish species in different development stages were investigated. Therefore the uncertainty with respect to the effect is considerable.*

Usually, the water reaches immediately the tailwater right after having left the powerhouse. Thus, the turbine water is diluted and the sediment concentration decreases at once. This means that the sediment concentration after the turbines can be higher than some 80 *mg/l*.

Ryan (1991) concludes that decisions regarding what constitutes acceptable levels of anthropogenic sediment in stream environments are essentially political. There will always be conflicting requirements for water and the levels ultimately arrived at will be compromises, often to no one's complete satisfaction.

1.4.3.3 Abrasion of turbine wheels and control devices

The process of the abrasion of the hydro-mechanical equipment like the hydraulic machinery and the control devices (Figure 1.11) is a problem of major concern, decreasing their efficiency and increasing maintenance costs (Varma et al. 2000, Krause and Grein 1993). Sediment concentration, the composition of the minerals (Quartz content), the size and the shape of the particles and the kinetic energy of the impact (jet velocity relative to the runner) on the solid surfaces are the main parameters influencing abrasion (Schleiss 2007 and Boes 2010). Additionally, the turbine characteristics like the number of the jets and buckets as well as the turbine material, all are influencing the abrasion evolution. The harder (content of Quartz) and the coarser the mineral and the larger the impact velocity is, the more severe is the expected damage. The latest development in the turbine industries are focused on the improvement of coatings for turbines reducing their vulnerability against abrasion (Huwyler 2002).

Turbine manufacturers have their own rarely published criteria to define the admissible sediment concentrations without requiring additional repairs. Das (2005) indicates silt concentrations in India (high Quartz content) to be respected as a function of the operating head: for low and medium head machines (up to 150 *m*) it is 200 *ppm* (530 *mg/l*), for high head machines ($\geq$ 150 *m*) he specifies 150 *ppm* (400 *mg/l*). In the case study of the hydropower plant Dorferbach the *SSC* = 1100 *mg/l* (400 *ppm*) was determined as the threshold to stop the turbines at short term, if exceeded, in order to limit abrasion (Boes 2010). Grein et al. (1996, cited in Schleiss et al. 2009) found that turbines with novel coating materials resist sediment concentrations of 2 to 5 *g/l* and even more with usual revision cycles of 3 to 5 years.

Minerals with a hardness 5.5 in Mohs' scale or higher (means Feldspar or harder) are considered to be harmful and are having an abrasion effect on turbines. Quartz is with 7 in the Mohs scale the most harmful mineral in the Alps. A significant portion (up to 60 % depending on the watershed) of the minerals content in the Alps is Quartz.

a)

b)

Figure 1.11 a) Damaged turbine runner and b) damaged guide vane in Nathpa Jhakri (India) (courtesy of Prof. H.-E. Minor)

The distribution of the grain sizes depends on the characteristics of the catchment basin. The majority of the sediments which are deposited in front of the dam of deep reservoirs usually consist of finest grains in the range of clay and silt. The density of the particles is often around $\rho_s = 2650\ kg/m^3$.

The turbines are usually made out of steel of the sort of X5 CrNi 13/4. Besides the abrasion resistance, the material needs to resist cavitation, corrosion and fatigue. A highly abraded wheel has to be dismantled and repaired in the factory. This also implies costs because of business interruption (loss of profits).

Today's usual coating is done with SXH70. The coating has its drawbacks: the turbine efficiency is diminished by about 0.5 to 1 %. Coatings also don't help against cavitations and makes it difficult to detect fissures on the blades. On the other hand the coating lasts 40 to 60 times longer (up to 200 times in the laboratory) against abrasion (Huwyler 2002).

1.4.3.4 Transport capacity in penstocks or headrace tunnels

If sediments are deposited in conduits, the cross-sections can be reduced and roughness can increase considerably. This can lead to significant energy losses. Therefore, the sediments have to be kept in suspension. Hence, it is important to know the transport capacity as a function of the flow rate, such that sedimentation in the conduit can be avoided (Sinniger and De Cesare 1996).

1.4.4 Concluding remarks

For successful desilting by means of the proposed jets different requirements need to be met:

- The majority of the sediments needs to be fine. Therefore, larger reservoirs are more suitable than smaller ones.
- An economical and sustainable method is aimed. Conventional methods are often expensive or have negative effects on the environment.
- The maximum outflow concentration is mainly determined by ecological aspects and hydraulic machinery abrasion. The latter is less limiting and requires concentrations of less than 400, 530 *mg/l* or even higher (depending on the operating head and sediment particle characteristics), whereas fish and bottom invertebrates are sensitive to high

suspended sediment concentrations: Concerning aquatic fauna the upper tolerance level mainly reported in the literature is 80 *mg/l* for permanent exposure, but it needs to be determined according to the needs of the concerned water reach. Nevertheless, the turbine water is usually reaching the tailwater when leaving the powerhouse and therefore immediately diluted. Consequently, the evacuated sediment concentration can be higher than the critical one determined by the fauna and flora.

1.5 Purpose, methodology and organisation of the present study

The main motivation for launching this research project is to find an efficient method of releasing sediment out of a reservoir. The transfer of sediment through the headrace tunnel and turbines is studied whereby a special focus is set on the fine sediment in the area in front of the power intake. In order to evacuate the sediments through power intakes and headrace tunnels during turbining sequences, they need to be in suspension in front of the water intake.

Hence, the purpose of the present study is to develop a way of using the energy head of available water transfer tunnels for keeping the sediments in suspension such that they can be drawn into the power intake.

A combination of two approaches, hydraulic modelling and numerical simulations, is followed. The experimental part is aimed to:

- Study the possibility of keeping the sediments in suspension by means of jets.
- Investigate the effect of a jet induced circulation.
- Assess the impact of two completely different jet arrangements and determine the optimal one with respect to sediment release.
- Determine the optimal geometrical parameter combination by studying their resulting flow pattern and sediment release.
- Define the required discharge or momentum flux to keep the sediment in suspension.
- Assess the long term sediment release when jets are used.
- Estimate the sediment release deficit in case of variations of the optimal parameter combination.
- Precise the efficiency of the optimal jet configuration compared to the situation without jets.

To obtain more information about flow patterns and circulations numerical simulations are conducted. The main objectives of numerical modelling are:

- Learn more about flow instabilities resulting from the installed jet configurations and assess their influence on suspension and sediment release.
- Continue the sensitivity analysis begun with the experiments by varying different parameters and evaluating their influence on sediment release.
- Evaluate the influence of an elongated basin shape with a different basin length over width ratio on the circulation and flow velocities.
- Simulation of a real case and assess the applicability of the jets.

The methodology of the present research project and the organisation of the project report are presented in Figure 1.12. The main objectives of each chapter are briefly described hereafter:

- Chapter 2 is dedicated to review existing studies related to the problems with which the author was confronted during the research study. Hence, the main physical characteristics of turbulent axisymmetric jets are summarized, studies of mainly chemical engineers concerning jet mixed and impeller stirred vessels, investigations about air-bubbler systems and mechanical mixers employed in lakes and reports about recirculating flow generated by jets and bubble plumes are outlined.
- Chapter 3 describes the experimental installation with its measuring devices. The testing procedures for experiments with and without jets are stated at the end.
- Chapter 4 gives an overview over the experimental observations, measurements and results. The results of experiments with two fundamentally different jet configurations and of experiments without jets are discussed and compared.
- Chapter 5 presents the principles and results of the numerical simulations. Comparisons with experimentally obtained results are made and the model is used for evaluation of a basin length over width ratio differing from the one investigated in the hydraulic laboratory.
- Chapter 6 contains a case study (reservoir of Mauvoisin) discussing up-scaling difficulties and economical aspects.
- Chapter 7 summarizes the experimental and numerical results, suggests recommendations for a real case, and finally presents proposals for further research.

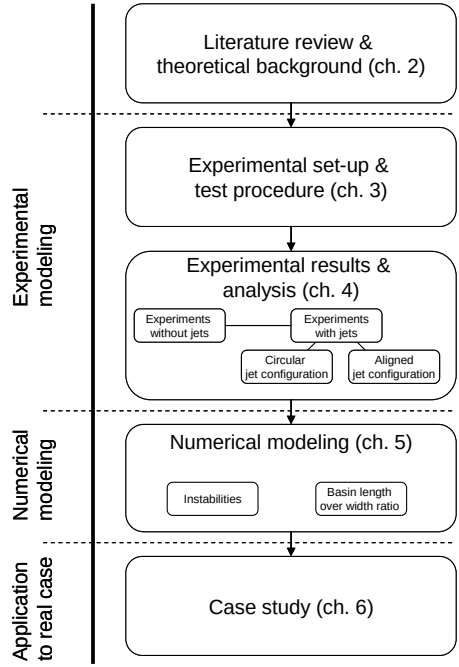

Figure 1.12 Methodology of the research project and structure of the chapters

2 Literature review and theoretical background

In this chapter background studies on sediment settling, turbulent jets, solid suspension, lake destratification by impeller aided stirring, jet mixing in tanks and recirculating flow generated by vertical jets and bubble plumes are reviewed. It has to be noted that none of these research domains covers exactly and comprehensively the theme of the present study.

The theory of the sediment settling process is well developed and documented. For the sake of completeness it is briefly touched in the literature review.

The knowledge about turbulent jets is essential when dealing with jet mixing and recirculating flows of vertical jets. For this reason a summary of the most important characteristics of turbulent axisymmetric submerged free jets is provided.

Jet mixing in tanks is one of the common unit operations employed in chemical industry. Jet mixers have become widely used as alternative to impellers.

Up to now jet mixing studies have focused mainly on improvements of the mixing process by studying the jet angle, jet location, jet length, tank geometry, and the jet characteristics like velocity, diameter, momentum flux, Reynolds number and Froude number. The flow pattern created by jets is subject of recent studies often supported by computational fluid dynamic (CFD) techniques. The authors of the CFD studies highlight the importance of the flow pattern on mixing time and try to find the most convenient jet configuration based on the flow pattern evaluation.

Stirring of solid suspensions by means of impellers in confined containers is well studied by chemical engineers. Here the researchers' goal is to establish a universal correlation for critical impeller speed and power needed for suspension. They observe that the impeller position within the vessel can completely change the flow pattern. At the same time they say that specific flow patterns are more conducive to facilitate suspension than others. It follows that the impeller position is important.

Mixing of big volumes such as lakes is important for lake remediation methods, when air-bubbler systems and mechanical mixers are applied.

While jet and impeller mixing relates to mixing of two or more substances in confined vessels, earlier studies on the recirculating flows generated by vertical jets and bubble plumes all ignore this mixing problem. They are concerned with the flow structure in the far field of a vertical jet (resp. bubble plume), and study the influence of the water depth, the cross-sectional geometry of the experimental setup, and the jet (and bubble plume) momentum flux as well as jet (respectively gas) flow rate on it. The conclusion drawn by Fanneløp et al. (1991) is that

bubble plumes (as well as vertical jets) are likely to produce recirculating cells rather than an unlimited horizontal current dissipating its energy in the far field.

Since these research domains (jet and impeller mixing in tanks and lakes and recirculating flow generated by vertical jets and bubble plumes) are relevant for the studied sedimentation problem, they have to be considered when analysing the results of the present study.

2.1 Submerged turbulent jet

2.1.1 General

A jet is a source of momentum and energy in a fluid reservoir. According to Revill (1992) a jet is fully turbulent at a jet Reynolds number Re_j above about 1'000-2'000 and laminar for Re_j below about 100. According to Blevins (1984) the limit between laminar and turbulent jet is around the Reynolds number of 3'000. The important characteristics of the jet are its momentum flux and its discharge.

$M_j = v_j^2 A_j$ jet momentum flux (*Eq. 2.1*)

$Q_j = v_j A_j$ jet volume flux (*Eq. 2.2*)

$\mathrm{Re}_j = \frac{v_j d_j}{\upsilon}$ jet Reynolds number (*Eq. 2.3*)

$Fr_j = \frac{v_j}{\sqrt{g' d_j}}$ densimetric jet Froude number (*Eq. 2.4*)

where

v_j: jet velocity at nozzle

A_j: nozzle opening

$A_j = \frac{d_j^2}{4}\pi = r_j^2 \pi$ for a round nozzle with diameter d_j and radius r_j (*Eq. 2.5*)

$g' = g \cdot c_s \cdot \left(\frac{\rho_s - \rho_w}{\rho_w} \right)$ reduced gravitational acceleration (*Eq. 2.6*)

In the present study submerged axisymmetric round turbulent jets are relevant. A submerged jet is a jet of fluid into a quiescent reservoir containing a similar fluid (Figure 2.1). It consists of three regions: an initial region, a transition region, and the fully developed jet. The initial region has axial length x_1 (according to Blevins 1984 ≈ 10 d_j, according to McCabe et al. 2005 ≈ 4.3 d_j, according to Revill 1992 ≈ 6 d_j) and it consists of the core flow and the surrounding shear layer. The velocity in the core flow is equal to the nozzle exit velocity v_j for a uniform exit velocity. The core flow is nearly free of shear; hence the terms potential flow or potential core are often used. The core flow is surrounded by a turbulent shear layer, also called a mixing layer, which forms the boundary between the core flow and the reservoir fluid. The flows in the core, the initial region, and the transition region bear the imprint of the details of the nozzle. However, at some point in the transition region, the turbulent eddies in the shear layer will obliterate the details of the nozzle core flow. The resultant eddy-dominated flow is called fully developed. The fully developed region of a submerged turbulent jet starts at about 10 d_j from the nozzle, and the mixing layer has penetrated to the jet axis.

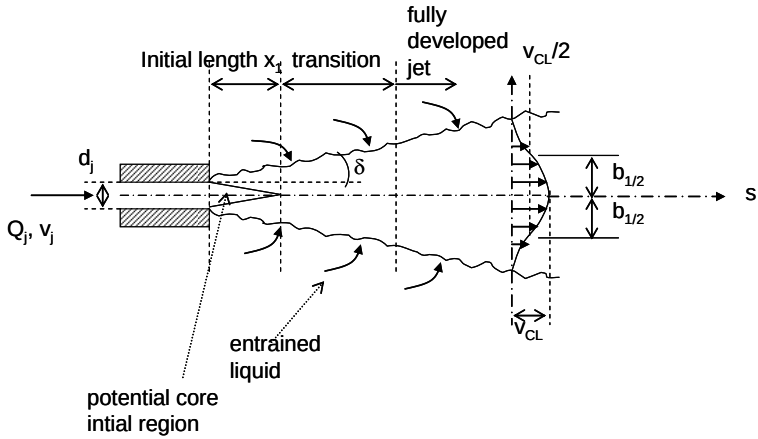

Figure 2.1 Jet flow behaviour according to Blevins (1984)

Extensive research work about the behaviour of turbulent jets has been done among others as by Rajaratnam (1976), Abramovich (1963), and Fischer et al. (1979).

2.1.2 Equations of motion

For axisymmetric flow at constant pressure, the momentum equation becomes (in polar coordinates):

$$u\frac{\partial u}{\partial s}+v\frac{\partial u}{\partial r}=-\frac{1}{r}\frac{\partial}{\partial r}\left(\nu\, r\frac{\partial u}{\partial r}-r\,\overline{u'v'}\right) \qquad (Eq.\ 2.7)$$

with

ν: kinetic viscosity

$\overline{u'v'}$: turbulent shear stress

and the continuity equation is written as (in polar coordinates):

$$\frac{\partial u}{\partial s}+\frac{1}{r}\frac{\partial rv}{\partial r}=0 \qquad (Eq.\ 2.8)$$

2.1.3 Axisymmetric round jets

2.1.3.1 Centreline jet velocity

In the fully developed region of the jet the centreline jet velocity v_{CL} continuously decreases with the distance *s* from the jet in the direction of jet flow. According to Jirka (2004) the following equations are applicable for turbulent axisymmetric round jets with the turbulent Schmidt Number λ_S = 1.20, assuming discharge in *s*-direction (analytical solutions):

$$v_{CL}(s)=\frac{1}{\sqrt{2\pi}\alpha_{jet}}\cdot\frac{\sqrt{M_j}}{s}\approx 6.43\frac{v_j d_j}{s} \qquad (Eq.\ 2.9)$$

v_{CL}: centreline velocity at distance *s* from nozzle

α_{jet}: a constant (α_{jet} = 0.055)

$$\lambda_s = \frac{\upsilon}{D} = \frac{viscous\ \ diffusion\ \ rate}{molecular\ (mass)\ diffusion\ rate} \qquad (Eq.\ 2.10)$$

Other authors found the centreline velocity at distance *s* from the nozzle as:

$$v_{CL}(s) = C_1 \frac{v_j \cdot d_j}{s} \qquad (Eq.\ 2.11)$$

where the constant C_1 varies between 5.75 and 7.32, depending on the author (Table 2.1).

Author	C_1
Goertler (1926, cited in Rajaratnam 1976)	*5.75*
Revill (1992)	*6*
Abramovich (1963, cited in Rajaratnam 1976)	*7.32*
Albertson et al. (1950, cited in Rajaratnam 1976)	*6.2*
Davies (1972, cited in Wasewar 2006)	*6.4*
Rajaratnam (1976)	*6.3*
Blevins (1984)	*6*
Schlichting (1968)	*7.31*

Table 2.1 The centreline jet velocity parameter C_1 according to different authors.

Revill (1992) writes that the mixing effect of a turbulent jet is generally considered insignificant after about 400 jet diameters.

2.1.3.2 Jet width and velocity at transverse distance

As the jet enters the bulk liquid it entrains fluid and expands. Jet expansion angle δ is difficult to measure; however, it is reported in the literature as varying between 15° and 25° for jet Reynolds numbers Re_j > 100 (Wasewar 2006).

The jet half-width $b_{1/2}$, defined as the transverse distance r for axial velocity *v(r)* to fall to one-half the centreline value, v_{CL}, is expressed by the following general equation:

$$b_{1/2} = C_2 s \qquad (Eq.\ 2.12)$$

where

$$v\left(r = b_{1/2}\right) = \frac{v_{CL}}{2} \cdot C_2 \qquad (Eq.\ 2.13)$$

and varies from author to author (Table 2.2).

Assuming a Gaussian distribution over jet width, the velocity in *s* direction at transverse distance *r* from the centreline can be written as

$$v(r) = v_{CL} \cdot e^{-C_3\left(r^2/s^2\right)} \qquad \text{(Eq. 2.14)}$$

Since at transverse distance $r = b_{1/2}$ the velocity in *s* direction amounts to one-half of the centreline velocity ($v(r = b_{1/2})/v_{CL} = 0.5 = e^{-0.7}$), C_3 can be expressed as a function of C_2, namely

$$C_3\left(r = b_{1/2}\right) = \frac{0.7}{C_2^{\,2}} \qquad \text{(Eq. 2.15)}$$

Assuming a Gaussian distribution of the transverse velocity, Table 2.2 summarizes the values of C_2 and the corresponding value of C_3.

Author	C_2	C_3
Tollmien (1926, cited in Rajaratnam 1976)	*0.082*	*104.1*
Corrsin (1946, cited in Rajaratnam 1976)	*0.084*	*99.2*
Abramovich (1963, cited in Rajaratnam 1976)	*0.097*	*74.4*
Albertson et al. (1950, cited in Rajaratnam 1976)	*0.0965*	*74.4*
Hinze and Zijnen (1949, cited in Rajaratnam 1976)	*0.094*	*70*
Rajaratnam (1976)	*0.1*	*79.2*
Blevins (1984)	*0.086*	*94*
Schlichting (1968)	*0.085*	*94*

Table 2.2 *The jet width parameters C_2 and C_3 according to different authors assuming that at jet width $b_{1/2}$ the velocity in s directionis equal to one-half of the centerline velocity.*

According to Jirka (2004) is $b_{0.37}$ the measure of the jet width where the excess velocity is defined in Eq. 2.16.

$$v(b_{0.37}) = e^{-1} \cdot v_{CL} = 0.37 \cdot v_{CL} \qquad \text{(Eq. 2.16)}$$

$$b_{0.37} = C_{2,0.37} s = 2\alpha_{jet} s = \sqrt{2}\sigma \qquad \text{(Eq. 2.17)}$$

$$C_{2,0.37} = 2\alpha_{jet} = 0.11 \qquad \text{(Eq. 2.18)}$$

$$\sigma = \sqrt{2}\alpha_{jet} s = 0.077 \cdot s \qquad (Eq.\ 2.19)$$

Jirka also assumes a Gaussian distribution over the jet width and expresses the velocity v(r) in s direction at transverse distance r from the centreline as follows:

$$v(r) = v_{CL} \cdot e^{-\left(r^2 / b_{0.37}^2\right)} \qquad (Eq.\ 2.20)$$

Bearing in mind that in Jirka's assumptions $b_{0.37}$ ($b_{0.37} = r(v = 0.37 v_{CL})$) is not the same length as in the formerly mentioned studies (where $b_{1/2} = r(v = 0.5 v_{CL})$), the value of $C_{3,0.37} = 1/C_{2,0.37}^2$ according to Jirka (2004) becomes 82.6.

According to Jirka (2004) the transverse distance σ (standard deviation) for relative velocity $v(r)$ falls to ~61 % of the centreline value v_{CL}.

$$\frac{v(\sigma)}{v_{CL}} = e^{-C_{3,0.37}\left(\frac{\sigma^2}{s^2}\right)} = e^{-C_{3,0.37}\left(2\alpha_{jet}^2\right)} \qquad (Eq.\ 2.21)$$

2.1.3.3 Volume flux due to entrainment

With larger distance from the nozzle, the total volume flux $Q(s)$ at distance s from nozzle increases due to the lateral entrainment. The volumetric flow rate of the bulk liquid entrained by the jet Q_e is difficult to measure and the available experimental data are widely scattered. Jirka (2004) describes the volume flux as a function of the square root of the momentum at the nozzle, and Blevins (1984) writes a simple expression with the discharge flow rate at the nozzle and the nozzle diameter. Developing the expression of Jirka (2004), it agrees with Blevins (1984). However, according to Donald and Singer (1959) the total volumetric flow rate in the jets is a function of the same parameters additionally multiplied by the kinematic viscosity at power 0.1333.

Jirka (2004): $$Q(s) = \sqrt{2\pi} \cdot 2\alpha_{jet} \cdot \sqrt{M_j}\, s = 4\sqrt{2}\alpha_{jet} \cdot \frac{s}{d_j} Q_j \qquad (Eq.\ 2.22)$$

Blevins (1984): $$Q(s) = 0.32 \frac{s}{d_j} Q_j \qquad (Eq.\ 2.23)$$

Donald and Singer (1959): $$Q(s) = Q_j \left(\frac{0.576 \cdot \nu^{0.133} s}{d_j} \right) \qquad (Eq.\ 2.24)$$

where ν is the kinematic viscosity of the system under consideration.

The liquid entrained per unit time at the distance s from the nozzle, Q_e, was early described by Folsom and Ferguson (1949, cited in Wasewar 2006) and confirmed by McCabe et al. (2005) as follows:

$$Q_e = \left(0.234 \cdot \frac{s}{d_j} - 1 \right) Q_j \qquad (Eq.\ 2.25)$$

2.2 Jet mixing in vessels

In jet mixers, a fast moving jet stream of liquid is injected into a slow moving or stationary bulk liquid. The relative velocity between the jet and the bulk liquid creates a turbulent mixing

layer at the jet boundary. This mixing layer grows in the direction of the jet flow, entraining and mixing the jet liquid with the bulk liquid. As a result, the jet grows in diameter but its centreline velocity and the turbulence of jet reduce in magnitude because the jet flow momentum is spread over a steadily increasing flow area. In addition to entrainment, strong shear stresses exist at the boundary between the jet and the surrounding liquid. These stresses tear off eddies at the boundary and generate considerable turbulence, which also contributes to the mixing action. Furthermore, a circulation pattern is created within the tank, which also causes mixing (Patwardhan and Gaikwad 2003). The flow pattern created by a jet can be described as follows (Revill 1992):

1. Rollover of the jet flow when it hits the wall or bottom of the tank or the liquid surface.
2. After rollover, a very weak liquid motion driven by the jet flow along the wall or bottom of the tank or the liquid surface.
3. Liquid flow induced by jet entrainment from remote regions towards the jet.

There have been many extensive studies on jet mixing over 60 years. The early work in this area was done by Fosset and Prosser (1949) and Fossett (1951) who reported performance figures of free jets for mixing fluids in large circular tanks, the studies having been conducted for the war-time purpose of utilizing existing underground storage tanks for blending aviation petrol. Fossett and Prosser (1949) and Fossett (1951) used laboratory scale models to study an inclined side-entry jet of tetraethyl lead into high octane fuel in large scale tanks up to 40 *m* in diameter. Their proposed simple correlation for the mixing time was a function of the tank and jet diameter and the jet velocity. The jet Reynolds number (based on jet velocity and diameter) covered in the study was between 4'500 and 80'000 although no explicit dependence on Reynolds number was included in the correlation.

Wasewar (2006) gives a critical analysis of the available literature data and some general conclusions concerning the various parameters.

Most of the studies have been conducted in vertical cylindrical tanks with flat bottoms, with a liquid height/tank diameter ratio between 0.2 and 1. Lane and Rice (1982) performed investigations in a vertical cylinder with hemispherical base. Jayanti (2001) found with the help of numerical simulations that a conical tank base is best in respect of mixing. Stefan and Gu (1992) observed in their destratification experiments that both the shape of a tank and the relative location of diffuser and intake affect the mixing processes. A prismatic tank is more rapidly mixed than a nonprismatic one when the diffuser is located at the bottom. The inversion of diffuser and intake location does not change the mixing characteristics in the prismatic tank, but in a parabolic tank, mixing occurs faster with the diffuser located near the surface rather than near the bottom. Perona et al. (1998) used an elongated horizontal cylindrical tank (3 m in diameter and 12 m in length). There are several studies about jet mixing in elongated containers (e.g. Perona et al. 1998, Zughbi 2006), but none suitable to study the circulation in the far field.

All of the authors aimed a minimum of mixing time and investigated the following parameters.

2.2.1 Tank dimensions (height and diameter)

Mixing was reported to be either directly proportional to the tank height (Grenville and Tilton 1997, cited in Wasewar 2006) or to the square root of the tank height (Fox and Gex 1956, Lane

and Rice 1982). With increase in height of the tank, mixing time increases with other parameters remaining the same.

From most of the experimental studies it follows that mixing time increases with the increase of the tank diameter for a constant set of the other parameters. Some authors find that the mixing time is proportional to the tank diameter (Fox and Gex 1956, Lane and Rice 1982), others proportional to the square of the tank diameter (Fosset 1951, Grenville and Tilton 1997, cited in Wasewar 2006).

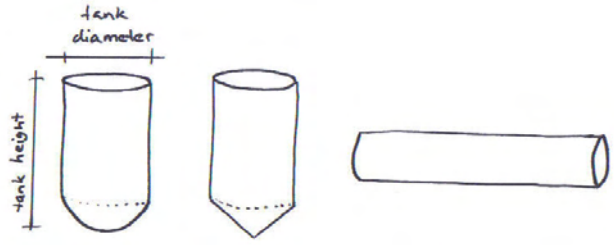

Figure 2.2 *from left to right: vertical cylindrical tank with hemispherical base and with conical base, elongated horizontal cylindrical tank.*

2.2.2 Jet velocity

Mixing time was found to decrease with increase in velocity and vice versa, when all other parameters are kept constant.

Fossett and Prosser (1949) proposed a condition for a big enough jet velocity in order to guarantee good mixing:

$$v_j \geq \sqrt{\frac{2gh}{\sin\theta}} \qquad \text{(Eq. 2.26)}$$

where h is the liquid height in the vessel and θ the jet angle to the horizontal. According to the authors this condition is valid for fluids of equal densities.

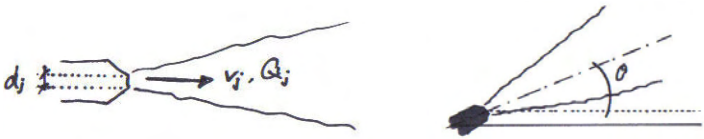

a) *b)*

Figure 2.3 *a) jet characteristics: jet nozzle diameter d_j, jet velocity v_j, jet discharge Q_j; b) jet angle θ*

2.2.3 Jet diameter

Coldrey (1978) found that under constant tank dimensions and at constant jet flow rate Q_j, mixing time is directly proportional to the jet diameter, which means that with increasing jet diameter, mixing time is increasing as well. After investigation of data of Perona et al. (1998) it is found that for the same flow rate, an increase in jet diameter will increase mixing time. From

the experimental results of Patwardhan and Gaikwad (2003) at the same power consumption level, an increase in diameter will lead to a decrease in mixing time. As the nozzle diameter increases, the flow rate as well as the momentum flux through the nozzle increase for the same level of power consumption. Based on the results of Fox and Gex (1956) it was postulated that a large-diameter low-velocity jet would require less power than a small-diameter high-velocity jet.

2.2.4 Jet momentum flux

In the mixing time correlations of Fossett and Prosser (1949) and Fossett (1951), Fox and Gex (1956), Lane and Rice (1982) and Grenville and Tilton (1997, cited in Wasewar 2006) the product of the jet velocity and the jet diameter appears as a package, and the mixing time is inversely proportional to this product with an exponent *n*. According to Fossett and Prosser (1949), Fossett (1951) and Grenville and Tilton (1997, cited in Wasewar 2006), *n* is equal to unity, whereas according to Fox and Gex (1956) and Lane and Rice (1982), n amounts to two third. Thus, even if not all of them associate apparently their correlations of mixing time with the momentum flux, through the squared product of the jet velocity and the jet diameter there is dependence expressed. Fox and Gex (1956) reported that mixing time could be correlated in terms of the momentum flux added to the tank in the laminar and turbulent regime. Stefan and Gu (1992) found that low momentum jets are more energy-efficient than high momentum jets. Ranade (1996) found that the mixing time was directly correlated to the Reynolds number and the jet momentum.

2.2.5 Jet location

Mewes and Renz (1991, cited in Wasewar 2006) and Perona et al. (1998) found that the position of the nozzle is one of the parameters affecting the mixing process. Maruyama et al. (1982, 1984) and Maruyama (1986) did extensive experiments to find the optimum location of the nozzle in the circulation regime, defined by the authors as Re > 30'000. Optimum nozzle depth varies in function of the relationship of the tank diameter to the tank height. Stefan and Gu (1992) found that both the shape of a tank and the relative location of the diffuser affect the mixing processes. Perona et al. (1998) found that in the elongated horizontal cylindrical tank (3 *m* in diameter and 12 *m* in length) the nozzle location in the centre of the tank and with horizontal direction is less effective than the location at ¼ tank length from the end of the tank. Zughbi (2006) concluded after a re-analysis of the horizontal cylinder of Perona et al. (1998) with the help of CFD simulations that the jet location is very important in determining the blending time.

2.2.6 Jet angle

Most commonly a single or multiple jets are located near the tank bottom, oriented at an angle to the vertical direction; some studies however have vertical jets (e.g. Fox and Gex 1956). According to Maruyama et al. (1982, 1984) and Maruyama (1986) the mixing time depends strongly on the jet angle, where the small angles up to 30° (wall jet excluded) and 75° provide a minimum of mixing time. As according to Maruyama et al. (1982) the mixing time is inversely proportional to the jet axis length, they state that the mixing time can be reduced by giving an angle to the jet which makes the jet axis length longer. Maruyama et al. (1982) conclude from their experiments that when the liquid depth is small, a horizontal or inclined jet is preferable to the vertical one. Patwardhan and Gaikwad (2003) reported that inclined jets at

the bottom give better mixing times. They found that horizontal jets give larger mixing times than inclined jets at the bottom, and an angle of 45° gives lesser mixing times than angles of 30° and 60°. Maruyama et al. (1982) as well as Grenville and Tilton (1997, cited in Wasewar 2006) point out the effect of the jet evolution from a circular jet into a wall jet. They found that mixing time was significantly increasing when the angle of injection was not adequate to exclude the wall effect. Maruyama et al. (1982) cite Davis and Winarto telling that the spreading rate of the jet is 8.5 times greater parallel to the wall than perpendicular to the wall. Therefore, the wall jet spreads widely along the wall, inducing circulations which consist mainly of vertical two-dimensional loops and thus reducing the mixing effect. Furthermore Patwardhan and Gaikwad (2003) point out that the jet flow along the tank bottom and the jet impingement on the wall opposite caused jet energy dissipate locally. The energy available for mixing within the rest of the tank then becomes small. Grenville and Tilton (1997, cited in Wasewar 2006) suggest that a cone which is concentric to the jet and of a vertical angle of approximately 15° should not contact the tank wall until the termination of the jet, i.e. hitting a tank wall or the liquid surface. Patwardhan and Gaikwad (2003) suggest for the same reason a higher angle of 30° and more. Revill (1992) concludes from the results of other authors that single axial jets should only be used in a certain range of the tank height/tank diameter ratio (0.75 to 3.0). The same he says for single side-entry jets (0.25 to 1.5). In case the jet is injected at an angle at the edge of the base Zughbi and Rakib (2004) found that the optimum angle appears to be 30° for the vessel geometry of Lane and Rice (1982). They conclude, however, that this optimum angle is not universal and varies with the location of the jet inlet.

Stefan and Gu (1992) found that destratification by a vertical jet is slightly more efficient than by a horizontal jet. The difference in mixing effects is small in the case of low jet density Froude numbers, but may be much larger in the case of high jet density Froude numbers.

2.2.7 Jet length

Coldrey (1978, cited in Wasewar 2006) suggested the use of the longest possible jet length (i.e. a jet which is directed towards the farthest corner of the vessel) which would produce more effective mixing and consequently reduced mixing time. Assuming that mixing time is inversely proportional to the amount of liquid entrained by the jet, an equation was proposed for mixing time. Coldrey formulated a mixing time equation independent of the jet Reynolds number for the turbulent jet regime. Lane and Rice (1982) confirmed these findings by their experiments. Grenville and Tilton (1996) refer to the jet path length too. Their correlation is based on a model that assumes that the mixing rate at the end of the jet's free path, estimated from the turbulent kinetic energy dissipation rate, controls the mixing rate for the whole vessel. The correlation reported by Grenville and Tilton (1997, cited in Wasewar 2006) indicates that mixing time is inversely proportional to the jet path length. The dimensionless mixing time used by Maruyama et al. (1982) comprises the dependence of the jet pathlength. Perona et al. (1998) used the same principle as Maruyama et al. (1981) to express the dimensionless circulation time in dependence of the jet path length. Patwardhan and Gaikwad (2003) prefer a longer jet path in order to provide an entrainment of the surrounding liquid to a larger extent. Patwardhan and Thatte (2004) conclude from their work that the definition of the jet length as the distance between the jet entry and the point where the jet would hit the wall of the tank on the opposite side is very crude, as it can happen that the jet may lose much of its momentum before it hits the opposite wall. According to them this would lead to an over-estimation of the

jet path length. They propose to consider the point along the axis on the jet where the centre line velocity reaches a certain fraction (1 to 5 %) of the velocity at the nozzle. They refer to the analogy of the estimation of boundary layer thickness, in which the thickness is considered to be the distance from the surface for flow velocity to achieve 95 or 99 % of the free stream velocity. They observed that mixing time decreases with an increase in the nozzle clearance (which is according to them comparable to the active jet length). Revill (1992) states that the centreline velocity of a jet falls to about 5 % of the initial values after an axial distance of 100 jet diameters. He emphasizes that after about 400 jet diameters the velocities have become so low that the mixing effect of the jet is insignificant at more remote positions.

Zughbi and Rakib (2004) show from their experiment that for a given geometric arrangement, the angle of injection is significantly more important in determining the time required for mixing than the length of the jet.

2.2.8 Multiple jets

There are few experiments investigating the influence of multiple jets. Fosset (1951) mentioned better mixing times using multiple jets, but no experimental results were reported. Perona et al. (1998) found that for a double jet of the same diameter and location mixing time was not significantly different from those of the single jet at the same flow rate. Simon and Fonade (1993) found that in biochemical applications alternating jets perform better than steady jets. Revill (1992) proposes that more than one jet need only be used in large-diameter, shallow tanks or in tall, small-diameter tanks.

2.2.9 Jet Reynolds number

Fox and Gex (1956) found that mixing time is a strong function of the jet Reynolds number in the laminar regime and a weak function in the turbulent regime. Maruyama et al. (1982) observed that mixing time was independent of the Reynolds number when $Re_j \geq 30'000$. This value of the lower bound of Re_j was found to coincide with that associated with a free jet, i.e. $Re_j \geq 25'000$, where the entrainment rate of a free jet becomes independent of Re_j according to Ricou and Spalding (1961). The above mentioned authors didn't study the influence of the viscosity. Orfaniotis et al. (1996, cited in Wasewar 2006)) reported that mixing time increases with viscosity. Ranade (1996) found that the mixing time was directly correlated to the Reynolds number or the momentum of the jet. Perona et al. (1998) reported a dependence of the mixing time on the Reynolds number. Based on their results Okita and Oyama (1963, cited in Maruyama 1982) concluded that, in the turbulent jet regime (above a jet Reynolds number of 5'000), mixing time is independent of jet Reynolds number. Lane and Rice (1982) observed that the mixing time t_m was strongly dependent on the jet Reynolds number in the laminar regime (below $Re_j = 2000$, $t_m \propto Re_j^{-1.333}$) and only marginally dependent on Reynolds number in the turbulent regime ($t_m \propto Re_j^{-0.166}$)). They explain the dependence on the jet Reynolds number in the turbulent regime by observing that the recirculation in the bulk of the tank still exhibits laminar-like flow.

2.2.10 Froude number

Stefan and Gu (1992) reported from laboratory experiments that with their destratification system using jets, mixing depends on the densimetric jet Froude number (Eq. 2.4).

Revill (1992), Fox and Gex (1956) and Lane and Rice (1982) express mixing time as a function of the jet Froude number.

2.2.11 Turbulent transfer by eddy motion

Grenville and Tilton (1996) correlated the mixing time with the theory of Corrsin (1964, cited in Grenville and Tilton 1996), where for low viscosity fluids the mixing time was expressed by means of the integral scale of the concentration fluctuations L_{cf} and the turbulent kinetic energy dissipation rate ε.

$$t_m = 2\left(\frac{L_{cf}^{\,2}}{\varepsilon}\right)^{1/3} \qquad (Eq.\ 2.27)$$

$$\varepsilon(s) \propto \frac{v_{CL}(s)^3}{d(s)} \qquad (Eq.\ 2.28)$$

where $d(s)$ and $v_{CL}(s)$ are the jet diameter and centreline jet velocity at distance s, respectively.

The best fit with their experimental data was obtained taking the conditions in the far region from the jet nozzle at the end of the free jet path, where the velocities and turbulence intensity are much lower. It is apparent that the correlation is based on a physical model; the mixing rates at the end of the jets free path, estimated from local turbulent kinetic energy dissipation rate at the end of the jet, controls the mixing rate for the whole vessel.

According to Lehrer (1981) mixing time is inversely proportional to the entrainment ratio which is an expression of the turbulent transfer by eddy motion. The entrainment ratio is defined by the mass flowrate of the jet in the established region divided by the mass flow rate of the injected stream. In other words, Lehrer formulated a model in which lateral transfer of momentum was considered to be due to eddy diffusion. The eddy viscosity was assumed to be the product of the nozzle Reynolds number and the molecular viscosity.

2.2.12 Residence time

Stefan and Gu (1992) used for their correlation a dimensionless time t^* defined by the real time divided by the residence time $\tau_m = V/Q_j$, where V is the tank volume and Q_j is the jet discharge rate (at the nozzle).

2.2.13 Circulation time

The dimensionless mean circulation time used by Maruyama et al. (1982) is normalized by the mean residence time and the ratio d_j/L_{axial} (d_j: nozzle diameter, L_{axial}: axial jet length), i.e. $(t_c/t_m)/(d_j/L_{axial})$. The mean circulation time t_c is a function of the liquid volume in the tank and the flow rate of the jet at its termination point (point where the jet axis collides with the inner wall of the tank or intersects the liquid surface): $t_c = V/Q_{j,termination\ point}$.

Grenville and Tilton (1997, cited in Wasewar 2006) observed that the mixing time was proportional to the circulation time (estimated form the volume of liquid in the tank and flow rate entrained by the jet).

2.2.14 Flow pattern

Ranade (1996), Zughbi and Rakib (2004), Jayanti (2001), Patwardhan (2002) and Zughbi and Ahmad (2005) as well as Zughbi (2006) all highlight the importance of flow patterns on mixing. Jayanti (2001) identified the dead zones by studying the flow patterns. By proposing a conical vessel bottom instead of a flat one, he was able to eliminate these zones and to reduce the mixing time.

2.2.15 Computational Fluid Dynamics (CFD)

Patwardhan (2002) states that until 2002 there have been only a few CFD investigations of the jet mixing process. Brooker (1993 cited by Patwardhan 2002) studied the performance of a jet mixer using CFD. It was found that the CFD model predicted mixing time with a maximum error of about 15 % when compared with experimental studies. However, the model validation consisted of a comparison of only overall mixing time and was restricted to one nozzle geometry and one location of the probe.

Hoffman (1996, cited by Patwardhan 2002) carried out CFD simulations of the mixing process in a large storage tank using jets (commercial computational fluid dynamic code FLUENT). These simulations were carried out for only one half of the tank and the total number of nodes was 24'360. The CFD model was not validated by comparison with the experimental measurements.

Ranade (1996) investigated the flow patterns and mixing in jet mixed tanks equipped with alternating jets using CFD simulations (code FLUENT). The CFD simulations were carried out using a standard 'k–ε' model for turbulence and first order upwind method was used to reduce CPU requirements. The whole tank was simulated with 60,486 nodes.

Jayanti (2001) carried out CFD simulations of the jet mixing process in 2D as well as 3D using the commercial code CFX. The overall mixing time predicted with CFD simulations was compared with those estimated from correlations. Jayanti validated his work by comparing the calculated velocity profile of a turbulent jet at various distances downstream of the nozzle with the analytical results given in Schlichting (1968). It was observed that the calculated velocity profiles at various distances, after non-dimensionalisation, collapse to a single curve and that this curve agrees very well with the theoretical one. Jayanti shows that mixing occurs mainly by advection and that the overall mixing time is governed by what happens in the low-circulation zones which are very much geometry dependent. The mixing time is strongly affected by the circulation pattern, especially on whether there are low-velocity regions. The point of the investigation is therefore to find a vessel form favouring the mixing process. Jayanti was working in the turbulent regime (Re = 40'000).

Patwardhan (2002) developed a CFD model to predict the mixing behaviour in jet mixed tanks. The model predictions of mixing time and concentration profiles were compared with the experimental measurements over a wide range of jet velocities, nozzle angles and nozzle diameters. It was found that the CFD model predicts the overall mixing time well, but the predicted concentration profiles are not in good agreement with the experimental measurements. One of the main reasons for the discrepancy is identified by the author to be the underprediction of the eddy diffusivity levels.

Zughbi and Rakib (2004) show from their results in CFD that the mixing time depends on the flow patterns which in turn depends on the angle of the jet injection, and that the angle of the

jet injection is significantly more important in determining the time required for 95% mixing than the length of the jet. The mixing time does not change monotonically with the angle of injection. The optimum angle is not universal and varies with the location of the jet inlet. They found that using two jets instead of one results in a substantial decrease in the blending time. However, the extent of the gain is not 100% and is found to depend on the value of Reynolds number.

Zughbi and Ahmad (2005) showed by numerical simulations that the location of the pump-around suction point was found to have some effect on the mixing time, and it was optimized using CFD results.

Zughbi (2006) simulated numerically jet mixing in a tank identical to the one used by Perona et al. (1998). An unstructured tetrahedral mesh was used to discretize the computational domain. A comparison with the experimental results of Perona et al. (1998) shows a reasonable agreement over a jet Reynolds number range from 33'000 to 85'000. Zughbi shows by numerical simulation that mixing time in a large horizontal cylindrical tank is a function of the flow patterns generated inside the tank by the jet. Consequently, the jet location is very important in determining the blending time, not so much due to its length but mainly due to the patterns of flow it creates inside the tank.

2.2.16 Concluding remarks

A lot of research has been done in the field of jet mixing. The influence of the tank dimensions in cylindrical tanks, jet characteristics like the jet velocity, jet diameter and their product, jet Reynolds number, and jet Froude number, the jet location, jet angle and jet length, and multiple jets on mixing time has been reported. Some authors studied the influence of the residence time and circulation time on mixing time; others investigated the flow patterns in respect to mixing time.

There are, however, some important differences between the goals, conditions and requirements of the chemical industry and the ones of the present study:

1. Chemical engineers usually aim a homogenisation of mixtures in the whole container, whereas in the present study high concentration is required locally (in front of the water intake).
2. Due to the homogenisation aimed in the whole container, the container walls confine the circulation. In the present study the problem has on three sides an open space (the water volumes in the rear and both lateral parts of the lake), that does not confine any circulation.
3. The chemical engineering studies are mainly focused on the minimization of mixing time, where the complete mixing is accomplished as soon as homogenisation of the physical properties is achieved. In the sedimentation problem, the already established suspension needs to be maintained over a long time.
4. The fluid and its components are in most of the chemical engineering problems conserved. In the present study the water-sediment mixture evacuated by the water intake is replaced by clear water, and hence, the sediment fraction is continuously reduced.

None of the cited studies reports about a jet arrangement to the one investigated in the present study. Nevertheless, the importance of the jet position, the jet diameter and velocity as well as

the residence time seems evident for every jet mixing case. The circular jet arrangement as it is presented in chapter 4 induces a flow pattern with a vertical jet similar like an impeller. Thus, this jet as it is induced from the unity of the four horizontally arranged jets needs to be regarded as such and the aforementioned characteristics might be applied for it as well.

The densimetric jet Froude number becomes relevant for high concentrations or high particle densities, respectively. The significance of the jet Reynolds number increases with higher fluid viscosity.

Time needed to reach steady state has not been reported as a subject of the studies.

2.3 Solid suspension in impeller stirred vessels

2.3.1 General

Since the pioneering work of Zwietering (1958) in the late 1950s, numerous empirical and semi-empirical investigations on solid suspension in stirred vessels have been reported in literature. Sharma and Shaikh (2003) also carried out suspension experiments with particulate solids in stirred tanks employing Pitched Blade Turbines (PBT) with four and six blades as the impellers in cylindrical glass vessels having flat bottoms with round corners and fitted with four standard baffles. They identified the main factors needed to reassembly the results obtained in many former studies. The main findings important for the present study are described hereafter.

Suspension by mixed flow turbines, like other agitators, in general takes place at the corners of the tank base. This is because the centrifugal action drives the particles to the corners where from they are ultimately suspended. The particles, travelling towards the corner, hit the wall, lose momentum and get trapped in the stagnant zone at the corner junction forming a kind of fillet through the deposition of the particles giving a rounding effect to the straight junction. This may be termed as self-filleting of the corners.

Thus, the most critical place for the suspension is the tank base and the ease or difficulty of suspension from it depends on the type of flow pattern that the agitator generates. Sharma and Shaikh (2003) confirmed from the results of Armenante and Nagamine (1998) showing that the flow pattern from an axial flow impeller is conducive to easier suspension in comparison to the flow pattern produced by a radial flow impeller (Figure 2.4). The suspension efficiency of the mixed-flow impellers remains in between.

2.3.2 Effect of off-bottom clearance

There are two zones at the tank base where weakly recirculated induced loops occur, one just below the impeller and the other at the junction of the tank base and wall. For the case of an axial impeller operating close to the tank base, the efficiency of energy transfer from impeller to particles is highest. The particulate mass trapped in the stagnant zone below the impeller is, therefore, easily driven to the corners with enough velocity to get suspended after sliding over the fillet. If the off-bottom clearance C/D_{tank} (C: clearance, D_{tank}: tank diameter) of the impeller is increased, the induced secondary loop (almost stagnant) below the impeller increases and gets wider, more particles are caught in it, and because of higher position of the impeller, less energy is imparted to them. As a consequence, higher speed of impeller rotation would be needed to force the higher amount of trapped particles out from this region and to drive them

towards the tank corner from where they may be suspended, if not, then still higher impeller speeds for ultimate suspension may be needed.

The flow, generated by a radial flow impeller (Figure 2.4), on reaching the tank base, would sweep the particles towards its central region, which is partly covered by an induced secondary loop. This is a very inconvenient situation for suspension. It is more difficult to lift the particles from the centre than to drive them towards the corners where from they are picked up. Sharma and Shaikh (2003) observed that at sufficiently higher position ($C/D_{tank} > 0.35$) PBTs' flow pattern changes from axial to radial. Particles are now caught in an inverted spinning vortex below the impeller just like a tornado touching the ground. A few particles at the vertex of the conical heap are lifted up apparently under the influence of the vortex while a few more particles at the circular periphery of the conical heap at the tank bottom are thrown by centrifugal force towards the corners and at high speeds are lifted before reaching there. When the particles strike the tank base later, they are again swept towards the centre. Sharma and Shaikh suppose that the hydrodynamics in which the central heap of particles are caught is possibly a combination of two phase forced and free vortex.

2.3.3 Effect of impeller diameter

Sharma and Shaikh (2003) found that for a given physical system, the critical speed of suspension decreases with increasing impeller size at constant tank diameter and increases with increasing tank diameter at constant impeller size. The relationships are not the same. For a given tank size, critical speed varies as $D_{impeller}^{-2}$ ($D_{impeller}$: impeller diameter). For a given impeller size critical speed varies as $D_{tank}^{1.15}$.

Axial Mixing Flow	*Radial Mixing Flow*
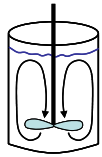	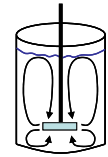
The fluid is parallel to an axis of rotation. It moves media from the top to the bottom. Axial flow impellers impose essentially bulk motion and are used for homogenization processes, in which it is important to increase fluid volumetric flow rate, for blending, solids suspension, solids incorporation, or draw down. It is most common in a low viscosity, high speed application. The most common impeller style is the propeller.	*The fluid is discharged radially outward to the vessel wall. Compared to axial flow impellers, radial flow impellers provide higher shear and turbulence levels with lower pumping. Radial flow draws the media from the top and bottom. They are used for liquid dispersion for low to medium viscosity fluids and high speed. The most common impeller styles are the straight blade and crossed blade.*

Figure 2.4 Axial and radial impeller type and their typical flow pattern

2.3.4 Concluding remarks

In the present study aiming maintaining the sediment in suspension axial mixer-like flow patterns are preferable to radial ones. This is due to the fact that in radial flow patterns the sediment has tendency to be thrown to the bottom and to be trapped below the impeller from where it is difficult to be released again. Off-bottom clearance is strongly influencing the flow pattern.

The impeller diameter in relation to the tank diameter has an influence on the critical impeller speed of suspension.

2.4 Air-bubbler systems and mechanical mixers in lakes

2.4.1 General

Mixing in large water volumes such as lakes has been subject of the development of lake remediation methods. Examples are air-bubbler systems and mechanical mixers.

There are various reasons for lake remediation:

1. Removal of polluted water from a locally limited patch, such as a coastal margin, by horizontal flushing (Morillo et al. 2009).
2. Cold water pollution (due to stratification) downstream of a reservoir when the cold water is released through the water intake (Australia). Cold water pollution decreases aquatic respiration and invertebrate productivity, and all biological metabolic processes in aquatic habitats slow down as temperature decreases (Sherman 2000).
3. Decrease of oxygen in the water column due to stratification. Dissolved oxygen is essential to the metabolism of all aquatic organisms that possess aerobic respiratory biochemistry, and it also affects the solubility of many inorganic compounds. Circulation and mixing in a reservoir is significantly decreased with the buildup of stratification, resulting in a lack of transport of oxygen from the relatively rich surface zones to the hypolimnion. However, bacterial consumption of oxygen continues, and since replenishment from the epilimnion is absent, the overall oxygen content of the hypolimnion may decrease rapidly, resulting in anoxic subsurface conditions with associated water-quality problems (Stephens and Imberger 1993).

Many methods have been proposed to remediate reservoirs. The three aforementioned motivations for lake remediation all are related to lake stratification. Therefore it seems obvious that traditionally, in-lake remediation methods have focused on enhancing vertical mixing.

2.4.2 Air-bubbler system

The mostly reported in the literature is the air-bubbler system, which involves injecting compressed air into the water body from a perforated pipe or diffuser located at the base of the reservoir. A short distance from the nozzle, the gas jet collapses into a series of bubbles which rise vertically. The bubbles entrain some of the surrounding liquid and carry it with them producing a buoyant turbulent plume of fluid above the aerator agitating the water column. Since the hydrostatic pressure of liquid increases with depth the bubbles expand as they rise and their buoyancy increases. Upon reaching the surface, the bubbles break, releasing their gas,

and the upwelling current spreads horizontally across the surface (Blevins 1984). Large volumes of water can generally be circulated for relatively low cost by using an unconfined system of this nature (Stephens and Imberger 1993). Bubble plumes in homogeneous and stratified ambient fluids have intensively been studied and reported in the literature.

Previous work, which mainly concentrated on plumes in homogeneous water, has revealed various characteristics of the flow: a Gaussian radial distribution of plume velocity and bubbles, the similarity of the radial profiles at different distances from the source, and the entrainment of surrounding water. There are similarities between a turbulent single-phase buoyant plume and a bubble plume. Both are driven by buoyancy and spread by the engulfing of quiescent environment fluid by turbulent eddies. It is reasonable to expect similar behavior in the two types of plume in the region where the flow is established, although there cannot be an exact analogy (Leitch and Baines 1989).

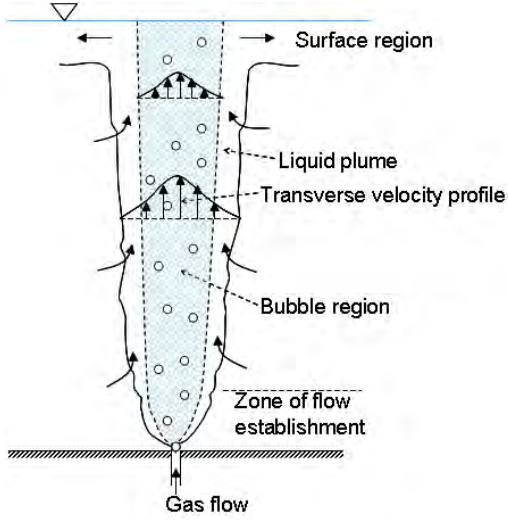

Figure 2.5 Schematic diagram of a bubble plume according to Leitch and Baines (1989).

Stephens and Imberger (1993) give a broad overview on the scientific work done by various authors in laboratory and field experiments. Satisfactory remediation results using an air-bubbler system were also reported for Lake Hallwil and Baldeggersee, Switzerland (Scheidegger et al. 1994 resp. Wüest et al. 1992).

2.4.3 Mechanical mixers

Mechanical mixers have also been studied in the context of destratification. If surface impellers are used, the researchers mainly make benefit from the vertical momentum inducing a simple vertical jet composed of surrounding water. Such unconfined jets propagate away from the impeller and entrain surrounding water as they descend.

In Lake Texoma Robinson et al. (1982) mounted an axial flow impeller with diameter 2.44 *m* on a floating support platform directly above the intake structure. The pumping rate was

calculated to be 4.06 m^3/s, and the velocity was 0.87 m/s, while the release rates through the intake were between 1.4 and 16.8 m^3/s. Situated 1.7 m below the water surface the impeller pumped high quality epilimnion water down to the outlet without destratifying the lake as a whole.

Busnaina et al. (1981) designed a three-dimensional mathematical model to predict the locally released water quality (degree of mixing) and jet penetration depth and to show the influence of the design parameters (densimetric Froude number, metalimnion location, propeller flow rate relative to the release flow rate, and propeller diameter and propeller depth below the surface) on the flow field. Robinson et al. (1982) and Busnaina et al. (1981) found in their destratification experiments with mechanical mixers a non-linear relationship between the release rate, Q_{out}, and the released temperature, T, when pumping with impellers.

Stephens and Imberger (1993) conducted laboratory tests of a mechanical mixing system in a confined environment to examine the efficiency of energy conversion from mechanical energy to buoyancy flux as a function of impeller diameter, rotational speed and the degree and type (linear or two-layer) of stratification. They concluded from their results that a maximum efficiency of the order of 12 % compares favorably with the more conventional air-bubbler system. Moreover, for a specific impeller type, they found direct scaling parameters enabling results found in the laboratory to be applied to a prototype situation and constructed a simple design methodology for prototype versions of mechanical systems. The first two experimental series were conducted in a 1 m x 1 m x 0.8 m glass tank, while for the third series a 2 m x 2 m x 2 m tank was used. Impeller sizes consisted of diameters ranging from 64 to 300 mm.

Mobley et al. (1995) present construction details and operational results for the surface pumps used at Douglass Dam on the French Broad River in Tennessee. The system consisted of nine 4.6 m diameter stainless steel impellers with a design pump rate of 15 m^3/s. The pumps worked more effectively when located side by side so that the plumes combined and entrainment was reduced. Apparently the system has performed satisfactorily.

Sherman (2000) mentions the application of draft tubes confining the impeller induced jet and therefore preventing unwanted entrainment in destratification problems.

Morillo et al. (2009) approached the pollution problem by horizontal flushing: the vertical jet induced by an impeller entrained surface water downward to depth, where upon reaching neutral buoyancy it intruded horizontally into the lake proper. The employed impeller consisted of two 1.25 m blades, and operated with an associated volume flux of approximately 4 m^3/s.

2.4.4 Concluding remark

With the application of mechanical mixers in lakes, the possibility of big water volume mixing was successfully tested and the evacuated water had satisfactory temperature. Nevertheless, in none of the cited studies the influence of the mixer on destratification in its far field was reported and none of them provides mixer induced flow patterns. Neither time dependence nor the regime (transient or steady state) was an investigated issue. Sediment particles were not concerned.

2.5 Bubble plumes and vertical upward pointing jets

2.5.1 Generated recirculating flow

Riess and Fanneløp (1998) investigated the flow structure in the far field of line-source bubble plumes in shallow water, and Fanneløp et al. (1991) investigated the flow structure associated with both a line bubble plume and a plane vertical jet. Recirculation cells form on both sides of the plume (Figure 2.6). Fanneløp et al. (1991) report that large-scale applications of bubble plumes in the ocean at depths typical of offshore fields, are likely to produce recirculating cells rather than an unlimited horizontal current. Riess and Fanneløp (1998) are convinced that there is little reason to believe that bubble plumes and vertical jets of comparable mass and momentum fluxes will produce very different flow patterns.

Riess and Fanneløp (1998) assumed that the width and the maximum plume velocity at the water surface are useful scaling parameters for the flow in the far field. They considered the horizontal surface flow resulting from deflection of the upward directed flow at the free surface as being similar to a free turbulent plane jet. This neglects damping of turbulence fluctuations at the free surface, but according to the authors it is physically a better assumption than setting the fluctuations at the surface to zero. Assuming similarity in the averaged velocity distribution and the fluctuating quantities, the width of the jet grows linearly, and the centre velocity decreases in inverse proportion to the square root of the distance to the origin. In the case of shallow reservoirs the entraining surface jet generates a horizontal counterflow for continuity reason. A localized outflow from the cell, near the surface, near the bottom or in between, could not be detected. It appears that the excess mass flow produced by the jet was distributed over the whole end surface and not, as expected, localized near the free surface. It was found from the experiments, that far away from the plume the observed flow is no longer similar to a turbulent plane jet, which was an assumption of the model (Riess and Fanneløp 1998).

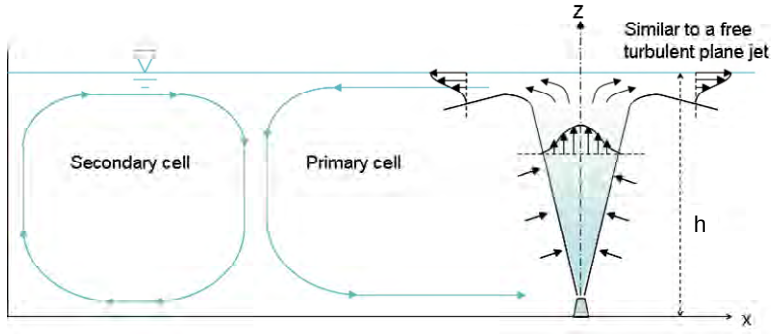

Figure 2.6 Plane jet geometry and recirculating cells according to Jirka and Harleman (1979).

The range of influence is the maximum distance from the plume or jet source, where the flow velocities can be clearly observed. Fanneløp et al. (1991) proposed observations of the free surface as a simple way to define the range of influence. The appearance of the surface is

rough (due to turbulence) in the recirculation region, but very smooth in the laminar flow outside.

In the following paragraphs various definitions of cell length as well as the relationship between cell length and water depth observed by different authors are discussed. Table 2.3 gives an overview in this regard.

Riess and Fanneløp (1998) cite varies authors reporting observed cell lengths between 2.5 and 7 times the water depth. They explain the differences in some cases with different definitions of the cell length and with the restricted length of the experimental setup. In a tank of limited length a very long recirculation zone cannot develop.

Fanneløp et al. (1991) observed that the outward flow from bubble plumes persists to almost 7 times the depth for the highest air flow rate investigated, whereas the cell length from vertical jets appears to be about 5 times the depth. Fanneløp et al. (1991) conclude that the length of the primary cell formed by bubble plumes is a weak function of the gas flow rate. Contrary to the observations made from bubble plumes, for the jet flow the cell length does not depend at all on volume flow rate. In the case of the vertical jet, the cell was asymmetric with the rotor core quite close to the jet (1.5 times the depth) in all cases investigated.

Author	*Definition of cell length*	*Cell length: value times depth*	*Experiments with*	*Remarks about dependencies*
Topham 1975, cited by Fanneløp et al. (1991)	*"Wave ring" and measurements of the velocities*	*0.5*	*Bubble plume*	
Goossens 1979	*Stagnation line of small pieces of paper*	*4 (model tests)* *7 (large-scale)*	*Bubble plume*	*Dep. on gas flow rate*
Jirka and Harleman 1979	*Location, where the depth of the surface current reached half the depth of the reservoir*	*2 to 2.5*	*Buoyant jets*	*Volumetric Froude number and relative depth*
Jirka 1982, cited by Fanneløp et al. (1991)	*?*	*?*	*Axisymmetric jets*	*Dep. on depth/jet-diameter ratio and on Froude number.*

Fanneløp et al. (1991)	*Observation of the surface appearance and velocity measurements*	*5 (jets)* *7 (bubble plumes)*	*Plane jets* *Bubble plume*	*Indep. of jet flow rate* *Weak function of gas flow rate, rotor core nearly indep. of volume rate*
Riess and Fanneløp (1998)	*Idem Fanneløp et al. (1991)*	*4 to 6*	*Bubble plumes*	*Dep. on depth/width ratio of experimental setup*

Table 2.3 Overview on observations regarding recirculation flow generated by jets and bubble plumes reported in the literature

According to Jirka (1982, cited by Fanneløp et al. 1991) we can expect recirculating cells for vertical axisymmetric jets for certain combinations of depth to jet-diameter ratio and Froude number. Jirka and Harleman (1979) estimated the cell length of about 2 to 2.5 times the water depth. This coincides with the location where the total jet width becomes equal to one half the total depth at a longitudinal position 1.5 *h*. According to Jirka and Harleman (1979) the breakdown of the jet behaviour must occur at this point since the velocities in the return flow become equal to the jet velocities. Jirka and Harleman (1979) mention the turbulent momentum transfer at the outer boundary of the primary cell driving the secondary cell. Even though experimental evidence was lacking so far, they expect that higher-order turbulent cells will be established.

Fanneløp et al. (1991) summarize that from his large-scale field experiments with bubble plumes at source depths down to 60 *m*, Topham (1975, cited by Fanneløp et al. 1991) reported the observation of a "wave ring" on the surface. This "wave ring" (Fanneløp et al. call it a stagnation line) separated the outward-directed surface current from a secondary inward current, and, in the sense of Fanneløp et al., defined the size of the primary recirculation cell. The actual cell radius was about half the ocean depth of 60 *m*, and Topham measured the outward as well as the inward velocity outside the "wave ring".

The limit of plume influence defined by Goossens (1979) appears at the distance where small pieces of paper placed in the plume region and carried outward remained stationary. Goossens proposed a region of influence in the range R/h = 4-7 (where R is the plume radius and h the depth of the tank), the smaller value representing model tests and the larger full scale. Goossens notes in particular the dependency of cell size on gas flow rate.

Riess and Fanneløp (1998) examined experimentally the influence of sidewalls on the flow and observed that the cross-sectional geometry parameter of the aspect ratio depth-to-width has a strong influence on the velocity distributions. The longest range of influence of the surface current was observed in the experiment with aspect ratio of unity. For values of this ratio higher than unity (narrow tank) the cell length is rather short. Only in the case of a narrow channel would the existence of a secondary cell seem at all possible. In a very wide channel

three-dimensional effects occur and a secondary flow was observed that reduced the range of influence.

Riess and Fanneløp (1998) concluded that without sidewalls (large-scale applications) new phenomena could appear which till date were not yet known.

2.5.2 Concluding remarks

As the influence of a bubble plume or a mechanical mixer on the far field was not an issue in the application in lakes (section 2.4.4), publications related to recirculated flow induced by vertical jets completes partially this lack of knowledge. But unfortunately, the obtained results of recirculation flow induced by jets and bubble plumes are not directly transferable to the problem of mechanical mixers in lakes. There are the following reasons:

- The mixer in the lake was introduced at some water depth, while the aforementioned bubble plumes and jets were placed at the bottom of the tank.
- The jet induced by the mixer is directed downwards. It is not mentioned whether it reaches the bottom as a jet, inducing an impinging radial jet. The jets induced by the authors investigating recirculating flows were directed upwards and reached the water surface, where they were considered to form a radial wall jet, instead.
- In the experiments conducted by the authors investigating recirculating flows (except of Topham 1975, cited by Fanneløp et al. 1991), the tank had an elongated shape such that the flow was laterally constrained (2D) except for Riess and Fanneløp (1998). Riess and Fanneløp (1998) detected for wide containers three-dimensional effects influencing the range of the primary cell. The latter finding is significant for investigations in lakes and reservoirs. But the phenomena in large scale applications (no side walls) are not yet known.
- The mixer induces the vertical jet with a swirl. This swirl could eventually have an influence on the flow pattern in the far field.

The expected cell length induced by a plane vertical jet under given test conditions is found to be 5 times the water height (Fanneløp et al. 1991).

2.6 Sediment settling process

2.6.1 Settling velocity of spherical cohesionless particles

Van Rijn (1990) stated that basically, the fall velocity is a behavioural property. The stationary settling velocity w_s (reached after having accelerated) of non-cohesive spherical particles in calm water is dependent on

- diameter of the particle d_s
- density of the particle ρ_s
- shape of the particle (SF)
- characteristics of the fluid (viscosity ν, density ρ_w)
- influence of the walls, the bed and other particles, etc.
- surface of the particles (roughness)

- concentration of the particles

The steady settling velocity can be simply described by the fall velocity when the flow resistance F_D (fluid drag force) on the particle is in equilibrium with the gravity force G reduced by the buoyancy, giving:

$$F_D = c_D \cdot \rho_s / 2 \cdot w_s^{\,2} \cdot d_s^{\,2} \cdot \frac{\pi}{4} = G = (\rho_s - \rho_w) \cdot g \cdot d_s^{\,3} \cdot \frac{\pi}{6} \qquad \text{(Eq. 2.29)}$$

$$w_s = \sqrt{\frac{4}{3} \cdot \frac{(\rho_s - \rho_w) \cdot g \cdot d_s}{\rho_w \cdot c_D}} \qquad \text{(Eq. 2.30)}$$

where the drag coefficient c_D is strongly dependent on the Reynolds number of the settling process:

$$\mathrm{Re}_s = \frac{w_s \cdot d_s}{\nu} \qquad \text{(Eq. 2.31)}$$

$$c_D = \frac{24}{\mathrm{Re}_s} \qquad \text{(Region of Stokes law, } \mathrm{Re}_s < 0.1\text{)} \qquad \text{(Eq. 2.32)}$$

$$c_D = \frac{24}{\mathrm{Re}_s}\left[1 + \frac{3}{16}\mathrm{Re}_s\right] \qquad 0.1 < \mathrm{Re}_s < 1.0 \text{ (Oseen, 1927)} \qquad \text{(Eq. 2.33)}$$

$$c_D = \frac{24}{\mathrm{Re}_s} + \frac{4}{\sqrt{\mathrm{Re}_s}} + 0.4 \qquad 1.0 < \mathrm{Re}_s < 2 \cdot 10^5 \text{ (Kaskas, 1970)} \qquad \text{(Eq. 2.34)}$$

A more sophisticated expression for the drag coefficient is given by Brown and Lawler (2003). It is valid for all Reynolds numbers smaller than $2 \cdot 10^5$.

$$c_D = \frac{24}{\mathrm{Re}_s}\left(1 + 0.150 \cdot \mathrm{Re}_s^{\,0.681}\right) + \frac{0.407}{1 + \frac{8.71}{\mathrm{Re}_s}} \qquad \text{(Eq. 2.35)}$$

For laminar flows around the particles friction forces are dominant, for turbulent flows, the inertial forces define the flow resistance. The c_D-value decreases rapidly outside the Stokes region and becomes nearly constant for $10^3 < Re_s < 10^5$, yielding w_s proportional to $d^{\,0.5}$. For larger Reynolds numbers the literature gives numerous empirical relationships between c_D and Re_s (Zanke, 1982).

An empirical equation for sand particles is proposed by Zanke (2002):

$$w_s = \frac{100}{9 \cdot d_s}\left(\sqrt{1 + 157 \cdot d_s^{\,3}} - 1\right) \qquad \text{(Eq. 2.36)}$$

where w_s: settling velocity in still water [mm/s]

d_s: particle diameter [mm]

This equation is valuable for:

$\frac{\rho_s}{\rho_w} = 2.65$ and T = 20°C in calm water.

Dietrich (1982) developed an empirical equation that accounts for the effects of size, density, shape and roundness on the settling velocity of natural sediment. This analysis was done in terms of four nondimensional parameters, namely, the dimensionless nominal diameter, D^*, the

dimensionless settling velocity, *W**, the Corey shape factor, and the Powers roundness index. He found that at low *D** the reduction in settling velocity due to either shape or roundness is much less. Hence, neglecting the influence of the shape and the roundness, the dimensionless nominal diameter *D** is calculated as follows:

$$D^* = \frac{(\rho_s - \rho) g D_n}{\rho \nu} \qquad \text{(Eq. 2.37)}$$

where D_n is the nominal diameter (diameter of the sphere of the same volume V_s of the particle, Wadell 1932) and ν the viscosity. The relationship between the settling velocity and the dimensionless nominal diameter, valuable for $0.05 < D^* < 6 \cdot 10^8$, is described by a forth order polynomial:

$$\log W^* = -3.76715 + 1.92944 (\log D^*) - 0.09815 (\log D^*)^2 - 0.00575 (\log D^*)^3 + 0.00056 (\log D^*)^4 \qquad \text{(Eq. 2.38)}$$

Since the dimensionless settling velocity *W** is expressed by the settling velocity w_s, the latter as well as the drag coefficient c_D can be drawn by the following equations:

$$W^* = \frac{\rho w_s^{\,3}}{(\rho_s - \rho) g \nu} \qquad \text{(Eq. 2.39)}$$

$$c_D = \frac{4}{3} \frac{(\rho_s - \rho) g D_n}{\rho w_s^{\,2}} \qquad \text{(Eq. 2.40)}$$

Bouvard (1984) collected and compared several analyses of the settling velocity of different authors. The results are summarized in Figure 2.7.

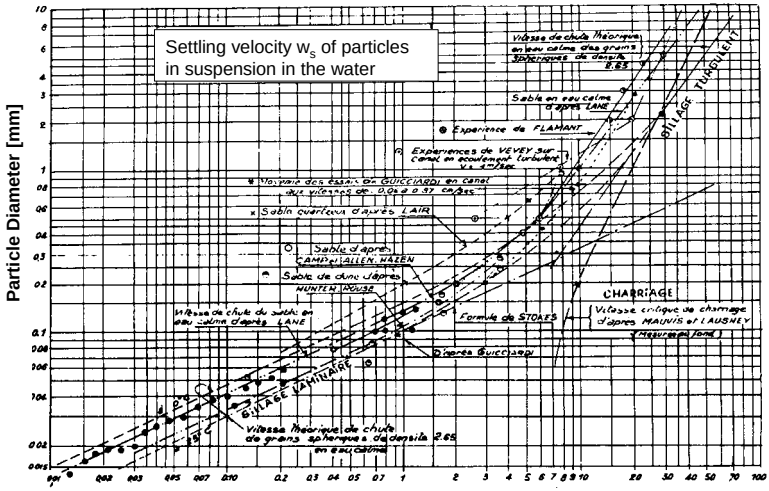

Figure 2.7 Diagram of Bouvard (1984) comparing settling velocities of different authors, valuable for particle densities of ρ_s = 2.65 t/m³

2.6.2 Non spherical particles

The above given relations between the drag coefficient, the Reynolds number and the settling velocity are valuable for perfectly spherical shaped particles. In the case of other shapes a shape factor *SF* should be considered.

$$SF = \frac{c_s}{\sqrt{a_s b_s}} \qquad \text{(Eq. 2.41)}$$

with a_s, b_s and c_s are the diameters of the particle, where c_s is the value for the shortest axis.

The expressions valid for a sphere cannot be applied for a natural sediment particle because of the differences in shape. The shape effect is largest for relatively large particles (> 300 μm) which deviate more from a sphere than a small particle. Experiments show differences in fall velocity of the order to 30% for *SF* (shape factor) in the range from 0.5 to 1.

$$w_s = \frac{(\rho_s/\rho_w - 1)\cdot g \cdot d_s^{\,2}}{18\upsilon} \qquad \text{for } 1 < d_s \le 100\ \mu\text{m} \qquad \text{(Eq. 2.42)}$$

$$w_s = \frac{10\upsilon}{d}\cdot\left[\left(1+\frac{0.01\cdot(\rho_s/\rho_w - 1)\cdot g \cdot d_s^{\,3}}{\upsilon^2}\right)\right] \qquad \text{for } 100 < d_s \le 1000\ \mu\text{m} \qquad \text{(Eq. 2.43)}$$

$$w_s = 1.1\sqrt{(\rho_s/\rho_w - 1)\cdot g \cdot d_s} \qquad \text{for } d_s > 1000\ \mu\text{m} \qquad \text{(Eq. 2.44)}$$

where d_s is the sieve diameter of the sediments (van Rijn 1990).

Other influences are yielded by the above listed parameters.

2.6.3 Effect of sediment concentration

The fall velocity of a single particle is modified by the presence of other particles. A small cloud of particles in a clear fluid will have a fall velocity which is larger than that of a single particle. Uniform suspensions of sediments have strongly reduced fall velocities than single particles. This effect, known as hindered settling, is largely caused by the fluid return flow induced by the settling velocities. A state of fluidization may occur when the vertical upward fluid flow is so strong that the upward drag forces on the particles become equal to the downward gravity forces resulting in no net vertical movement of the particles. According to Oliver (1961), the fall velocity in a fluid-sediment suspension can be determined as (Figure 2.8):

$$w_{s,m} = (1 - 2.15\cdot c)\cdot(1 - 0.75\cdot c^{0.33})\cdot w_s \qquad \text{(Eq. 2.45)}$$

$w_{s,m}$: particle fall velocity in fluid with suspended material

w_s: particle fall velocity in a clear fluid

c: volumetric sediment concentration

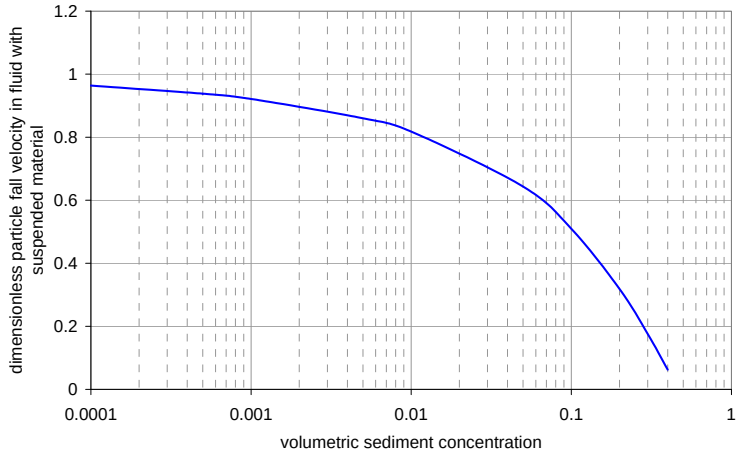

Figure 2.8 Dimensionless particle fall velocity in fluid with suspended material (according to Oliver 1961)

2.7 Concluding remarks

For both foreseen jet arrangements, circular and aligned, no specific research was yet reported in the literature. Nevertheless, since there are jets involved in a mixing process, the literature reporting about jet mixing might contribute some findings to the present study, even if there are some differences in tank shape and general test requirements: the jet position, the jet diameter and velocity as well as the residence time are important in any jet mixing case. Moreover, as it is discussed in chapter 4, the circular jet arrangement induces a vertical downward jet out from the centre of the jet arrangement. This jet needs to be regarded as such and the aforementioned characteristics might be applied for it as well.

Moreover, the circular jet arrangement induces a circulation similar to the one induced by a propeller type impeller. Thus, reflections about similarity with mechanical mixers and their flow patterns are advisable. According to the literature flow fields induced by axial mixers are more conducive to easier suspension than those induced by radial mixers.

Research reporting about mixing in lakes and reservoirs with air-bubblers or mechanical mixers provide an insight into mixing in large water volumes. The influence of the impeller induced flow rate as well as of the release flow rate on mixing was reported. Unfortunately, the goal of these studies is different and there is no hint about circulation in the far field and the flow patterns.

This lack of knowledge could be partially covered by the experiments performed within the research domain of recirculating flow where relations between recirculation cell length and water depth were related. Although the general conditions are different to the ones using mixers in lakes, and although, consequently, the results cannot be easily transferred, the

findings of the cited authors give certain advice about the length due to an impeller induced cell.

Based on the existing knowledge, the effect of circular and aligned jet arrangements in reservoirs on suspension and sediment release need, therefore, further investigation.

3 Experimental set-up and test procedure

3.1 Description of the experimental facility

3.1.1 Laboratory tank

The physical experiments were carried out in a prismatic tank with vertical walls. Different jet arrangements assumed to be enhancing for solid suspension as well as reference tests without jets were performed. Since it is a priori assumed that the influence of the proposed jet arrangements on the flow is locally limited, the tank only represents a limited part of the reservoir located in front of the dam. Its elongated shape with a total inner basin length of 4 *m*, an inner width of $B = 1.97$ *m* and a total basin height of 1.50 *m* simulates with its water body in the upper part (length equals twice the width) a boundary condition as it exists in nature. The front wall of the tank is considered to represent the dam, and the two lateral walls confine the reservoir volume in analogy to valley slopes (Figure 3.1 and Figure 3.2).

Figure 3.1 Photograph of the laboratory tank

The horizontal bottom is made of a steel plate. Three quarters of the right lateral wall and the majority of the front wall are made of glass providing transparency for visual observations, whereas the other walls are made out of steel plates. In the middle of the front wall there is a vertical stripe of PVC, into which the water intake is insertable at three different levels: 0.25, 0.50 and 0.75 *m* above the bottom (Figure 3.2). This allows varying the level of the power intake. The water intake has been designed to reduce the head losses and the turbulences

disturbing the flow in the vicinity of the outlet. It consists of an elliptical bell mouth shaped intake followed by a cylindrical throat with an inner diameter of 48 *mm* (Figure 3.3).

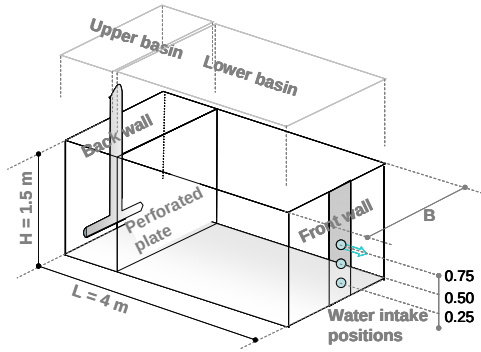

Figure 3.2 Sketch of the experimental tank

A pipe of a 50.8 *mm* diameter and approximately 1.5 *m* length guides the outflowing water into a small energy dissipating basin (0.7 x 0.7 m^2 ground surface). The end of the pipe is submerged in the dissipating basin (Figure 3.4). Turbidity of the outflowing water is measured in the dissipating basin, with the turbidity sensor installed right at the end of the incoming pipe. In the dissipating basin, the flow rate is monitored visually when falling over a 2 *mm* thin, 30° angle V-notched weir plate made out of a metal sheet. It is controlled manually by means of guide vanes.

At a distance of 0.50 *m* from the back wall of the basin, a perforated steel plate is inserted vertically. The holes have a diameter of 2 *mm* with 4 *mm* spacing. From other physical experiments it is known, that this metal sheet tranquilizes the water introduced from the back of the basin and favours equal distribution when flowing into the bigger part of the basin (Figure 3.2). No flow velocities were measured and the flow was not visualized in this area and, hence, this tranquilizing effect was not qualified.

Figure 3.3 Nozzle at the water intake with an ellipsoidal inlet coupled to a cylindrical throat.

Figure 3.4 Photograph of the turbidity sensor position within the energy dissipating basin relative to the submerged jet restituting the evacuated water sediment mixture.

A 150 *mm* diameter pipe, supplied by the laboratory pump with an available head of $1.5 \cdot 10^5$ *Pa* and a maximum discharge of 5 *l/s*, leads clear water from the laboratory reservoir vertically downward along the middle axis of the inner side of the back wall into the upper part of the experimental basin. This pipe has at its end a T-shaped bifurcation with two arms going horizontally along the lower edge of the back wall. The submerged pipe segment is perforated all around with holes having a diameter of 12 *mm*. The distance between two holes averages 82 *mm* on the horizontal arms and 125 *mm* in the vertical section.

3.1.2 Jet installation

A 50.8 *mm* diameter pipe, supplied by the same laboratory pump as described above, leads clear water to a level 150 *mm* above the upper basin edge, where it is distributed from a horizontal chamber into four rotameters. The use of the rotameters allows an equal distribution of the total flow rate into the four nozzles. On the top of each rotameter a valve is installed, which can release trapped air. Each rotameter feeds a horizontally attached flexible pipe with an inner diameter of 25.4 *mm* each. The flexible pipes lead the water into rigid pipes leading the water downward into the basin.

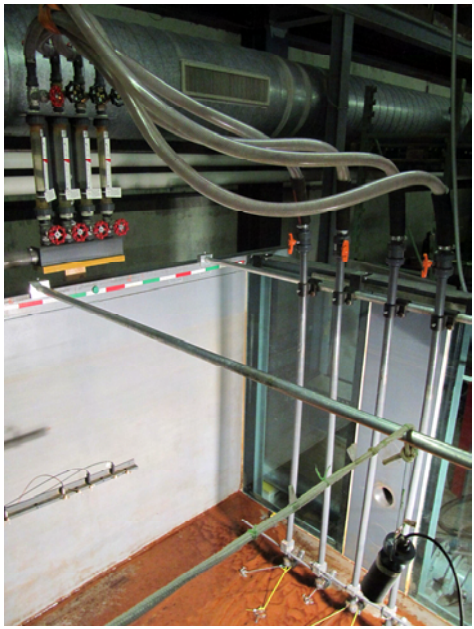

Figure 3.5 *Inside of the basin the four rotameters on the left with valves controlling the flow to the four nozzles. Shown here is the linear jet configuration. In the foreground on the right lower edge of the picture one of the turbidity meters is suspended by a rope.*

The rigid pipes are fixed at their upper end on two horizontal bars running across the width of the tank. Their position can be varied. The fixation on the horizontal bars allows rotations in all three degrees of freedom. The nozzles are fixed at the lower end of the rigid pipes at the angle to be investigated (45°, 0° or -45° to the horizontal). The nozzle diameter can be varied by exchanging the nozzle (3, 6 and 8 *mm*). In the lower section the rigid pipes are held in a frame, avoiding flow induced vibration and therefore maintaining the exact nozzle position during the experimental run (Figure 3.6).

In the lower part of the basin, three flexible and flat irrigation pipes are put longitudinally and in equal distance (0.5 *m*) on the bottom of the basin as well as on the bottom of the upper part of the tank. On their upper surface they have every 100 *mm* a tiny hole. This arrangement gives the possibility to let rise pressurized air through these holes provoking a whirling pool and ensuring homogeneous sediment mixing. The installed air pressure has a maximum of $6 \cdot 10^5$ *Pa*. This whirl pool, turned on during the filling process helps to maintain the sediments in suspension and to reach a quasi homogeneity of the sediment concentration in the entire basin.

Figure 3.6 *Circular jet configuration. The rigid pipes are held in a frame, avoiding flow induced vibration and therefore maintaining the exact nozzle position during the experimental run.*

3.1.3 Measurement equipment

Apart from the mentioned rotameters controlling the jet discharge, two types of measurements were carried out during the experiments:

- Flow velocity measurements
- Turbidity measurements

3.1.3.1 Flow velocity measurements

Takeda (1995) developed an Ultrasonic Velocity Profiling technique (UVP) to measure instantaneous velocity profile of liquid flows by using the Doppler shift of echoes reflected by small particles flowing with the liquid. The principles of UVP operation and the related theoretical explanations are presented in the manual provided by Met-Flow (2005). The UVP technique is quasi non-intrusive and does, hence, not disturb the flow circulation. De Cesare and Schleiss (1999) report successfully performed UVP-measurements using the mapping technique when monitoring turbidity currents in the laboratory. Kantoush (2008) used the same technique to investigate the 2D-flows developing in a shallow reservoir.

In order to get the required flow velocity measurements an L-shaped rack was built with two wings hosting five equally distanced UVP-transducers, each. This rack was fixed at the lower end of a vertical stem (Figure 3.7). The lateral distance from one sensor to another was 200 *mm*; the distance between the sensors and the wall was 230 *mm* when positioned vertically, and 100 *mm* for horizontal measurements. This rack was moved within the front tank cube from one quadrant to another. Four displacements were needed to get all records on one level (Figure 3.8), providing a horizontal 2D flow pattern on a plane of 2 x 2 m^2 (Figure 3.9). Such horizontal measurements were performed at four different levels: 0.10, 0.30, 0.50 and 0.70 *m* from the bottom. Vertical measurements were recorded on two axes: the longitudinal middle axis corresponding to the water intake axis, and the transversal axis, crossing the jet circle centre (in case of circular jet arrangement) or following the jet line (in case of linear jet arrangement, Figure 3.9).

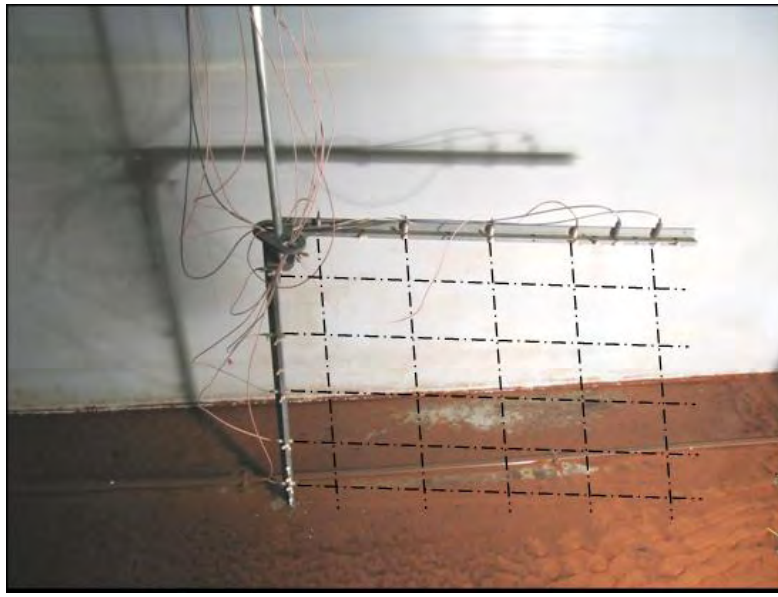

Figure 3.7 *Rack of 5 x 5 UVP-transducers fixed at the lower end of a vertical stem. The sensor emitting axes are schematically indicated.*

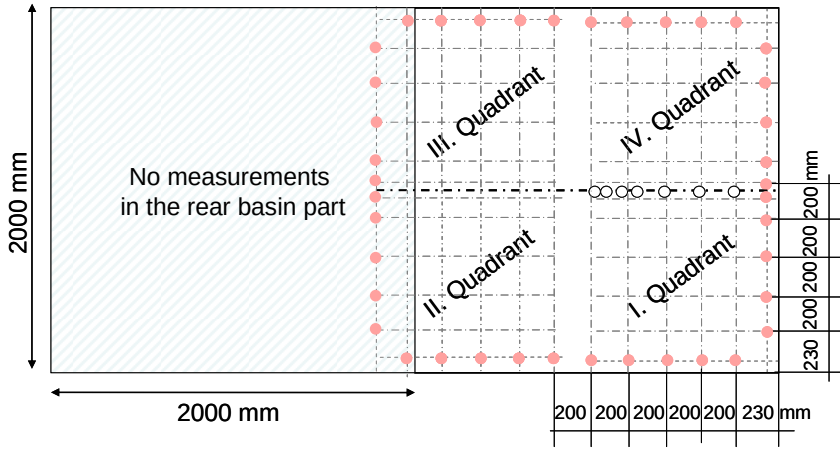

Figure 3.8 *Top view of the measurement points in the front cube of the experimental basin. Full dots: Positions of the UVP-sensors in the four quadrants; circles: Periodic positions of the turbidity meter on the longitudinal axis.*

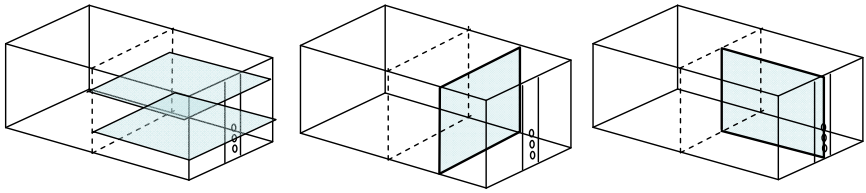

Figure 3.9 *Schematic view of the position of the UVP-sensor-frame for, right: horizontal 2D-flow patterns, middle: transversal 2D-flow pattern, left: longitudinal 2D-flow pattern.*

Parameter	*Value*
Ultrasonic frequency, f_0	*2 MHz*
Transducer diameter	*10 mm*
Measurement window start / end	*84.92 mm / 907.8 mm*
Maximum velocity, U_{max}	*±150 mm/s*
Number of cycles	*4*
Channel width = channel distance	*1.48 mm*
Max. depth	*913.9 mm*
Number of repetitions	*128*
Sound velocity, c_{US}	*1480 m/s*
Number of channels	*557*
Overlap	*none*
Output voltage	*90 V*
Number of multiplexer cycles	*8 with 6 profiles per burst*
Multiplexer parameters (flow mapping)	
Number of cycles	*8*
Cycle delay	*10 s*

Table 3.1 *Main characteristics of the ultrasonic Doppler velocity profiler measurements (MetFlow 2005)*

3.1.3.2 Turbidity measurements

Two SOLITAX sc sensors (brand Hach) were employed. Their measuring principle is based on an infrared absorption scattered light technique, where the sensor is equipped with a LED (light-emitting diode) light transmitting a beam of infrared light into the sample stream at an angle of 45° to the sensor face. A pair of photoreceptors in the sensor face detects light scattered at 90° to the transmitted beam. The relationship between the suspended sediment concentration and the turbidity signal was derived in the laboratory by placing the probe in

suspensions of known crushed walnut shells concentrations. The resulting calibration relationship is linear (Figure 3.10).

One of the turbidity sensors was installed in the dissipation basin right below the exit of the headrace tunnel and recorded suspended sediment concentration continuously (Figure 3.4). The concentration of the outflowing suspended sediment and the flow rate provide an indication of the efficiency of the sediment evacuation method.

The second turbidity meter is used to measure sporadically (5 to 8 times per experiment) suspended sediment concentration on the horizontal axis through the water intake (at a distance of 0.25, 0.45, 0.65, 0.75, 0.85, 0.95 and 1.00 *m* from the front wall) and on the rotational (vertical) axis of the jets configuration (on levels 0.10, 0.20, 0.30, 0.40, 0.50, 0.75 and 1.00 *m* over bottom). The chronological evolution of the sediment concentration measured within the basin gives further information on the evacuation efficiency.

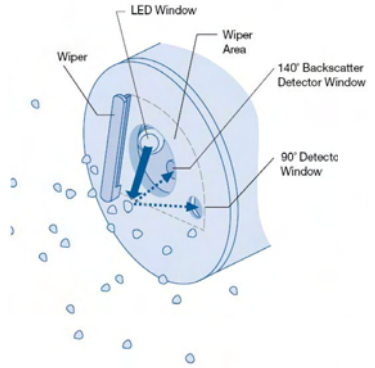

Figure 3.10 Optical measuring principle (SOLITAX sc, User Manuel, 2005)

3.1.3.3 Laboratory calibration of the two turbidity measurement devices

The sediment concentration of the suspended crushed walnut shells was plotted against the resulting turbidity determined from laboratory measurements. This relationship was derived in the laboratory by placing the probe in suspensions of crushed walnut shells of known concentration in a range between 0.05 and 1.5 *g/l*. The resulting calibration relationships of the two different sensors are shown in Figure 3.11.

The adopted calibration relationships for the suspended sediment concentration (*SSC*) are as follows:

$SSC\ [g/l] = 0.0041 \cdot Turbidity\ [FNU]$ placed in the experimental basin (*Eq. 3.1*)

$SSC\ [g/l] = 0.0045 \cdot Turbidity\ [FNU] + 0.001$ placed in the dissipation basin (*Eq. 3.2*)

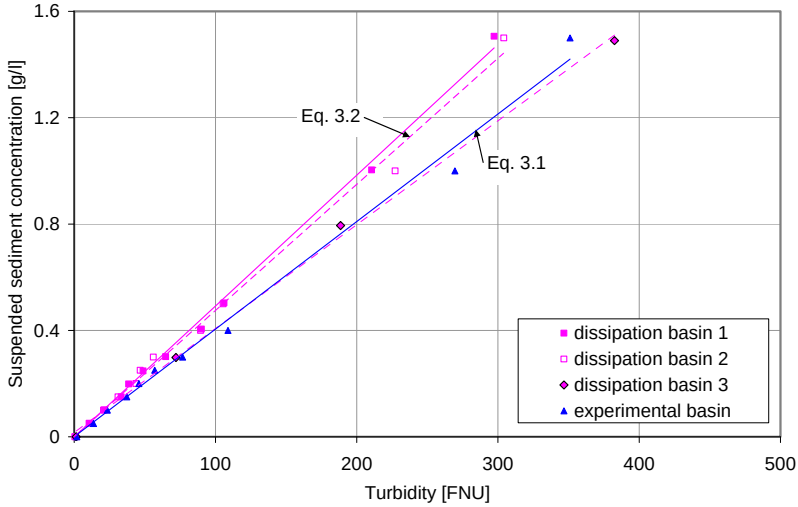

Figure 3.11 Calibration relationship of the sensor within the dissipation basin and the experimental basin respectively.

3.1.3.4 Data reliability and errors

Assuming that there is a close relationship between fluctuations in sediment concentration and turbidity and considering, first, the reliability of the point measurement of SSC provided by a turbidity probe installed at a particular point, errors may stem from several sources, including:

- instrument errors associated with the equipment used,
- systematic errors introduced by the calibration procedure employed, and
- methodological errors caused by indirect measurement of the variable under study.

Further uncertainties are introduced if the point measurement of sediment concentration is assumed to be representative of a bigger water volume, since it is well known that suspended sediment concentrations will vary through space.

To determine the error of the concentration measurement, 5 pairs of samples (suspended sediment concentration and turbidity) were again used. The turbidity values were substituted into the regression equation and a set of concentration values was obtained. The average error in suspended sediment concentration associated with the soil method calibration established, using the following equation:

$$error = \sqrt{\sum \frac{\left(SSC_{calc} - SSC_{known}\right)^2}{n-1}} \qquad (Eq.\ 3.3)$$

where SSC_{calc} [g/l] refers to the estimated suspended sediment concentration using the laboratory-derived calibration equation and SSC_{known} refers to the known suspended sediment concentration using the known sediment weight and water volume. The average error

associated with the calibration was estimated to be +/- 0.044 *g/l* and +/- 0.035 *g/l* for the sensor within the basin and the sensor in the dissipation basin respectively.

It was verified if during long term experiments the turbidity measurements were influenced by swelling of the organic sediment in water. In a test with constant sediment concentration lasting for five days no swelling was detected, or swelling did not falsify the turbidity measurements (section 3.4.1, Figure 3.14).

3.2 Measurement errors

After four hours experiment duration the total average error (root mean square deviation) of the evacuated sediment ratio resulting from the experiments with basic geometric parameters (Table 4.2) depends linearly on the discharge, and its relationship has been found to be the following (Figure 3.12):

$$Error = 8 \cdot 10^{-6} \cdot Q\,[l/h] \qquad (Eq.\ 3.4)$$

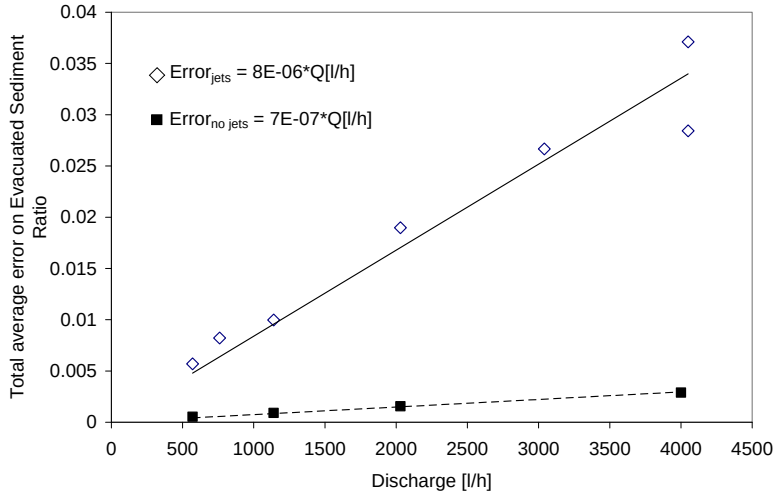

Figure 3.12 Total average error of evacuated sediment ratio (ESR) due to turbidity, sediment weight balance, and rotameter or electromagnetic flow measurements, respectively, showed for the jet experiments with basic parameters and the experiments without jets.

The error is established after the following error propagation laws:

Generally, for sum and subtraction of the form $a = b \pm c$, the average error of a is

$$\sigma_a^2 = \sigma_b^2 + \sigma_c^2. \qquad (Eq.\ 3.5)$$

For multiplication and division of the form $f = x \cdot y$ and $f = x/y$, the average error of f is

$$\left(\frac{\sigma_f}{f}\right)^2 = \left(\frac{\sigma_x}{x}\right)^2 + \left(\frac{\sigma_y}{y}\right)^2 \qquad (Eq.\ 3.6)$$

Thus, the average error of the sum $\Sigma c_{s,i}$ calculated for 4 hours is with the turbidity measurement error of 0.035 *g/l* (section 3.1.3.4) and a logging interval of Δt = 5 *s*:

$$\sigma^2_{(\Sigma c_{s,i})} = 2880 \cdot 0.035\ g/l \qquad (Eq.\ 3.7)$$

The total average error of the evacuated sediment ratio for experiments with jets is estimated as follows:

$$\left(\frac{\sigma_{ESR}}{ESR}\right)^2 = \left(\frac{\sigma_{(\Sigma c_{s,i})}}{\Sigma c_{s,i}}\right)^2 + (error\ due\ to\ rotameter)^2 + (error\ due\ to\ balance)^2 \qquad (Eq.\ 3.8)$$

The error of a rotameter is assumed to be approximately ± 5 %; the error of the employed balance is indicated to be 0.05 *g*.

For experiments without jets the error due to rotameter does not apply and is replaced by the error due to the electromagnetic flow measuring system (Promag 50, Endress and Hauser) which amounts to ± 0.5 %.

As Figure 3.12 shows, the total error resulting from experiments with jets is higher than the one from experiments without jets. Moreover, it increases linearly with higher discharge. The maximum total average error corresponding to the highest tested discharge is after four hours experiment duration approximately 3.5 % (with jets), whereas without jets it is approximately 10 times smaller.

3.3 Similarity rule

Usually, free surface hydraulic models are run according to the criterion of Froude similarity. This means that the same relationships for inertia and gravity forces apply in the prototype (subscript *p*) and in the model (subscript *m*).

Introducing the geometrical length scale:

$$\lambda_L = \frac{L_p}{L_m} \qquad (Eq.\ 3.9)$$

Froude similarities have to follow the relation:

$$Fr_L = \frac{v_L}{\sqrt{\lambda_g \cdot \lambda_L}} = 1 \qquad (Eq.\ 3.10)$$

The acceleration due to gravity is equal in the prototype and in the model (λ_g = 1), the relations presented in Table 3.2 are obtained for a Froude similarity.

Type of parameter	*Parameter*	*Froude-scale condition*
geometric	*length*	$\lambda_L = L_{prototype} / L_{model}$
cinematic	*velocity*	$\lambda_v = \lambda_L^{1/2}$
	discharge	$\lambda_Q = \lambda_L^{5/2}$
	time	$\lambda_t = \lambda_L^{1/2}$

Table 3.2 Scale relations for a Froude similarity

The jet Reynolds number and the Reynolds number at the water intake are in every tested configuration considered to be turbulent.

The range of tested jet Reynolds numbers: Re_j : 8400 – 60'000

The range of tested water intake Reynolds number: Re_i : 4030 – 29'000

Therefore, the Reynolds similarity is not an issue.

3.4 Selection of experimental parameters

This section is dedicated to evaluate the physics of involved components in the sediment release problem out of a reservoir. The jet characteristics and the reservoir (tank) dimensions influence the sediment release, or the trap efficiency, respectively. To achieve reliable results, the suspended material and physical boundary conditions should be as representative as possible for real cases.

3.4.1 Selection of materials

3.4.1.1 Properties of reservoir water

The temperature of the water used for the experiments varied between 15 and 20°*C*. The viscosity influencing the settling velocity of the sediment does not vary significantly within this range.

3.4.1.2 Properties of the sediment materials

For the present study ground walnut shell powder was used. This material has been tested in former studies of sedimentation in shallow reservoirs (Kantoush 2008 among others) and has been found to be very well adapted to this problem. It is very easy to mix, almost cohesionless and lightweight. Specifically, the density is $\rho_s = 1500\ kg/m^3$. The grain size distribution of the sediment material was determined with a Laser-Particle-Sizer Instrument (Analysette 22). The particle size distribution is relatively narrow and the settling velocity is small (according to Stokes' theory: $w_s \approx 0.8\ mm/s$ in water at 15°*C*). The particles have a median diameter of $d_m = d_{60} = 0.06\ mm$ (Figure 3.13, Table 3.3). With a dispersion, σ_g, of 2.4 some grain sorting effects can be expected to occur. The particles are not spherical, but have slightly angular shapes, like natural sediments.

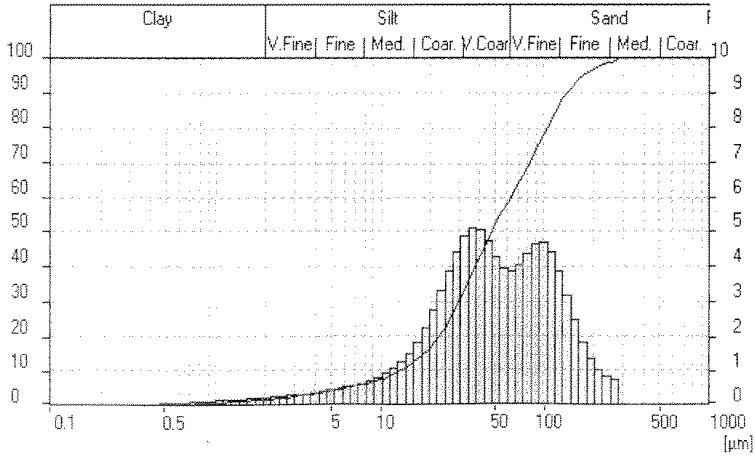

Figure 3.13 Grain size distribution of ground walnut shells

Because they are organic swelling tests were performed on the sediments in order to estimate their behaviour over a long term. Turbidity measurements carried out over five days showed only minor evidence of swelling: the sensor used in the experimental basin showed a linear suspended sediment concentration increase of 1.45 % per day, whereas the sensor used in the dissipation basin detected an insignificant variation of 1.7 ‰ per day (Figure 3.14). Both sensors were placed in the same mixture during the test period. For tests lasting for four hours, swelling is considered to be negligible.

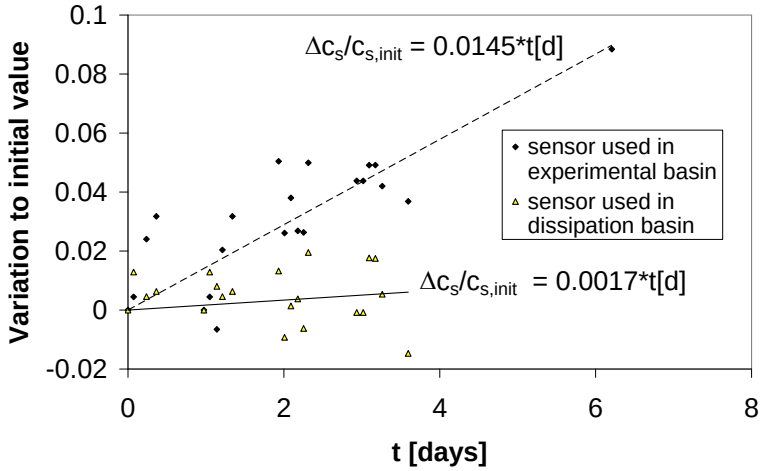

Figure 3.14 Detected variation of sediment concentration in function of time due to swelling of used organic sediment (crushed walnut shells).

In case of small, almost spherical particles and low Reynolds numbers, the Stokes' law can be applied to estimate the settling velocity as:

$$w_s = g\frac{\rho_s - \rho_w}{\rho_w}\frac{1}{18\nu}d_s^{\,2} \qquad (Eq.\ 3.11)$$

The influence of the shape and the sediment concentration was discussed in sub-chapter 2.6. With the particle size distribution shown in Figure 3.13 the calculated w_s is 0.8 *mm/s* (for d_{60}, $T = 15°C$).

The characteristics of the ground walnut shells are listed in Table 3.3.

As shown in Figure 3.15, the grain size distribution of the ground walnut shells is in the range of the grain size distribution of the fine sediments encountered in front of the dam of three large reservoirs in Switzerland (Grimselsee, Turtmann, Luzzone), where data are available (Sinniger et al. 2000) .

Diameter d_{60}	*0.060 mm = 60 μm*
Diameter d_{50}	*0.050 mm = 50 μm*
Diameter d_{84}	*0.115 mm = 115 μm*
Diameter d_{16}	*0.022 mm = 22 μm*
$\sigma_g = \sqrt{d_{84}/d_{16}}$	*2.4*
Density ρ_s	*1500 kg/m^3*
Settling velocity w_s according to Stokes' law with d_{60}	*~ 0.83 mm/s (T = 15°C)*
Critical shear velocity $u_{*cr} = 6 \cdot w_s$	*~ 4.8 mm/s*
(Kantoush 2008)	
$\mathrm{Re}_s = w_s d_s / \upsilon$	*0.048 (Stokes' domain)*
$c_D = 24/\mathrm{Re}_s$	*520*

Table 3.3 Characteristics of the sediment material (ground walnut shells)

The Reynolds number of a natural grain with the same average diameter of 60 μm is Re_s = 0.138, the corresponding drag coefficient is c_D = 240. Thus, the behavior of the natural grain is in the Stokes' domain as well. Both Reynolds numbers are in the same range and therefore, viscosity effects are same for physical experiments and real case. Consequently, the Reynolds model scale doesn't need to be applied.

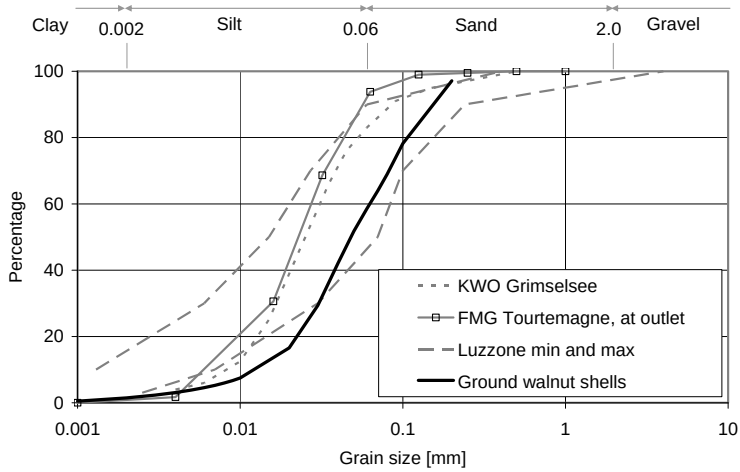

Figure 3.15 Grain size spectrum of the ground nut shells in comparison with the sediment grain size measured in three Swiss Alpine reservoirs in front of the dam. Continuous line: ground walnut shells, dotted: Lake Grimsel, the dash-dotted line: Lake Tourtemagne, the range between the dashed lines: Luzzone dam.

3.4.2 Selection of jet characteristics

Since the jets of a prototype are fed by the water of transfer tunnels, the characteristics of the jets in the experimental installation are chosen in a range comparable to what is available in natural conditions. The available head defines the jet velocity, and the discharge can only be changed if the water is caught in a reservoir located above the main reservoir.

The head of the feeders of Lake Grimsel (239 *m*), Tourtemagne (35 to 170 *m*) and Mauvoisin (69 *m*) are in the range between approximately 35 and 240 *m*. Thus, the jet velocities are expected to be equal to the theoretical velocities in the penstock at the water level of the reservoir, i.e. between v_j = 25 and 70 *m/s* (head losses neglected). The experiments were carried out with the following jet velocities: v_j = 2.8 *m/s*, 5.6 *m/s* and 7.5 *m/s*. If Froude similarity with scale factor λ = 100 applied, the chosen velocities would cover the range between v_j = 28 and 75 *m/s* and, thus, be congruent with the corresponding velocity range observed in prototype. The nozzle diameters employed in the experiments were d_j = 3, 6 and 8 *mm*. If Froude similarity with scale factor λ = 100 applied, in nature the nozzle diameters would be d_j = 0.3, 0.6 and 0.8 *m*.

Combining jet nozzle diameters and jet velocities, six different jet discharges were used: 570, 760, 1140, 2030, 3040 and 4050 *l/h*. With a scale factor λ = 100 this would correspond to a discharge range of 15.8 to 113 m^3/s.

Figure 3.16 Water transfer from a neighbor catchment with a head of 170 m (Tourtemagne)

3.4.3 Tank dimensions

The tank dimensions are outlined in section 3.1.1. The length and the width of the tank were not varied during the experiment campaign. Three water depths of 1, 1.2 and 1.3 *m* were chosen as indicated in Table 3.5.

3.5 Experimental program

During the thesis work four different series of experiments were carried out. In the following paragraphs each series is briefly discussed. Experimental conditions and other useful information for these 4 series of runs are summarized in Table 3.4 to Table 3.6.

3.5.1 Preliminary experiment

This series consists of a unique experiment, the so called preliminary experiment, exploring the temporal evolution of the suspended sediment concentration in case of no induced circulation (no flow source, no evacuation). Two turbidity sensors were installed, each on a different level (at 0.5 and 0.25 *m* over bottom). The experiment lasted for 178 hours. No flow velocity measurements were carried out.

Results are presented in the sub-chapter 4.2.

3.5.2 Experiments without jets – Reference tests (R series)

The second series contained reference experiments, in which no jets were employed. The evacuated discharge through the water intake was replaced by water flowing in from the back wall of the basin, while the water level was maintained constant. Only local suspended sediment concentration measurements were executed within the basin. Velocities were assumed to be very small (except for area within the perimeter influenced by the outflow).

Thus, no flow velocity measurements were performed. This experiment shows which quantity of sediments is evacuated without jets, i.e. when no measures were undertaken.

Parameter variations are given in Table 3.4.

Results are presented in sub-chapter 4.5.

Exp [-]	*h* [m]	h_i [m]	Q_{out} [l/h]	$c_{s,init}$ [g/l]
R1	*1.2*	*0.5*	*570*	*0.2943*
R2	*1.2*	*0.5*	*1140*	*0.30053*
R3	*1.2*	*0.5*	*2030*	*0.28905*
R4	*1.2*	*0.5*	*4050*	*0.29766*

Table 3.4 Experimental conditions for reference tests

3.5.3 Jet experiments

Two series of jet experiments with fundamentally different jet arrangements were carried out:

1. Circular jet arrangement
2. Linear jet arrangement

Both of them employed the same jet characteristics.

3.5.3.1 Circular jet arrangement (C series)

The circular jet experiments are arranged as follows: The jet configuration consists of four water jets with equal nozzle diameter and jet velocity, arranged in a circle in a horizontal plane. Each jet is pointing in a 90°-angle to axis of the neighbouring jet (Figure 3.18 and Figure 3.19). In this way a rotational flow is introduced, sucking water vertically from above, and spreading it either horizontally or vertically downward out of the jet's circle. This jet arrangement is installed in the front part of the tank. The parameters influencing the effectiveness of the jets are the jet velocity, jet diameter, and the geometry of their arrangement.

In the first configuration (C1 to C7), also called basic configuration, experiments with six different combinations of the three jet velocities and the three diameters were performed. Each diameter and each velocity were combined twice. This resulted in six different jet discharges (between 570 and 4050 *l/h*) but, due to the proper choice of parameter combinations, in only three different total momenta ($0.887 \cdot 10^{-3}$, $1.579 \cdot 10^{-3}$ and $6.3 \cdot 10^{-3}$ m^4/s^2). In the subsequent configurations only a set of three different or even only one jet parameter combination was employed.

Apart from the jet characteristics five geometrical parameters were individually varied while keeping the others parameters constant (Figure 3.17): the off-bottom clearance, C (C8 to C15), the water intake height, h_i (C16-C21), the water height, h (C22 to C24), the distance between the circle centre and the front wall, d_{axis} (C25 to C32), the distance between two neighboring jets, l_j (C33 to C42). One experiment with a jet direction angle of $\theta = 45°$ with respect to the horizontal was performed (C43), with the other geometrical parameters

remaining the same as in the first experiments (C1 to C8). Parameter variations are given in Table 3.5.

Results are presented in sub-chapters 4.6 and 4.8.

l_j *the horizontal distance between two neighbouring jets*

C *the off-bottom clearance*

d_{axis} *the horizontal distance from the rotational axis to the front wall*

B *the width of the basin characterizing one of the boundary conditions*

h *the water height*

h_i *the water intake height*

θ *the jet direction angle with respect to the horizontal*

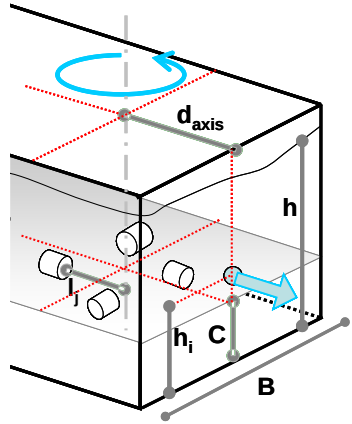

Figure 3.17 Geometrical parameters varied in the circular jet configuration.

Exp [-]	h [m]	h_i [m]	Q_{out} [l/h]	v_j [m/s]	d_j [mm]	$M_j \cdot 10^{-3}$ [m^4/s^2]	d_{axis} [m]	l_j [m]	C [m]	$c_{s,init}$ [g/l]	θ [°]
C1	1.2	0.5	570	5.6	3	0.9	1.05	0.3	0.35	0.359	0
C2	1.2	0.5	760	7.5	3	1.6	1.05	0.3	0.35	0.344	0
C3	1.2	0.5	1140	2.8	6	0.9	1.05	0.3	0.35	0.283	0
C4	1.2	0.5	2030	2.8	8	1.6	1.05	0.3	0.35	0.262	0
C5	1.2	0.5	3040	7.5	6	6.3	1.05	0.3	0.35	0.299	0
C6	1.2	0.5	4050	5.6	8	6.3	1.05	0.3	0.35	0.308	0
C7	1.2	0.5	4050	5.6	8	6.3	1.05	0.3	0.35	0.267	0
C8	1.2	0.5	760	7.5	3	1.6	1.05	0.3	0.2	0.271	0
C9	1.2	0.5	2030	2.8	8	1.6	1.05	0.3	0.2	0.299	0
C10	1.2	0.5	4050	5.6	8	6.3	1.05	0.3	0.2	0.279	0
C11	1.2	0.5	4050	5.6	8	6.3	1.05	0.3	0.2	0.271	0
C12	1.2	0.5	760	7.5	3	1.6	1.05	0.3	0.5	0.353	0
C13	1.2	0.5	760	7.5	3	1.6	1.05	0.3	0.5	0.267	0
C14	1.2	0.5	2030	2.8	8	1.6	1.05	0.3	0.5	0.283	0

Exp [-]	h [m]	h_i [m]	Q_{out} [l/h]	v_j [m/s]	d_j [mm]	$M_j \cdot 10^{-3}$ [m^4/s^2]	d_{axis} [m]	l_j [m]	C [m]	$c_{s,init}$ [g/l]	θ [°]
C15	1.2	0.5	4050	5.6	8	6.3	1.05	0.3	0.5	0.287	0
C16	1.2	0.25	760	7.5	3	1.6	1.05	0.3	0.5	0.3075	0
C17	1.2	0.75	760	7.5	3	1.6	1.05	0.3	0.5	0.2665	0
C18	1.2	0.25	760	7.5	3	1.6	1.05	0.3	0.2	0.2923	0
C19	1.2	0.75	760	7.5	3	1.6	1.05	0.3	0.2	0.2993	0
C20	1.2	0.75	760	7.5	3	1.6	1.05	0.3	0.35	0.328	0
C21	1.2	0.25	760	7.5	3	1.6	1.05	0.3	0.35	0.3075	0
C22	1.4	0.5	760	7.5	3	1.6	1.05	0.3	0.35	0.287	0
C23	1.4	0.5	760	7.5	3	1.6	1.05	0.3	0.35	0.2747	0
C24	1	0.5	760	7.5	3	1.6	1.05	0.3	0.35	0.3177	0
C25	1.2	0.5	760	7.5	3	1.6	0.6	0.3	0.35	0.2829	0
C26	1.2	0.5	2030	2.8	8	1.6	0.6	0.3	0.35	0.2911	0
C27	1.2	0.5	4050	5.6	8	6.3	0.6	0.3	0.35	0.3534	0
C28	1.2	0.5	760	7.5	3	1.6	0.8	0.3	0.35	0.2993	0
C29	1.2	0.5	2030	2.8	8	1.6	0.8	0.3	0.35	0.328	0
C30	1.2	0.5	4050	5.6	8	6.3	0.8	0.3	0.35	0.3157	0
C31	1.2	0.5	760	7.5	3	1.6	1.3	0.3	0.35	0.287	0
C32	1.2	0.5	760	7.5	3	1.6	1.55	0.3	0.35	0.3075	0
C33	1.2	0.5	760	7.5	3	1.6	1.05	0.2	0.35	0.1886	0
C34	1.2	0.5	4050	5.6	8	6.3	1.05	0.2	0.35	0.287	0
C35	1.2	0.5	760	7.5	3	1.6	1.05	0.45	0.35	0.246	0
C36	1.2	0.5	760	7.5	3	1.6	1.05	0.45	0.35	0.246	0
C37	1.2	0.5	2030	2.8	8	1.6	1.05	0.45	0.35	0.2665	0
C38	1.2	0.5	2030	2.8	8	1.6	1.05	0.45	0.35	0.2665	0
C39	1.2	0.5	4050	5.6	8	6.3	1.05	0.45	0.35	0.3198	0
C40	1.2	0.5	760	7.5	3	1.6	1.05	0.6	0.35	0.3444	0
C41	1.2	0.5	2030	2.8	8	1.6	1.05	0.6	0.35	0.287	0
C42	1.2	0.5	4050	5.6	8	6.3	1.05	0.6	0.35	0.2665	0
C43	1.2	0.5	4050	5.6	8	6.3	1.05	0.3	0.35	0.328	45
C44	1.2	0.5	760	7.5	3	1.6	1.05	0.3	0.35	0.5945	0
C45	1.2	0.5	760	7.5	3	1.6	1.05	0.3	0.35	0.1517	0

Table 3.5 Experimental conditions for jet tests in circular arrangement

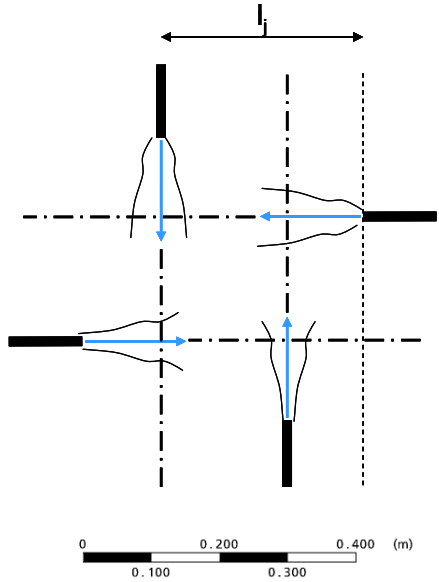

Figure 3.18 Schematic top view of the circular jet configuration. Each jet points to the location on the axis of its neighboring jet where the transition zone starts.

Figure 3.19 Circular jet arrangement in front of the front wall with the water intake in the front wall.

3.5.3.2 Linear jet arrangement (L series)

Four jets were installed along a line parallel to the front wall. All of the four jets pointed towards the front wall. The lateral distance between the jets was 0.2 *m*, and the set was installed at mid-width of the tank. Their height over bottom was always 0.1 *m*.

First, three experiments with a jet direction angle $\theta = 45°$ to the horizontal (L1 – L3) were carried out, and thereafter, three experiments with $\theta = 0°$ (L4 – L4), with the other geometrical parameters remaining constant. In subsequent two experiments (L7 – L8) the distance between the jets and the front wall was varied, with $\theta = 45°$. Parameter variations are given in Table 3.6.

Results are discussed in sub-chapters 4.7 and 4.9.

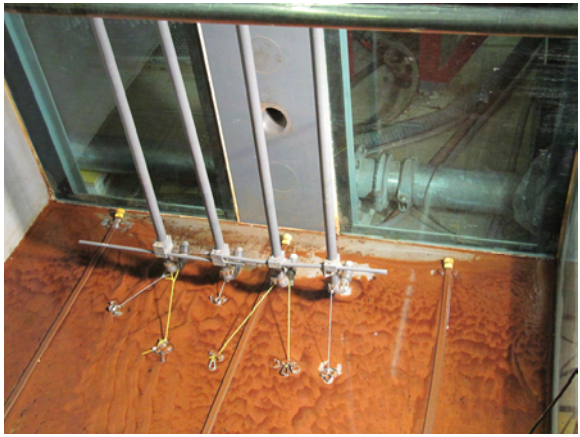

Figure 3.20 Linear jet arrangement with four jets pointing to the front wall after an experiment.

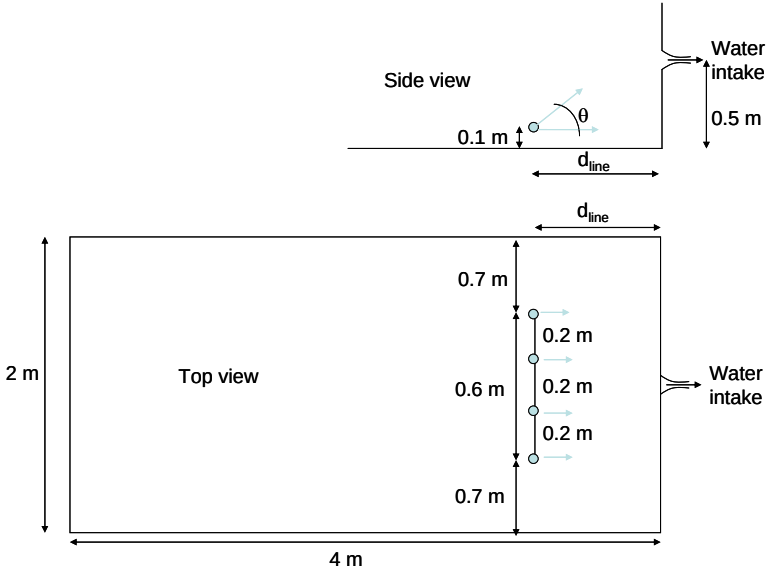

Figure 3.21 Schematic view of the linear jet arrangement.

Exp	*h*	h_i	Q_{out}	v_j	d_j	$M_j .10^{-3}$	d_{line}	θ	$c_{s,init}$
[-]	*[m]*	*[m]*	*[l/s]*	*[m/s]*	*[mm]*	*[m^4/s^2]*	*[m]*	*[°]*	*[g/l]*
L1	*1.2*	*0.5*	*1.125*	*5.60*	*8*	*6.29*	*0.4*	*45*	*0.287*
L2	*1.2*	*0.5*	*0.564*	*2.80*	*8*	*1.58*	*0.4*	*45*	*0.3239*
L3	*1.2*	*0.5*	*0.211*	*7.47*	*3*	*1.58*	*0.4*	*45*	*0.2952*
L4	*1.2*	*0.5*	*1.125*	*5.60*	*8*	*6.29*	*0.4*	*0*	*0.25625*
L5	*1.2*	*0.5*	*0.564*	*2.80*	*8*	*1.58*	*0.4*	*0*	*0.2788*
L6	*1.2*	*0.5*	*0.211*	*7.47*	*3*	*1.58*	*0.4*	*0*	*0.2624*
L7	*1.2*	*0.5*	*1.125*	*5.60*	*8*	*6.29*	*0.6*	*45*	*0.2788*
L8	*1.2*	*0.5*	*1.125*	*5.60*	*8*	*6.29*	*0.2*	*45*	*0.2665*

Table 3.6 Experimental conditions for tests with jets pointing to the front wall

3.6 Experimental procedure

3.6.1 Experiment preparation

At first, a liquid water-sediment mixture consisting of 3 *kg* of ground walnut shells and around 16 *l* of tap water was spread on the bottom of the experimental tank. Thereafter, the tank was slowly filled with laboratory water from the back wall, while pressurized air (approx. $6 \cdot 10^5$ *Pa*) is continuously blown out of the irrigation pipes creating a strong whirling pool flow condition. The bubbles and the circulation induced by them have the effect of maintaining the sediments in suspension. The filling process took around 1.5 hours. Once the tank was filled up to the selected water level, and a nearly homogeneous mixture existed in the whole tank. The pressurized air was then interrupted, the water intake opened and the experiment started at $t = 0$ *s*. The homogenised sediment-water mixture represents the simplified situation existing in the reservoir close to the dam, when turbidity currents have reached the dam area and right before their sediments start settling (muddy lake, section 1.1.5).

In case of an experiment employing jets, the jets were put in operation a few minutes before the experiments started. This measure allowed installing equal discharge to the four jets preliminarily to the beginning of the experiment.

With the chosen mixing process based on air bubbles the initial suspended sediment concentration at the start of the experiment was not consistently identical in spite of the equal feed charge in every experiment (3 *kg* of ground walnut shells). As a result the initial suspended sediment concentration was noted and subsequently used for calibration.

3.6.2 Experimental run

During all the experiments a constant water level was maintained. This means that the water discharge evacuated through the water intake corresponded, depending on the experiment

type, either to the total jet discharge or, in case of no jets, to the compensating clear water discharge flowing into the upper part of the tank.

Concerning jet experiments all four jets had the same jet diameter. The jet configuration and the jet diameters could not be changed during an experiment.

Most of the experiments lasted for four hours. This duration has been chosen from a preliminary experiment (3.5.1). In this pure settling experiment with no inflow and no outflow the highest suspended sediment concentration drop was registered within the first four hours. After this period, suspended sediment concentration changes became moderate.

Since the discharges were constant during an experiment, the experiment reaches after a while steady state with respect to flow circulation. Regarding the sediments behaviour, the experiment has transient character.

4 Experimental results and analysis

4.1 Outline of the chapter

As mentioned in the introduction (chapter 1) the main purpose of the study is to quantify the amount of fine sediments which can be evacuated from the reservoir by creating turbulence, i.e. a rotational flow in front of the dam by the means of jets. In this chapter, the effect of two different jet arrangements creating an artificial turbulence is discussed and compared to the case where no jets are used.

Before starting the jet experiment series, the duration of the experiments is chosen based on sediment settling investigations in the absence of any current. Subsequently, some general observations on turbidity measurements when using jets are analysed. The evolution of the suspended sediment distribution within the experimental tank when employing jets is discussed.

The experiments started with a quasi homogeneous suspended sediment concentration, simulating the presence of a muddy layer in front of the dam induced by a turbidity current.

By comparing the sediment amount evacuated during the experiment with the initially added amount, the sediment release resulting from the current test conditions is quantified. This ratio can be adopted for experiments with or without jets.

The influence of the parameters describing the jet arrangements as well as the influence of the jet discharge is discussed. Also, the respective flow patterns are analysed in order to understand and explain the different results.

A comparison of the laboratory results with idealized test conditions (no settling and perfectly homogeneous suspended sediment distribution) reveals that with any jet configuration the process to achieve a steady circulation needs a certain time. A transient starting phase is observed where sediment is settled on the bottom. Once steady conditions are established, sediment is resuspended and the suspended sediment distribution becomes homogeneous. In other words, the present test conditions are approaching idealized test conditions.

4.2 Turbidity measurements

4.2.1 Sediment settling experiment and choice of experiment duration

The knowledge about the sediment settling behaviour of the crushed walnut shells is fundamental for the following analysis. Therefore, a preliminary experiment in the tank with no out- and no inflow was conducted. Suspended sediment concentration was measured at two different positions: at 0.25 and 0.375 normalized height over bottom (z/B).

Figure 4.1 shows the with the initial concentration normalized sediment concentration (*SSC*) evolution as a function of time. It can be seen that during the first hour the sediment concentration decreases from the starting value defined as unity to approximately 0.4. After this period until the duration of four hours, the suspended sediment concentration decreases with a reduced rate. After these first 4 hours, the sediment concentration decreases very slowly and with an almost constant rate, without ever reaching the value zero within the observed time period of 178 hours. This can be explained by the non uniform grain size distribution, when a grain sorting process occurs. The smaller grains keep staying in a sort of a cloud, where the gravity force of an individual grain equalizes the viscosity effects in its surroundings. Due to the strong sediment concentration decrease limited within the first 4 hours of the experiment, this period is chosen as reference period of the subsequent experiments.

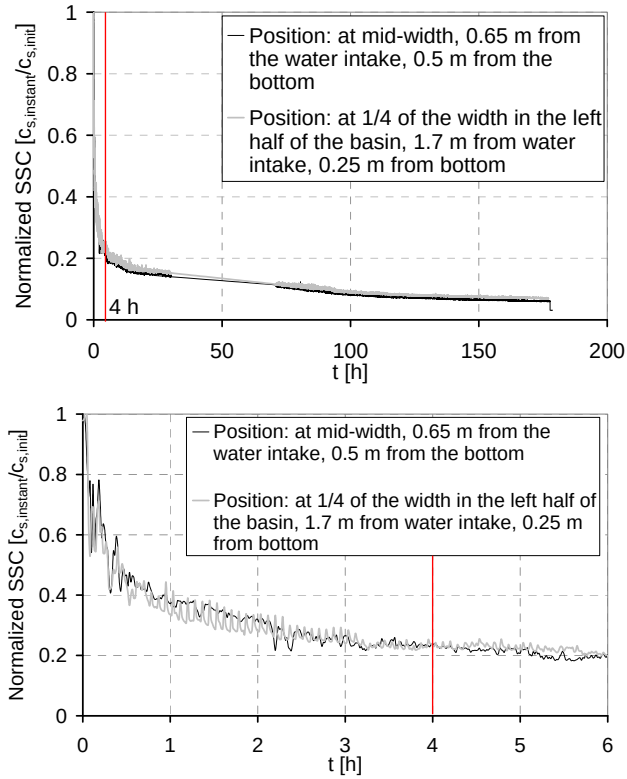

Figure 4.1. Normalized sediment concentration on two different levels (0.5 and 0.2 m above bottom), top: during a preliminary experiment lasting 178 hours, bottom: during the first 6 hours. Normalization of $c_{s,instant}$, the instantaneously measured sediment concentration, with $c_{s,init}$, the initial sediment concentration.

4.2.2 Suspended sediment concentration measurements

As mentioned in section 3.1.3.2, turbidity was measured during the subsequent regular experiments at two different positions:

- within the experimental tank itself
- in the outlet dissipation tank

In each tank one turbidity sensor was installed.

4.2.2.1 Suspended sediment concentration measured within the experimental tank

The sensor in the experimental tank was sporadically moved in order to provide point measurements at different positions. Measurements were taken on the horizontal axis of the water intake (at a distance of 0.25, 0.45, 0.65, 0.75, 0.85, 0.95 and 1.00 *m* from the front wall) and on the rotational (vertical) axis of the jet configurations (on levels 0.10, 0.20, 0.30, 0.40, 0.50, 0.75 and 1.00 *m* above the bottom).

These point measurements give an indication on the turbidity distribution within the tank as well as on the turbidity time evolution at a certain point. They give a cross-check of both suspended sediment concentration registrations (in the experimental and the dissipation tank).

The jet configurations of the experiments C1 to C3 as well as C5 and C6 (Table 3.5) were analysed to assess homogeneity of the turbidity, and the standard deviation of all normalized records on the horizontal as well as on the vertical axis were drawn as a function of time (Figure 4.2). The standard deviation decreases rapidly within the first experimental hour. After roughly two hours it is below 0.02. This observation indicates that a high degree of homogeneity was reached and that mixing was effective. The same conclusion can be drawn from *Figure 4.3* to Figure 4.8 where the normalized suspended sediment concentration at the different measurement positions on the vertical axis is shown for different times. It appears that mixing with air bubbles during filling was less effective than jet mixing: in the first minutes of the experiments suspended sediment concentration is visibly higher at the bottom of the tank, and tends to be lower close to the water surface. This gravity forced distribution is less accentuated and turbidity is more equilibrated by the end of the four hours of experiment duration.

Figure 4.3 to Figure 4.8 illustrate that the suspended sediment concentration is decreasing with time. The tendency can be seen that with higher discharge out of the tank (as well as higher jet discharge) suspended sediment concentration decreases faster.

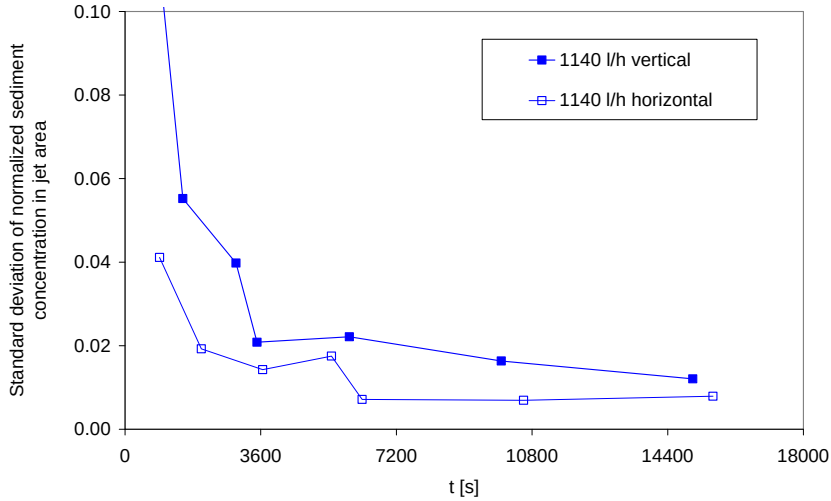

Figure 4.2 *Standard deviation of the normalized sediment concentration registered near the jet area. Exact measurement positions are given in section 3.1.3.2. As the standard deviation of the measurements decreases with time, turbidity tends to be homogeneous in the whole area.*

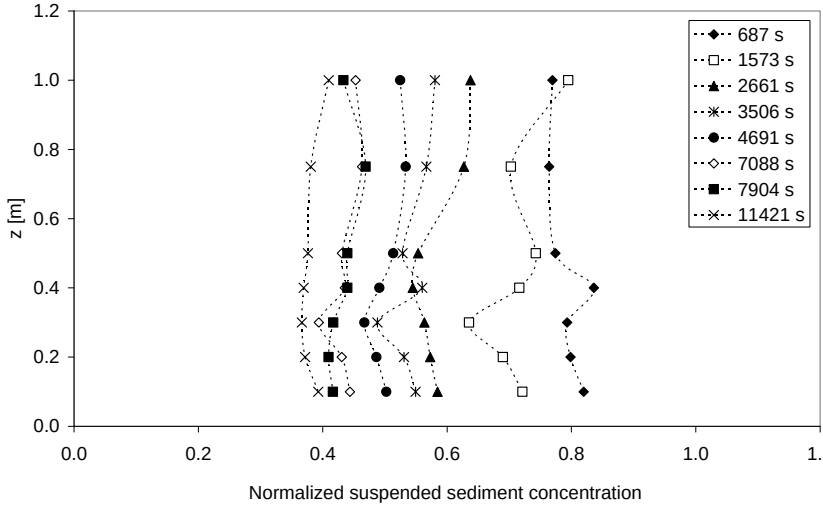

Figure 4.3 Normalized suspended sediment concentration SSC as a function of time at different positions z on the vertical axis in the experiment C1, $Q_{out} = \Sigma Q_j = 570$ l/h

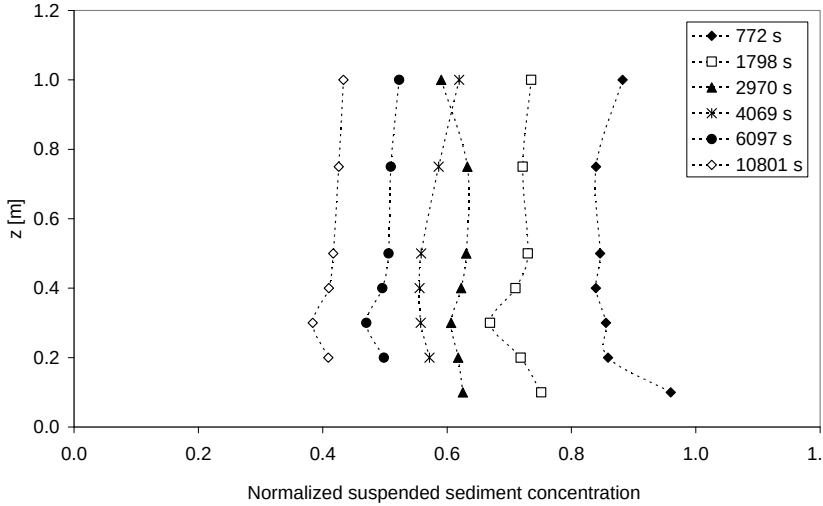

Figure 4.4 Normalized suspended sediment concentration SSC as a function of time at different positions z on the vertical axis in the experiment C2, $Q_{out} = \Sigma Q_j = 760$ l/h

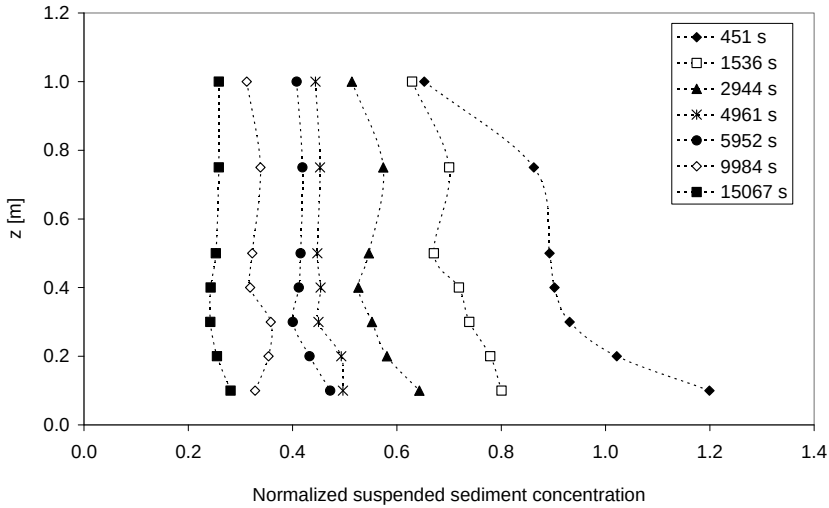

Figure 4.5 Normalized suspended sediment concentration SSC as a function of time at different positions z on the vertical axis in the experiment C3, $Q_{out} = \Sigma Q_j$ = 1140 l/h

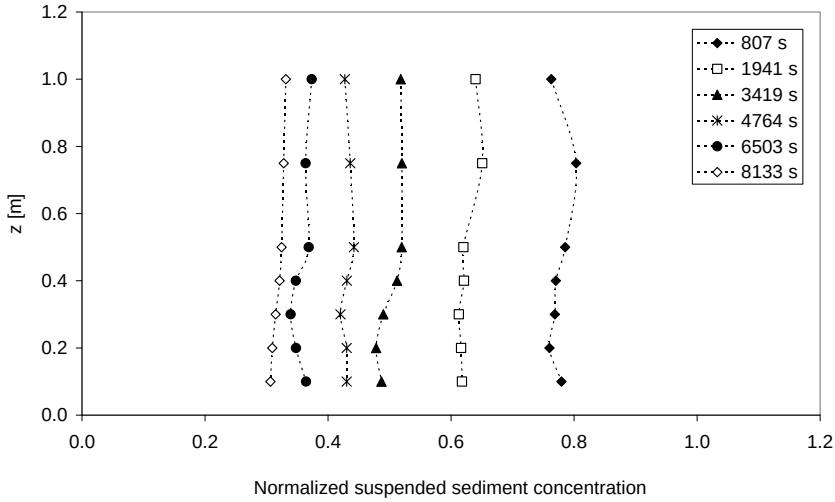

Figure 4.6 Normalized suspended sediment concentration SSC as a function of time at different positions z on the vertical axis in the experiment C5, $Q_{out} = \Sigma Q_j$ = 3040 l/h

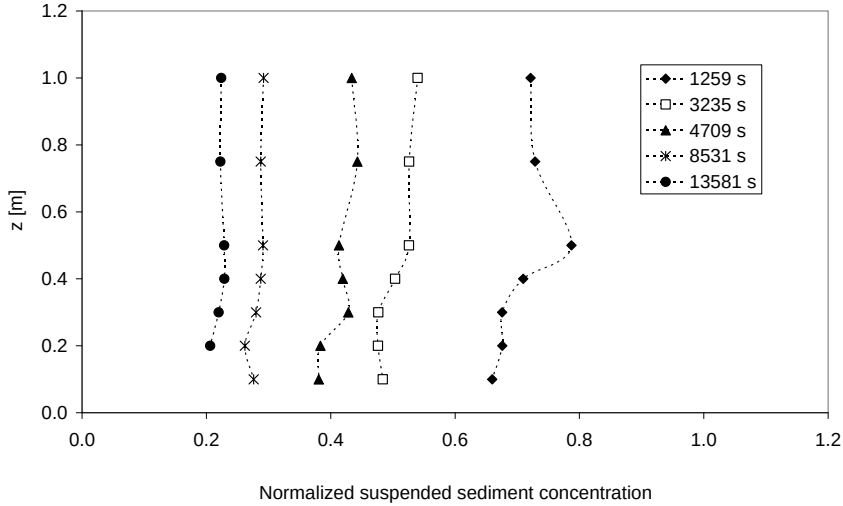

Figure 4.7 Normalized suspended sediment concentration SSC as a function of time at different positions z on the vertical axis in the experiment C6, $Q_{out} = \Sigma Q_j$ = 4050 l/h

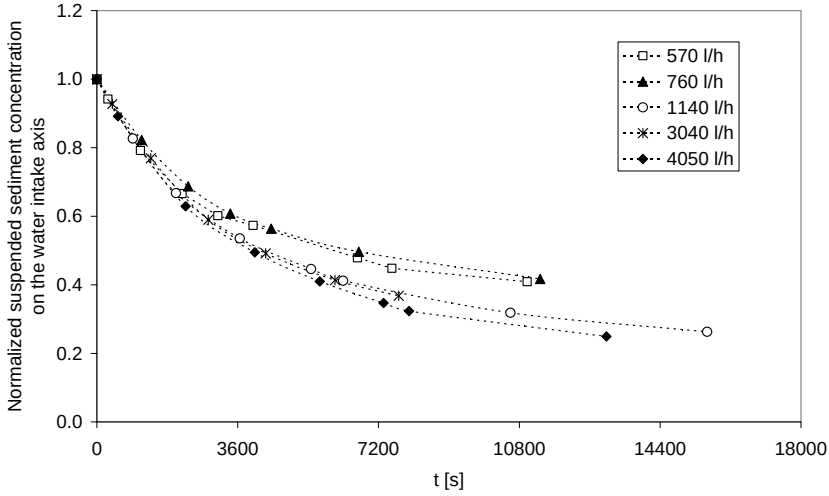

Figure 4.8 Normalized suspended sediment concentration within the experimental tank measured and averaged over the axis through the water intake as a function of time for five different discharges.

4.2.2.2 Suspended sediment concentration measured in the dissipation tank

The evacuated sediments are released through a pipe into the dissipation tank. The turbidity sensor in the dissipation tank is positioned such that its probe volume is situated within the turbulent jet entering this tank.

Furthermore, from what has been observed in the previous section (4.2.2.1), quasi complete sediment concentration homogeneity (within the front part of the lower part of the experimental tank) can be assumed.

These are two reasons why consequently the sediment concentration of the outflowing discharge through the water intake is misleadingly expected to be identical with a slight discrepancy due to the time lag initiated by the transit time through the pipe. But as Figure 4.9 shows the two measurements are slightly delayed in time. The differences can be explained as follows.

At the beginning of the experiment the dissipation tank was filled with clear water up to the level of the down-tip of the V-notched weir. Measuring turbidity of clear water the records in the dissipation tank start with a value close to zero. As time goes on, turbidity increases quite quickly. Despite its position the sensor actually measures the turbidity of a mixture and not just the turbidity of the inflowing jet. This mixture consists of an instantaneously incoming and already present water-sediment mixture. In spite of the turbulence generated by the submerged jet originating from the water intake the sediment distribution in the dissipation tank is hardly homogeneous.

Moreover, during the experiment a small, but non-defined part of the sediment is retained in the dissipation tank while the other part is continuously evacuated over the V-notched weir. The time to peak of the measurements registered in the dissipation tank is somehow related to its mean residence time as well as to its retention ratio during the experiment. Residence time and retention depend on both the dissipation tank volume and the water intake discharge. Retention depends on the evacuated sediment concentration also. The complexity of these three factors, their dependencies and the fact that the concentration in the experimental tank is not perfectly homogeneous, are the reasons why there is no shortcut to simply correlate the two normalized suspended sediment concentration measurements as a function of time. Therefore, turbidity within the experimental tank can hardly be reconstructed from the measurements registered in the dissipation tank.

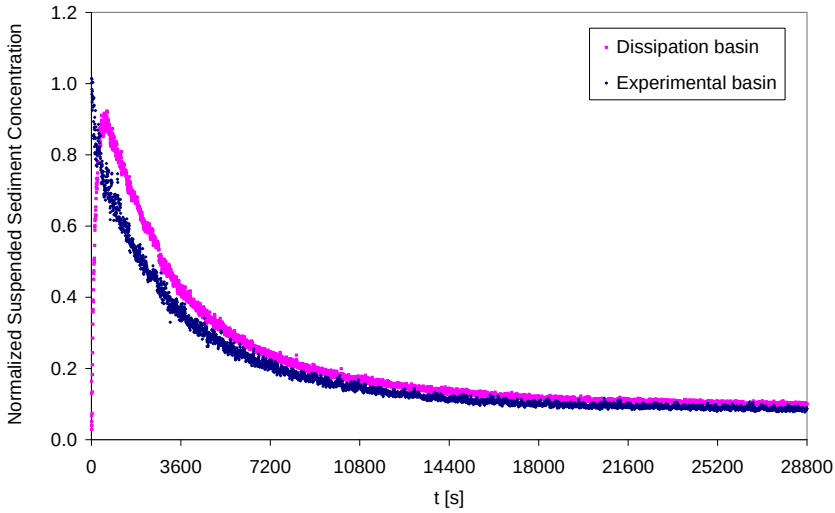

Figure 4.9 *Normalized SSC values measured inside and outside of the experimental tank during the experiment C7 (Q_{out} = ΣQ_j = 4050 l/h, off-bottom clearance C/B = 0.175, distance between jet circle axis and front wall d_{axis}/B = 0.525, distance between two neighboring jets l_j/B = 0.15, water intake height h_i/B = 0.25).*

4.3 Dimensional analysis

Using a dimensional analysis, the ratio of evacuated sediment to its maximum value (P_{out}/P_{in}) can be expressed as:

$$\frac{P_{out}}{P_{in}} = \phi\left(geometrical\ \ parameters,\ jet\ characteristics, tank\ dimensions, t, w_s, c_{s,i}\right) \qquad (Eq.\ 4.1)$$

The geometrical arrangement parameters are outlined in section 3.5.3, the jet characteristics are summarized in section 3.4.2, the tank dimensions are the width *B* and length *L*.

Since always one single geometrical arrangement parameter was varied, the inter-dependence of these parameters was not comprehensively grasped and a non-dimensionalisation based on one of these doesn't make sense.

The jet characteristic d_j (nozzle diameter) and the jet momentum M_j themselves did not have any influence on the sediment outflow. The densimetric jet Froude number Fr_j has no relevance since the density difference between the sediment laden water within the experimental tank and the clear water jets is negligible. Since viscosity effects can be neglected, the Reynolds numbers Re_s and Re_j didn't influence the sediment outflow either.

The settling velocity w_s as well as the tank dimensions (*B* and *L*) was kept constant.

Nevertheless, in the research field of impeller stirred suspension the tank diameter is taken as normalizing basic dimension. Since the findings of the present study are strongly related with

the ones of this research field, accordingly, the tank width B was taken as reference dimension for non-dimensionalizing lengths.

The evacuated sediment ratio is then expressed as in section 4.4.

4.4 Sediment evacuation efficiency

In order to compare and evaluate the different experiments and to identify the most efficient jet configuration composed by the optimal parameter combination, the evacuated sediment ratio was determined. This ratio is defined as the evacuated sediment weight P_{out} divided by the sediment weight initially added to the tank P_{in} (3 kg dry sediment, Eq. 4.2 and 4.3). It represents the normalized temporal integral of the released sediment amount. The evacuated sediment ratio helps in quantifying the sediment evacuation efficiency.

$$ESR = P_{out} / P_{in} \qquad (Eq.\ 4.2)$$

$$ESR = \frac{P_{out}}{P_{in}} = \frac{\sum c_{s,i}\left[g/l\right] \cdot Q_{out}\left[l/s\right] \cdot \Delta t\left[s\right]}{P_{s,in}\left[g\right]} \qquad (Eq.\ 4.3)$$

where $\sum c_{s,i}$ is the integrated suspended sediment concentration measurements recorded in intervals of Δt (mostly equal to 5 seconds). Q_{out} is the discharge released through the water intake.

The evacuated sediment ratio for $Q_{out} = \Sigma Q_j = 3040\ l/h$ is shown in Figure 4.10 for an experiment duration of four hours.

The highest evacuated sediment ratio (respecting test conditions) can theoretically be achieved when assuming no sediment settling and homogeneous suspended sediment concentration in the experimental tank (section 4.8.2). Figure 4.10 depicts a difference between the theoretically idealized and the measured evacuated sediment ratio when employing jets. The conditions related to the theoretically idealized sediment release are presented in section 4.8.2.2.

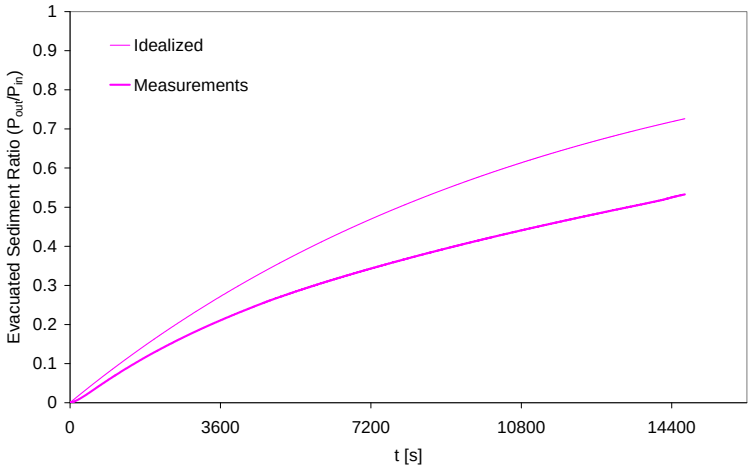

Figure 4.10 *Evacuated sediment ratio calculated for the experiment C5 with $Q_{out} = \Sigma Q_j$ = 3040 l/h. Comparison between the evacuated sediment ratio as a function of time based on the turbidity measurements (bold line) and the evacuated sediment ratio calculated for theoretically completely homogeneous suspended sediment concentration within the experimental tank and no settling (fine line).*

4.5 Experiments without jets

4.5.1 Outline of subchapter

A first series of experiments was carried out without jets. The sediment load evacuated through the water intake was examined while the outflowing water was continuously replaced by clear water through the back wall as presented in section 3.5.2. The resulting flow pattern is almost stagnant and not suitable for velocity measurements. In this subchapter, the influence of the evacuated discharge on the evacuated sediment load as well as on the settling behavior is investigated.

4.5.2 Sediment release without jets

Figure 4.11 depicts the evacuated sediment ratio *ESR* as a quasi linear function of the evacuated discharge through the water intake. Such linear relationship is not surprising in the presence of equal suspended sediment concentration in front of the water intake. A higher discharge evacuates a proportionally higher sediment load.

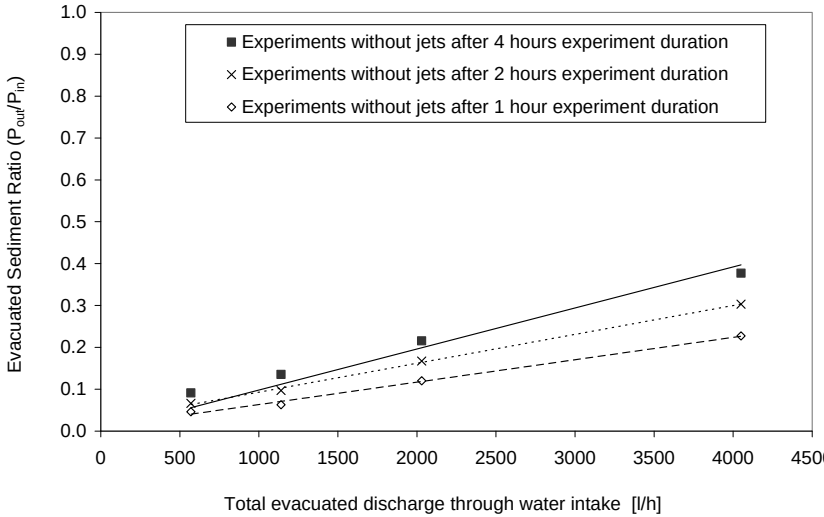

Figure 4.11 Evacuated sediment ratio ESR as a function of the evacuated discharge through the water intake shown for the reference experiments R1 to R6 (water intake height $h_i/B = 0.25$).

Figure 4.12 illustrates a strong increase of the evacuated sediment ratio in the first experimental hour. After this time the increase becomes smaller and nearly constant. Figure 4.13 to Figure 4.16 underline this statement showing the evacuated sediment ratio rate as a function of time. A very similar observation was also described in section 4.2.1 where the suspended sediment concentration within the experimental tank was measured (Figure 4.1). If no mixing takes place in the experimental tank, the suspended sediment concentration is significantly decreasing during the first hour due to sediment settling. As a consequence, less sediment is evacuated per time. Between one and four hours duration, the suspended sediment concentration is decreasing more slowly. After four hours its decrease is even more reduced. The sediment release is strongly driven by this evolution.

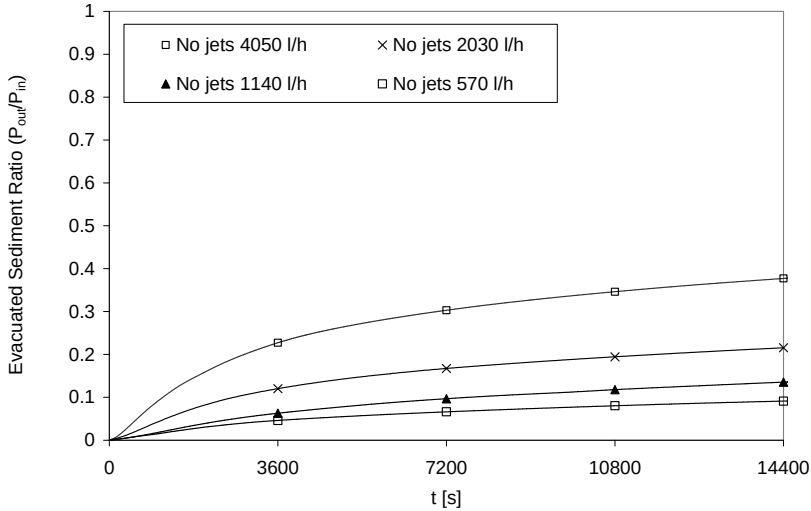

Figure 4.12 Evacuated sediment ratio as a function of time for the different investigated evacuated discharges in experiments without jets.

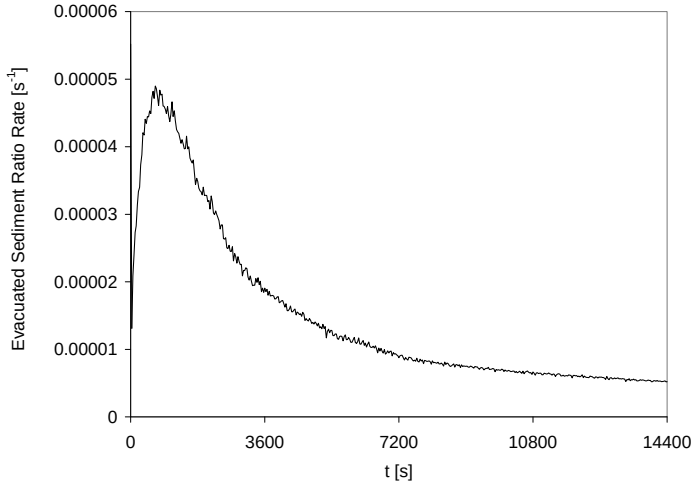

Figure 4.13 Evacuated sediment ratio rate as a function of time for the experiment without jets R3 (Q_{out} = 2030 l/h). The reason why the evacuated sediment ratio rate increases at the start is explained in detail in section 4.2.2.

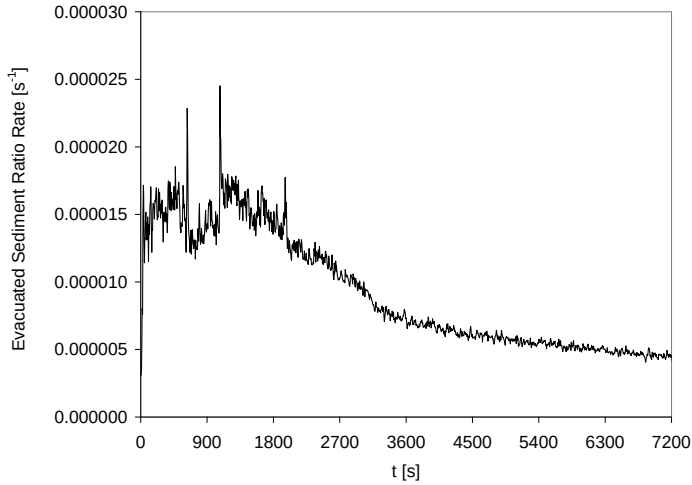

Figure 4.14 *Evacuated sediment ratio rate as a function of time for experiment without jets R1 (Q_{out} = 570 l/h). The reason why the evacuated sediment ratio rate increases at the start is explained in detail in section 4.2.2.*

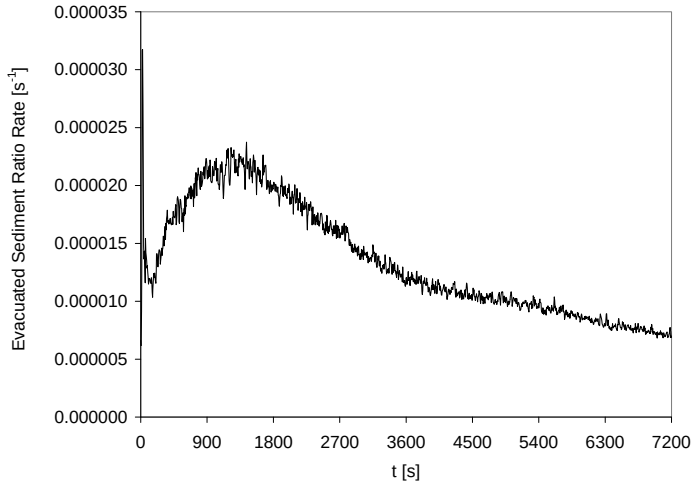

Figure 4.15 *Evacuated sediment ratio rate as a function of time for the experiment without jets R2 (Q_{out} =1140 l/h). The reason why the evacuated sediment ratio rate increases at the start is explained in detail in section 4.2.2.*

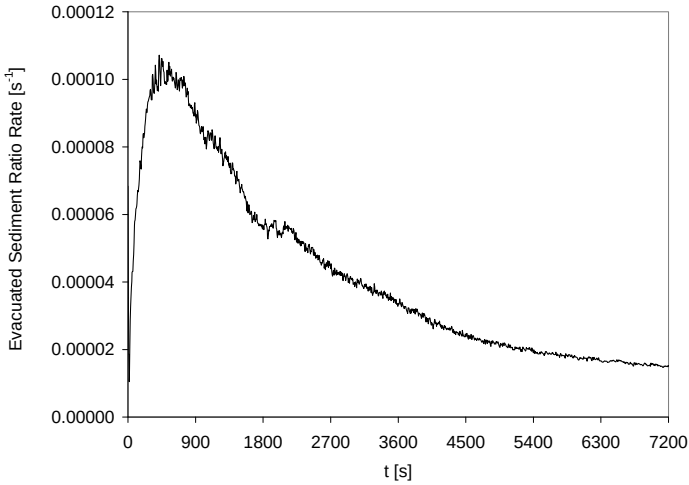

Figure 4.16 Evacuated sediment ratio rate as a function of time for the experiment without jets R4 (Q_{out} = 4050 l/h). The reason why the evacuated sediment ratio rate increases at the start is explained in detail in section 4.2.2.

4.5.3 Settled sediment without jets

As mentioned in section 4.2.2 two turbidity measurements at two different locations were executed: the suspended sediment measurements within the experimental tank and the evacuated sediment measurements in the dissipation tank. The sum of the three normalized evacuated, suspended and settled sediments must be unity. Thus, with the availability of the aforementioned measurements, the settled sediment ratio can easily be derived.

Nevertheless, there is an uncertainty concerning the measurement of the suspended sediment concentration. In all the experiments without jets the sensor was positioned at one location only. Nevertheless, in the experiments without jets, the concentration can be non-homogeneous due to gravity forced sediment settling and vary therefore from the water surface to the bottom. The tank volume is only weakly mixed by the current from the back wall. Consequently, if the sensor was positioned in the top area of the water column, it measured rather low concentrations, whereas close to the bottom it is certainly higher than the average concentration. Thus, if calculating the settled sediments by the aforementioned sum, taking into account a suspended sediment concentration measurement at one single position, the so established settled sediment ratio might be biased and should be carefully used.

In Figure 4.17 the three fractions established from the measurements are shown as a function of normalized time for a discharge of Q_{out} = 4050 *l/h*. The part above the upper thin line represents the evacuated sediment ratio, while below it is the ratio of the sediments remaining in the experimental tank. The remaining sediments are split by the lower thin line into the suspended (upper part) and the settled sediment ratios (lower part) respectively. Time is

normalized by the mean residence time, which is defined as the quotient of the water volume in the experimental tank divided by the discharge Q_{out}. Stefan and Gu (1992) used for their mixing time correlation the same dimensionless time t/τ_m.

Figure 4.17 shows that the evacuated and settled sediment ratios have asymptotic behaviour, while the suspended sediment ratio is continuously decreasing and tending to zero. From the available measurements of four hours duration it seems that, if test conditions are maintained, the settled sediment is not going to be resuspended and its ratio will in this example (Q_{out} = 4050 *l/h*) reach a magnitude close to 0.6. Consequently, the maximum evacuated sediment ratio is expected to be smaller than 1, and in the present case close to 0.4.

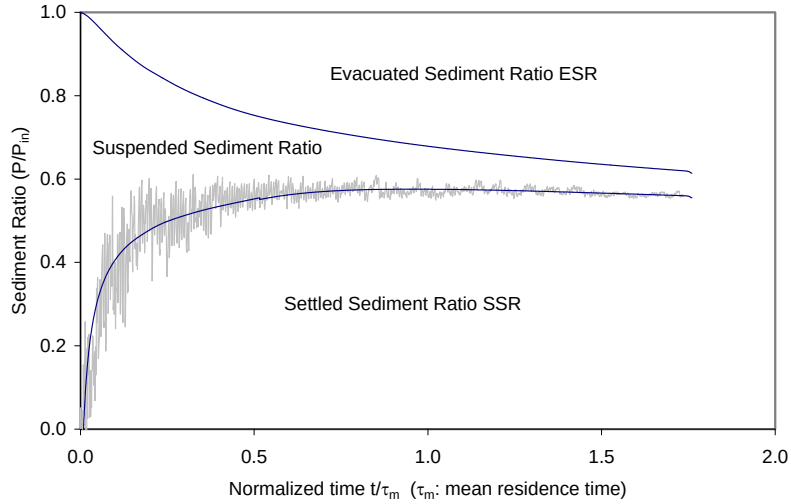

Figure 4.17 Evacuated, suspended and settled sediment ratios as a function of normalized time with a discharge Q_{out} = 4050 l/h and without jets. The part above the upper thin line represents the evacuated sediment ratio, while below it is the ratio of the sediments remaining in the experimental tank. The latter part can be split into the suspended and the settled sediment ratios. The separation is represented by the lower thin line, below which is the settled and above which is the ratio of suspended sediment.

4.5.4 Long term evolution of sediment release

The evacuated sediment ratio rate (Figure 4.13 to Figure 4.16) reveals that the largest amount is evacuated during the first hour. When assuming a flow field only influenced by the outflow through the water intake, an inflow from the back wall and a quasi homogeneous sediment concentration at the experiment start, the peak at the beginning is explained by the entrainment of the sediment close to the water intake. From the vicinity of the water intake sediment of all grain sizes is entrained. Later, the lighter sediment particles from further away are driven to the water intake by, on one hand, the settling velocity, and on the other hand, the potential flow

generated by the water intake and the flow from the back wall. The heavier grains are settling towards the bottom.

Assuming that the trajectory of a sediment particle is only determined by the flow field induced by the water intake discharge and by the current from the back wall as well as by the settling velocity, the longest possible trajectory from the water surface to the water intake can be calculated and is shown in Figure 4.18 for three different settling velocities: w_s = 0.8, 0.2, and 0.04 *mm/s*. According to Stokes the settling velocity of a particle of diameter d_s = 0.06 *mm* in water of 17°C is w_s = 0.8 *mm/s*. The settling velocity w_s = 0.2 *mm/s* corresponds to a diameter of d_s = 0.03 *mm* and w_s = 0.04 *mm/s* to a particle diameter of d_s = 0.013 *mm*. As presented in section 3.4.1.2 d_s = 0.06 *mm* is the average diameter (60 *%* of the grains), d_s = 0.03 *mm* represents 30 *%* and d_s = 0.013 *mm* 10 *%* of the grains.

The flow velocity field generated by the discharge approaching the water intake can be assumed as potential flow and is, hence, radial towards the water intake. With decreasing radial distance r_i of the particle from the water intake, the magnitude of the velocity v_a increases with inverse proportion to the square of the distance r_i (Equation 4.4).

$$v_a = \frac{Q_{out}}{2\Pi r_i^{\,2}} \qquad (Eq.\ 4.4)$$

The flow velocity through the back wall v_b is defined by the discharge Q_{out} and the wetted surface B_0 (Equation 4.5).

$$v_b = \frac{Q_{out}}{B_0} \qquad (Eq.\ 4.5)$$

The calculation of the sediment trajectory is done iteratively as follows:

Position in the horizontal *x*-coordinate:

$$x_{i+1} = x_i + \max(v_b, v_a \cos\beta \cdot \Delta t) \qquad (Eq.\ 4.6)$$

$$\text{with } v_a = \frac{Q_{out}}{2\Pi\left(x_i^{\,2} + z_i^{\,2}\right)} \qquad (Eq.\ 4.7)$$

and β being the angle between the line joining the position (x_i, z_i) with the water intake, and the horizontal plane:

$$\beta = \arctan\frac{z_i}{x_i} \qquad (Eq.\ 4.8)$$

The iteration time step is expressed by Δt.

Position in the vertical *z*-coordinate:

$$z_{i+1} = z_i + \left(v_a \sin\alpha + w_s\right) \cdot \Delta t \qquad (Eq.\ 4.9)$$

Since the bottom roughness is neglected, in this simplified model even a sediment particle initially staying in the farthest lower corner could reach the water intake. In order to provide more realistic trajectories and to take into account bottom roughness the longest trajectories

were chosen such that the particles were allowed to touch shortly upon the bottom but not to settle down and drag along the bottom.

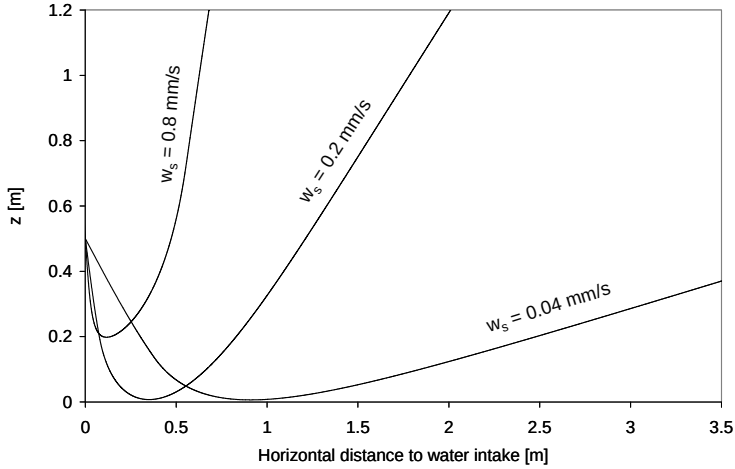

Figure 4.18 Longest possible trajectory from the water surface to the water intake for Q = 2030 l/h and for three different settling velocities: w_s = 0.8 mm/s (d_{60} = 0.06 mm), w_s = 0.2 mm/s (d_{30} = 0.03 mm), and w_s = 0.04 mm/s (d_{10} = 0.013 mm). Water intake is located on z = 0.50 m.

A high amount of the particles contained in the half volume of revolution limited by the boundary determined by the longest trajectory of the particle d_{60} is expected to reach the water intake. From the particles contained in the half volume of revolution between the longest trajectories corresponding to d_{30} and d_{60}, 30 % of the grain spectrum are expected to reach the water intake. A 20 % of the grains contained in the half volume of revolution between the longest trajectories corresponding to d_{30} and d_{10}, respectively, will probably reach the water intake. The time to travel from the farthest position to the water intake corresponding to d_{10} varies with the discharge as follows (Table 4.1):

Q_{out} [l/h]	Travel time from farthest position to water intake [h]	Calculated sediment weight [kg]	Calculated ESR	Measured ESR
570	11	0.34	0.11	0.09
1140	6.9	0.47	0.155	0.136
2030	3.9	0.64	0.216	0.214
4050	2	1	0.28	0.37

Table 4.1 *Travel time from the farthest position to the water intake for d_{10} of the grain size distribution depending on the discharge. Calculated evacuated sediment weight, calculated and measured evacuated sediment ratio, calculated settled sediment ratio.*

The estimated water volumes for Q_{out} = 2030 *l/h* as a function of grain sizes is as follows:

d_{60}: $V_{60} = 0.73\ m^3$

d_{30}: $V_{30} = 3.30\ m^3$

d_{10}: $V_{10} = 7.28\ m^3$

It is assumed that from the volume V_{60} all sediment particles smaller than d_{60} are entrained into the water intake, means 60 % of the contained particles. This estimated water volume is the closest one to the water intake, and it was not more refined. Nevertheless, larger particles which are closer to the water intake than the longest estimated trajectory corresponding to d_{60} are also likely to be entrained. Therefore, 90 % of the particles contained in V_{60} are supposed to reach the water intake. Assuming that 30 % of V_{30} and 20 % of V_{10} are reaching the water intake, a total sediment weight of 0.64 *kg* is evacuated through the water intake, which corresponds to an evacuated sediment ratio of 0.214 (Table 4.1). This is equal to the measurements effectuated under the same test conditions (0.216 for t = 4 hours). The rest of the sediment (~ 78.5 %) is settled and will never be evacuated.

The same approach has been done for Q_{out} = 1140 *l/h* (Figure 4.20) and Q_{out} = 570 *l/h* (Figure 4.19). It was found that the estimated evacuated sediment ratio was in both cases higher than the measured one (14.5 % and 33 %, respectively). This can be explained by the following:

The experimental test duration was four hours. Within this period the farthest particle from the water intake didn't reach this for Q_{out} = 570 and 1140 *l/h* (Table 4.1). However, the previously established approach gives a final evacuated sediment ratio, for the case that all the sediments in the volumes defined by the longest trajectories have reached the water intake. This is the reason why the measured evacuated sediment ratio after four hours is smaller than the estimated final ratio. In the case of Q_{out} = 2030 *l/h*, the farthest particle needs 3.9 hours to travel which corresponds approximately to the experiment duration of four hours. The agreement between estimation and measurement is almost perfect.

In the case of the highest discharge (Q_{out} = 4050 *l/h*, Figure 4.21) the estimation is 9 % smaller than the measurements. The farthest located particle had theoretically reached the water intake

already after half of the experiment duration (approximately two hours). For comparison, the measured evacuated sediment ratio was after two hours 11 % higher and after three hours 3 % smaller than the estimated one.

There is a lack of measurements to definitely conclude if this difference is due to resuspension or if there is an error of 9 % in the previous estimation of the evacuated sediment ratio. According to the observation in section 3.2 the error for this magnitude of discharge (Q_{out} = 4050 *l/h*) is expected to be lower, namely approximately 0.35 %.

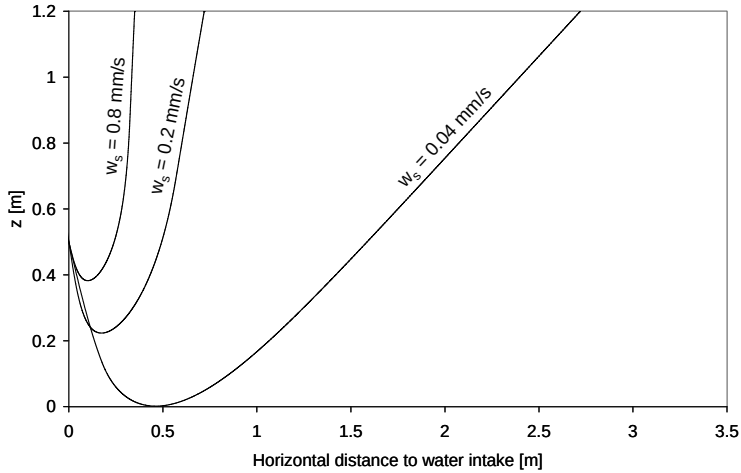

Figure 4.19 Longest possible trajectory from the water surface to the water intake for Q = 570 l/h and for three different settling velocities: w_s = 0.8 mm/s (d_{60} = 0.06 mm), w_s = 0.2 mm/s (d_{30} = 0.03 mm), and w_s = 0.04 mm/s (d_{10} = 0.013 mm). Water intake is located on z = 0.50 m.

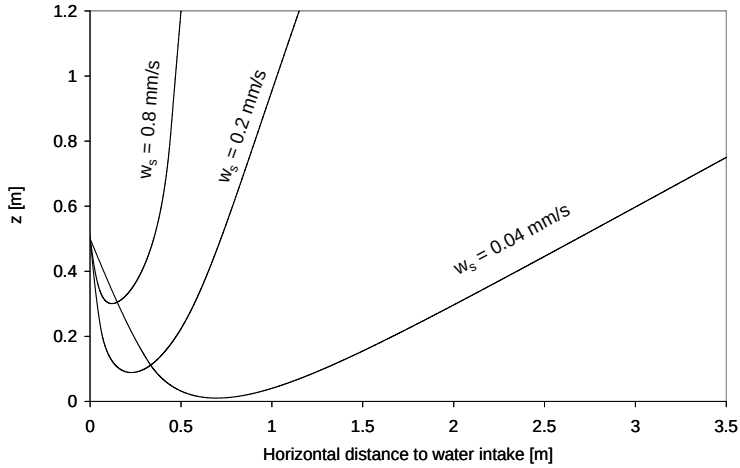

Figure 4.20 Longest possible trajectory from the water surface to the water intake for Q = 1140 l/h and for three different settling velocities: w_s = 0.8 mm/s (d_{60} = 0.06 mm), w_s = 0.2 mm/s (d_{30} = 0.03 mm), and w_s = 0.04 mm/s (d_{10} = 0.013 mm). Water intake is located on z = 0.50 m.

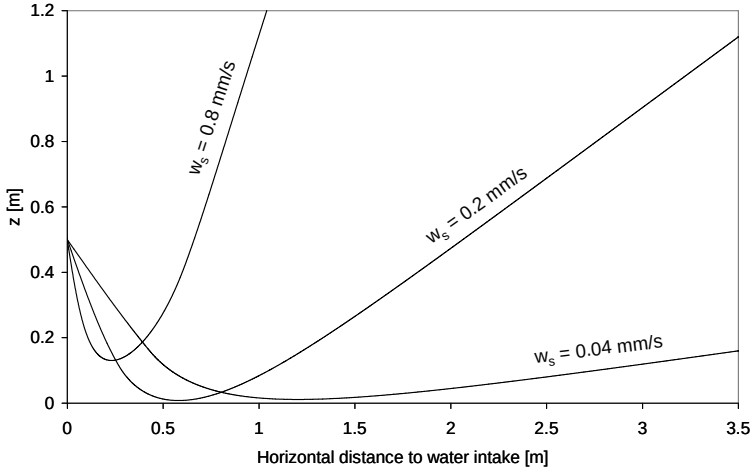

Figure 4.21 Longest possible trajectory from the water surface to the water intake for Q = 4050 l/h and for three different settling velocities: w_s = 0.8 mm/s (d_{60} = 0.06 mm), w_s = 0.2 mm/s (d_{30} = 0.03 mm), and w_s = 0.04 mm/s (d_{10} = 0.013 mm). Water intake is located on z = 0.50 m.

4.5.5 Concluding remarks on the long term evolution of sediment release without jets

The experiments revealed a quasi linear relation between the water discharge and the evacuated sediment ratio: the higher the discharge, the higher the evacuated sediment ratio.

By summing the evacuated and the suspended sediment ratios (both obtained from turbidity measurements) and subtracting this sum from unity, the settled sediment ratio can be quantified. Its evolution in time shows that no resuspension takes place.

For a constant discharge the evacuated sediment ratio as well as the settled sediment ratio is easily estimated by a physical approach taking the settling velocity, the potential velocity generated by the discharge through the water intake, and the homogeneously distributed velocity through the back wall into account. For the tested range of Q_{out} between 570 and 4050 *l/h*, and for the condition that the discharge flowing out equals the discharge flowing in, the final evacuated sediment ratio is between 0.09 and 0.37. Consequently, the settled sediment ratio is between 0.91 and 0.63.

4.6 Flow patterns with circular jet arrangements

4.6.1 Outline of subchapter

In section 3.1.3.1 the method and position of the Ultrasonic Velocity Profilers (UVP) was presented. The flow velocity measured by the UVP-sensors are useful for flow pattern analysis. The flow pattern gives local information about the circulation created by the jets. As reported in the literature, there are flow patterns which are more suitable for maintaining sediment in suspension in comparison with others. There is no such information available regarding sediment release.

In this section flow patterns are analyzed and the influence of different geometrical parameters is discussed by varying a single parameter while keeping the others constant like in the basic set (section 4.6.2, Table 4.2).

As mentioned in section 3.1.3.1 the longitudinal plane is located on the mid-width axis of the tank. The transversal plane is located perpendicularly to the longitudinal plane and passes through the jet circle centre.

In both vertical planes (transversal and longitudinal) flow velocity was measured from the bottom up to $z/B = 0.5$. Consequently, there is not the complete water height presented (except for a single experiment where the water height was $z/B = 0.5$). Moreover, in the transversal plane flow velocity was measured in the whole tank width, whereas in the longitudinal plane only the part between the water intake ($x/B = 0$) and $x/B = 1.75$ was measured.

There is a basic geometrical parameter set (Table 4.2) with which the highest number of different discharges was tested. These experiments are used like basic experiments and serve as comparison for all the others.

Each flow pattern is composed of two parts measured at two different instants. The time lag is approximately half an hour.

4.6.2 Flow patterns for basic geometrical parameters

In the experimental tank, the basic circular jet configuration is defined as follows (metric indication in model scale):

off-bottom clearance	$C = 0.35$ *m*	$C/B = 0.175$
distance between jet circle centre and front wall	$d_{axis} = 1.05$ *m*	$d_{axis}/B = 0.525$
distance between two neighbouring jets	$l_j = 0.30$ *m*	$l_j/B = 0.15$
water intake height	$h_i = 0.50$ *m*	$h_i/B = 0.25$
water height	$h = 1.20$ *m*	$h/B = 0.6$

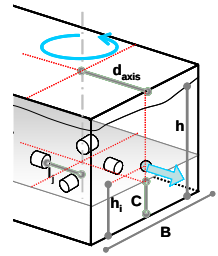

Table 4.2 Geometrical parameters of the basic circular jet configuration.

The measured flow pattern generated by the basic circular jet configuration is shown in Figure 4.22 (transversal plane), and Figure 4.23 (longitudinal plane) for $Q_{out} = \Sigma Q_j = 760$ *l/h*.

The transversal flow pattern (Figure 4.22) is similar to the one of a typical axial mixer where the fluid is parallel to the rotation axis and flow media is moving from the top to the bottom. There is one rotor core on each side, the two sides being measured at two different instants. Since the rotor cores are lying on a different level, they are supposed to move up and down.

Sharma and Shaikh (2003) reported that for the case of an axial impeller operation close to the tank base, the efficiency of energy transfer from impeller to particles is maximal. The particles trapped in the stagnant zone below the impeller is, therefore, easily transported to the corners with enough velocity to get suspended after sliding over the fillet[1].

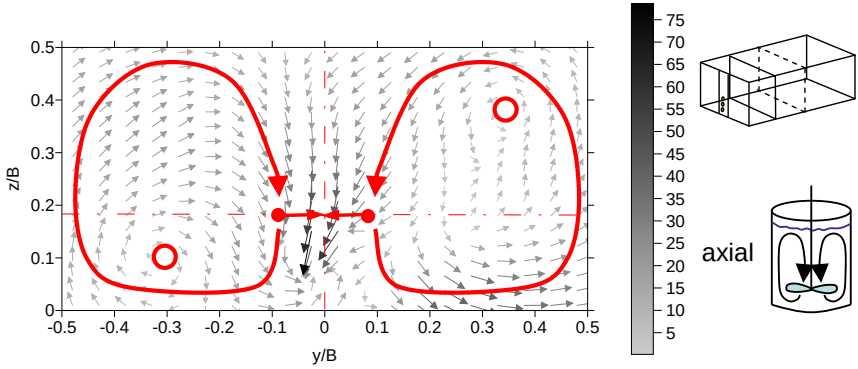

Figure 4.22 Velocity vectors [mm/s] in the transversal plane for off-bottom clearance $C/B = 0.175$, water intake height $h_i/B = 0.25$, distance between neighbouring jets $l_j/B = 0.15$, distance between jet circle centre and front wall $d_{axis}/B = 0.525$, water height $h/B = 0.6$, total jet discharge $\Sigma Q_j = Q_{out} = 760$ l/h. Axial flow pattern indicated by arrows, rotor cores indicated by circles.

[1] Stagnant zone at the corner junction filled up by deposited particles giving a rounding effect to the straight junction, called fillet (Sharma and Shaikh 2003)

The flow pattern in the longitudinal plane (Figure 4.23) shows two strong currents issuing from the jets. One is pointing to the front wall and part of it directly to the water intake. Close to the jets an eddy is formed beneath this current. The other current is directed to the rear part of the tank. It has a vertical component downwards. At approximately $x/B = 0.9$ a rotor core is formed on the level of the jet arrangement. This flow pattern is very similar to the one generated by a radial mixer.

The longitudinal flow pattern shows only the front part of the tank. Information in the rear part is lacking. Nevertheless, all needed information is available.

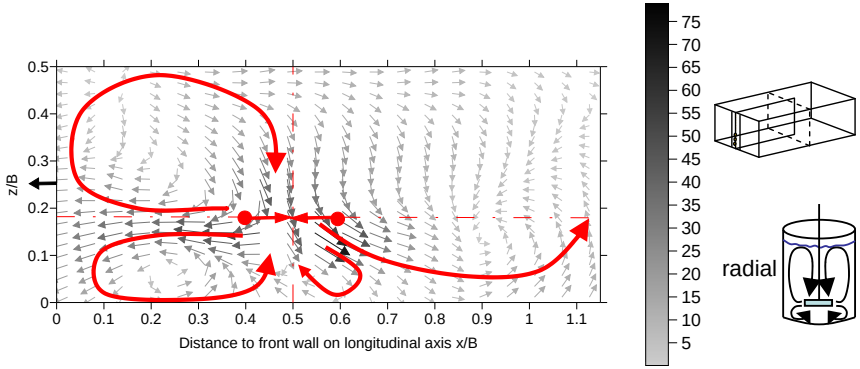

Figure 4.23 *Velocity vectors [mm/s] in the longitudinal plane for off-bottom clearance $C/B = 0.175$, water intake height $h_i/B = 0.25$, distance between neighbouring jets $l_j/B = 0.15$, distance between jet circle centre and front wall $d_{axis}/B = 0.525$, water height $h/B = 0.6$, total jet discharge $\Sigma Q_j = Q_{out} = 760$ l/h. Radial flow pattern indicated by arrows.*

4.6.3 Flow patterns for different discharges

In this section the flow patterns for experiments with basic circular jet configuration are analyzed (Table 4.2). Only the discharge was varied.

4.6.3.1 Transversal plane

In the transversal plane the flow patterns are quite similar for different discharges. They are all axial mixer-like flow patterns. The difference consists only in having the rotor cores more or less eccentric regarding the off-bottom clearance. The smaller the discharge is the more accentuated is the eccentricity found (Figure 4.24). Interestingly, the upper rotor core is in all of the transversal flow patterns on the right side. There is a possible explanation:

For the smaller discharges, at the time of the measurement, the jet induced circulation was not yet in a steady state. Thus, the final equilibrium was not yet achieved. The flow pattern represents an instantaneous status in the transient phase. It even might be influenced by a tiny discrepancy of the perfect jet positioning. The higher the discharge is the closer is the steady state at measurement time and the more equilibrated are the rotors.

Appendix B includes flow patterns of all tests.

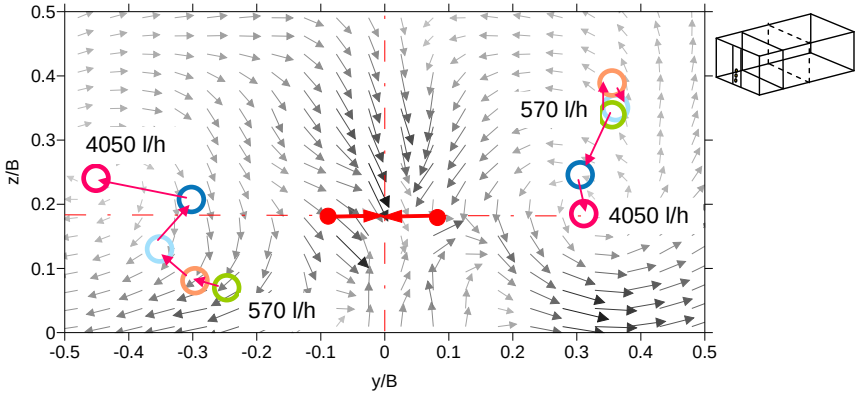

Figure 4.24 *Transversal flow pattern for total jet discharge $\Sigma Q_j = Q_{out}$ = 4050 l/h. The rotor cores are indicated by circles demonstrating their decreasing eccentricity for increasing discharge.*

4.6.3.2 Longitudinal plane

The interpretation of the longitudinal flow patterns is more complex:

For the smaller discharges (ΣQ_j = 760 *l/h* in Figure 4.23 and ΣQ_j = 570 *l/h* in Figure 4.25) the strong current ejected from the jets is almost horizontally pointing towards the front wall. For ΣQ_j = 760 *l/h* (Figure 4.23) there is a small rotor underneath this current making the flow pattern come close to the one induced by a radial mixer, while for the smallest tested discharge no well developed rotor can be identified between the jets and the front wall (Figure 4.25, dotted arrow). Nevertheless, in Figure 4.25 the water underneath the jets is sucked by them which is typical for a radial mixer. Moreover, the rotor below the horizontal current pointing towards the rear part of the tank is clearly recognizable. This confirms the identification of a radial mixer-like flow pattern in the longitudinal plane in case of small discharges.

For discharges ΣQ_j = 1140 and 3040 *l/h* (Figure 4.26) this current is deflected downward pointing into the lower corner. It is part of a rotor whose core is situated right in front of the water intake. The rotor expands probably from the bottom to the water surface.

The flow pattern of the highest tested discharge (ΣQ_j = 4050 *l/h*, Figure 4.27) is quite different. The rotor in the area of the front wall is missing. Moreover, the current ejected from the jets towards the front wall cannot be identified. In contrast, the current directed to the opposite side (rear of the tank) can be observed in all longitudinal flow patterns. With increasing discharge it is more pronounced and sinking deeper. For ΣQ_j = 4050 *l/h* (Figure 4.27) it reaches quickly the bottom and flows along it to the rear part.

Appendix B includes flow patterns of all tests.

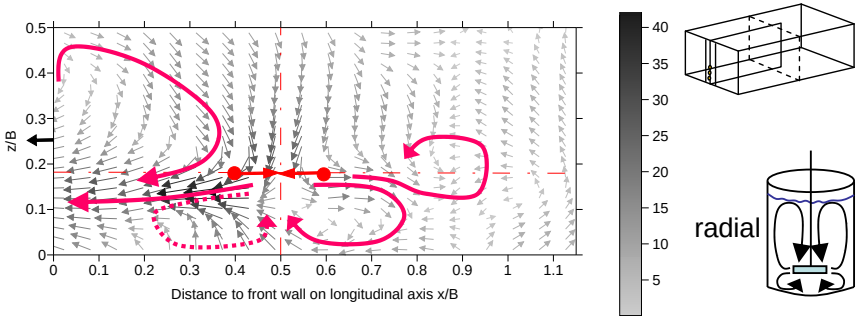

Figure 4.25 *Velocity vectors [mm/s] in the longitudinal plane for total jet discharge ΣQ_j = Q_{out} = 570 l/h, off-bottom clearance C/B = 0.175, water intake height h_i/B = 0.25, distance between neighbouring jets l_j/B = 0.15, distance between jet circle centre and front wall d_{axis}/B = 0.525, water height h/B = 0.6. Radial flow pattern is indicated by arrows.*

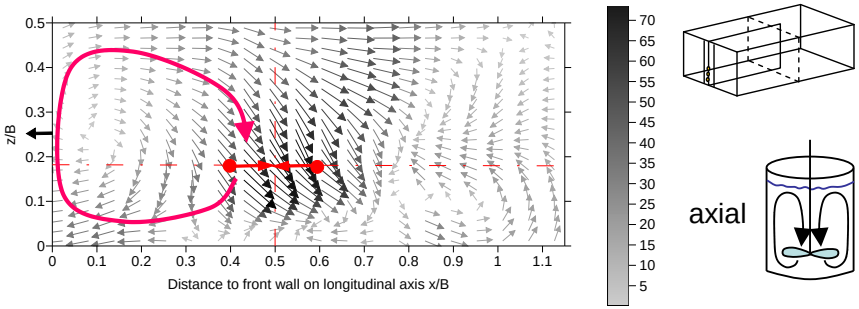

Figure 4.26 *Velocity vectors [mm/s] in the longitudinal plane for total jet discharge ΣQ_j = Q_{out} = 3040 l/h, off-bottom clearance C/B = 0.175, water intake height h_i/B = 0.25, distance between neighbouring jets l_j/B = 0.15, distance between jet circle centre and front wall d_{axis}/B = 0.525, water height h/B = 0.6. Axial flow pattern is indicated by arrows.*

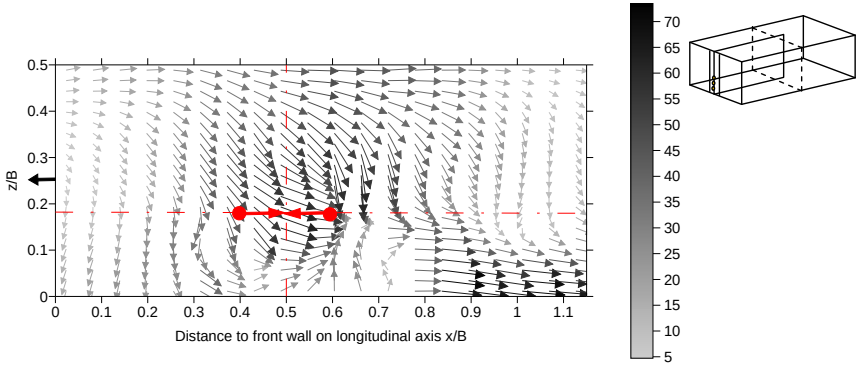

Figure 4.27 *Velocity vectors [mm/s] in the longitudinal plane for total jet discharge ΣQ_j = Q_{out} = 4050 l/h, off-bottom clearance C/B = 0.175, water intake height h_i/B = 0.25, distance between neighbouring jets l_j/B = 0.15, distance between jet circle centre and front wall d_{axis}/B = 0.525, water height h/B = 0.6.*

4.6.3.3 Concluding remarks on the influence of the jet discharge

Although the transversal flow patterns were probably still measured in the transient phase, they are quite similar for the investigated discharges. No instabilities could be observed. Once steady state is achieved, the rotor cores are expected to be situated on the jet mixing level. Axial mixer-like flow pattern is found.

The longitudinal flow pattern is more complex and probably more influenced by the third dimension (tank width). The differences of the flow pattern near the front wall are not necessarily due to the discharge, but probably to instabilities since the measurements were taken in the transient phase. For flow patterns resulting from higher discharge, a single rotor is found between jets and front wall (axial mixer-like flow pattern). For smaller discharges the flow pattern comes close to the one of a radial mixer.

4.6.4 Flow patterns for different off-bottom clearance

An unambiguous difference can be observed between the flow patterns resulting from higher (*C/B* = 0.25) and from lower off-bottom clearances (*C/B* = 0.1 to *C/B* = 0.175), respectively.

Higher off-bottom clearance (*C/B* = 0.25, Figure 4.28 and Figure 4.29):

Figure 4.28 (transversal plane) and Figure 4.29 (longitudinal plane) demonstrate a strong similarity between the flow pattern for jets installed at the off-bottom clearance *C/B* = 0.25 and a typical flow pattern of a radial mixer: the fluid is distributed radially outward to the tank wall. This results in four rotors in both planes as shown in Figure 4.28 and Figure 4.29. Armanante and Nagamine (1998) and Sharma and Shaikh (2003) found that this kind of mixer is not suitable for high suspension. According to Sharma and Shaikh (2003) the flow generated by a radial flow impeller sweeps the particles towards its central region when reaching the tank base. The central region is partly covered by an induced secondary loop. This is an unfavorable situation for suspension. It is more difficult to lift the particles from the centre than to drive them towards the corners where from they are picked up.

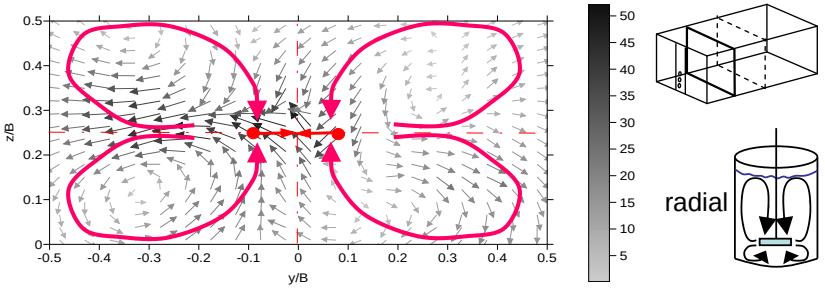

Figure 4.28 *Velocity vectors [mm/s] in the transversal plane for off-bottom clearance C/B = 0.25, water intake height h_i/B = 0.25, distance between neighbouring jets l_j/B = 0.15, distance between jet circle centre and front wall d_{axis}/B = 0.525, water height h/B = 0.6, total jet discharge $\Sigma Q_j = Q_{out}$ = 760 l/h. Radial flow pattern is indicated by arrows.*

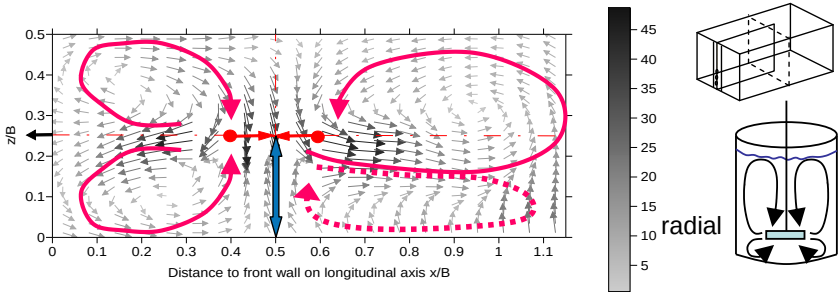

Figure 4.29 *Velocity vectors [mm/s] in the longitudinal plane for off-bottom clearance C/B = 0.25, water intake height h_i/B = 0.25, distance between neighbouring jets l_j/B = 0.15, distance between jet circle centre and front wall d_{axis}/B = 0.525, water height h/B = 0.6, total jet discharge $\Sigma Q_j = Q_{out}$ = 760 l/h. Radial flow pattern is indicated by arrows.*

Lower off-bottom clearance (*C/B* = 0.1 to 0.175, Figure 4.30 and Figure 4.31):

The flow pattern induced by the jets with an off-bottom clearance of *C/B* = 0.1 (Figure 4.30 for transversal plane and Figure 4.31 for longitudinal plane) is, just like the off-bottom clearance of *C/B* = 0.175 (Figure 4.22), similar to the one of a typical axial mixer. As it can be seen in Figure 4.30, for the lowest off-bottom clearance *C/B* = 0.1 the rotor cores are on both sides (measured at two different instants) at the same low position.

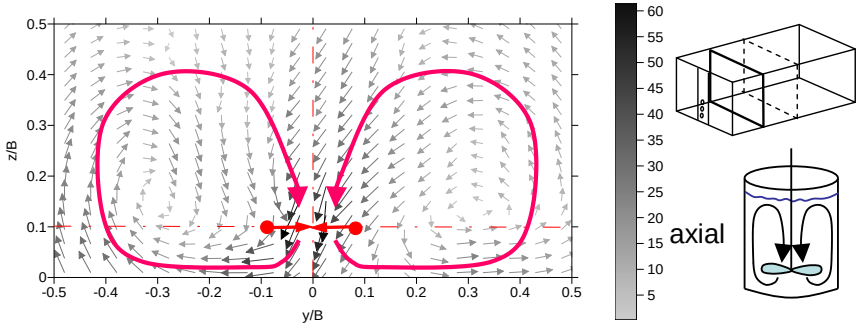

Figure 4.30 *Velocity vectors [mm/s] in the transversal plane for off-bottom clearance C/B = 0.1, water intake height h_i/B = 0.25, distance between neighbouring jets l_j/B = 0.15, distance between jet circle centre and front wall d_{axis}/B = 0.525, water height h/B = 0.6, total jet discharge $\Sigma Q_j = Q_{out}$ = 760 l/h.*

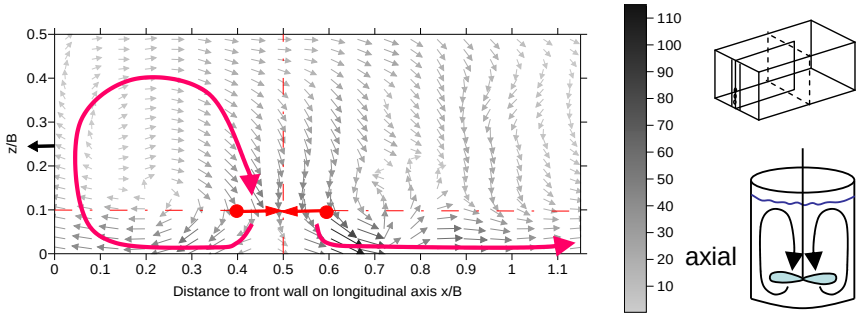

Figure 4.31 *Velocity vectors [mm/s] in the longitudinal plane for off-bottom clearance C/B = 0.1, water intake height h_i/B = 0.25, distance between neighbouring jets l_j/B = 0.15, distance between jet circle centre and front wall d_{axis}/B = 0.525, water height h/B = 0.6, total jet discharge $\Sigma Q_j = Q_{out}$ = 760 l/h.*

Appendix B includes flow patterns of all tests.

4.6.4.1 Concluding remarks

When keeping the water intake constant at h_i/B = 0.25 axial mixer-like flow patterns occur in the transversal plane for the lowest and the middle off-bottom clearance (C/B = 0.1 and 0.175). For the highest off-bottom clearance a radial mixer-like flow pattern is observed. According to the literature, the radial mixer-like flow pattern is less suitable for suspension than the axial mixer-like flow pattern. Therefore, optimal conditions are achieved for an off-bottom clearance of the circular jet arrangement between C/B = 0.1 and 0.175.

4.6.5 Flow patterns for different water intake heights

The investigated combinations of water intake heights h_i/B and off-bottom clearances C/B are summarized in Table 4.3.

Off-bottom clearance C/B	*Water intake height h_i/B*
0.1	*0.125*
	0.25
	0.375
0.175	*0.125*
	0.25
	0.375
0.25	*0.125*
	0.25
	0.375

Table 4.3 Studied combinations of off-bottom clearance C/B of the circular jet arrangement and the water intake height above tank bottom.

4.6.5.1 Transversal plane

All the flow patterns resulting from configurations with the jets on $C/B = 0.1$ are very similar among each other and very close to the flow pattern induced by an axial mixer (Figure B.15, Figure 4.30, Figure B.12, Figure B.16, Figure 4.32). The water intake height has no significant influence on the flow in the transversal plane and the rotor cores are located on both sides on a level close to the mixing level.

If the jets are arranged on the central plane ($C/B = 0.175$, Figure 4.32), the flow patterns are different when the water intake height is varied. With the lowest and the middle position of the water intake ($h_i/B = 0.125$ and 0.25, Figure B.17 and Figure B.2, Figure 4.22) the flow pattern is still axial mixer-like with more or less eccentric rotor cores (as discussed in section 4.6.3, Figure 4.24). For the highest height of the water intake ($h_i/B = 0.375$, Figure B.18) the flow pattern is completely changed and is not clearly identified, i.e. it cannot definitely be assigned to a specific mixing flow pattern (Figure 4.32 and Figure B.18). The dominating current comes horizontally from both sides to the central axis where it is deflected to the vertical direction, heading to the jets from below and above.

This is also the case for both right flow pattern sides when the off-bottom clearance is $C/B = 0.25$ and the water intake height is $h_i/B = 0.125$ (Figure B.19) and 0.375 (Figure B.20), respectively (Figure 4.32). On their left sides (different point in time), one single rotor with quite irregular appearance develops. The fully developed radial mixer flow pattern as observed for the water intake at the same level as the jets does not occur. Thus, the influence of the water intake on the flow in the transversal plane is evident.

As discussed in section 4.6.4 for the highest off-bottom clearance ($C/B = 0.25$) combined with the water intake height on $h_i/B = 0.25$, the flow pattern is very similar to a radial mixer induced flow pattern (Figure 4.28, Figure B.11).

Appendix B includes flow patterns of all tests.

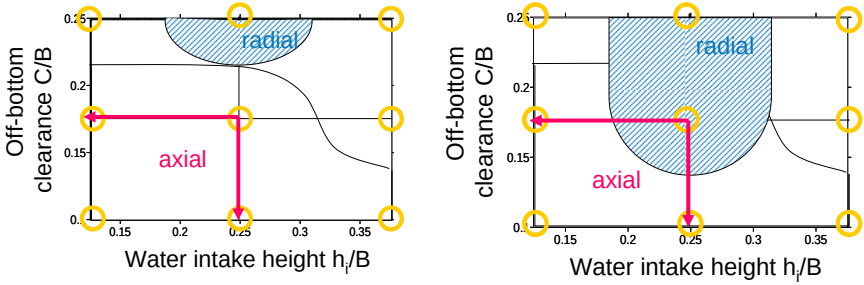

Figure 4.32 Superposition of the flow pattern characteristics in transversal and in longitudinal planes resulting from different combinations of off-bottom clearance and water intake height. Left: high discharges (ΣQ_j = 1140 l/h and 3040 l/h), right: low discharges (ΣQ_j = 570 to 760 l/h). Circles indicate performed experiments with corresponding combination of off-bottom clearance and water intake height.

4.6.5.2 Longitudinal plane

With the lowest off-bottom clearance (C/B = 0.1) the flow pattern is independently of the water intake height axial mixer-like. For the lowest and the highest water intake height (h_i/B = 0.125 and 0.375, respectively), the corresponding rotor cores are installed at the same level as the water intake (Figure B.21 and Figure B.22). This is not exactly true for the middle height (h_i/B = 0.25, Figure 4.31 and Figure B.14), where the core is approximately 0.1 normalized height (0.20 *m* model scale) deeper than the water intake. Due to the spin of the rotor, the water intake is fed from the bottom up to its height. Hence, the water intake determines the lowest possible position of the rotor core in the vertical direction. Minimum energy is spent when the distance from the rotor core to the jets is shortest. Thus, the position of the rotor core is defined.

Axial mixer-like flow patterns are also found in the case where the jets are arranged on the middle height (C/B = 0.175) and the water intake is on its lowest level (h_i/B = 0.125, Figure B.23).

However, with the jets on C/B = 0.175 and h_i/B = 0.25, as discussed in section 4.6.3, for low discharges (ΣQ_j = 570 to 760 *l/h*) a radial mixer-like flow pattern was generated and the current issued from the jets went rather straight to the water intake (Figure 4.23, Figure B.7 and Figure 4.25). For higher discharges (ΣQ_j = 1140 *l/h* and 3040 *l/h*) the flow pattern was axial mixer-like (Figure 4.26).

In case h_i/B = 0.375, the flow is not clearly identified (Figure B.24). It seems that the measurements were made when the flow field was changing. Just one small rotor close to the bottom is present. The radial flow issued by the jets, is damped by the surrounding flow.

As has been seen in section 4.6.4, higher located jets (C/B = 0.25) in combination with the water intake height on h_i/B = 0.25 generate a flow pattern similar to the one of a radial mixer. This is visualized in Figure 4.28 (transversal) and Figure 4.29 (longitudinal). The flow issued from the jets and generating the two rotors above and below goes straight towards the water intake. In Figure B.25 where the water intake is at the lowest tested level (h_i/B = 0.125) the

tendency of forming two rotors is visible at the rear side of the tank, but definitely cannot be identified at the side facing the front wall. If the water intake is located at its highest level (h_i/B = 0.375, Figure B.26) the formation of two rotors is possibly disturbed by the water intake: the formerly mentioned flow issued by the jet is deflected upwards. Only the upper rotor is created. The deflected jet does not directly flow towards the water intake. Thereby, the lower rotor is not formed. Instead, a wide current is generated coming from the lower corner, and being divided by the upper rotor, one part joins the jets from below, the other part flows around the aforementioned rotor. Consequently, the flow pattern generated by the combination of C/B = 0.25 and h_i/B = 0.125 and 0.375, respectively, are not clearly identified and cannot be assigned to a typical mixing flow pattern.

Appendix B includes flow patterns of all tests.

4.6.5.3 Concluding remarks on the influence of the off-bottom clearance and the water intake height

The flow created by the circular jet arrangement at the lowest level (C/B = 0.1) seems to be the best developed and hard to disturb. Well defined axial mixer-like flow pattern occurs. Nevertheless, for the higher tested off-bottom clearances (C/B = 0.175 and 0.25) the flow pattern type and the position of the rotor cores is strongly influenced by the water intake height (Figure 4.32) and flow instabilities might occur.

From the literature it follows that axial mixer-like flow patterns are more favorable for suspension in comparison with others. The radial mixer-like flow pattern in the longitudinal direction might be favorable for sediment release, because the so created horizontal current issued from the jets towards the front wall may enhance sediment entrainment into the water intake.

The circular jet arrangement with off-bottom clearance C/B = 0.175 and with water intake height h_i/B = 0.25 creates a flow pattern having both: a clearly axial mixer-like flow pattern in the transversal direction and a radial or axial mixer-like flow pattern in the longitudinal direction, depending on the discharge (Figure 4.32). It may be concluded that this configuration generates the optimal flow pattern regarding sediment release.

4.6.6 Flow patterns for different water heights in tank

The flow patterns of the experiments having water heights in tank other than h/B = 0.6 (1.20 *m* in model scale) all are quite irregular. There is no well developed rotor, and both sides of the transversal and longitudinal patterns are quite different. The flow field is highly asymmetrical.

As a concluding remark it can be noted, that in both directions, only with water height h/B = 0.6 a suspension favoring flow pattern (axial mixer-like) was observed.

Appendix B includes flow patterns of all tests.

4.6.7 Flow patterns for different distances of jet circle centre to the front wall

4.6.7.1 Transversal plane

The flow patterns in the transversal plane are quite different depending on their distance between jet circle centre and the front wall, d_{axis}.

With d_{axis}/B = 0.3 (Figure B.31, ΣQ_j = 4050 l/h), the flow pattern on the left side seems to have two rotor cores (radial), whereas on the right side there is a single rotor core (axial) with a

strong current along the bottom. As the two sides are not measured at the same time, this combined figure may reveal instabilities in the flow. The same can be concluded from Figure 4.33 (Figure B.32) showing the flow pattern on the transversal plane with d_{axis}/B = 0.4 (ΣQ_j = 4050 l/h), and where on both sides the rotors are well developed, with left an axial and right a radial mixer-like flow pattern.

In Figure B.34 (d_{axis}/B = 0.65, ΣQ_j = 760 l/h) no clearly visible rotors are present. Nevertheless, two rotors on the right side seem to develop and, thus, a tendency to a radial mixer-like flow pattern is shown. On the left side axial mixer-like flow pattern is assumed. The rotors in Figure B.35 (d_{axis}/B = 0.775, ΣQ_j = 760 l/h) are more pronounced and show a characteristic axial mixer-like flow pattern.

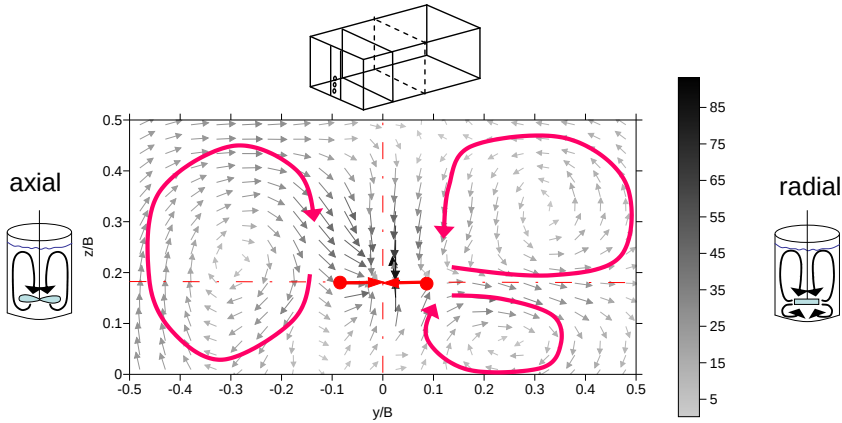

Figure 4.33 Velocity vectors [mm/s] in the transversal plane for off-bottom clearance C/B = 0.175, water intake height h_i/B = 0.25, distance between neighbouring jets l_j/B = 0.15, distance between jet circle centre and front wall d_{axis}/B = 0.4, water height h/B = 0.6, total jet discharge $\Sigma Q_j = Q_{out}$ = 4050 l/h.

4.6.7.2 Longitudinal plane

A generally valuable observation can be made for the flow patterns measured in the longitudinal plane with a distance between jet circle axis and front wall longer or equal than d_{axis}/B = 0.4 (Figure B.37 to Figure B.39, ΣQ_j = 760 *l/h*): In the space between the jets and the front wall, there is a flow pattern similar to the one induced by a radial mixer with a strong current issuing just beneath the jet plane towards the front wall. In the vicinity of the jets a small rotor is formed near the bottom underneath of this current (Figure 4.34 and Figure 4.35). In the case of d_{axis}/B = 0.525 the current is almost horizontal from the jets towards the front wall (Figure 4.23). The upper part of it is directed towards the water intake. For d_{axis}/B longer than 0.525 (Figure B.38 and Figure B.39), the current is deflected downwards and there is no direct current from the jets to the water intake (Figure 4.35). Moreover, the velocity of the current decreases when approaching the front wall. The flow pattern for d_{axis}/B = 0.525 (Figure 4.23) seems to have two rotors in the space between the jets and the front wall, even if the

upper one is not perfectly developed. This is not the case for d_{axis}/B other than 0.525. For d_{axis}/B = 0.3 (Figure B.36, ΣQ_j = 4050 *l/h*), the aforementioned horizontal current is not visible, and is supposed to be deflected by the strong vertical current from above.

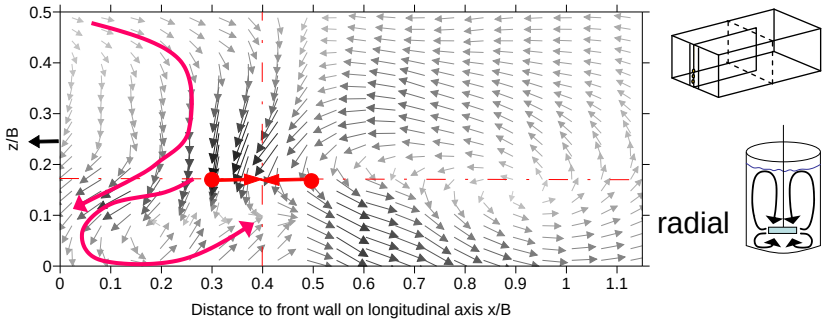

Figure 4.34 *Velocity vectors [mm/s] in the longitudinal plane for off-bottom clearance C/B = 0.175, water intake height h_i/B = 0.25, distance between neighbouring jets l_j/B = 0.15, distance between jet circle centre and front wall d_{axis}/B = 0.4, water height h/B = 0.6, total jet discharge $\Sigma Q_j = Q_{out}$ = 760 l/h.*

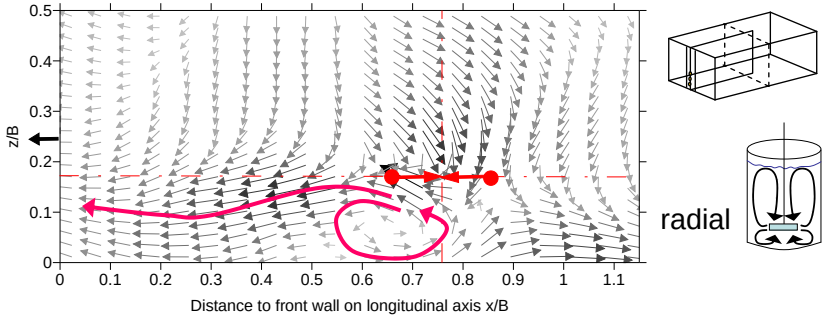

Figure 4.35 *Velocity vectors [mm/s] in the longitudinal plane for off-bottom clearance C/B = 0.175, water intake height h_i/B = 0.25, distance between neighbouring jets l_j/B = 0.15, distance between jet circle centre and front wall d_{axis}/B = 0.775, water height h/B = 0.6, total jet discharge $\Sigma Q_j = Q_{out}$ = 760 l/h.*

4.6.7.3 Concluding remarks on the influence of the distance of the jet arrangement to the front wall

Above described observations can be summarized in the following illustration (Figure 4.36).

It may be concluded that only for d_{axis}/B = 0.525 the transversal flow pattern is stable. In the case of the longitudinal flow pattern a single rotor between the jets and the front wall has only been observed for d_{axis}/B = 0.525 (for higher discharges as discussed in section 4.6.3).

Moreover, at this distance the current issuing from the jets heading towards the front wall (if present) is still horizontal. With increasing distance it is weakened and deflected downwards.

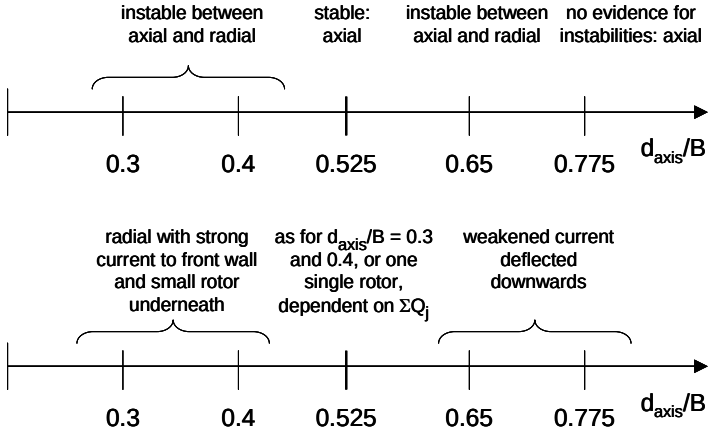

Figure 4.36 Observations regarding the distance between the jet circle centre and the front wall d_{axis}/B. Above: transversal plane, below: longitudinal plane.

4.6.8 Flow patterns for different distances between neighboring jets

4.6.8.1 Transversal plane

Independently on the distance between neighboring jets the flow pattern is typically axial mixer-like (Figure 4.37).

For the smallest distance between neighbouring jets l_j/B = 0.1 (Figure B.40) the rotors are not well developed compared to the flow pattern associated with l_j/B = 0.15 (Figure 4.22 and Figure 4.37). It is interesting to note that the vertical current coming from the top extends to a larger width than the region of the jets (as observed for l_j/B = 0.15) and sinks to the bottom. The detected rotor on the left side is located beyond this current, oriented towards the side wall and limited by it. On the right side, no such cell can be identified. Moreover, the flow underneath the jets has a rather chaotic pattern.

For the distance l_j/B = 0.225 (Figure 4.37, Figure B.41 and Figure B.42), a very distinct vertical downward current is formed in the axis of the jets circle, extending laterally over the region of the jets. Furthermore, pronounced instabilities occur as confirmed by the double rotors (Figure 4.38). They have been observed during the same experiment, but a few minutes later.

For l_j/B = 0.3 this vertical downward current is still strong but distributed on the larger distance between the jets. The remaining space for the rotors between the jets and the side wall becomes with increasing inter-jet distance narrower (Figure 4.37).

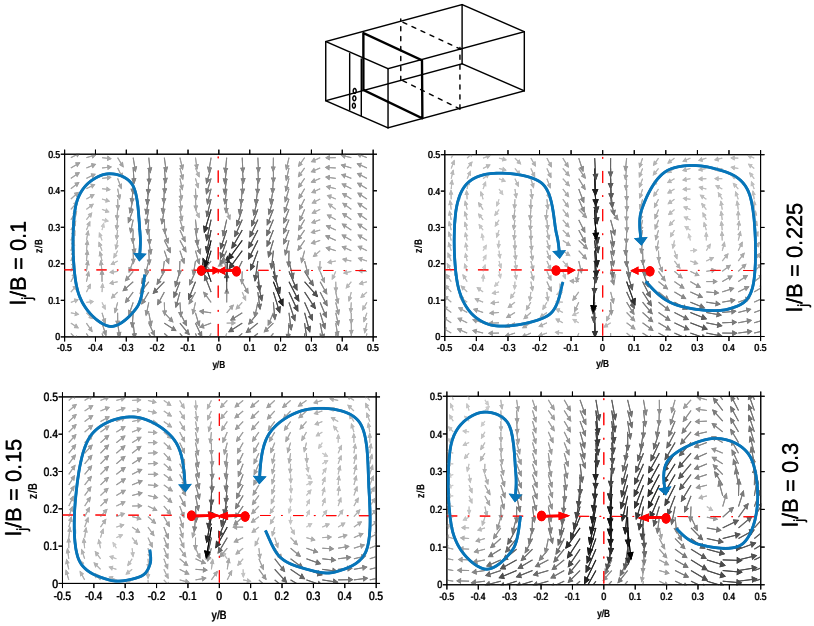

Figure 4.37 Flow patterns in the transversal plane for different distances between neighboring jets (l_j/B = 0.1 to 0.3). Grey surfaces indicate the expansion of the rotor cells.

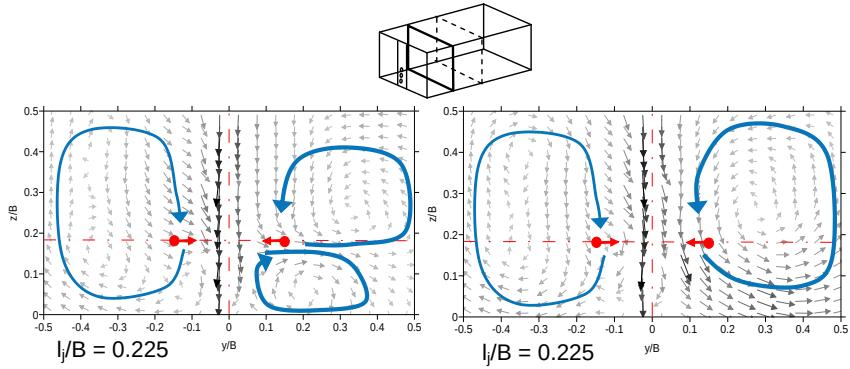

Figure 4.38 Flow instabilities observed in the transversal plane for the distance between neighboring jets lj/B = 0.2.

4.6.8.2 Longitudinal plane

For all values l_j/B other than 0.15, there is a single rotor between the jets and the front wall (Figure B.44 (l_j/B = 0.1), Figure B.45 (l_j/B = 0.225) and Figure B.46 (l_j/B = 0.3)). Its longitudinal position is stable, whereas its vertical position varies little. The current issuing

from the jets towards the front wall is for l_j/B = 0.1 slightly deflected towards the bottom. For l_j/B = 0.225 (Figure B.45) it is almost horizontal and for l_j/B = 0.3 (Figure B.46) it is deflected upward. In none of these three flow patterns a second rotor is formed as has been observed for l_j/B = 0.15 for lower discharges (Figure 4.23). The current issued from the jets towards the rear part of the tank is less pronounced for all three cases compared to l_j/B = 0.15 (Figure 4.23).

4.6.8.3 Concluding remarks on the influence of the distance between two neighboring jets

For l_j/B = 0.1 the vertical (axial) downward current extends in the transversal plane laterally further than the region of the jets, whereas for higher l_j/B this current is as wide as the jet circle diameter. Hence, the laterally available space for rotors decreases with increasing distance between jets. For l_j/B = 0.1 the rotor is formed beyond the vertical current and difficult to identify. In the longitudinal direction the presence of a single rotor between the jets and the front wall, thus, an axial mixer-like flow pattern, is persistent for all inter-jet distances.

4.6.9 Flow patterns for a jet inclination angle of 45°

In this experiment the jet configuration was the same as in the basic circular jet configuration (Table 4.2) except that the jet nozzle was inclined from the horizontal 45° upwards. The transversal flow pattern (Figure 4.39, Figure B.47) is similar to the flow pattern of the basic configuration (Figure 4.22), with the important distinction that the rotors are rotating in the opposite sense. Moreover, the rotor cores are situated in the upper part. Beneath and above the jets the flow is clearly moving upward. There is a small disturbed zone above z/B = 0.3.

Since the rotors are rotating in the opposite sense compared to an axial mixer it can be assumed that this movement is hindering suspension. Therefore, sediment may be accumulated underneath the jets. The sediment is moving along the side walls towards the bottom, where it is difficult to pick it up again.

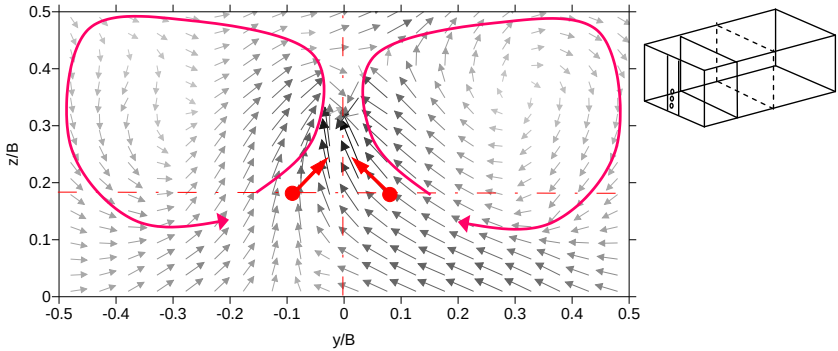

Figure 4.39 Velocity vectors [mm/s] in the transversal plane for off-bottom clearance C/B = 0.175, water intake height h_i/B = 0.25, distance between neighbouring jets l_j/B = 0.15, distance between jet circle centre and front wall d_{axis}/B = 0.525, water height h/B = 0.6, angle θ = 45°, total jet discharge $\Sigma Q_j = Q_{out}$ = 760 l/h.

In the longitudinal plane (Figure B.48) the flow pattern is dominated by a vertical upward flow. Thus, the rotors observed in the transversal plane are apparently not axisymmetric to the jet circle axis. The vertical upward movement may be favorable for suspension. Nevertheless, due to continuity, there must be areas with downward flow compensating the upward movement.

Concluding remarks for jets with an angle of 45°

The transversal flow pattern for a jet angle of 45° is similar to the flow pattern of the basic configuration with horizontal jets, beside the important difference that the rotors are rotating in the opposite sense. From the available longitudinal flow pattern it is hard to judge if this configuration is favorable in view of sediment release. It may be concluded that inclined jets do not create flow patterns which are more favorable in view of suspension than horizontal jets.

4.7 Flow patterns for linear jet arrangement

With the linear jet arrangement different configurations regarding the distance of the jet line from the front wall, the jet angle, as well as jet discharges were experimentally tested. The distance between the jets, their off-bottom clearance, the water height, and the water intake height were always kept constant (Figure 3.21). The transversal plane is located along the jet line.

Figure B.49 shows the flow pattern in the transversal plane induced by the jets with the distance of the jets to the front wall $d_{line}/B = 0.2$. Figure B.50 shows the same flow pattern with $d_{line}/B = 0.3$. Both flow patterns are very similar and have a rotor with a core at mid-height of the tank ($z/B \sim 0.3$), close to the vertical middle axis. Both sides are symmetric and there is a sharp interface separating them. The sense of rotation is unfavourable in view of suspension since the sediment is drawn down to the bottom and settled near the longitudinal middle axis. At this position the sediments are difficult to put in suspension again.

In the longitudinal plane a small rotor can be observed beneath the jets ($d_{line}/B = 0.2$, Figure B.51). In this configuration ($d_{line}/B = 0.2$) for $C/B = 0.1$, $h_i/B = 0.25$ and a nozzle angle of 45° the jet is expected to extend directly to the water intake. However, this is not observed in Figure B.51, since a horizontal current towards the water intake is forming. Thus, the jet is deflected downwards. The flow in the back of the jet line is mainly in vertical direction. Intuitively, such a circulation seems favourable for sediment release. The longitudinal flow pattern for $d_{line}/B = 0.3$ (Figure B.52) reveals a general current having the same direction as the jet. Nevertheless, this current is disturbed in the area between the jets and the water intake where the flow is mostly in upward direction and away from the front wall. The energy of the jet was reduced along its long path in a way that there is no current possible in direction to the water intake. This leads to the assumption that this configuration is less sediment release conducive than the former one even if the ratio d_{line}/h_i is in the same range.

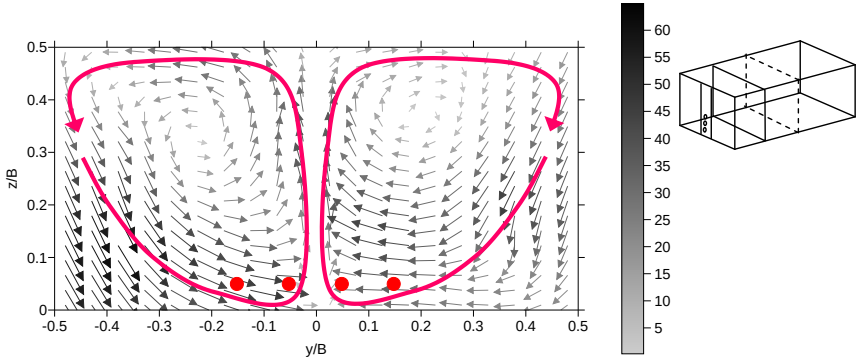

Figure 4.40 *Velocity vectors [mm/s] in the transversal plane for off-bottom clearance C/B = 0.05, distance of jet line to front wall d_{line} /B = 0.3, water height h/B = 0.6, angle θ = 45°, total jet discharge $\Sigma Q_j = Q_{out}$ = 4050 l/h.*

Near the water surface a stagnation area was detected visually (Figure 4.41). PVC particles put on the surface and which reached this area were accumulating there. During the experiment the separation line remained quite stable at approximately *x/B* = 1.1 (for d_{line}/B = 0.1, experiment L8). Unfortunately, no UVP measurements are available for this experiment. However, since the longitudinal flow fields for d_{line}/B = 0.2 and d_{line}/B = 0.3 are quite similar, a similar flow field can be also expected for d_{line}/B = 0.1. The separation line was outside of the performed UVP measurements in the longitudinal plane. Therefore, its deveolping current and the eventual counter-current cannot be seen in Figure B.51 and Figure B.52. Moreover, the observed current near the water surface (*h/B* = 0.6) was in the opposite direction than the measured velocities at *z/B* = 0.5. Thus, obviously, there is a flat but strong rotor near the top of the water column, which was unfortunately outside of the measurement area.

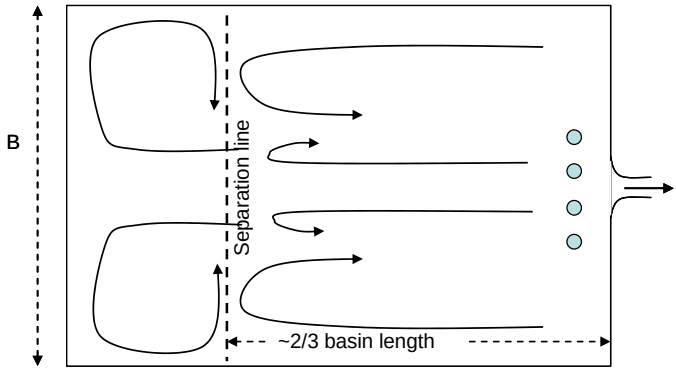

Figure 4.41 *Schematic view of the visually observed circulation of the water surface with a stagnant area in the rear of the tank (water intake on the right side). The dashed line indicates the approximate position of the separation line.*

Concluding remarks for linear jet arrangement

The direction of transversal rotation is unfavorable regarding suspension. The sediment seems to be drawn down to the bottom where it settles near the longitudinal middle axis. It is hard to lift it up from this position.

4.8 Sediment release with circular jet arrangement

4.8.1 Overview

In this subchapter, the effect of a circular jet arrangement on the efficiency of sediment evacuation for different geometrical jet arrangement parameters is discussed.

The geometrical parameters as well as the jet and water intake discharges were varied as presented in section 3.5.3.1.

For the basic geometrical parameters six different discharges were analyzed. These experiments are used as reference for comparison when varying the other parameters (section 4.6.2, Table 4.2).

4.8.2 Influence of jet discharge on sediment release

4.8.2.1 Introduction

Following the procedure as described in subchapter 4.5, the effect of the discharge on sediment release efficiency was examined. The water in the tank becomes well mixed during the experiments with jets. The suspended sediment concentration becomes nearly homogeneously distributed (see section 4.2.2). Consequently, less sediment is settled and the suspended sediment concentration in front of the water intake is higher than without jets. Therefore, after four hours, the sediment release efficiency expressed by the evacuated sediment ratio is higher than without jets, as expected. This is illustrated in Figure 4.42 for a circular jet arrangement with the basic geometrical parameter set (section 4.6, Table 4.2):

off-bottom clearance	$C/B = 0.175$
horizontal distance between jet circle axis and front wall	$d_{axis}/B = 0.525$
horizontal distance between two neighbouring jets	$l_j/B = 0.15$
water intake height	$h_i/B = 0.25$.

Within the range of the experimental conditions Figure 4.42 reveals an almost linear relationship between the measured evacuated sediment ratio (circular jet arrangement experiments and reference experiments after four hours experiment duration) and the discharge. It has to be mentioned that jet discharge ΣQ_j and released discharge through water intake Q_{out} are identical (see section 3.6.2).

Remark: The initial suspended sediment concentration was varied twice (experiments C44 and C45) when 6 and 2 kg, respectively, were initially supplied to the tank instead of 3 kg. The so reached concentrations did not have any remarkable influence on the settling velocity. Consequently, the sediment release (evacuated sediment ratio) was the same.

4.8.2.2 Idealized theoretical released sediment ratio

Assuming no sediment settling and perfectly homogeneous suspended sediment within the experimental tank at the beginning of the experiments, an idealized theoretical evacuated

sediment ratio is established and illustrated in Figure 4.42. Within the same discharge range the relationship between evacuated sediment ratio and discharge appears to be clearly non linear. Figure 4.42 illustrates, that for higher discharges the influence of the discharge becomes smaller.

The idealized theoretical evacuated sediment ratio is developed as follows:

The initial suspended sediment concentration $c_{s,init}$ is expressed by the initially added sediment weight P_{in} and the tank volume V:

$$c_{s,init} = \frac{P_{in}}{V} \qquad \text{(Eq. 4.10)}$$

After one time step the suspended sediment concentration c_{s1} can be expressed as follows:

$$c_{s1} = \frac{P_{in} - P_{out1}}{V} = \left[\left(c_{s,init} \cdot V\right) - \left(Q_{out} \cdot c_{s,init} \cdot \Delta t\right)\right] \cdot \frac{1}{V} = c_{s,init}\left(1 - \frac{Q_{out}}{V}\right) \qquad \text{(Eq. 4.11)}$$

After two time steps the remaining sediment concentration c_{s2} can be written as in Eq. 4.12.

$$c_{s2} = \frac{P_{in} - P_{out1} - P_{out2}}{V} = c_{s1} - \frac{P_{out2}}{V} = \left[\left(c_{s1} \cdot V\right) - \left(Q_{out} \cdot c_{s1} \cdot \Delta t\right)\right] \cdot \frac{1}{V} \qquad \text{(Eq. 4.12)}$$

By substitution of Eq. 4.11 in Eq. 4.12 it follows

$$c_{s2} = c_{s,init}\left(1 - \frac{Q_{out}\Delta t}{V}\right)^2 \qquad \text{(Eq. 4.13)}$$

Accordingly, the suspended sediment concentration after i time steps c_{si} can be written as

$$c_{si} = \left(1 - \frac{Q_{out}}{V}\Delta t\right)^i \cdot c_{s,init} \qquad \text{(Eq. 4.14)}$$

i: time step i

Δt: time step length

By considering the definition of the mean residence time (Eq. 4.15)

$$\tau_m = \frac{V}{\Sigma Q_j} = \frac{V}{Q_{out}} \text{ mean residence time} \qquad \text{(Eq. 4.15)}$$

Eq. 4.14 can be rewritten as in Eq. 4.16

$$c_{si} = \left(1 - \frac{\Delta t}{\tau_m}\right)^i \cdot c_{s,init} \qquad \text{(Eq. 4.16)}$$

According to Eq. 4.2 and Eq. 4.3 the evacuated sediment ratio after i time steps is established as follows:

$$ESR_i = \frac{\sum_{j=0}^{i}\left(1 - \frac{\Delta t}{\tau_m}\right)^i \cdot c_{s,init} \cdot Q_{out} \cdot \Delta t}{c_{s,init} \cdot V} = \frac{\Delta t}{\tau_m} \cdot \sum_{j=0}^{i}\left(1 - \frac{\Delta t}{\tau_m}\right)^i \qquad \text{(Eq. 4.17)}$$

After i time steps of duration Δt a total duration of t is achieved deriving:

$$t = i \cdot \Delta t \qquad \text{(Eq. 4.18)}$$

with

t: experimental duration of interest

With the substitution of Eq. 4.18 in Eq. 4.17 the evacuated sediment ratio at time *t* is expressed.

$$ESR(t) = \frac{\Delta t}{\tau_m} \sum_{j=0}^{i=t/\Delta t} \left(1 - \frac{\Delta t}{\tau_m}\right)^i \qquad \text{(Eq. 4.19)}$$

If the time step Δt tended to have duration 0, Eq. 4.19 leads to Eq. 4.20

$$ESR(t) = \lim_{\Delta t \to 0} \frac{\Delta t}{\tau_m} \sum_{j=0}^{t/\Delta t} \left(1 - \frac{\Delta t}{\tau_m}\right)^i \qquad \text{(Eq. 4.20)}$$

Consequently, the following exponential expression is obtained (Eq. 4.21)

$$ESR_{ideal} = 1 - e^{-t/\tau_m} \qquad \text{(Eq. 4.21)}$$

with

ESR_{ideal}: idealized theoretical evacuated sediment ratio, assuming homogeneous distribution of suspended sediment and no sediment settling

The above idealized theoretical evacuated sediment ratio may indicate that the relationship between discharge and experimentally measured evacuated sediment ratio is also not linear.

The idealized theoretical evacuated sediment ratio allows comparing the performance of the different jet configurations and, thus, finding the optimal configuration.

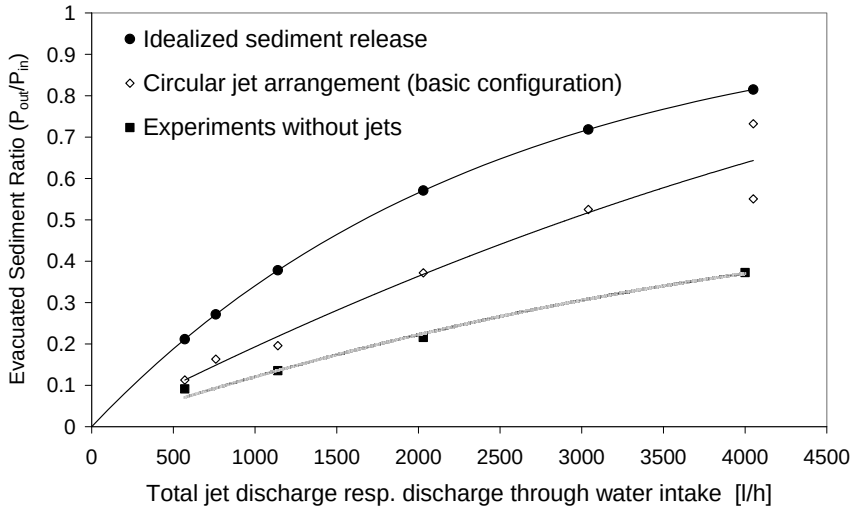

Figure 4.42 *Evacuated sediment ratio ESR after four hours as a function of the total jet discharge (resp. discharge through water intake) shown for the jet experiments C1 to C7 (circular jet arrangement with off-bottom clearance C/B = 0.175, water intake height h_i/B = 0.25, horizontal distance between jet circle centre and front wall d_{axis}/B = 0.525, horizontal distance between neighboring jets l_j/B = 0.15), as well as for the experiments without jets and for idealized conditions (i.e. with homogeneous suspended sediment concentration and no sediment settling).*

Analogous to Figure 4.17 showing the different sediment ratio without jets, Figure 4.43 represents the distribution of the evacuated sediment ratio and the ratio of the remaining sediments in the experimental tank. The remaining sediments can be divided into the suspended (upper part) and the settled sediment ratios (lower part) respectively. The thin line in Figure 4.43 separates the evacuated and the suspended sediment ratios for idealized conditions where there is no settled sediment ratio.

How the difference between the idealized theoretical and the experimentally measured evacuated sediment ratio can be explained?

The ideal conditions represent the steady state conditions. There is no transient phase, whereas the experiments need to run for a certain while before reaching steady state.

Two observations underline that at the beginning of the experiment the circulation is in a transient phase:

- As discussed in section 4.2.2 the suspended sediment concentration distribution within the experimental tank is at the beginning of the experiment not homogeneous. Concentration homogeneity is only reached after a certain while.
- Sediment settling is observed in the first period of the experiments (Figure 4.43). The

measurements show that after a while the settled sediments are resuspended again. At the point in time where the settled sediment ratio is maximal and resuspension starts (in Figure 4.43 indicated by a small square), the transition from transient phase to steady state is assumed.

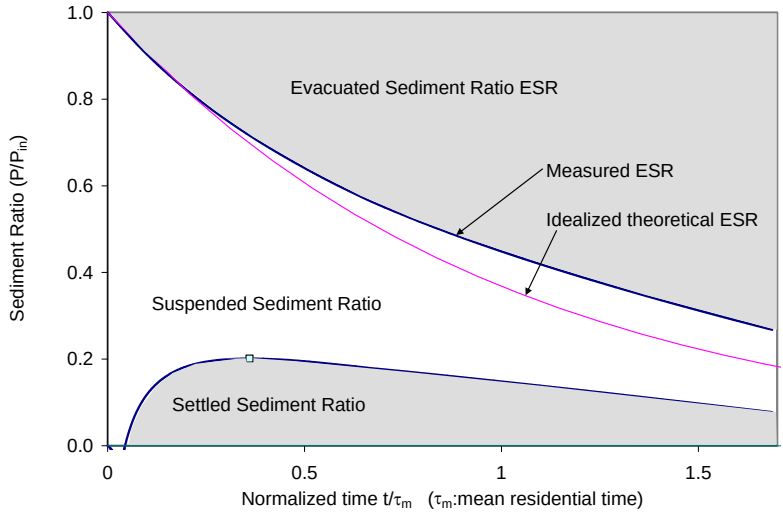

Figure 4.43 *The three sediment fractions: evacuated, suspended and settled sediment ratio in the experiment C6 ($\Sigma Q_j = Q_{out}$ = 4050 l/h). The settled sediment reaches a maximum at approximately 0.3 normalized time. After this point in time, the transition from transient phase to steady state is assumed and resuspenstion takes place.*

4.8.2.3 Comparison with other research

It is interesting to note that Robinson et al. (1982) found in their destratification experiments with axial mechanical mixers (2.44 *m* of diameter) a non-linear relationship between the release rate, Q_{out}, and the temperature, *T*, when pumping (Figure 4.44). They conclude that the discharge has an influence on the temperature of the outflow. A similar observation has been discussed in the former section (4.8.2.2) regarding evacuated sediment ratio. Moreover, the relationship between release rate and temperature in Robinson et al. (1982) (evacuated sediment ratio respectively) is similar to the idealized case discussed above: with higher discharge its influence becomes less effective (Figure 4.44, Figure 6 in Robinson et al., 1982). Nevertheless, the Garton pumps in the experiments in Lake Texoma operated only for 30 minutes at each of the five release rates. Thus, and bearing in mind the magnitude of the reservoir volume of Lake Texoma, there is some doubt that steady state was achieved within this short period.

Busnaina et al. (1981, Figure 4.44) observed that the release water quality, expressed by a dilution factor, is strongly improved with an increase of the flow-rate ratio ($Q^* = Q_p/Q_{out}$); a condition achieved with low release rate and high propeller flow rates. Analogously, in the present study only two different flow-rate ratios have been tested: 0 (no jets) and 1 (with jets). Thus, it doesn't make sense to adopt the same flow-rate ratio for comparison, and a direct comparison is therefore not accurate. Nevertheless, Busnaina et al. (1981) found, that with higher flow-rate ratio its influence becomes less effective. This behavior reminds the one observed assuming idealized test conditions.

Evoking the research work in the field of jet mixing, none of the cited authors did mention a direct relationship between the discharge and the mixing time. Chemical engineers often keep the jet discharge constant while varying the jet velocity or jet nozzle diameter, such as Coldrey (1978) who found for increasing jet diameter an increasing mixing time. Perona et al. (1998) confirmed this finding. In the present study the sediment release is not directly related to jet diameter or jet velocity.

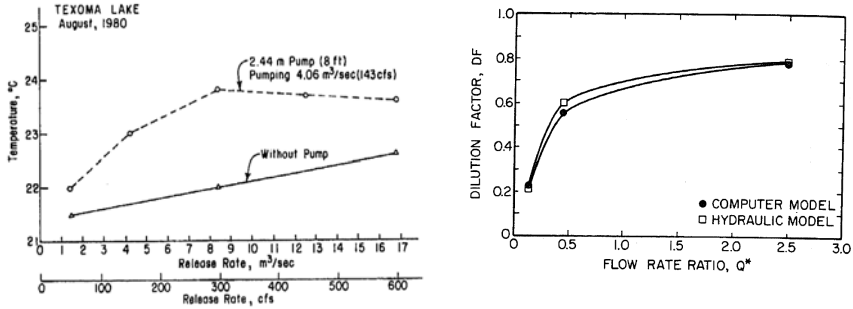

Figure 4.44 Left: Figure from Robinson et al. (1982): Temperature as function of release rate at Lake Texoma. Right: Figure from Busnaina et al. (1981): Dilution Factor as a function of flow rate ratio (propeller flow rate divided by the release flow rate)

4.8.3 Mixing time

When in chemistry fluid is mixed by mechanical mixers, no volume is normally extracted from the experimental mixing volume. When using jets for mixing procedures, the jet is fed by the mixture from an intake in the tank itself (closed circuit). In the present study the extracted water is replaced by clear water and the sediment amount within the experimental tank is, hence, decreasing with time. According to the mentioned authors the mixing time obtained under their own test conditions depends on various factors (chapter 2) and is determined by the degree of homogeneity. In most of the cases 95 % mixing is required (Wasewar, 2006), i.e. when the following equation is fulfilled.

$$\frac{|c-\bar{c}|}{\bar{c}} = 0.05 \qquad \text{(Eq. 4.22)}$$

c: instantaneous concentration

$\bar{c}$: concentration in case of perfect mixing

In the present study this condition is achieved in the first half experimental hour (section 4.2.2). At this time the circulation is obviously still in the transient phase and sediment is still settling.

Particle settling and resuspension as well as the influence of transient phase and steady state in correlation with mixing time have not been reported in the literature so far.

4.8.4 Long term evolution of sediment release

Within the four hours of experimental duration the initially supplied sediments were not evacuated completely in any of the experiments and the water in the tank was not clear. The chosen duration in the steady state was too short to achieve a final state regarding sediment release.

The following questions may be discussed:

- How can the experimental data be extrapolated for long term evolution?
- Are finally all sediments going to be evacuated or is there a settled rest remaining on the bottom unable to be resuspended?
- How long does it take until all suspended sediments are evacuated?
- What's the value of the final evacuated sediment ratio?

As already mentioned in section 4.8.2, the experimentally established evolution of the evacuated sediment ratio doesn't exactly follow the idealized one (Figure 4.45). However, the higher the jet discharge the closer they are. However, even if the equation describing the evacuated sediment ratio under idealized conditions is useful for the steady state, it is not suitable to describe the experimental results during the transient phase and therefore also not for extrapolation.

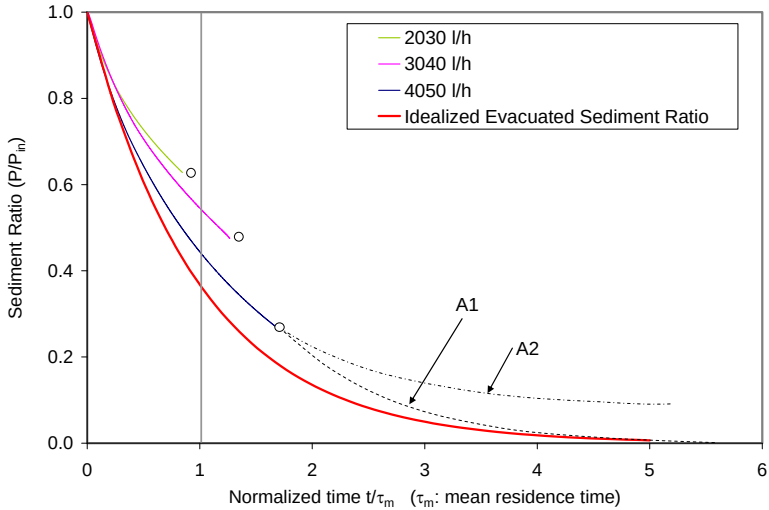

Figure 4.45 *Evacuated sediment ratio in function of normalized time (above the lines). For the experiment with ΣQ_j = 4050 l/h after the experiment duration of 4 hours two extreme extrapolation possibilities are presented: dashed line: Assumption A1 that all the sediments are resuspended instantly; dash-dotted line: Assumption A2 that the settled sediment is not resuspended.*

In Figure 4.45 two extreme possibilities of sediment ratio evolution in long time are sketched for the experiment with a discharge of ΣQ_j = 4050 l/h:

The dashed line is based on the assumption A1 that right after the last measurement all settled sediment is instantly resuspended and that all the remaining suspended sediment is homogeneously distributed within the experimental tank. As a consequence the curve follows the idealized one starting at the same evacuated sediment ratio, but with a certain time lag which is due to the preceding experimental transient conditions.

The dash-dotted line is based on the assumption A2 that after the last measurements no more sediment is resuspended, and the suspended sediment is homogeneously distributed. Therefore, the evolution of the evacuated sediment ratio follows the idealized curve. However, there is on one hand the time lag due to the preceding transient conditions (like encountered with the former assumption). On the other hand the curve continues with a higher evacuated sediment ratio, i.e. with the evacuated sediment ratio increased by the suspended sediment ratio measured at the end of the experiment. At long term, the settled sediment fraction remains in the tank (Figure 4.45).

Both assumptions are extreme cases and it seems obvious that the real evolution is somewhere in between. Consequently, the observation made in the first four hours regarding the behavior of the settled sediment is very important for extrapolation.

4.8.4.1 Behavior of settled sediment

In Figure 4.46 the lower lines represent the evolution of the settled sediment ratio. In all experiments settling was observed at the very beginning of the experiment with quite a high rate. Then the rate decreased and for the three higher discharges a maximum of the settled sediment ratio was reached. After this, resuspension starts, that means that the overall resuspension rate is stronger than the settling rate. For the three lower discharges (570, 760 and 1140 *l/h*), the transition from settling to resuspension was not reached and the maximum settling sediment ratio could not be evaluated. These experiments were not long enough to reveal when resuspension occurs. It has to be remembered that for smaller discharges it takes even more time to reach the transition from transient to steady state.

It can be assumed that before the maximum settled sediment ratio is reached, the circulation is in a transient phase, whereas afterwards it is in a steady state.

Moreover it can be seen in Figure 4.46 that the resuspension rate is approximately constant. Figure 4.47 doesn't confirm this firmly, but for a rough estimate, this hypothesis is considered as accurate. None of the experiments reached the end of resuspension. It remains unsure if a constant resuspension rate is ever reached, and if ever all sediments are resuspended. It seems obvious that some sediments are always remaining in the tank, like those settled in the corners (Sharma and Shaikh, 2003). They are very difficult to be lifted by any circulation.

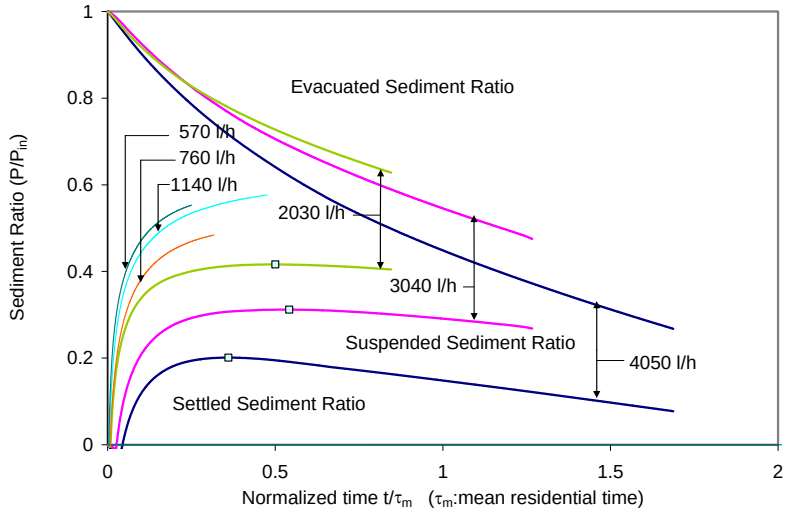

Figure 4.46 *Sediment ratio as a function of normalized time. Small squares indicate maximal settled sediment ratio for $\Sigma Q_j = Q_{out}$ = 2030 l/h, 3040 l/h and 4050 l/h.Grey areas are bounded by the curves belonging to $\Sigma Q_j = Q_{out}$ = 4050 l/h.*

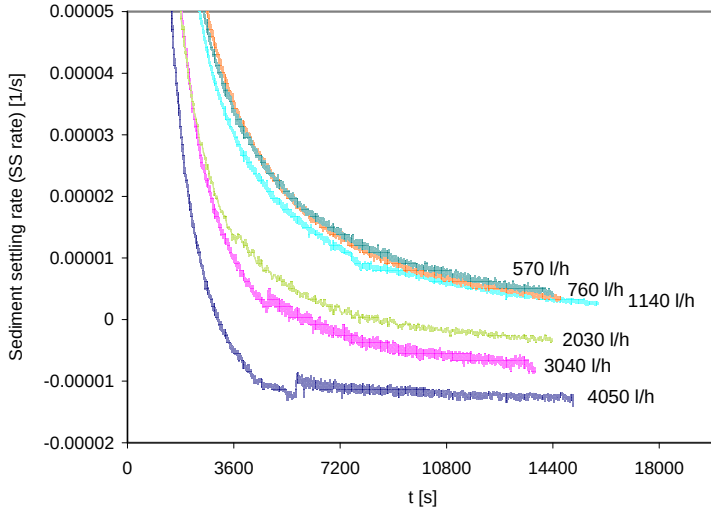

Figure 4.47 Sediment settling rate for the standard geometrical parameter set. Positive values mean settling, negative values mean resuspension. During the experiment, the resuspension rate tends towards a constant value.

4.8.4.2 Assumptions for extrapolation

From the above discussion three assumptions which are related to each other can be given:

Assumption 1. Once the jet induced circulation has achieved steady state, no more sediment is settled, and the suspended sediment distribution within the experimental tank is homogeneous. The evolution of the evacuated sediment ratio follows the idealized one with a time shift.

Assumption 2. Steady state is achieved once the settled sediments start resuspending, in other words, more sediment is resuspended than is settled.

Assumption 3. The resuspension rate is constant from the start and all sediment is resuspended.

With these three assumptions the evolution of the sediment release for the highest three discharges can be extrapolated (Figure 4.48 to Figure 4.50).

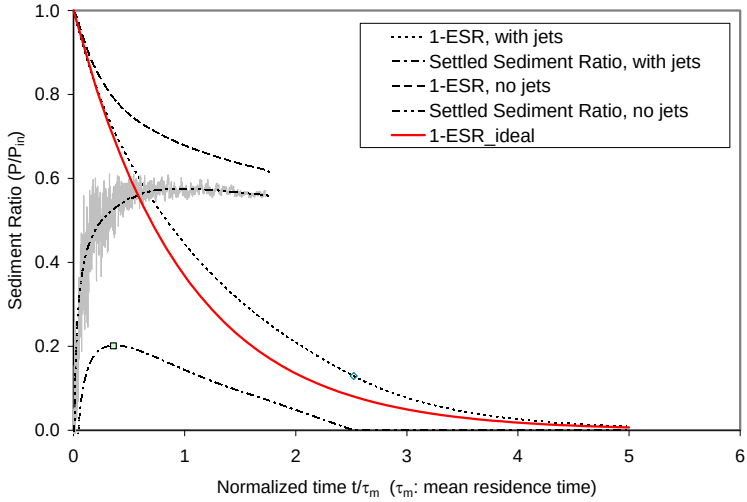

Figure 4.48 *Extrapolated long term evolution of the evacuated sediment ratio and settled sediment ratio for the experiment with jets for Q_{out} ($=\Sigma Q_j$) = 4050 l/h. The corresponding curves of the experiments without jets are not extrapolated. The curve of the idealized evacuated sediment ratio is also given.*

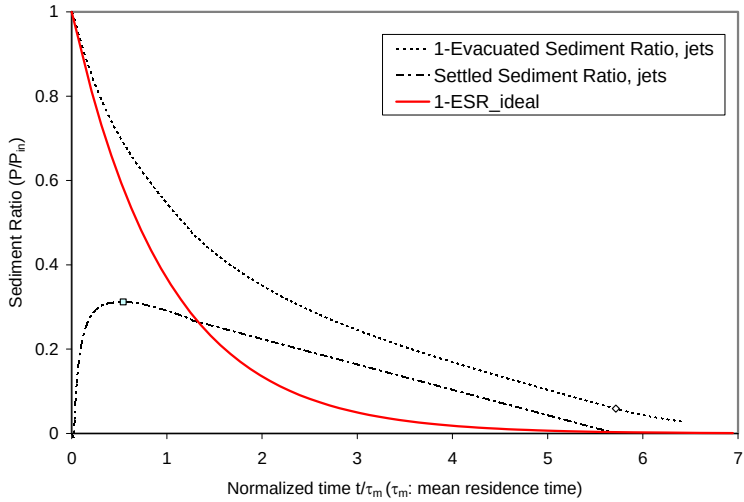

Figure 4.49 *Extrapolated long term evolution of the evacuated sediment ratio and settled sediment ratio for the experiment with jets for Q_{out} ($=\Sigma Q_j$) = 3040 l/h. The curve of the idealized evacuated sediment ratio is also given.*

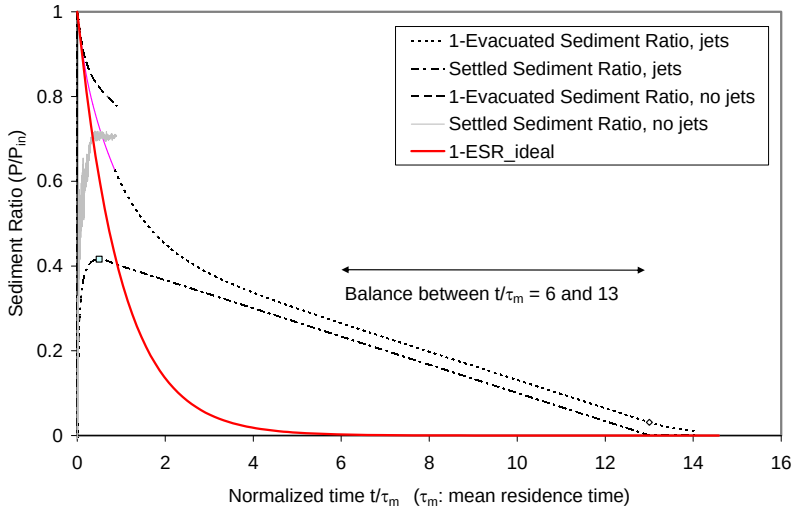

Figure 4.50 *Extrapolated long term evolution of the evacuated sediment ratio and settled sediment ratio for the experiment with jets for Q_{out} ($=\Sigma Q_j$) = 2030 l/h. The corresponding curves of the experiments without jets are not extrapolated. The curve of the idealized evacuated sediment ratio is also given.*

For ΣQ_j = 1140 *l/h* and smaller the maximal settled sediment ratio was not achieved during the four experimental hours. Thus, the maximum settled sediment ratio has to be estimated.

Therefore four more assumptions have to be discussed:

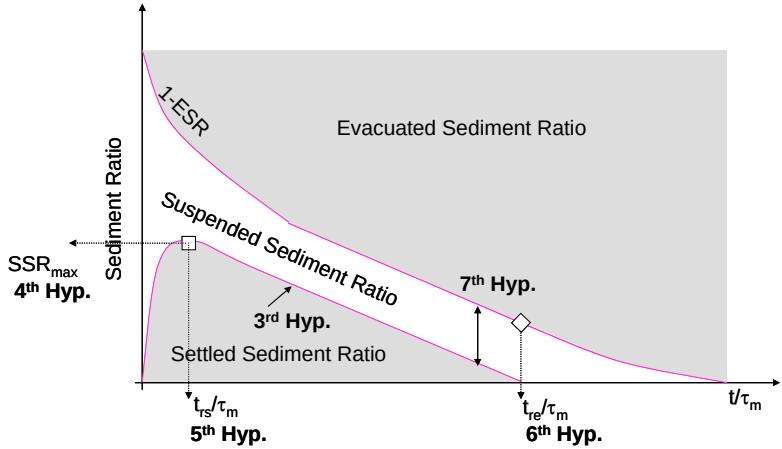

Figure 4.51 Schema of the seven hypotheses made for extrapolation.

Assumption 4. Linear relationship between the maximal settled sediment ratio and the inverse of the mean residence time $1/\tau_m$ (Figure 4.52 a)

Assumption 5. Linear relationship between mean residence time τ_m and start of resuspension t_{rs} (Figure 4.52 b)

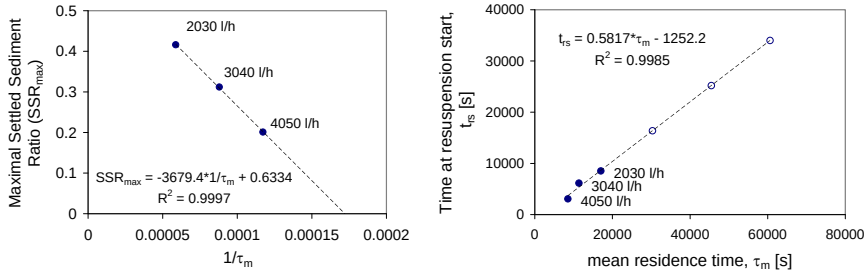

(a) *(b)*

Figure 4.52 (a) Fourth assumption: Linear relationship between the maximal settled sediment ratio, SSR_{max}, and the inverse of the means residence time $1/\tau_m$ (b) Fifth assumption: Linear relationship between mean residence time τ_m and the point in time of the resuspension start, t_{rs}. Full dots: measurements, circles: extrapolation.

Assumption 6. Linear relationship between the normalized end time of resuspension t_{re} and mean residence time τ_m

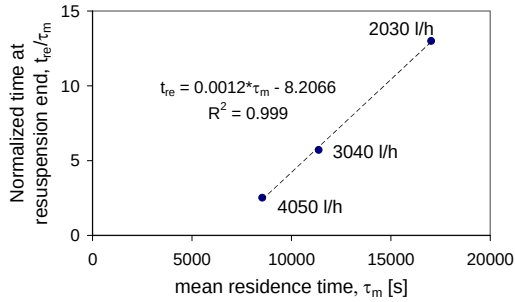

Figure 4.53 Linear relationship between the normalized point in time of resuspension end, t_{re}, and mean residence time τ_m.

From these relationships the resuspension rate can be estimated by the following equation:

$$\text{Resuspension rate} = \frac{\text{maximal settled sediment ratio}}{(\text{resuspension end} - \text{resuspension start})} \qquad (Eq.\ 4.23)$$

The resuspension rate can therefore be expressed as a function of the mean residence time for these three smaller discharges (570, 760 and 1140 *l/h*). As can be seen in Figure 4.54, the resuspension rate of the three higher discharges (previously assumed constant) fit very well in this relationship.

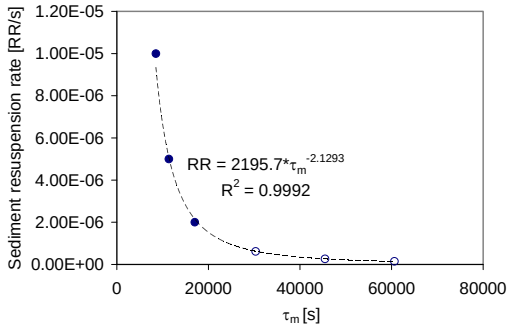

Figure 4.54 Exponential relationship between the sediment resuspension rate and the mean residence time. (RR: resuspension rate). Full dots: measurements (ΣQ_j = 2030, 3040 and 4050 l/h); circles: extrapolation (ΣQ_j = 570, 760 and 1140 l/h). Full dots: measurements, circles: extrapolation.

Assumption 7. Equilibrium between resuspended and evacuated sediments during the last resuspension period (see Figure 4.49). The resuspended sediment is evacuated while the suspended sediment ratio remains constant. This balance has been observed for the extrapolated mean residence time of τ_m = 17'000 *s* and is therefore considered to be valuable for τ_m > 17'000 *s*.

The seventh assumption leads to a logarithmic relationship between the evacuated sediment ratio at end time of the resuspension and the normalized resuspension rate (Figure 4.55a). The evacuated sediment ratio at the end time of resuspension can also be expressed as a logarithmic function of normalized time (Figure 4.55b). Between the last measurements and the obtained equilibrium between resuspension rate and evacuation rate, the evolution needs to be accomplished visually.

These seven assumptions allow the long term extrapolation of the experimental results.

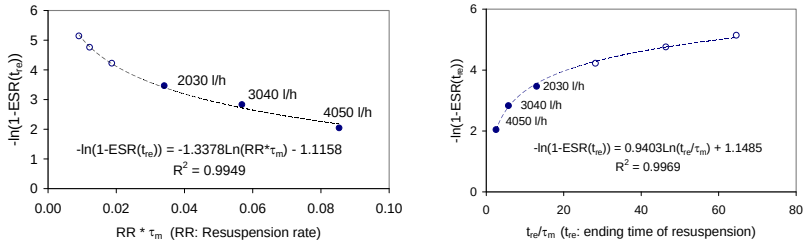

(a) *(b)*

Figure 4.55 *(a) Logarithmic relationship between the evacuated sediment ratio and the normalized resuspension rate. (b) Logarithmic relationship between the evacuated sediment ratio at the point of time of resuspension end and the normalized ending time of resuspension. Full dots: measurements (ΣQ_j = 2030, 3040 and 4050 l/h); circles: extrapolation (ΣQ_j = 570, 760 and 1140 l/h).*

4.8.4.3 Concluding remarks on long term extrapolation

Since no experiment reached the end of resuspension, the proposed extrapolation can unfortunately not be validated. Nevertheless, the assumptions seem to be reasonable, but with a certain uncertainty.

As is observed in Figure 4.47 the resuspension rate is close to zero for a discharge of ΣQ_j = 2030 *l/h*. For smaller discharges resuspension was not reached. Moreover, from the observed evolution of the resuspension rate it is not clear if it ever comes to resuspension. If resuspension takes place it is expected to be negligible.

Consequently, the ΣQ_j = 2030 *l/h* is a threshold below which no resuspension is assumed. In other words, a certain discharge is necessary to generate resuspension. At the final stage the sediment release would not be unity, but thanks to more efficient mixing it would (for test conditions) still be higher than the ratio achieved without jets.

For geometrical parameters other than the basic ones resuspension was not observed.

4.8.5 Influence of off-bottom clearance of jets on sediment release

A series of experiments was carried out with the jets installed on different off-bottom clearances *C/B*. First, only the off-bottom clearance was varied keeping the other geometrical parameters constant. Afterwards the off-bottom clearance was varied while the water intake height was changed at the same time (sections 3.5.3.1, 4.8.5 and 4.8.6).

Figure 4.56 and Figure 4.57 reveal an optimum off-bottom clearance near the middle of the investigated off-bottom clearances *C/B* (0.10, 0.175 and 0.25). The evacuated sediment ratio is obviously the highest for the off-bottom clearance of *C/B = 0.175*.

As it has been discussed in section 4.6.4 a flow pattern similar to a radial mixer as found for the off-bottom clearance *C/B* = 0.25 is not suitable for suspension. This explains why the highest investigated off-bottom clearance didn't provide the best results regarding sediment release.

Sharma and Shaikh (2003) observed that with increased off-bottom clearance the induced secondary loop below the impeller increases and gets wider, and more particles are caught in it, and because of the higher position of the impeller, less energy is imparted to them. As a consequence and in the case of a mechanical impeller, higher speed of impeller rotation would be needed to force the higher amount of trapped particles out from this region and to drive them towards the tank corner from where they may be suspended. If they are not suspended, then still higher impeller speeds for ultimate suspension may be needed. The interpretation of the results of Sharma and Shaikh (2003) might be true for their proper test conditions but cannot be transferred to the results of the present study, since the optimum has not been found on the lowest off-bottom clearance.

One reason for this difference is that in the present study water is extracted from the tank which is not the case in the study of Sharma and Shaikh (2003). Sharma and Shaikh are looking at the suspension ease whereas the goal of the present study is a high sediment release. Moreover, the vessel in their tests was axisymmetric whereas in the present study an elongated tank with an open space in the rear was used.

Another reason might be the instable rotor core position. The instabilities might be favorable for sediment release. The regions with high velocities are alternated and possibly the stagnant zones are not permanent. This could allow reaching sediments staying permanently in the same zone if there were no instabilities.

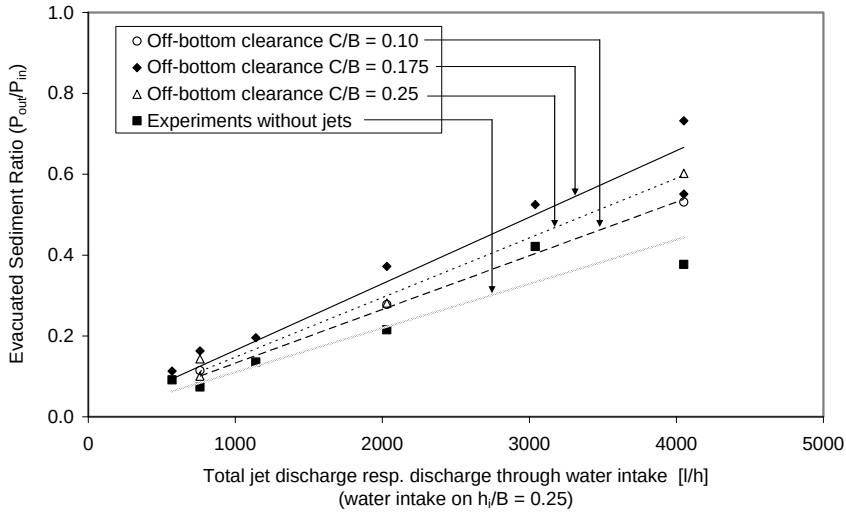

Figure 4.56 Evacuated sediment ratio ESR as a function of the total jet discharge (resp. discharge through water intake) varying the off-bottom clearance while holding the others geometrical parameters constant.

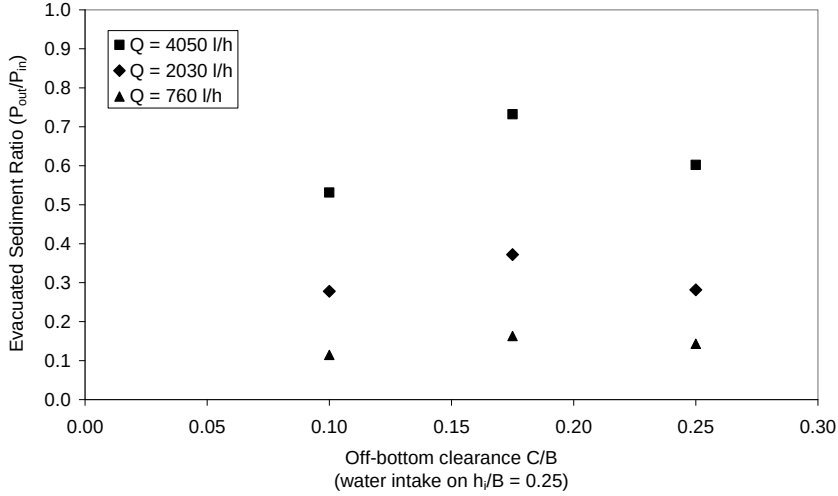

Figure 4.57 The evacuated sediment ratio depends on the off-bottom clearance C/B, records after four hours.

The part of the sediment not released due to a variation to the optimal off-bottom clearance is given in Figure 4.58. It increases with time. For the lower off-bottom clearance the increase is higher than for the higher off-bottom clearance. Both have a similar reduction of released sediment after one hour (approximately 13 %), but the deficit increases faster for the lower off-bottom clearance and becomes after four hours approximately 26 %, whereas for the higher off-bottom clearance it is 18 %.

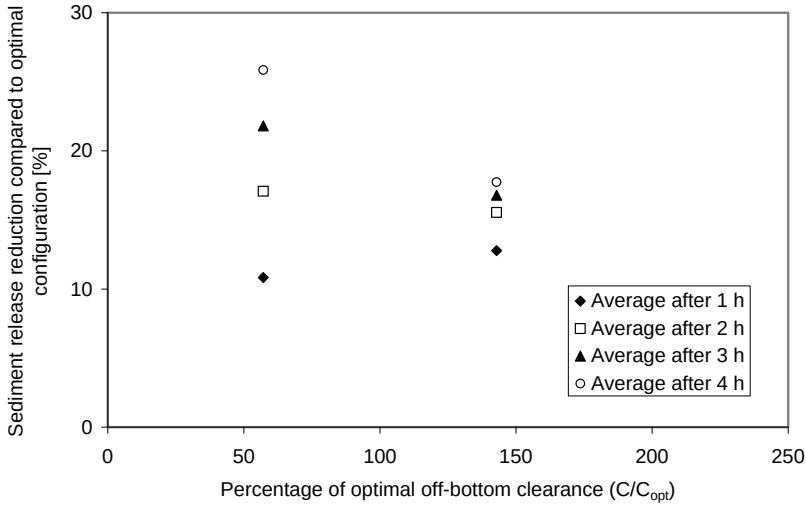

Figure 4.58 *Reduction of released sediment ratio as a function of the off-bottom clearance normalized with the optimum off-bottom clearance C/B =0.175 (while holding the water intake height constant at h_i/B = 0.25). This reduction is given as the average of all tested discharges.*

4.8.6 Influence of water intake height on sediment release

The optimal water intake height was found to be in the middle of the three test heights, at 0.50 *m* in model (h_i/B = 0.25, Figure 4.59). The reduction in sediment release due to a variation of the water intake is shown in Figure 4.60 for a constant off-bottom clearance C/B = 0.175. A water intake placed on half of the optimal height has after four hours a reduction of sediment release of more than 30 %. If it is installed 50 % higher it is even 40 %.

As discussed in section 4.6.5 the water intake height and the off-bottom clearance are strongly interacting. Therefore, the flow patterns and their influence on the sediment release need to be interpreted studying both parameters simultaneously (section 4.8.8).

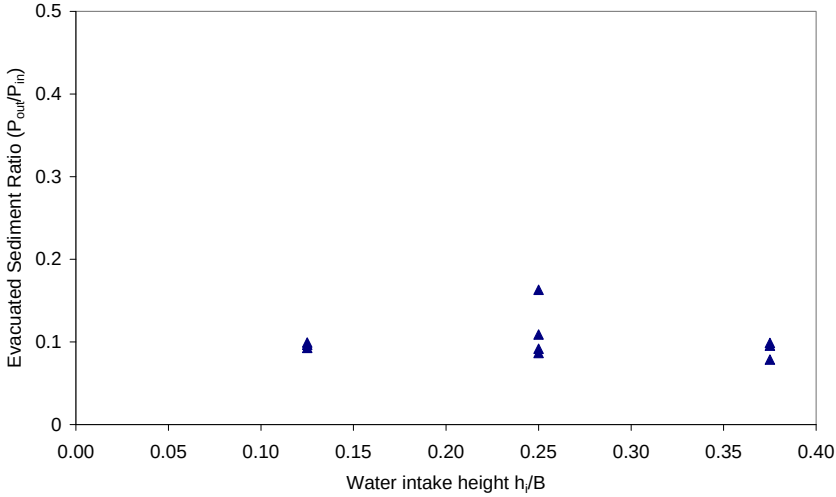

Figure 4.59 Evacuated Sediment Ratio as a function of the normalized water intake height after four hours experiment duration. $\Sigma Q_j = Q_{out}$ = 760 l/h.

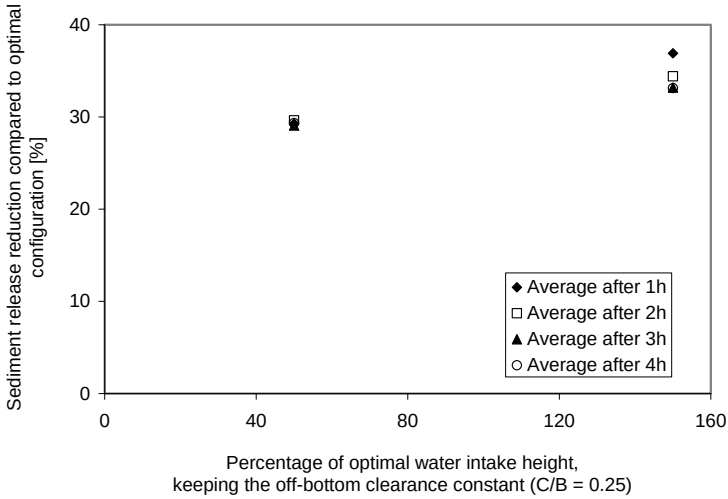

Figure 4.60 Reduction of released sediment ratio as a function of the water intake height normalized with the optimum water intake height h_i/B =0.25 (while holding the off-bottom clearance constant at C/B = 0.175). This reduction is given as the average of all tested discharges.

4.8.7 Influence of water height in tank on sediment release

From Figure 4.61 and Figure 4.62 it can be seen that the water height has a certain influence on the sediment release. The experiments varying the water height were all carried out with the same discharge of ΣQ_j = 760 *l/h*, the releasing discharge being equal to the jet discharge. The evacuated sediment ratio in the case of h/B = 0.6 is approximately 0.16, whereas for h/B = 0.5 and h/B = 0.65, it is between 0.08 and 0.1. Thus, the optimum water height in the tank seems to be at h/B = 0.6. For this optimum water height, the sediment release is approximately double as high as for a change of water height of 5 to 10 *%*.

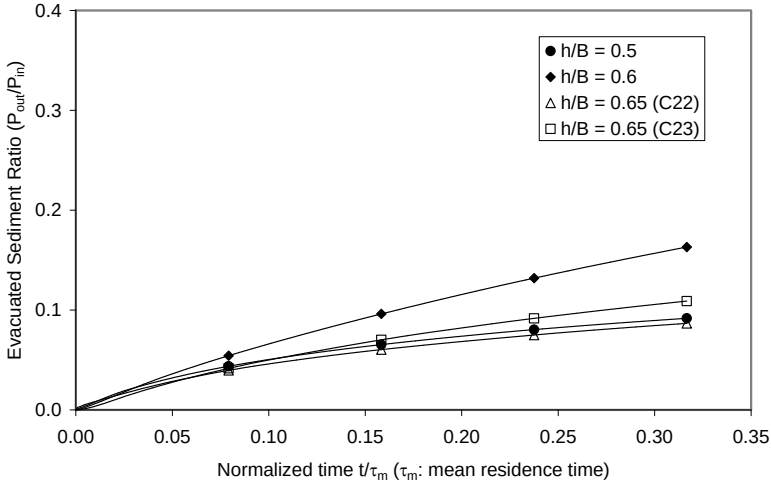

Figure 4.61 Evacuated Sediment Ratio as a function of normalized time for different water heights during the first four experimental hours for ΣQ_j = 760 l/h. (Experiments C22, C23 and C24).

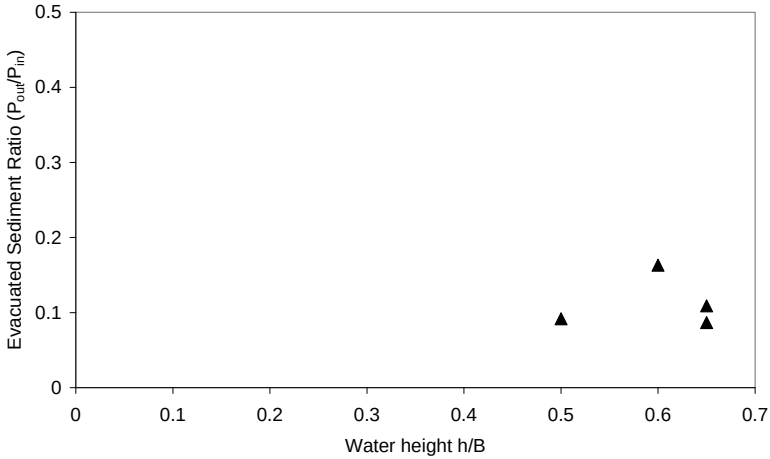

Figure 4.62 Evacuated Sediment Ratio as a function of the normalized water height h/B in the tank (Experiments C22, C23 and C24).

Figure 4.63 confirms that the optimum water height for the performed tests is at $h/B = 0.6$. For smaller water height ($h/B = 0.5$) the reduction of sediment release compared the optimum water height ($h/B = 0.6$) is after one hour between 20 and 25 % and increases after four hours to more than 30 %. With the higher water height ($h/B = 0.65$) the reduction remains constant during the whole experiment duration and is approximately 27 %.

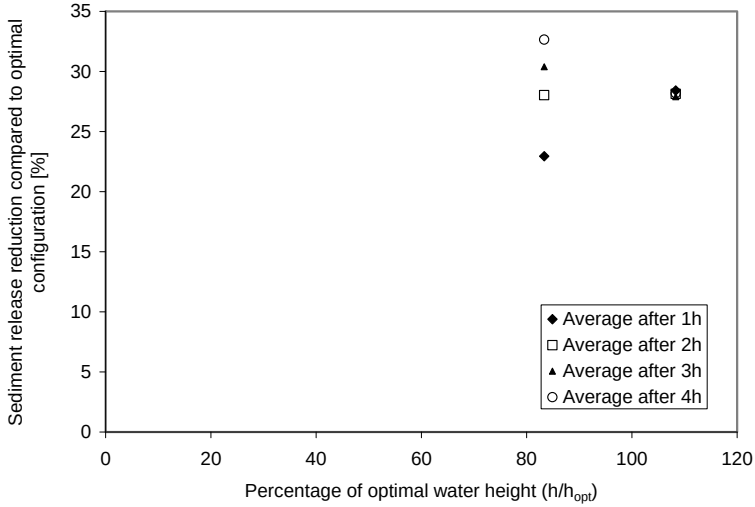

Figure 4.63 Reduction of released sediment ratio as a function of the water height in the tank normalized with the optimum water height h/B =0.6. This reduction is given as the average of all tested discharges.

4.8.8 Influence of combinations of off-bottom clearance of jets and water intake height

As discussed in sections 4.8.5, 4.8.6 and 4.8.7, the tests revealed optimum values of off-bottom clearance of jets, the height of intake above bottom as well as the water height in the tank regarding sediment release. Additionally, experiments combining different off-bottom clearances and water intake heights have been carried out, which results are presented in Figure 4.64. The optimum combination is given by the isolines which give the fraction regarding the optimum expected to be released when respective heights are available for a discharge of ΣQ_j = 760 *l/h*. The optimum combination is the following:

$C/B = 0.175$

$h_i/B = 0.25$

$h/B = 0.6$.

In section 4.6.5 the flow patterns are discussed when varying both the water intake and the off-bottom clearance. The influence of the interaction of both heights on the flow pattern can be clearly seen.

The flow pattern with the lowest tested off-bottom clearance ($C/B = 0.1$) was, independently of the water intake height, identified to be the most stable and close to the axial mixer-like flow pattern (in both planes, transversal and longitudinal). If the jet plane is on its middle position ($C/B = 0.175$) and the water intake on its lowest position ($h_i/B = 0.125$) also an axial mixer-like flow pattern develops. This flow pattern is known to be favorable for keeping the sediments in

suspension (Sharma and Shaikh 2003). Nevertheless, the experiments revealed that an axial mixer-like flow pattern in the longitudinal plane is not favorable regarding sediment release.

For the jet plane on its highest tested position (C/B = 0.25), a radial mixer-like flow pattern was found in the transversal plane. Such flow pattern is known as unfavorable regarding suspension (Sharma and Shaikh 2003), what has been confirmed in the present study.

If the jet plane is on its middle tested position (C/B = 0.175) and the water intake at its highest position (h_i/B = 0.375), the flow in the longitudinal plane is disturbed. The radial mixer-like flow pattern is not well developed. There is no more a straight current from the jets towards the water intake.

If the jet plane and the water intake are on their middle tested heights (C/B = 0.175 and h_i/B = 0.25) the flow pattern in the transversal plane is axial mixer-like, whereas the flow pattern in the longitudinal plane is rather radial mixer-like. This combination has been observed to be the most favorable regarding sediment release. This may be explained by the fact that the axial mixer-like flow pattern in the transversal plane is responsible for the most efficient suspension while the radial mixer-like flow pattern in the longitudinal plane provides a straight jet towards the water intake.

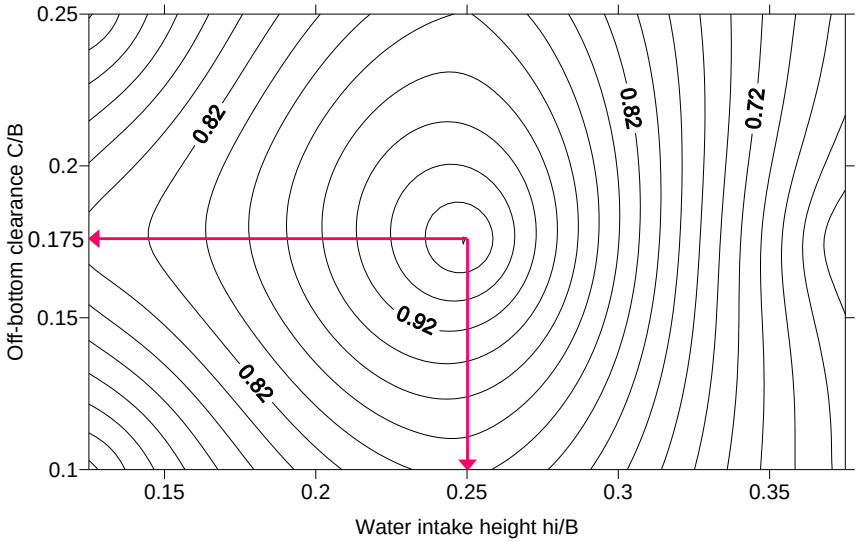

Figure 4.64 *Isolines of normalized evacuated sediment ratio. The normalized evacuated sediment ratio of the combination of the optimal off-bottom clearance and water intake height above bottom for basic geometrical parameters (Table 4.2) and ΣQ_j = 760 l/h is unity (in the centre of the figure).*

4.8.9 Influence of horizontal distance between jet circle centre and front wall

The influence of the horizontal distance d_{axis} between the jet circle centre and the front wall is shown in Figure 4.65 and Figure 4.66 after four hours experimental duration. From Figure 4.65 it appears that there is an optimum for d_{axis}/B around 0.525. For smaller and higher values the evacuated sediment ratio decreases.

The presentation as a function of the total jet discharge (resp. discharge through water intake, Figure 4.66) shows that optimum value was observed for $d_{axis}/B = 0.525$ over the total range of discharge investigated in the tests. For all values d_{axis}/B except $d_{axis}/B = 0.525$ the corresponding evacuated sediment ratio is found to be in the same range. For $d_{axis}/B < 0.525$, this is confirmed for three different discharges (ΣQ_j = 760, 2030 and 4050 l/h). For d_{axis}/B = 0.65 and 0.775, only experiments with discharge ΣQ_j = 760 l/h were performed.

The analysis of the flow pattern can give the reason why there is an optimum value for the horizontal distance between the jet circle centre and the front wall d_{axis}.

As indicated in section 4.6.7 it seems that for $d_{axis}/B < 0.525$ the flow pattern is changing with time, hence, the flow is instable. There are observations with one and with two rotor cores on each side depending on time. Two rotor cores on one side of the circular jet arrangement are typical for a radial mixer, whereas one rotor core indicates circulation of an axial mixer. According to Sharma and Shaikh (2003) an axial mixer is more favorable for suspension. The particles are easier lifted up and are not accumulating beneath the mixer blades. A radial flow pattern may hinder a successful suspension.

Moreover, the flow pattern of $d_{axis}/B = 0.3$ is more chaotic than the flow pattern of $d_{axis}/B = 0.4$. Figure 4.22 shows the flow pattern in the transversal plane for $d_{axis}/B = 0.525$. There is only one rotor core on each side. The instability seems to be limited by the fact that the rotor core may be wandering up and down. As discussed in section 4.6.7 this instability even might be due to the fact that steady state is not yet achieved.

Based on the observations discussed in section 4.6.7, it may be concluded that there are two possible explanations for the optimal distance between the jet circle centre and the front wall $d_{axis}/B = 0.525$:

1. The horizontal current in the longitudinal plane issuing from the jets towards the front wall in direction to the water intake favors the direct transport of suspended sediment laden water towards the water intake.
2. Bearing in mind that the experimental tank has a width of $B/B = 1$ (2 *m* in model scale) and the jet circle centre has a distance to both side walls of $B/B = 0.5$ (1 *m* in model scale), the jets are symmetric to the side walls. $d_{axis}/B = 0.525$ is close to the lateral distance. Such position would allow an axisymmetric configuration at least for three sides, since the back wall is further away (1.225 normalized length). An axisymmetric position may favor flow stability. The longitudinal flow pattern of the axisymmetric position is most regular and has the most developed rotors. The measurements unfortunately didn't reveal that even in the longitudinal plane there might be sporadically a single rotor between the jets and the front wall. Nevertheless, because of axisymmetry this possibility cannot be excluded and would even better explain the optimal distance at $d_{axis}/B = 0.525$.

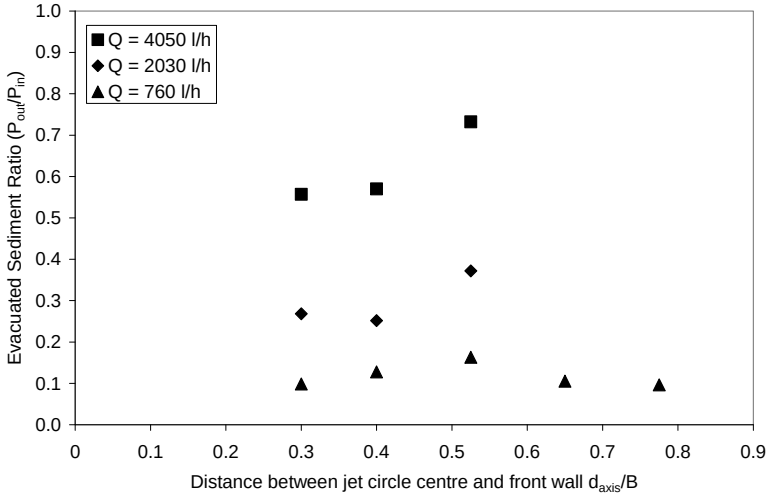

Figure 4.65 *Influence of the horizontal distance between the jet circle centre and the front wall d_{axis}/B on the evacuated sediment ratio for three different total jet discharges (resp. discharges through water intake) after four hours experiment duration.*

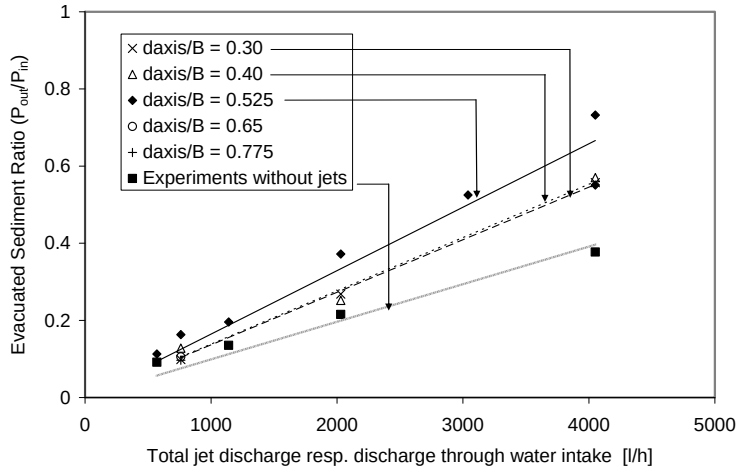

Figure 4.66 *Evacuated sediment ratio after four hours as a function of the total jet discharge (resp. discharge through water intake) for different horizontal distance between the jet circle centre and the front wall d_{axis}/B and for basic geometrical parameters.*

Figure 4.67 depicts the relative reduction in sediment release when using a distance between rotational axis and front wall smaller or longer than the optimal one. The higher the relative difference in distance is the higher is the reduction. The reduction is in the range between 20 and 35 %, depending on the experiment duration (between one and four hours). For shorter distances the reduction increases with time, for longer distances it decreases. After four hours experiment duration the deficit is for all distance variations approximately 25 %.

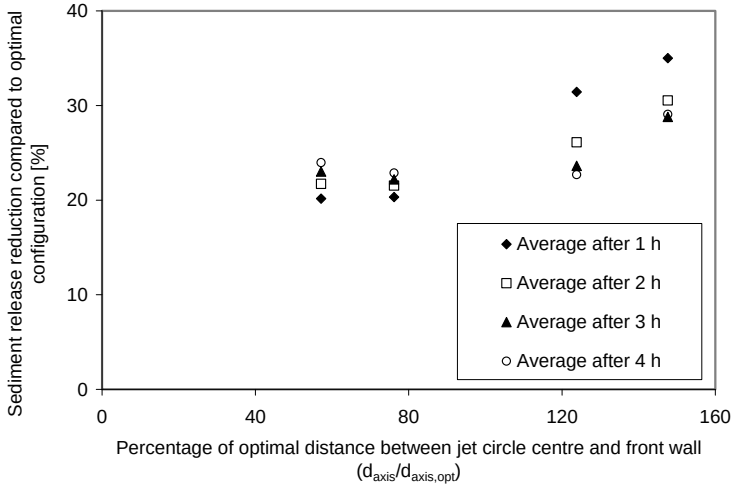

Figure 4.67 Reduction in sediment ratio as a function of the relative optimal distance between jet circle centre and front wall. This reduction is an average over the whole tested discharge range.

4.8.10 Influence of distance between neighbouring jets on sediment release

The horizontal distance l_j between neighboring jets gives indirectly the diameter of the circle on which the jets are lying. In the following the notion of the distance between the jets is employed.

It appears that with the smallest distance $l_j/B = 0.1$, the evacuated sediment ratio after the experiment duration of four hours is rather low. For $l_j/B = 0.15$, there seems to be an optimum, and with $l_j/B \geq 0.225$, the efficiency is decreasing again (Figure 4.68 and Figure 4.69). This was confirmed for all three tested discharges.

The weakly developed rotor in the case of the smallest tested distance between the jets ($l_j/B = 0.1$) and the rather chaotic flow beneath the jets might be the reasons for observed sediment release.

According to Sharma and Shaikh (2003) the critical speed for suspension decreases with increasing impeller size at constant tank diameter. For a given tank size, critical speed varies with $D_{impeller}^{-2}$ ($D_{impeller}$: impeller diameter, Sharma and Shaikh, 2003). The proportionality, however, is given only up to a value of $D_{impeller}/D_{tank}$ (D_{tank}: tank diameter), which

approximately is equal to 0.35. This is opposite to the observations in the present study, where starting from $l_j/B = 0.15$ with increasing diameter the sediment release decreases, which must be related to the different test conditions. In chemistry mostly axisymmetric (baffled) vessels are used, whereas in the present study the tests were performed in an elongated tank. Moreover, in the present study the sediment release is the purpose, whereas in the mechanical mixer studies the focus is set on the suspension process itself.

Busnaina et al. (1981) found in their destratification field tests and numerical simulations for a constant propeller flow rate an optimal non-dimensional propeller diameter, below which dilution is ineffective. Non-dimensionalisation was made by dividing by the water height, which confirms the findings of the present study.

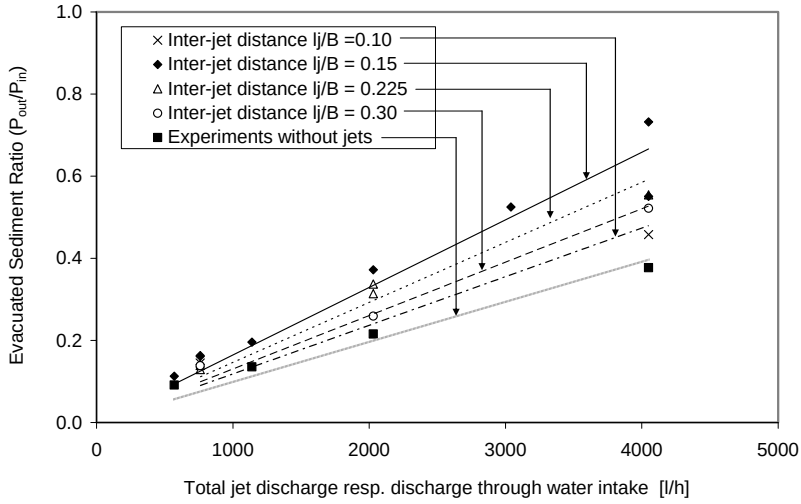

Figure 4.68 Evacuated sediment ratio after four hours as a function of the total jet discharge (resp. discharge through water intake) for different horizontal distance l_j/B between two neighbouring jets while keeping the others geometrical parameters constant.

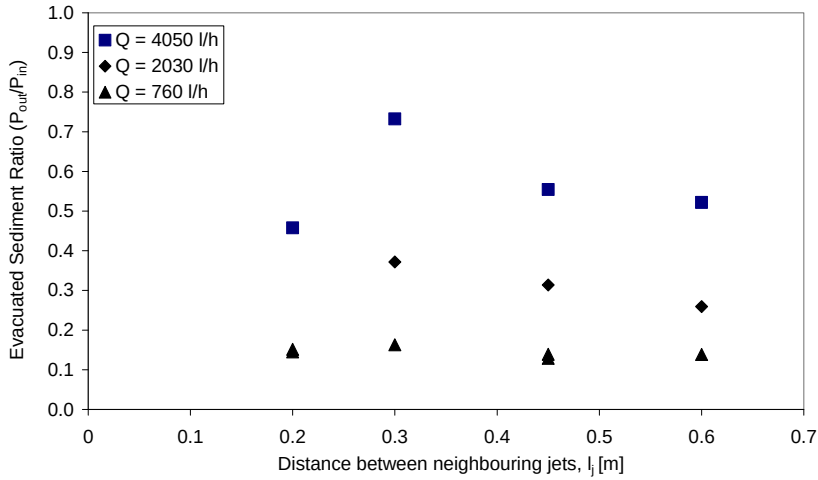

Figure 4.69 Evacuated sediment ratio as a function of the horizontal distance between two neighboring jets, lj.

In Figure 4.70 the reduction in sediment release due to a variation in the distance between neighboring jets is presented. It can be seen that with test duration the reduction increases for all tested distance variations. The reduction generated by employing a shorter distance is higher than with longer distances. With shorter distance the reduction is around 20 % after 1 hour test duration and reaches almost 35 % at the end of the experiment (four hours). Both longer distances have after one hour approximately a 10 % deficit, whereas after four hours the longest distance causes a reduction of 27 % and the second longest distance one of approximately 18 %. The optimum corresponds to a jet circle diameter close to the quarter of the tank width ($0.222 \cdot B$).

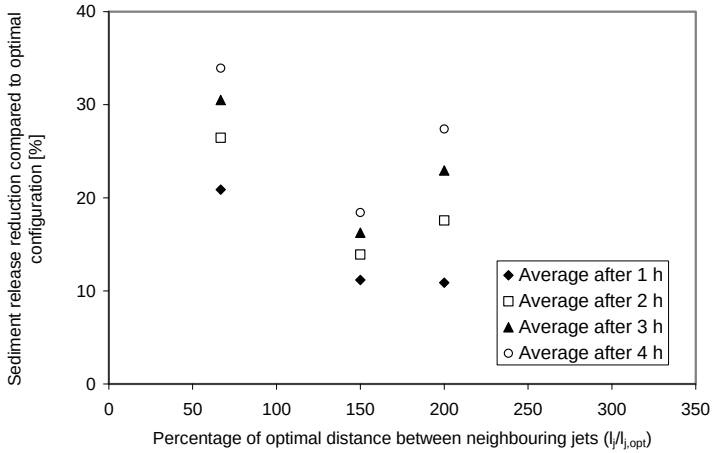

Figure 4.70 Reduction of sediment ratio as a function of the optimal distance between neighboring jets. This deficit is an average over the whole tested discharge range.

4.8.11 Influence of jet angle on sediment release

One experiment was carried out installing the jets with an angle of 45° in respect to the horizontal plane. The others geometrical parameters were held like in the basic configuration (Table 4.2). As can be seen in Figure 4.71 the basic configuration is more efficient and releases more sediment in the same time period. According to Figure 4.72 the reduction of sediment ratio due to the angle variation is increasing with time reaching 35 % after four hours experiment duration.

The corresponding flow patterns presented in Figure B.47 and Figure B.48 show one rotor on each side in the transversal plane having its core closely beneath the water surface. The circulation is well developed. The rotors are directed in the opposite sense of those induced by horizontal jets and are similar to what is expected if an axial mixer is introduced upside down. According to the reflections of Sharma and Shaikh (2003) this movement accumulates sediment beneath the jets and is therefore adverse in view of suspension. The upward movement observed in the longitudinal plane is for continuity reasons compensated in other tank areas, where it might have an unfavorable effect concerning suspension, too. These two considerations may explain the inefficiency of the jets oriented upward.

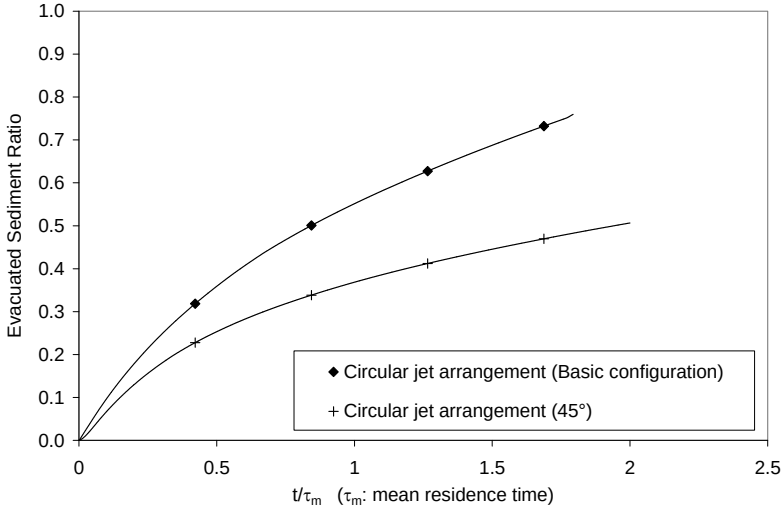

Figure 4.71 Evacuated Sediment Ratio for basic configuration with jet angle 0° and with jet angle 45°, respectively, as a function of normalized time.

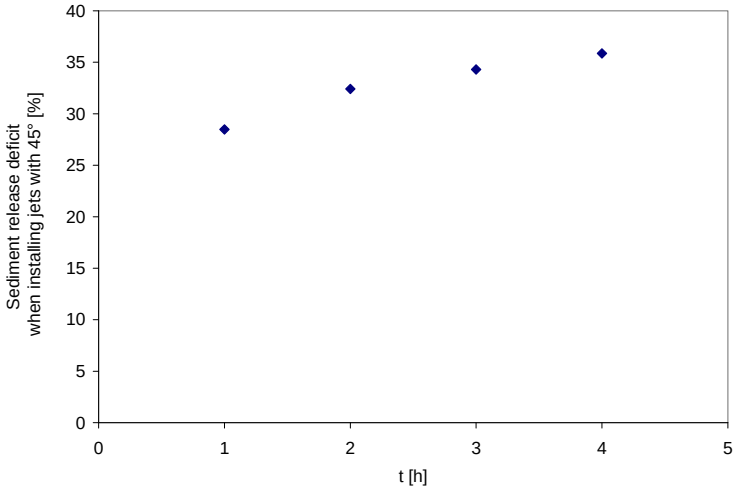

Figure 4.72 Reduction in sediment release for jets inclined by 45°.

4.8.12 Concluding remark

For all performed experiments and for the duration of four hours a quasi linearity between discharge and sediment release has been observed. As expected with increasing discharge the sediment release increases.

In analogy to the experiments without jets, sediment settling was observed. However, contrary to experiments without jets, resuspension of settled sediment is observed for discharges higher than ΣQ_j = 2030 *l/h*. Based on this finding and on the results of three experiments, where a settled sediment ratio peak had been reached, a long term prediction of sediment release was established. The observed resuspension rate suggests that for discharges higher than ΣQ_j = 2030 *l/h* at a final stage all of the initially supplied sediment is evacuated. For smaller discharges resuspension has not been observed.

An optimal geometrical parameter set for circular jet arrangements has been identified: off-bottom clearance 0.175, water intake height 0.25, and distance between neighbouring jets 0.15, distance between jet circle centre and front wall 0.525, water height 0.6, and jet angle 0° in respect to the horizontal.

A variation of a single geometrical parameter within the tested range (i.e. 60 to 200 % of the optimum value) caused a sediment release reduction of up to 40 %, depending on the parameter and the duration.

4.9 Sediment release with linear jet arrangements

Although in the case of d_{line}/B = 0.2 the flow pattern in the longitudinal plane seems rather favorable for sediment release, the evacuated sediment ratio doesn't reach the magnitude of the circular jet arrangement (Figure 4.73 and Figure 4.74). Evoking the observations discussed in section 4.7 the transversal flow patterns are not favorable in view of suspension. The sediment is drawn down along the side walls to the bottom and is accumulated in the longitudinal tank middle axis from where it is difficult to be eroded again. This explains the generally worse evacuated sediment ratio result.

The best tested experiments (with distance between jet line and front wall d_{line}/B = 0.2, jet angle 45°, and water intake height h_i/B = 0.25) provide evacuated sediment ratios in the range of the reference tests (without jets). In this case the jets are pointing directly to the water intake. If the jets are installed too close or too far from the front wall, the arrangement is even contra productive and there is less sediment evacuated than in case of no jets.

It may be concluded that the linear jet arrangement tested in the presented experiments is not favourable regarding sediment release. The comparison of the results reveals that the circular jet arrangement is much more favourable.

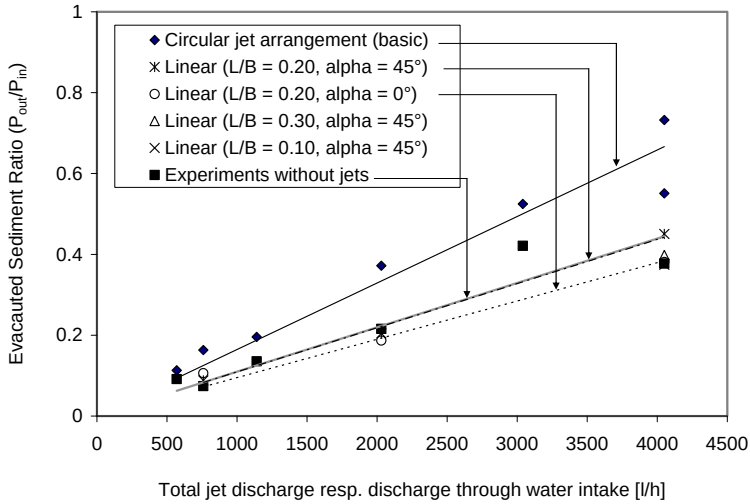

Figure 4.73 Evacuated Sediment Ratio for optimal circular jet arrangement and different linear jet arrangements as a function of the discharge. (Total jet discharge equals water intake discharge $\Sigma Q_j = Q_{out}$ = 4050 l/h).

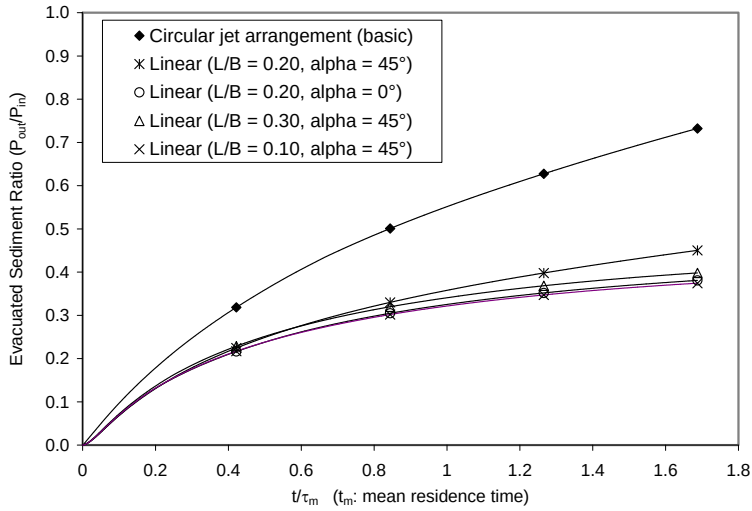

Figure 4.74 Evacuated Sediment Ratio for four different aligned jet arrangements tested with ΣQj = 4050 l/h compared to the circular jet arrangement with basic geometrical parameters as a function of normalized time.

4.10 Optimal jet configuration

The discussions concerning flow patterns (sections 4.6 and 4.7) and sediment release (sections 4.8 and 4.9) reveal that an axial mixer-like flow pattern in the transversal plane is favorable regarding suspension. This finding is confirmed by Sharma and Shaikh (2003). Moreover, it can be seen that in the longitudinal plane a radial mixer-like flow pattern is favorable for sediment release, if the current issuing from the jets towards the front wall goes straight towards the water intake. A stable single rotor between the jets and the front wall seems also to provide good results.

As a conclusion the optimal flow pattern is in a rectangular tank achieved with the basic circular jet configuration arranged with the following geometrical parameters (Table 4.4):

off-bottom clearance	$C/B = 0.175$
water intake height	$h_i/B = 0.25$
distance between neighbouring jets	$l_j/B = 0.15$
distance of jet circle centre to front wall	$d_{axis}/B = 0.525$
water height in the tank	$h/B = 0.6$
jet inclination angle	$\theta = 0°$

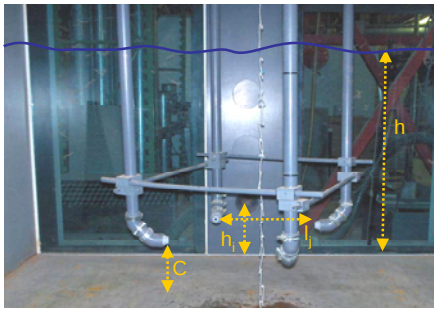

Table 4.4 Optimal jet configuration

A variation of a single geometrical parameter within the tested range (i.e. 60 to 200 % of the optimum value) caused a sediment release reduction of up to 40 %, depending on the parameter and the duration.

4.11 Empirical relationship

4.11.1 Experiments with jets

As discussed in 4.8.4 the prediction of the long-term evolution of the sediment release when employing jets is based on several assumption. Moreover, the prediction has been tried for experiments performed with the configuration basic geometrical parameters (Table 4.2) only. A general formula determining the evacuated sediment ratio for any duration, discharge and geometrical parameter is more of interest.

4.11.1.1 Empirical relationship for sediment release efficiency based on all measurements with circular jet arrangement

Based on all hourly measurements of the circular jet arrangements an empirical relationship was established. Despite its simplicity the proposed empirical equation (Equation 4.24) was developed using a genetic programming tool: Evolutionary Polynomial Regression-EPR (Giustolisi and Savic 2003).

$$ESR_{jet} = 1.033 \frac{\sqrt{t \cdot \tau_s}}{\tau_m} \quad \text{(Eq. 4.24)}$$

with ESR_{jet}, the evacuated sediment ratio when employing jets, t, the experimental duration, τ_s the normalized settling time defined by the water height divided by the settling velocity, and τ_m the mean residence time defined by the tank volume divided by the total jet discharge (equal to discharge through water intake).

This empirical relationship gives direct proportionality between evacuated sediment ratio and discharge. Nevertheless, as discussed in section 4.8.2 a non-linear relationship was found for idealized conditions. Likewise, the relationship according to idealized conditions does not have the same proportionality regarding time as found in the empirical relationship. Moreover, it appears that in this equation there is just one single geometrical variable: the water height, contained in the normalized settling time τ_s and the tank volume. Nevertheless, the correlation coefficient is 0.967 while the average error is 14.1 %. In this relationship all the considered experiments are equally weighted.

The average error over the four hours in respect to the basic geometrical configuration is 17.6 %. But the evolution of this error is inconsistent with time: after one hour the average error is 22 %, after two hours 6.7 %, after three hours 16.3 % and after four hours 25 %.

4.11.1.2 Empirical relationship for sediment release efficiency exclusively based on extrapolated basic geometrical parameters

If the three aforementioned experiments (basic configuration with ΣQ_j = 4050, 3040, and 2030 l/h) are considered temporally extrapolated (section 4.8.4), the proposed empirical equation would be Equation 4.25 with 15.3 % average error for the basic configuration and 14.8 % for all the considered experiments:

$$ESR_{jet} = 1.082 \frac{\sqrt{t \cdot \tau_s}}{\tau_m} \quad \text{(Eq. 4.25)}$$

Thus, this equation fits better the measurements of the basic configuration. Figure 4.75 shows the comparison between the predicted (Eq. 4.25) and the measured evacuated sediment ratio. With a correlation coefficient of 0.969 the agreement is very good.

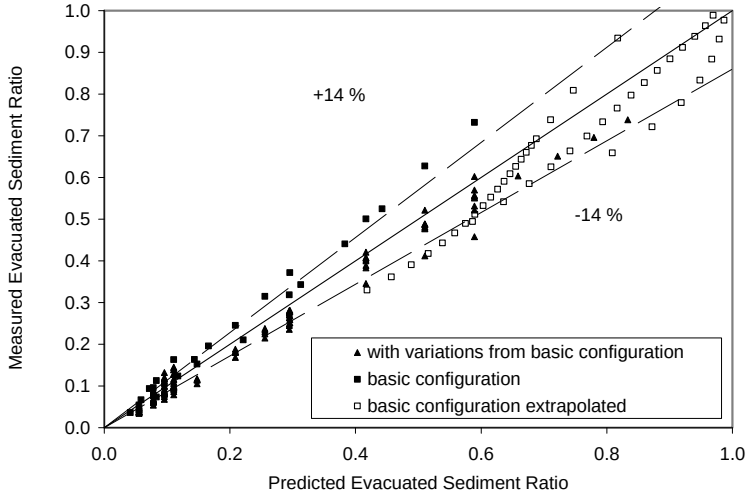

Figure 4.75 Comparison between predicted (Eq.4.25) and extrapolated evacuated sediment ratio.

4.11.1.3 Empirical relationship for sediment release efficiency exclusively based on measurements with basic circular jet arrangement

In case only the measurements of the basic configuration are taken into consideration, the prediction equation becomes

$$ESR_{jet} = 1.2859 \frac{\sqrt{t \cdot \tau_s}}{\tau_m} \qquad \text{(Eq. 4.26)}$$

with a correlation coefficient of 0.9883 and with an average error of 10.3 % (Figure 4.76). If the extrapolated data are added the prediction equation becomes

$$ESR_{jet} = 1.102 \frac{\sqrt{t \cdot \tau_s}}{\tau_m} \qquad \text{(Eq. 4.27)}$$

with a correlation coefficient of 0.9279 and with a average error of 10.5 % (Figure 4.76).

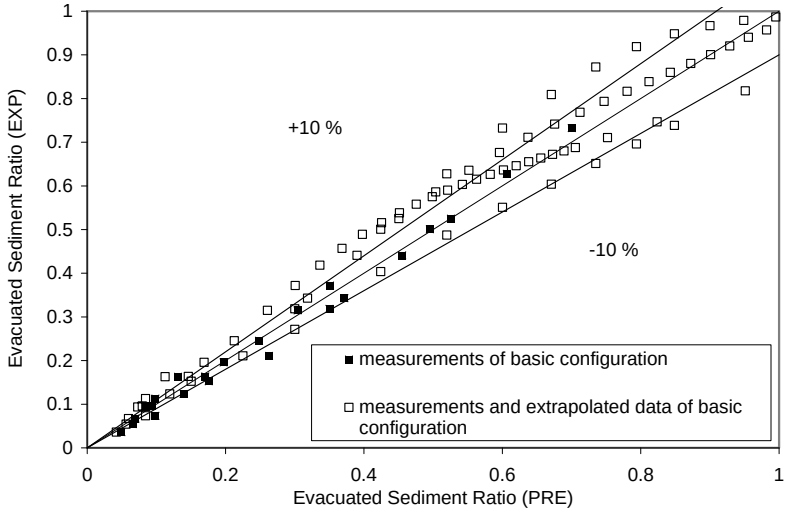

Figure 4.76 Comparison between the experimental results (EXP) and the predictions (PRE) of Equation 4.26 (measurements only) and Equation 4.27 (measurements and extrapolated data) for experiments with the basic configuration only.

4.11.2 Experiments without jets

Concerning the experiments without jets the empirical equation proposed by EPR is the following

$$ESR_{no\ jets} = 0.7742 \frac{\sqrt{t \cdot \tau_s}}{\tau_m} \qquad \text{(Eq. 4.28)}$$

with $ESR_{no\ jets}$, the evacuated sediment ratio in case no jets are used.

The correlation coefficient is 0.958 and the average error is 15.3 % (Figure 4.77).

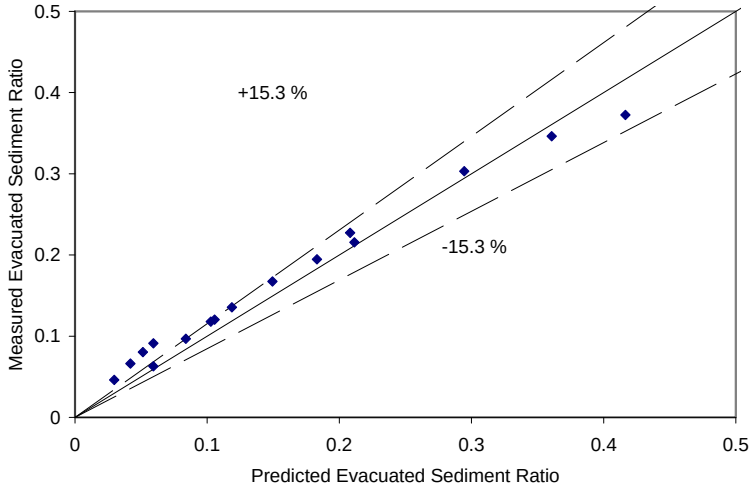

Figure 4.77 Comparison between predicted (Eq.4.28) and measured evacuated sediment ratio (no jets).

4.11.3 Concluding remarks

The established empirical equations for the case with jets all have an excellent correlation coefficient, i.e. higher than 0.93. Nevertheless, for sediment release predictions in optimal conditions it is certainly accurate to use the relationship based on the basic configuration expressed with a constant of approximately 1.29 (Eq. 4.26). In case of a variation of a single geometrical parameter within the tested range (i.e. 60 to 200 % of the optimum value) Eq. 4.24 applies with its characteristic constant of 1.033.

As discussed in section 4.8.4.3 the long term extrapolation is based on certain uncertainties. Therefore, the empirical relationships based on the extrapolated values should be carefully used. Nevertheless, the according correlation factors are also very high, namely 0.93 for all measurements included extrapolated values and 0.97 for basic circular jet configuration with extrapolated values. Their characteristic constant (1.082 and 1.102, respectively) is in the range of the empirical equations based on measurements only. Thus, the committed error would not be high.

The characteristic constant of the empirical relationship for experiments without jets is low, namely 0.77.

All of the established empirical formulae give unlimited evacuated sediment ratio for long duration *t*. This is physically not correct since the ratio cannot be higher than unity. Moreover, it doesn't take into account if resuspension takes place or not. If it doesn't come to resuspension the ratio should asymptotically fall to a value smaller than unity. This is important for the case without jets and for the jet configuration with a discharge below the threshold.

4.12 Efficiency of circular jet arrangement

4.12.1 Introduction

The efficiency of jets is established by comparing the results obtained for the cases with and without jets.

With the previously elaborated results there are two ways of comparison: one is based on the prediction equations (empirical relationship), the other on a direct comparison of measurements.

4.12.2 Predicted efficiency based on empirical relationships

For the first approach the prediction equations obtained for the case with jets are compared with prediction equation 4.28 (without jets):

$$Efficiency = \frac{ESR_{jet}}{ESR_{no\ jets}} \qquad \text{(Eq. 4.29)}$$

In case all the measurements are considered (prediction equation 4.24) the sediment evacuation efficiency is 1.30±0.34, regardless the position, the duration, and the discharge of the jets. In case only the measurements of the basic configuration are considered (prediction equation 4.26) the sediment evacuation efficiency is 1.66±0.30. This means that by using the jets in the optimal position the gain is 66±30 %. Since the long term extrapolation of the data resulting from the basic configuration is based on several assumptions the extrapolated values are uncertain. Nevertheless, taking into account additionally the long term evolution as established in section 4.8.4 (prediction equation 4.27) the estimated sediment evacuation efficiency is 1.42±0.29.

4.12.3 Measured efficiency

A direct comparison between the data obtained in experiments with and without jets is made. Figure 4.78 shows the sediment evacuation efficiency when employing jets as a function of normalized time. It can be observed that it exceeds quickly unity. In other words, by this approach it is confirmed that the jets generate a circulation such that the sediment release is significantly higher than without jets. This is true for both the transient phase (until approximately $t/\tau_m = 0.5$) and the steady state.

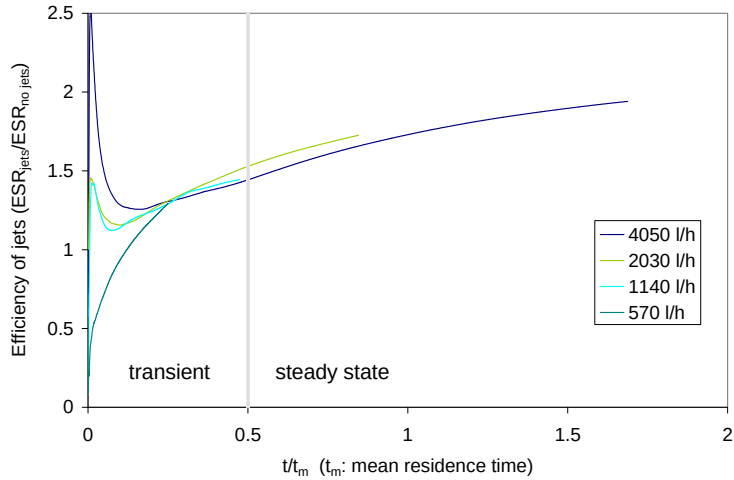

Figure 4.78 *Efficiency of jets by comparing the evacuated sediment ratio obtained with and without jets, respectively.*

Assuming no resuspension in the case of the experiments without jets the settled sediment ratio reaches a maximum when no sediment is in suspension any more. The final efficiency becomes then:

$$\text{Efficiency} = \frac{1}{\text{1-settled sediment ratio (no jets)}} = \frac{ESR_{jets}}{ESR_{no\ jets}} \qquad \text{(Eq. 4.30)}$$

The evacuated sediment ratio for the case without jets is given in Table 4.1. Table 4.5 gives the final efficiency derived from Eq. 4.30 as a function of the discharge.

Discharge	*Final efficiency*
$Q_{out} = \Sigma Q_j$ = 570 l/h	*(9.1)*
$Q_{out} = \Sigma Q_j$ = 1140 l/h	*(6.5)*
$Q_{out} = \Sigma Q_j$ = 2030 l/h	*4.6*
$Q_{out} = \Sigma Q_j$ = 4050 l/h	*2.7*

Table 4.5 *Final efficiency as a function of the discharge. Values in parentheses are theoretical.*

4.12.4 Discussion

Between t/τ_m ~ 0.5 and 1.7 the measured efficiency and the efficiency based on the empirical equations are in the same range (section 4.11). The efficiency obtained with the empirical

equations is time and discharge independent, whereas the efficiency obtained by the measurements depends on both, time and discharge. This can be discussed as follows:

With a low discharge and in the absence of jets only a relatively small sediment ratio is evacuated and a part of the sediments remains on the bottom of the tank. With a higher discharge there is more sediment evacuated per time. Thus, the final settled sediment amount is smaller than for low discharge. As a consequence, in the course of time and assuming that all sediment is evacuated when using jets, the final efficiency using jets is higher for lower discharges.

This statement is confirmed by extrapolating the corresponding experiments. The final efficiency derived from Eq. 4.30 is given in Table 4.5 as a function of the discharge. Since for $Q_{out} = \Sigma Q_j = 1140$ *l/h* and for $Q_{out} = \Sigma Q_j = 570$ *l/h* no resuspension was observed, the so established final efficiencies as given in Table 4.5 are biased.

The efficiencies summarized in Table 4.5 are based on the assumptions of constant discharge and equal discharges flowing out of the tank and in. However, in a real reservoir discharges are permanently varying and it becomes, hence, difficult to derive the efficiency for a real reservoir. The sediment release itself is in a real reservoir of much more interest, since a sediment release as high as possible is aimed.

It can be concluded from the experiments that thanks to the jet induced circulation the whole water volume in the tank is well mixed. So is the water volume in front of the water intake, which by the purpose of the present study, shall be liberated from sediments. Moreover, with a persisting jet discharge $Q_{out} = \Sigma Q_j \geq 2030$ *l/h* almost all initially supplied sediments are expected to be evacuated at long term. This is a big advantage compared to the conditions without jets and very promising for the real case.

For discharges $Q_{out} = \Sigma Q_j < 2030$ *l/h* no resuspension had been observed during the four experimental hours. Nevertheless, with jets still better mixing was achieved than without jets, and the efficiency of approximately 1.5 is reached even if no resuspension takes place (Figure 4.78).

4.13 Application range

The results of the present study were obtained under given test conditions. Thus, it is certain that they apply to the employed rectangular laboratory tank, the used sediment (crushed walnut shells) as well as to the used jet discharge, velocity and diameter range.

It is, as usual, difficult to apply the obtained results to other conditions. Since the ratio of the tank length over width was not varied in the experiments, its influence on mixing and on sediment release is not known. Moreover, the influence of other sediment grain size distributions and densities has not been investigated either. Thus, when varying the tank dimensions and/or the sediment characteristics, the discharge range used in the present study will not have the same effect on mixing and sediment release as discussed above.

5 Numerical modelling of flow patterns

5.1 Introduction

In this chapter results of the numerical simulations are presented and discussed. Numerical models can provide a better understanding of instabilities in the flow field. Moreover, the influence of different tank geometries on the jet induced circulation can be easily highlighted.

Furthermore, the numerical models guarantee exact discharge input through exactly positioned nozzles, whereas in an experimental set-up rotameters have an error of ±5 % and nozzles position have an error of about ±3 *mm*. Furthermore, although the rigid pipes with the nozzles were fixed at a frame small vibrations could not completely be ruled out. Compared to the ideal situation in the numerical model the experimental installation has therefore some imprecision as it would also be the case in real case installation.

Simulations with clear water only were performed since it is not absolutely sure if the numerical model can represent correctly the sediment release efficiency quantitatively.

5.2 Methodology of numerical study

The flow is simulated using the software package ANSYS-CFX 12. The simulations are performed using the *k-ε* turbulence model. Other turbulence models were tested (RNG *k-ε,* Shear Stress Transport, Standard k-ω), but the *k-ε* model has proven to give satisfactory results for the simulation of the jets (centerline velocity and velocity at transverse distance are in good agreement with the theory). In a first step the simulations are run in steady state, with gradually increasing time steps. As for the laboratory experiments the steady state calculation requires at least a duration as observed in the experiments to reach the end of the transient phase. For two of the presented cases transient simulations were performed as soon as steady state was expected to be achieved. For two other cases simulations it is assumed that the simulation time was too short to reach steady state.

5.3 CFD Model

Three simulations were performed with the same tank dimensions as in the laboratory experiments (chapter 3). The fourth simulation had an elongated tank (7 *m* long instead of 3.5 *m*). Only circular jet arrangements were modeled, mainly with the basic geometrical parameters, but by varying the off-bottom clearance and the water intake height. The total discharge through the nozzles was fixed in each case at a constant rate of ΣQ_j = 760 *l/h*.

Simulation number	*Off-bottom clearance C/B*	*Water intake height h_i/B*	*Length over width ratio L/B*	*Forerun in steady state*
N1	*0.1*	*0.175*	*1.75*	*3 h*
N2	*0.175*	*0.25*	*1.75*	*1.5 h*
N3	*0.25*	*0.325*	*1.75*	*2.6 h*
N4	*0.175*	*0.25*	*3.5*	*33 min*

Table 5.1 Overview of the numerical simulations with their varied geometrical parameters

5.3.1 Mesh generation

For mesh generation the ANSYS attached software ICEM was used. The area in the vicinity of the jets was modelled with hexahedral elements (Figure 5.3 to Figure 5.6). For the round jet nozzles the O-grid application was used (Figure 5.4 and Figure 5.5). Because of the small nozzle diameter (3 *mm*) and the relatively high velocities (7.5 *m/s* at the inlet) the smallest element had its smallest dimension with 0.5 *mm* in length (Figure 5.4). In order to allow coarser mesh elements in the rear part of the tank, a transition mesh made of tetrahedral elements was modelled around the jets mesh (Figure 5.2 and Figure 5.3). Around the tetrahedral mesh the coarser hexahedral mesh was attached. The hexahedral mesh modelling the bell-shaped water intake was integrated in the tetrahedral mesh part (Figure 5.7). For the fluid fluid interfaces between the different mesh pieces conservative interface flux is defined. The GGI (General Grid Interface) connection was used creating an interface between two meshes with different node locations and element types.

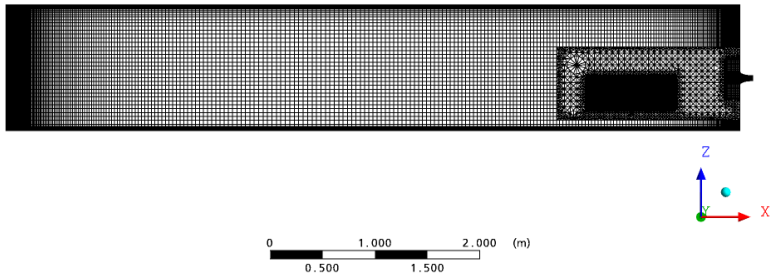

Figure 5.1 Longitudinal cross section through the mesh of simulation N4 (elongated tank with L = 7 m instead of 3.5 m). A zoom of the mesh near the jets is given in Figure 5.2 and Figure 5.3.

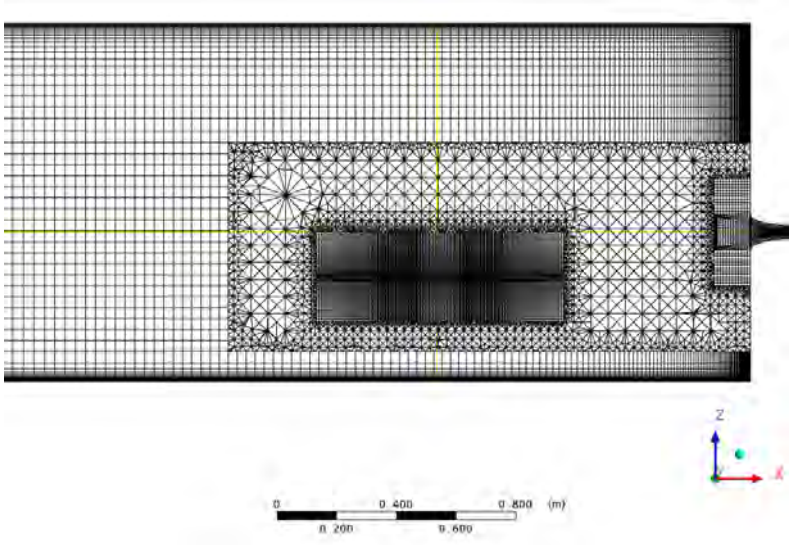

Figure 5.2 *Front part of the longitudinal cross section through the mesh of simulation N4 (elongated tank).*

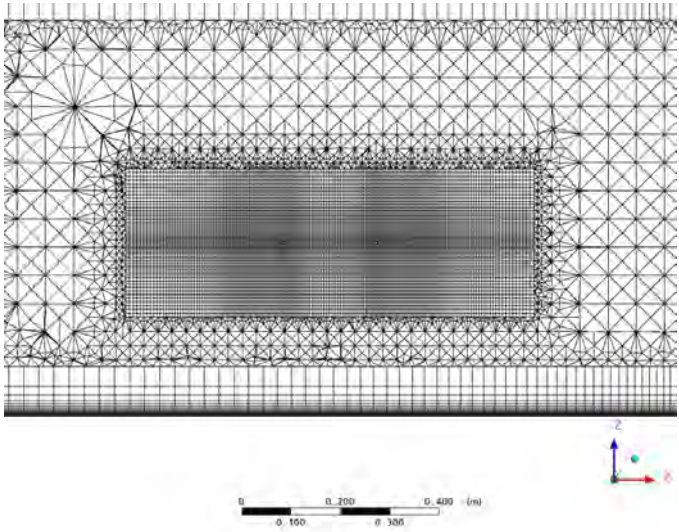

Figure 5.3 *Zoom on the jets area modeled with hexahedral elements. Longitudinal cross section.*

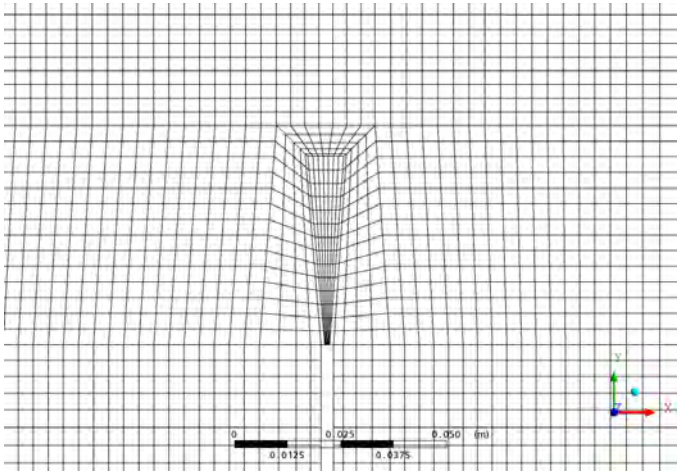

Figure 5.4 Zoom of the top view on a single jet on its installation height.

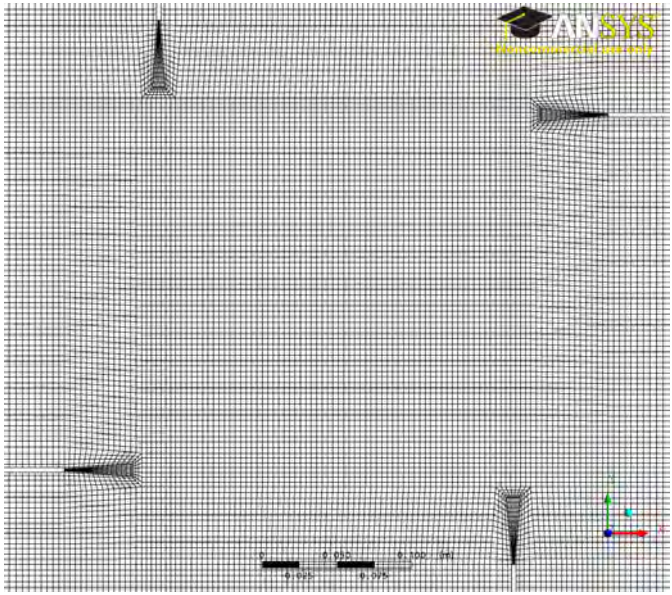

Figure 5.5 Zoom of the top view on the four jets on their installation height.

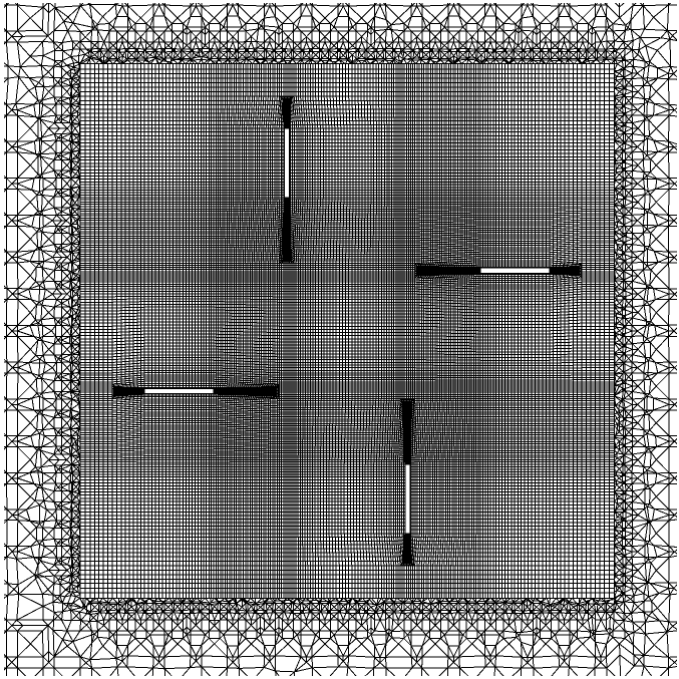

Figure 5.6 Zoom of the top view on the four jets on their installation height.

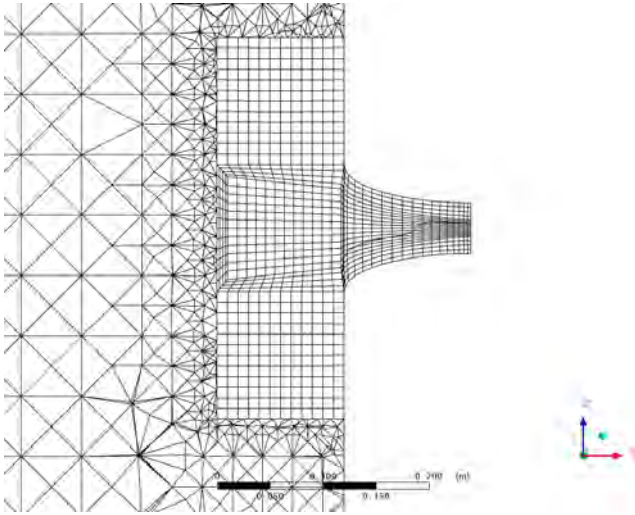

Figure 5.7 Zoom on the cross section of the water intake.

5.3.2 Boundary conditions

Following conditions were set at each boundary of the model:

Free-surface:	free-slip wall condition with no shear was applied
Bottom and tank walls:	no-slip wall condition was considered
Nozzles:	the inlets having a diameter of 3 *mm*, the fluid velocity was uniform with a magnitude of 7.5 *m/s*
Water intake:	average static pressure in order to maintain the water level was considered. Equilibrium between the sum of the inlet discharges and the outlet discharge is conditioned

5.4 Results

5.4.1 Comparison of numerical and experimental flow patterns

The flow patterns obtained from numerical simulation (N2) with basic geometrical parameters (Table 4.2) are compared with the experiments. The numerically obtained flow pattern in the transversal plane (Figure 5.8 above) is very similar to the experimentally obtained flow pattern (Figure 5.8 below), because all the geometrical parameters and jet characteristics are equivalent.

The longitudinal flow patterns obtained by numerical simulation (Figure 5.9 above) and by experiments (Figure 5.9 below) are quite similar. Nevertheless, the rear part matches better than the front part. In the front part the numerical flow pattern approaches the experimentally observed flow pattern for higher discharges having a single rotor (Figure 4.26, Figure B.8 and Figure B.9). As discussed in section 4.6.3 this could be due to two different reasons and might not necessarily be related with the discharge:

1. The numerical forerun of 1.5 hours was not long enough and the numerical simulation is still in the transient phase, whereas the experiment was more advanced in time.
2. There are significant flow instabilities and the flow pattern is changing as a function of time.

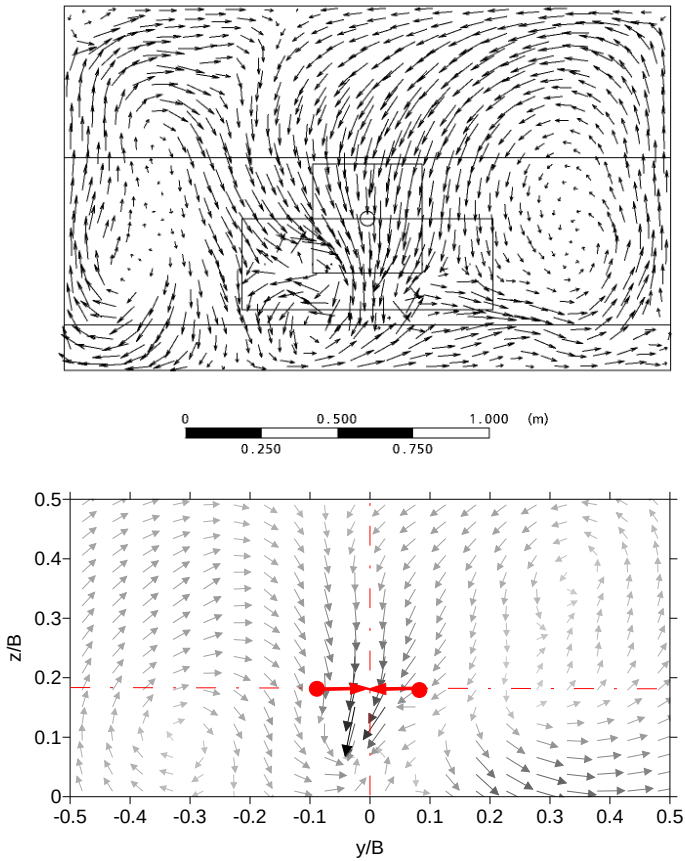

Figure 5.8 Above: numerically obtained transversal flow pattern of simulation N2, below: experimentally obtained transversal flow pattern for ΣQ_j = 760 l/h and basic geometric parameters (Table 4.2)

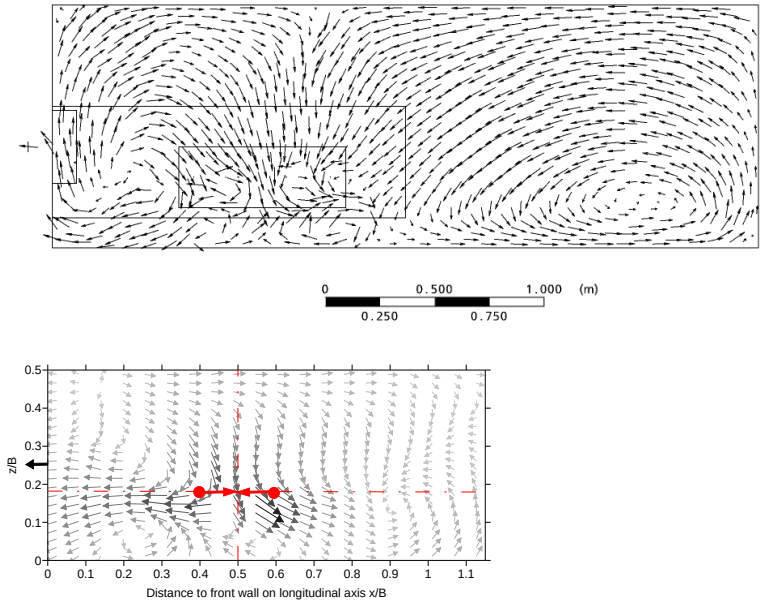

Figure 5.9 *Above: numerically obtained longitudinal flow pattern of simulation N2, below: experimentally obtained longitudinal flow pattern for ΣQ_j = 760 l/h and basic geometric parameters (Table 4.2)*

5.4.2 Test of congruence

Comparison between the experimentally and numerically obtained flow fields gives only the approximate congruency of circulations. Therefore, for validation of the numerical simulations the measured flow velocities on the water intake axis and on the vertical axis passing through the jet circle centre were also compared with the corresponding velocities obtained by the numerical simulations. Figure 5.10 to Figure 5.15 visualize this comparison for the case with the basic geometrical parameters (Table 4.2) and for ΣQ_j = 760 *l/h* (numerical simulation N2 and hydraulic experiment C2). The numerical simulation was running for 1.5 hours before the results were extracted (Table 5.1). As mentioned in subchapter 5.2 this might be an insufficient duration and the circulation might still be transient.

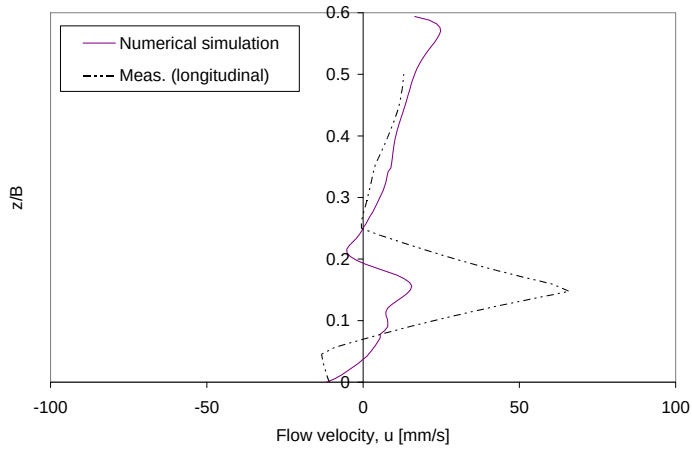

Figure 5.10 *Horizontal flow velocity u on the vertical axis passing through the jet circle centre, in longitudinal direction of the tank for numerical simulation (continuous line) and experiments measured in the longitudinal plane (dashed-dotted line). Positive values correspond to a movement from the front wall inward.*

According to Figure 5.10 the horizontal flow velocities *u* for the experiments as well as for the numerical simulations are almost along the whole water column positive and, hence, directed to the back of the tank. The experimentally obtained pronounced current on the jet level is reproduced by the numerical simulations, but with smaller magnitude. Below the jets a counter current is visible.

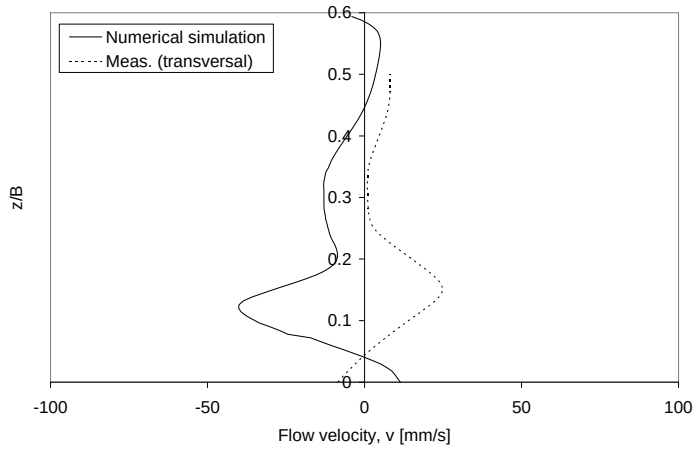

Figure 5.11 Horizontal flow velocity v on the vertical axis passing through the jet circle centre, in transversal direction of the tank for numerical simulation (continuous line) and experiments measured in the transversal plane (dotted line). Positive values correspond to a movement from right to left viewed in flow direction.

The transversal velocity *v* has a peak with similar magnitude at the jets level as the longitudinal velocity (Figure 5.11). This peak is present in the numerical simulations as well as in the measurements. Nevertheless, in the numerical simulation it is stronger and on the opposite side. On the one hand this might be due to instabilities on the axis and the current flips from one side to the other. On the other hand there might be a sharp line along the vertical rotation axis separating the currents issuing to the opposite directions. Thus, experimentally the current heading to the right side might be measured, and from the numerical simulations the opposite current might be visualized.

The developing of the transversal velocity *v* above the jets is similar for both, numerical approach and measurements, and is close to zero. The velocities in the longitudinal direction are in this section more important (Figure 5.10).

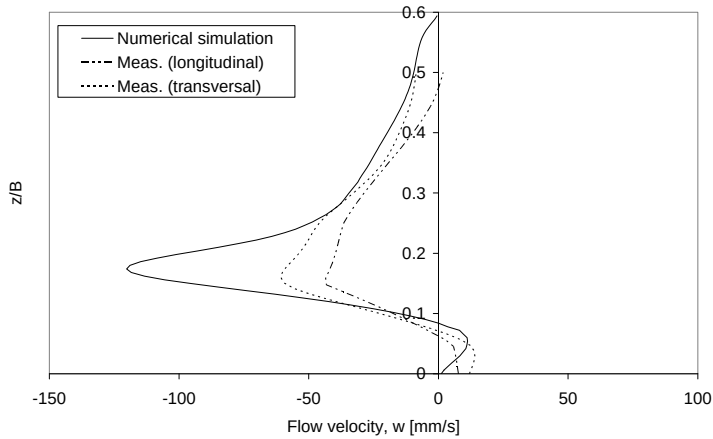

Figure 5.12 *Vertical flow velocity w on the vertical axis passing through the jet circle centre, in transversal direction of the tank for numerical simulation (continuous line) and experiments measured in the transversal plane (dotted line) and in the longitudinal plane (dash-dotted line).*

The vertical flow velocities *w* measured on both, longitudinal and transversal plane reveal a clear peak on the jets level. It is the same for the result obtained by the numerical simulation (Figure 5.12). Although the magnitudes of the vertical velocity are not identical for the three cases, the shape of the curves is very similar. The movement is almost all along downward and accelerated in the area of the jets. For $z/B < 0.1$ the movement is in upward direction and indicates the presence of a counter current.

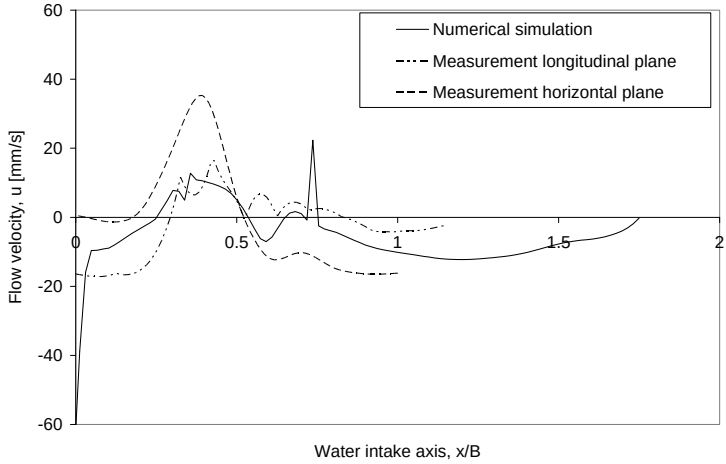

Figure 5.13 *Horizontal flow velocity u on the water intake axis, in longitudinal direction of the tank for numerical simulation (continuous line) and experiments measured in the longitudinal plane (dashed-dotted line) and in the horizontal plane (dashed line). Positive values correspond to a movement from the front wall inward.*

According to Figure 5.13 all the flow velocity *u* curves have positive values around $x/B = 0.4$. Moreover, the experimentally obtained measurements as well as the numerical simulations have a peak in this area, corresponding to the location of the longitudinally oriented jet in the vicinity of the front wall. At the jet circle centre ($x/B = 0.5$) the measurements have a transition from positive to negative values indicating the separation of the two radial currents. At $x/B = 0.6$ the numerical simulations reveal a smooth negative peak. This position corresponds to the location of the opposite longitudinally oriented jet.

According to the measurements the flow field generated by the jets is influenced by the presence of the wall. Since the location $x/B = 0.5$ corresponds to the centre of the jet arrangement and the jets are arranged point symmetrically to it, the flow velocity curve should also be point symmetrical to the centre location. This can be observed in Figure 5.13, but the jet circulation is visibly disturbed by some other circulation, which is probably influenced by the wall and the water intake or by the larger far field at the opposite side of the jet arrangement, respectively. At distances $x/B > 0.75$ the flow on the water intake axis is oriented in direction to the water intake. The numerical simulation gives the same tendency, whereby the velocity magnitude is not in all curves the same and is between 5 and 20 *mm/s*.

The peak at $x/B = 0.75$ is due to intermesh boundary interpolation.

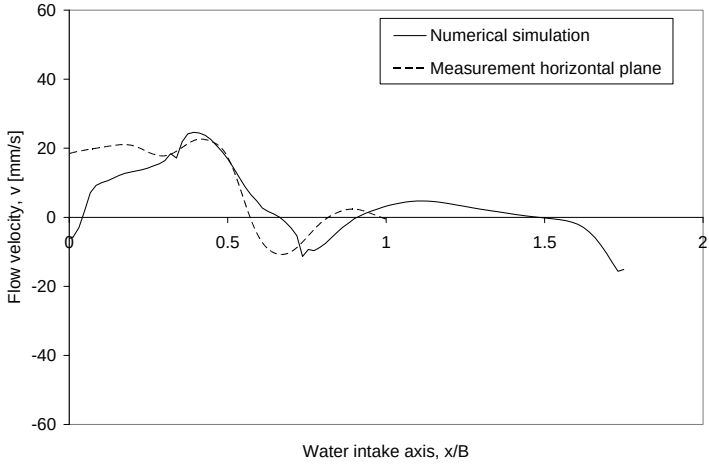

Figure 5.14 Horizontal flow velocity v on the water intake axis, in transversal direction of the tank for numerical simulation (continuous line) and experiments measured in the horizontal plane (dashed line). Positive values correspond to a movement from right to left viewed in flow direction.

The horizontal flow velocities *v* are in the numerical simulations and the experiments positive in the area between the jets and the wall. This is due to the direction of the jet located nearest to the wall. The flow direction changes approximately at location $x/B = 0.5$ which corresponds to the jet arrangement centre. This is observed numerically and experimentally and is explained by the presence of the opposite jet. At the location of the latter jet the velocity is high, whereas at some distance it decreases. The experimental results even show a direction change behind the location where the longitudinal jet intervenes; but the velocities remain low.

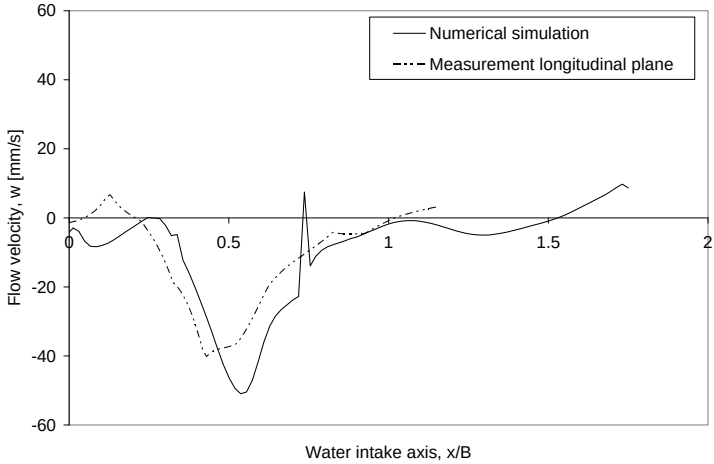

Figure 5.15 Vertical flow velocity w on the water intake axis. Positive values mean upward flow direction for numerical simulation (continuous line) and experiments measured in the longitudinal plane (dashed-dotted line)

Although the experimentally measured velocities are smaller than the ones obtained numerically, both vertical flow velocity *w* curves are similar. Even the change from upward to downward flow in the area between the jets and the front wall takes place at almost the same location. The only important difference is found in front of the water intake, where according to the measurements the flow goes upward, whereas the numerical simulations show a downward oriented flow.

The peak at $x/B = 0.75$ is due to intermesh boundary interpolation.

5.4.2.1 Concluding remarks

As already mentioned above, the numerical simulation was running for 1.5 hours before the results were extracted. This might be an insufficient duration. The circulation is probably still transient. This would imply that the circulation is not yet fully developed. As a comparison, the measurements in the horizontal plane were taken within the first experimental hour, whereas the vertical planes (longitudinal and transversal) were registered one or two hours later. The confronted curves obtained by both techniques, numerically and experimentally, are quite similar. The velocity magnitudes are not much different. The variations could also be explained by probable instabilities as discussed in section 5.4.3.

5.4.3 Flow instabilities

5.4.3.1 Numerical simulation N1

As discussed in chapter 4 flow instabilities were detected in various experiments and revealed the combination of two different half parts of the flow pattern, which were measured at different times. Therefore, instabilities are expected to be observed in numerical simulations as well. The obtained results confirm these assumptions partly as discussed in the following paragraphs.

In chapter 4 the experiments with the lowest off-bottom clearance (C/B = 0.1) appeared to be the most stable (section 4.6.5). A time sequence of 300 *s* with transversal flow patterns every 60 *s* of the numerical simulation N1 (Table 5.1) with C/B = 0.1, but with the water intake lying in between (h_i/B = 0.175 instead of 0.125 or 0.25, respectively) is presented in Figure C.1. Although a forerun of even 3 hours was used, for this configuration flow instabilities occur.

Figure C.1 shows in the transversal plane dominatingly an axial mixer-like flow pattern and confirms hereby the finding of sections 4.6.4 and 4.6.5 where the experiments with the same off-bottom clearance were presented. Despite the instabilities, the flow pattern in the longitudinal plane obtained by numerical simulation has mainly two single rotors at both sides of the jets and confirm the flow pattern found by the experiments.

The same time sequence but for the longitudinal flow patterns shows only slight instabilities (Figure C.3). There is a permanent cell between the jets level and the water intake, and another cell in the rear part of the tank. The rear cell is persistent during the first three minutes of the sequence; afterwards a perturbation is visible probably coming from the third dimension decreasing the size of the rear cell.

5.4.3.2 Numerical simulation N2

The time sequence of the numerical simulation N2 (Table 5.1) corresponding to the experiment C2 (basic geometrical parameters) has slight instabilities in the transversal plane. Nevertheless, the axial mixer-like flow pattern can be at any time recognized, although the forerun of the simulation was only 1.5 hours.

In the longitudinal plane the flow pattern remains stable in the rear part of the tank where a single cell is located, which is strongly influenced by the back wall. During most of the time (5 minutes out of 6) the single cell in the front part of the tank was persistent and changed only its shape.

As already discussed in section 5.4.1 the flow patterns as well as the velocity magnitudes are in quite good agreement with the experiments.

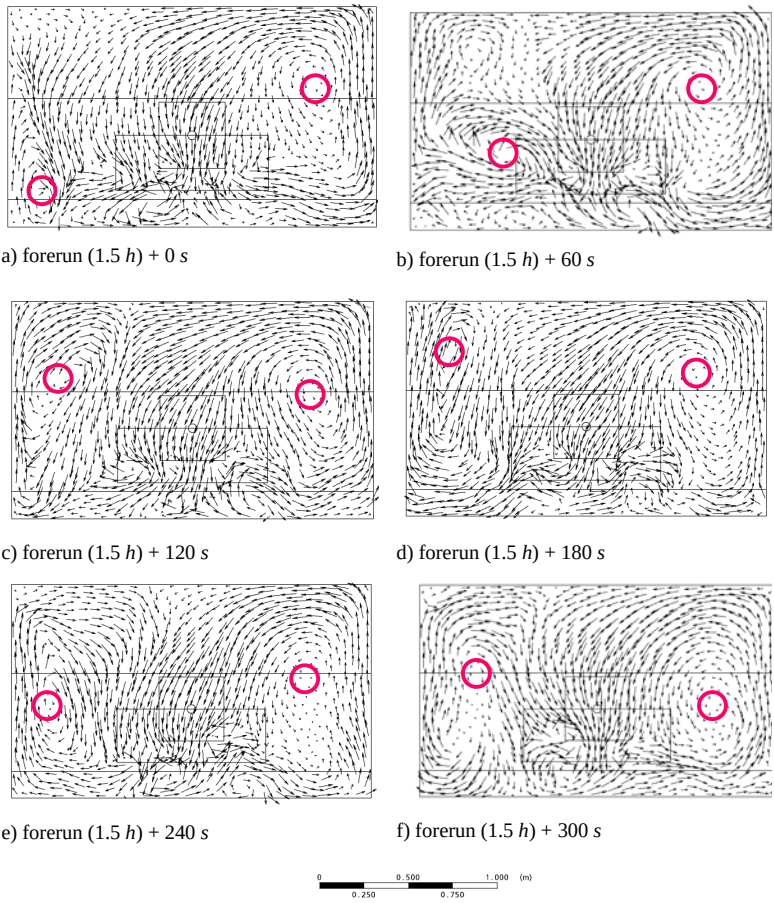

a) forerun (1.5 *h*) + 0 *s*

b) forerun (1.5 *h*) + 60 *s*

c) forerun (1.5 *h*) + 120 *s*

d) forerun (1.5 *h*) + 180 *s*

e) forerun (1.5 *h*) + 240 *s*

f) forerun (1.5 *h*) + 300 *s*

Figure 5.16 Time sequence of transversal flow patterns of the numerical simulation N2 (C/B = 0.175, hi/B = 0.25). From a) to f): forerun (1.5 h) + 0 s, 60 s, 120 s, 180 s, 240 s, 300 s. The level of the water intake is indicated by the circle.

5.4.3.3 Numerical simulation N3

The forerun of the simulation N3 with a high off-bottom clearance (*C/B* = 0.25, Table 5.1) was 2.6 hours. As can be seen in Figure C.7 the right side is more stable than the left side. On the right side the radial mixer-like flow pattern is persistent, whereas on the left side strong instabilities are observed to destroy these characteristic flow fields.

The longitudinal flow field is characterized by numerous cells appearing and disappearing during the observed period of 6 minutes. The typical radial mixer-like flow pattern is not all the time present.

The flow patterns of the experiments are more regular (section 4.6.4) than the simulated. It is not clear whether the reason for this difference is the higher position of the water intake (h_i/B = 0.325 in numerical simulation, h_i/B = 0.25 in experiments).

5.4.3.4 Numerical simulation N4

The numerical simulation N4 (Table 5.1) corresponds to the experiment with basic geometrical parameters, but with a double tank length instead. The forerun was 33 minutes. Nevertheless, in the transversal flow pattern through the jet circle centre and during three minutes, no major instabilities were observed (Figure C.1).

In the flow pattern in the longitudinal plane also no any major instability can be observed.

5.4.4 Length of recirculation cell

The increased tank length was simulated in order to assess the effect of a longer reservoir and a different length over width ratio (L/B = 3.5 instead of 1.75). Is there a recirculation cell forming, how long is it, what is its length in proportion to the off-bottom clearance, and what is its height?

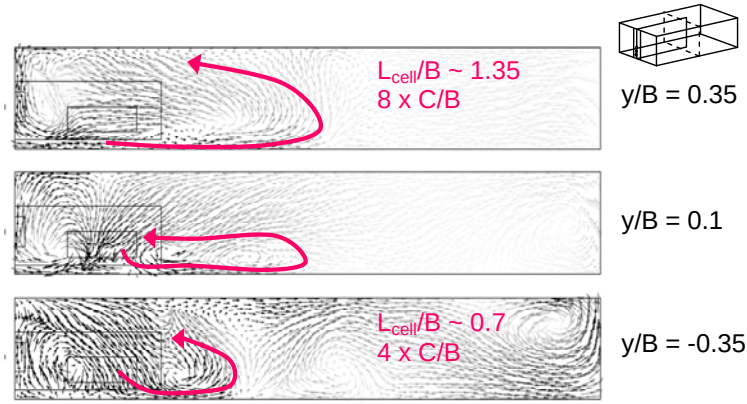

Figure 5.17 Flow pattern in three longitudinal planes (y/B = 0.35, 0.1 and -0.35). Arrows are indicating the recirculation cell.

5.4.4.1 Length of recirculation cell

As can be seen in Figure C.13 and Figure 5.17 the longitudinal flow pattern varies from one tank side to the other. Both tank half-widths are not symmetric. At y/B = 0.45 there is a recirculation with a length of approximately 1.6, what corresponds to approximately 9 times the off-bottom clearance (C/B = 0.175). The cell length decreases by shifting the longitudinal plane to the other tank side. At y/B = -0.35 the cell is 0.7 normalized length long. Consequently, this length is 4 times the off-bottom clearance. Coming closer to this side (y/B = -0.3 to y/B = -0.45) the recirculation cell disappears as such and is replaced by a strong current flowing from the jets to the rear.

Although on 80 % of the width a recirculation cell is present, no information about the relationship between the recirculation length and the off-bottom clearance can be given. The over-all flow is asymmetric and 3D-effects are very high. Nevertheless, it is sure that there is a recirculation cell which is shorter than the available tank length.

Moreover, even though in section 5.4.3 almost no major instability was discovered for the present simulation (Figure C.10 and Figure C.11), the forerun was with 33 *min* (Table 5.1) very short and the simulation was probably still in the transient phase. This would mean that the whole circulation is not yet well developed and that the described circulation could continue to change.

Remembering the findings of Riess and Fanneløp (1998) the recirculation cell resulting from a vertically upward oriented jet placed on the bottom of an elongated tank has a length of approximately 4 to 6 times the water depth. Although a direct comparison is incorrect (the reasons are discussed in section 2.5.1) it is interesting to note that their results are close to those found in the present study.

5.4.4.2 Height of recirculation cell

The recirculation cell is generally little higher than the off-bottom clearance.

5.4.4.3 Discussion

Bearing in mind the uncertainties due to the short forerun and related instabilities, the strong asymmetrical flow pattern can be explained. This asymmetry makes the assessment of the length of the recirculation cell difficult.

As can be seen in Figure C.12, Figure C.13 and Figure C.14 the flow velocities of the recirculation cell are certainly not high enough to bring back the sediments thrown to the rear of the tank.

5.5 Concluding remarks

Only numerical simulations with clear water were performed since it is not sure whether the numerical model can represent correctly the sediment release quantitatively.

The simulated forerun might not be enough and the circulation was probably still in the transient phase. Nevertheless, comparisons of the flow patterns from numerical simulations with experiments show that they are in quite good agreement.

In order to reduce the number of finite elements in numerical simulations of jets in large water volumes such as real reservoirs the jets could be simulated by momentum fluxes induced at points. By this method the required computer calculation time could be reduced as well. Consequently, numerical simulations of case studies could be performed with a reasonable expenditure of time.

Two major findings result from the numerical simulations:

1. Despite the rather short forerun only slight instabilities were observed.
2. In the tank with increased length (L/B = 3.5 instead of 1.75) a recirculation cell occurs. Since both half-widths of the tank are not symmetric its length varies strongly from one side to the other. Nevertheless, it is sure that there is a recirculation cell which is shorter than the available tank length and little higher than the jet off-bottom clearance.

6 Prototype case study

6.1 General reflections

In this chapter a case study of a jet installation in a real reservoir is presented. This case study is partially based on a master thesis (Graf 2009) which was co-supervised by the author.

Such a case study requires first some reflections about the application of jets in a prototype and its feasibility. When designing such an installation it is of high interest to know how to up-scale from the model to the prototype, and how many tons of sediment are evacuated per year when using jets, and what there efficiency is. The installation costs must be assessed and an economic analysis has to be done.

Subsequently, the implementation of best conditions in a real reservoir is discussed. Further, the economic analysis of a jet installation is considered.

6.2 Expected sediment release and efficiency

As presented in chapter 1 the major part of the sediment is entering the reservoirs during floods particularly when turbidity currents occur. The turbidity currents transport the sediment along the reservoir to the dam and after the flood a muddy layer with high sediment concentrations remains in front of the dam. Erosion and sediment transport decrease and almost clear water enters to the reservoirs. This state was chosen as initial condition for the experiments.

On one hand the experiments with no jets revealed as expected that with the current from upstream there is almost no mixing in the dam area. Only the particles close to the water intake are drawn into it, provided that the turbine is in operation. The flow velocity from upstream and the potential flow field generated by the flow entrained into the water intake define the sediment quantity to be released (section 4.5.4). The rest of the sediment is settling down and the water in front of the dam becomes more and more clear.

On the other hand with an optimal circular jet arrangement and if the jets are permanently operating, the water in front of the dam is well mixed. Even if the discharge of the jets is temporally slightly varying, the jet induced circulation is probably permanently close to steady state. This assumption implies ideal conditions, i.e. homogeneous sediment concentration distribution, no settling and, in the absence of cohesion, even resuspension. Thus, if test conditions are preserved, it is assumed, that in the best case all of the sediments initially arrived at the dam will be evacuated.

As discussed in sub-chapter 4.12 the efficiency of the jets has to be calculated according to the specific conditions. In a case study, however, the notion of efficiency looses its meaning due to the following reflections:

The magnitude of the yearly sediment yield is usually calculated based on the bathymetry which has changed during a series of years due to sediment settling. The sediment inflow is rarely measured. Thus, the sediment amount released without jets is usually not known and the

efficiency cannot be quantified. However, it is important to compare the yearly sediment volume deposited when no jets are used (indicated by the yearly sediment yield) with the corresponding volume when jets are correctly used.

6.3 Up-scaling from model to prototype scale

As discussed in chapter 4, the geometrical parameters were all non-dimensionalized by the basin width *B*. This had a physical sense. The jet induced circulation was strongly influenced by this geometrical dimension. Namely, the lateral circulation extended in test conditions to the side walls. Consequently, the optimal distance between the jet circle centre and the front wall was, probably due to symmetry reasons, found to be equal to half of the basin width, and the jet circle diameter was found to have its optimum at approximately *B/4*. So is the water intake height. These relationships were the same for all tested discharges and are, hence, expected to be the same for larger volumes such as real reservoirs. The nozzle diameter had no influence on the sediment release in the physical experiments.

The jet discharge and velocity, however, depend on the local conditions of the reservoir. The available head of the transfer tunnel defines the jet velocity, and the maximal discharge is determined by hydrological conditions.

6.3.1 Froude similarity, jet discharge and settling velocity

When up-scaling to a prototype, i.e. to the dimensions of a real reservoir, Froude similarity has to be satisfied. However, real case conditions show that the available jet discharge and velocity are not necessarily in the same relationship with the geometrical dimensions as in the hydraulic model.

The experiments showed that in the rectangular laboratory tank with a discharge exceeding the tested discharges ($\Sigma Q_j > 4050$ *l/h*) suspension and sediment release are expected to be more favorable. The higher the discharge the closer it comes to the idealized conditions (Figure 4.45). However, with discharges smaller than the tested range ($\Sigma Q_j < 570$ *l/h*) the jet discharge is probably too small to either reach the neighboring jet or to generate the optimal circulation. If Froude similarity is preserved, this is also a concern for a real case.

Moreover, the circulation velocity compared to the settling velocity should at least be the same as in test conditions. If Froude similarity between the velocity and the geometrical parameters of the test conditions is preserved, the efficiency should be the same as in the scaled model. However, the jet velocity was not explicitly identified as an influencing parameter in the investigated range. Instead, it is implicitly included in the jet discharge. Thus, the relationship based on settling velocity combined with the discharge, as proposed by the following dimensionless number, has to be satisfied:

$$\frac{\tau_s}{\tau_m} = \frac{h/w_s}{V/Q_{out}} > 0.088 \qquad \textit{(Eq. 6.1)}$$

where 0.088 was obtained for the smallest tested discharge having still resuspension ($\Sigma Q_j =$ 2030 *l/h*).

Consequently, the available discharge and the available velocity or head, respectively, as well as the settling velocity together define the model scale factor.

6.3.2 Reservoir dimension

The relationship between the reservoir dimensions and the available discharge is usually higher than in the performed experiments. Consequently, the jet induced circulation is not confined like in the laboratory tank. In the contrary, the circulation is expected to create a three-dimensional recirculation cell as has been found in the numerical simulations (chapter 5). Consequently, it will not be extended over the whole reservoir width. Nevertheless, the sediment in the region of the water intake can be released through the water intake or thrown out of this area. Thus, the area in front of the water intake can be kept free of sediment which is the main purpose.

6.3.3 Up-scaling procedure

The following conditions should be satisfied when up-scaling the experiments to prototype:

1. The scale factor λ_L is given by the relationship between the sums of the jet discharges:

$$\lambda_L = \left(\frac{\Sigma Q_{j,p}}{\Sigma Q_{j,m}} \right)^{2/5} = \lambda_Q^{2/5} \qquad (Eq.\ 6.2)$$

2. The dimensionless number τ_m/τ_s should exceed 0.088 (considering the threshold beyond which resuspension is expected), when the length of the considered volume is assumed to be 1.75 times, and the water height of the considered volume to be 0.6 times the up-scaled width. This leads to the condition that

$$\lambda_L = \sqrt{\frac{\Sigma Q_{j,p}}{\Sigma Q_{j,m}}} \sqrt{\frac{w_{s,m}}{w_{s,p}}} = \sqrt{\frac{\lambda_Q}{\lambda_{w_s}}} \qquad (Eq.\ 6.3)$$

Finally, both conditions can be combined in the following expression:

$$\lambda_L = \min\left(\lambda_Q^{2/5}; \sqrt{\frac{\lambda_Q}{\lambda_{w_s}}} \right) \qquad (Eq.\ 6.4)$$

In other words, if $\lambda_Q^{2/5} \leq \lambda_{ws}^2$, the influence of the settling velocity on the design of the jet arrangement becomes significant.

6.4 Preliminary case study of Mauvoisin

6.4.1 Circumstances and history

The seasonal Mauvoisin Reservoir, built in the early 1950s, is situated in the canton of Valais (Switzerland) in the valley of the river Drance. It is a typical alpine reservoir with a pronounced sedimentation concern. Namely, in 1985, part of the sediment was flushed. From 1989 to 1991, the dam was heightened by 13.5 *m* to 250 *m* in order to increase the storage capacity. Ten years after (2001 – 2006), the water intake and the bottom outlet were also heightened (by 38 and 36 *m*, respectively) due to sedimentation.

A water conveying tunnel exists which transfers water from neighboring catchments (Corbassière and Séry). This water falls like a waterfall out of the tunnel exit into the reservoir (Figure 6.1). The available head is between 70 and 183 *m*, depending on the reservoir water level. Thus, there is no extra energy needed for the jets. This water is brought by a penstock down to a certain elevation above the ground, where the jets should be installed.

Figure 6.1 Reservoir of Mauvoisin with the water transfer tunnel from Corbassière and Séry (Source: Wikipedia.org, author: Goudzovski)

6.4.2 Characteristics of Mauvoisin

6.4.2.1 Design of jet discharge

The present transfer tunnel is designed for a discharge of Q = 10 m^3/s and has on its major length a slope of 0.5 %. At the intake the water passes through a sand trap such that it is already clear and does harm neither the pressure pipe nor an eventually added turbine.

The hydrograph of this transfer tunnel dating from the year 2007/08 illustrates that between mid-October and mid-April the discharges are very low, i.e. smaller than 1 m^3/s (Graf 2009). This is due to the fact that the considered catchments are situated in a glacial area. Remember that turbidity currents mainly occur during summer.

The highest daily discharges were registered in the range of 5 to 7 m^3/s, being equal or exceeded during 50 days per year (Q_{50d}). Thus, during one turbidity current event, 5 to 7 m^3/s can be expected from the water transfer tunnel.

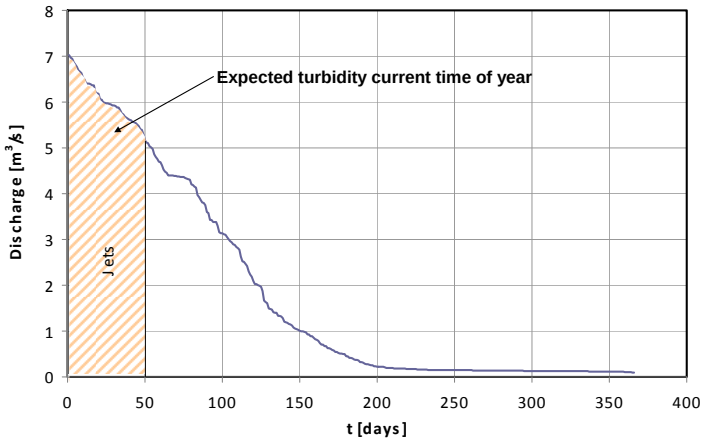

Figure 6.2 Flow duration curve for daily measured discharges of the hydrological year 2007/08.

6.4.2.2 Sediment yield

The yearly sediment yield into the dead storage of the Mauvoisin reservoir is estimated at 155'000 m^3 based on regularly carried out bathymetry (Schleiss et al. 1996). Until 1985, in the dead storage area (approx. 25 *ha*) an average increasing sediment level rate of 0.6 *m* per year was observed.

6.4.2.3 Settling velocity

The grain size distribution of the sediment in Mauvoisin can be assumed the same as used in the experiments. As discussed in section 3.4.1.2 this grain size corresponds well with those found in three different Swiss alpine reservoirs: Grimsel, Tourtemagne and Luzzone.

The mean summer temperature of the lake is indicated to be 10°*C*. The corresponding settling velocity after Stokes is therefore $w_{s,p}$ = 0.0024 *m/s*.

6.4.3 Circular jet installation

6.4.3.1 Design

Following the formerly established up-scaling criteria (section 6.3.3) the optimal jet installation for Mauvoisin is preliminarily designed.

The designated model scale factor would be 38, based on the real discharge of 5 m^3/s and on lowest discharge in model scale with which resuspension was observed (ΣQ_j = 2030 *l/h)*.

$$\lambda_L = \min\left(\lambda_Q^{2/5}; \sqrt{\frac{\lambda_Q}{\lambda_{w_s}}}\right) = 38 \qquad \text{(Eq. 6.5)}$$

Thus, the optimal interaction width would be 76 *m*, the water height 45 *m*, the distance between neighboring jets 11.4 *m*, the distance of the jet circle centre to the front wall 38 *m*, and the considered length 133 *m*.

It appears that in Mauvoisin the relationship of $w_{s,p}/w_{s,m}$ is not significant compared to the relationship of the discharges.

6.4.3.2 Combination with a mini-hydropower plant

If a circular jet arrangement is available the power plant operator can profit from the installed penstock and mount an additional turbine. The mean head is H_{avg} = 117 *m*. The available discharge has to be determined based on the flow duration curve (Figure 6.2) and taking into account the water needed for the jets. The discharge would be variable and therefore, an economic assessment would be needed.

6.4.3.3 Installation description of circular jet configuration

As is visualized in Figure 6.3 the water intake of the Mauvoisin reservoir is situated laterally and its opening is also laterally faced. This situation is different to the experimental one where the water intake located in the front wall and therefore orientated frontally to the main flow.

Moreover, in section 6.4.3.1 the required width was chosen with 76 *m* long. This is definitely shorter than the dam width on the today's level of the reservoir bottom (approximately 200 *m* wide at 1803 *m a.s.l.*).

There are several possible positions for the circular jet arrangement. Two of them are discussed hereafter:

1. The circular jet configuration is arranged on a parallel line to the thalweg crossing the water intake (Figure 6.3 left).
2. The circular jet configuration is arranged on the axis through the water intake (Figure 6.3 right).

Since in the first position the jet arrangement is located close to the left valley slope (Figure 6.3 left) the jet induced circulation may be laterally confined by it. This confinement has a similar effect like the side wall in the laboratory tank. Nevertheless, since the opposite side is missing the resulting circulation is asymmetric. Moreover, the water intake is not integrated in a wall like it was in the experiments. Therefore, it is located in the middle of the jet induced circulation.

In the second position the jet induced circulation is probably confined by both, the left valley slope and the dam (Figure 6.3 right). Moreover, the water intake is arranged laterally when comparing with the laboratory tank.

Thus, both situations are different from the experiment and a prediction of the flow is difficult. In view of the sediment release it is probably more favorable with two confined sides than with a single one and, hence, the second position would be preferred (Figure 6.3 right).

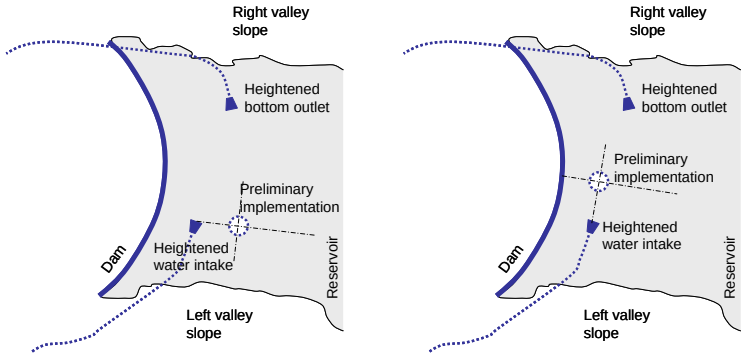

Figure 6.3 Circular jet configuration arranged on a parallel line to the thalweg crossing the water intake (left) and arranged on the axis through the water intake (right).

Concerning the jet installation itself, a platform with four pillars in its corners would be built and sunken to the bottom of the lake. On each pillar top a jet nozzle would be mounted and oriented in the proper direction (Graf 2009). The water of the jets is fed by a penstock like presented in section 1.3.2.

6.4.4 Cost estimation of a jet installation

Based on the constructions costs put at 924'000 *CHF* (construction site installation, salaries, exploitation and maintenance inclusive, Graf 2009) and with an interest rate of 5.6 % and duration of 20 years the amount of annuity is 78'000 *CHF*.

Additional turbine recoating and repair costs are not included. The sediment characteristics would have to be evaluated regarding abrasion as well as the sediment concentration of a typical turbidity current in Mauvoisin would have to be measured and compared to the abrasion threshold values (section 1.4.3.3).

6.4.5 Extraction costs in case of no jets

The removal costs differ according to the methods, circumstances and the references (Molino 2006 and Broccard 2010) between 9 (dilution method) and 30 *CHF*/m^3 (mechanical extraction, pump and others). Transport and disposal costs are included. Consequently, the annual removal and disposal costs for the considered yearly sediment supply (section 6.4.2.2) are between $1.4 \cdot 10^6$ and $4.65 \cdot 10^6$ *CHF*, if feasible.

The heightening of the bottom outlet and the water intake in the years 2001-2006 required an investment of approximately 50 millions *CHF* (Graf 2009). This construction was executed after roughly 45 years of operation. This means that the annual cost, calculated under the same conditions as the jet installation (section 6.4.4), would be 4.22 millions *CHF*.

If a subsequent heightening was required the investment would be less, since the expensive tunneling works are already accomplished. A rough estimate gives 15 millions *CHF* resulting in an annual cost of 1.27 millions *CHF*.

6.4.6 Economic analysis

The aforementioned investment, respectively its annual costs, compared with the costs of yearly sediment removal by other means provides a quick profitability assessment. Hereby, the monetary value of production loss, and disposal and treatment of polluted sediment are not considered, neither the cost of a new hydraulic scheme in case of an eventual complete damage due to reservoir filling.

For the economic analysis it is assumed that the jet installation is working successfully and that half of the incoming fine sediment could be released through the turbines.

The annual costs of the different alternatives are compared in Table 6.1.

	Without jets	With jets
Annual costs	0.7 – 2.3	0.08
[10^6 CHF]	(dilution and mechanical removal for half of the supplied fines)	(20 years payback period)
	1.27 (bottom outlet and water intake heightening with 20 years payback period)	

Table 6.1 *Comparison of annual expenses in two different cases: sediment removal without jets and outlet heightening, sediment release through turbines by means of jets.*

From Table 6.1 it can be derived that even if only 7 % of the yearly incoming sediment amount was released by means of the jets, with the available discharge and head a circular jet installation is economical and recommended in view of a sustainable reservoir operation.

6.5 Concluding remarks

The implementation of a circular jet arrangement in the real reservoir Mauvoisin was studied.

This reservoir is already accomplished and in operation for many years. Consequently, the position of the water intake was chosen regardless of an eventual circular jet installation.

The location of the water intake and the complex bathymetry are obviously different from the situation in the laboratory tank. The proportion between the reservoir dimensions and the available head and discharge of the water transfer tunnel is also different from the laboratory conditions. Consequently, the jet induced circulation will also be different.

Nevertheless, two possible positions of circular jet arrangements were discussed and a first attempt to up-scale the research results was made. With two confinements given on one hand by the dam and on the other hand by the valley slope, the circulation flow is still difficult to predict. Nevertheless, by means of the jets a much higher sediment release is expected than without jets. Moreover, the area in front of the water intake will be free of sediment and the problem of clogging can be ruled out. Further numerical simulations could provide optimal jet

arrangement position and a better estimate of the quantitative effect of the jets on the circulation and the sediment release.

A comparison between the annual costs of equivalent sediment volume extraction, on one hand due to mechanical removal and on the other hand due to release with jet mixing, states that the jet option is more profitable. Even if only 7 % of the yearly incoming sediment amount was released by means of the jets, a circular jet installation is still economical and strongly recommended in view of a durable power scheme.

In other words, if the yearly sediment yield of 5‘000 to 10‘000 m^3/a is exceeded it is economical to install a circular jet installation.

Consequently, it is definitely recommended to implement a circular jet arrangement to delay reservoir filling and counteract reservoir sedimentation.

7 Concluding Summary, Recommendations and Outlook

7.1 Summary and Conclusion

7.1.1 Sedimentation problem and new sediment evacuation concept

Reservoir sedimentation is a subject of major importance in many alpine reservoirs. It has its origin particularly during flood events when sediment is eroded and transported by the rivers into the reservoirs. Turbidity currents with a high suspended sediment concentration carry a large quantity of sediment along the reservoir to the dam and its outlet devices endangering the sustainable use of the reservoir. In view of the current mitigation measures alternative and more sustainable solutions are required.

In long and deep reservoirs the sediment particles are well sized along the thalweg with the finest ones in front of the dam. Approximately 80 % of the total sediment is smaller than sand and, hence, hard difficult to be retained by sand traps at intakes.

The present study focuses on these fine sediment particles. The purpose is to maintain the fine sediment in suspension in front of the dam by means of a specific jet arrangement inducing a rotational flow circulation. During turbine operation suspended sediment is entrained into the water intake and released through the headrace tunnel out of the reservoir. Evacuating sediment out of the area in front of the water intake and, thus, avoiding its clogging, is specially aimed.

The effect of two different jet arrangements on turbulence and flow pattern in front of the intakes as well as the sediment release out of the reservoir was investigated by physical experiments and numerical simulations.

7.1.2 Description of experimental set-up and conditions

The experiments were carried out in a rectangular 2 *m* wide, 4 *m* long and 1.5 *m* deep tank, with and without jets. Two jet arrangements were tested, namely a circular and an linear configuration.

The initial conditions for each experiment represented the muddy layer left in front of the dam after the passage of a turbidity current. It was simulated by a quasi homogeneous sediment concentration generated by three evenly over the tank bottom spread air bubble curtains.

The water height was always kept constant. In case of experiments without jets the outflowing water was replaced by feeding clear water from the back wall of the tank. In case of experiments with jets, the clear water fed by the jets into the tank was equal to the outflow through the water intake.

In case of a circular jet arrangement, four water jets with equivalent nozzle diameter and jet velocity were placed at the same spacing in a horizontal circle. Each jet was pointing perpendicularly to the transition zone of the neighbouring jet. For circular jet arrangements, the

influence of the off-bottom clearance, the water intake height, the water height, the distance between the jet circle centre and the front wall, the distance between two neighbouring jets, and the jet angle to the horizontal on the sediment release have been investigated.

Additionally, an linear jet arrangement consisting of four jets installed in a line parallel to the front wall was investigated. All jets were directed with the same angle (0 and 45°, respectively) towards the front wall. Similar to the circular jet arrangement, the influence of the distance between the jet line and the front wall and of the jet angle to the horizontal on the sediment release has been studied.

7.1.3 Sediment release and flow pattern

The sediment release was continuously measured by means of a turbidity meter in the dissipation tank where the evacuated water from the reservoir was restituted. The sediment release (evacuated sediment ratio, *ESR*) is defined as the evacuated sediment weight P_{out} divided by the sediment weight initially supplied P_{in} and represents the normalized temporal integral of the released sediment amount: $ESR = P_{out}/P_{in}$.

Turbidity was also measured within the experimental tank providing information about the evolution of sediment concentration and distribution during the experiments. Combining the measurements in the reservoir with those in the dissipation tank settled sediment fraction as a function of time is obtained. Analogously to the sediment release, the settled sediment ratio is the settled sediment divided by the sediment weight initially supplied P_{in}.

At the start of the experiments a certain sediment amount settles to the bottom. For experiments with a circular jet arrangement and a discharge exceeding an experimentally determined threshold, after a certain while the peak of the settled sediment ratio is reached and resuspension is observed. It is assumed, that at the time resuspension starts, the transition between transient phase and steady state takes place.

For experiments with and without jets, in the investigated discharge range and time period, the sediment release has been found to be in quasi linear relationship with the discharge. Nevertheless, for theoretically idealized conditions (i.e. steady state, no sediment settling and perfectly homogeneous sediment concentration distribution) this relationship is not linear, and for higher discharges its influence becomes less effective.

7.1.3.1 Circular jet arrangement

Depending on the jet position in the circular jet arrangement different flow patterns measured by a set of ten ultrasonic velocity profilers (UVP) could be observed.

For lower off-bottom clearances of the jet arrangement on one hand, the flow pattern was in the transversal plane similar to the one of an axial mixer. On the other hand, if the off-bottom clearance was high radial mixer-like flow patterns were detected in the same plane. As reported in the literature radial mixers are not as favourable as axial mixers concerning particle suspension. This is indirectly confirmed by the present study since the sediment release was less significant if radial mixer-like instead of axial mixer-like flow patterns were detected in the transversal plane. Nevertheless, contrary to what would be expected for classical impeller mixing problems from the literature, the lowest off-bottom clearance was not the most efficient one concerning sediment release.

The height of the water intake had its influence mainly on the flow pattern in the longitudinal sense. Depending on the water intake position in respect of the off-bottom clearance, the current issued horizontally out of the jets circle was more or less deflected. A straight horizontal current pointing almost directly towards the water intake resulted in very effective sediment release.

Consequently, the combination of an axial mixer-like flow pattern in the transversal plane and a radial mixer-like flow pattern in the longitudinal plane revealed to be optimal regarding sediment release.

The hydrodynamic numerical simulations with steady state and one single phase (clear water) confirmed the observed flow patterns for the optimal configuration. Moreover, slight flow instabilities were detected whose influence on sediment release are not yet investigated.

The water height played a major role. There is an optimum on a certain water height where the flow pattern was very well developed. If the water height was higher or deeper than this optimum, the flow pattern was more chaotic and the sediment release was significantly lower.

For a non-optimal distance between the jet circle centre and the front wall, instabilities are detected in the transversal flow pattern changing from axial mixer-like to a radial mixer-like flow pattern. With increasing distance, the current issued from the jets becomes weaker in the longitudinal plane and is therefore deflected before reaching the front wall. Consequently, the sediment release decreases with increasing distance when moving away from the optimal distance. With decreasing distance from the optimal one, the horizontal current issued from the jets disappears and the sediment release decreases accordingly. The optimal distance is the same as the distance between the jet circle centre and the side walls, thus, half of the tank width.

Regarding the distance between neighbouring jets the optimum corresponds to a jet circle diameter close to a quarter of the tank width. Shorter and longer distances are less sediment release effective.

The investigated jet angle of 45° turns out to be less sediment release effective than horizontal jets. This can be easily explained by the flow pattern which is similar to an axial mixer introduced upside down.

Thus, under optimum conditions and with the highest tested jet discharge ($\Sigma Q_j = Q_{out}$ = 4050 *l/h*) after four hours a sediment release of *ESR* = 0.73 was achieved. Without jets and with the same discharge through the water intake the sediment release reached was *ESR* = 0.37.

The normalized optimal geometrical parameter combination regarding sediment release was obtained as follows:

Off-bottom clearance:	$C/B = 0.175$
Water intake height:	$h_i/B = 0.25$
Water height:	$h/B = 0.6$
Distance between jet circle centre and front wall:	$d_{axis}/B = 0.525$
Distance between neighboring jets:	$l_j/B = 0.15$
Jet angle to the horizontal:	0°

The efficiency of the jets was established by comparing the sediment release obtained under different conditions: once when jets were employed, once without jets. The predicted efficiency based on time and discharge independent empirical relationships is around 1.7 for

the optimum jet configuration. Using the measured data the efficiency depends on discharge and increases with time. At the end of the transient phase and when resuspension started the efficiency was approximately 1.5. With the highest tested discharge the efficiency reached after four hours almost 2 (ΣQ_j = 4050 *l/h*).

7.1.3.2 Linear jet arrangement

As for the circular jet arrangement, an optimal geometrical parameter set concerning sediment release has been identified also for the linear jet arrangement. Nevertheless, even with the optimal parameter set the resulting sediment release is only marginally higher than for the experiments without jets. For higher distances from the jet line to the front wall than the optimal one the sediment release became even smaller than without jets. The highest resulting sediment release after four hours was *ESR* = 0.45. This can be explained by the direction of the induced rotation which is unfavourable regarding sediment suspension: the sediment is drawn to the bottom where it is settled and difficult to be put in suspension again.

7.2 Recommendation for practical application

The location of the water intake and the bathymetry of a real reservoir are obviously different from the rectangular laboratory tank. The proportion between the reservoir dimensions and the available head and discharge of a real water transfer tunnel is also different from the laboratory conditions.

Nevertheless, for the reservoir of Mauvoisin, with a 250 *m* high dam creating a large reservoir in Switzerland, a possible position for a circular jet arrangement was proposed where the resulting circulation is confined on two sides: by the dam and by the left valley slope. The jet forced circulation flow is difficult to predict. For better understanding of the flow and a better estimate of the quantitative effect of the jets on the circulation and the sediment release numerical simulations have to be done.

Even though, by means of the jets a much higher sediment release is expected than without jets. Moreover, the area in front of the water intake will be free of sediment and the problem of clogging can be ruled out.

A comparison between the annual costs of equivalent sediment volume extraction, on one hand due to mechanical removal and on the other hand due to release with jet mixing, states that the jet option is more profitable. Even if only 7 % of the yearly incoming sediment amount was released by means of the jets, a circular jet installation is still economical and strongly recommended in view of a sustainable reservoir operation.

7.3 Suggestions for further research

The following points are suggested to be addressed in a possible progression of the present research:

- Experiments with a 45° jet angle pointing downwards. From the performed experiments with 0° and 45° upwards angles the resulting flow pattern is expected to be the inverse of the 45° upwards angle. Thus, this third angle could be promising in view of sediment release.
- Experiments with variations of the tanks length over width ratio to learn more about the influence of the back and the side walls or of the far field, respectively, on the jet

induced circulation and the related sediment release.

- Experiments with inclined side walls as in real reservoirs. Their influence on the circulation and the sediment release has not been investigated yet.
- Experiments with asymmetric arrangement of the water intake. Its influence on the circulation and the sediment release has not been investigated yet.
- Calibration of three-dimensional numerical simulations with two phases (water and sediment) by comparing with the experimental results.
- Extensive three-dimensional numerical simulations with two phases (water and sediment) in a tank with up-scaled dimensions to assess the influence of the settling velocity of a natural sediment particle and to provide more certain up-scaling criteria.
- Numerical simulations with a calibrated model and two phases of a real reservoir.
- Prototype testing

References

Abramovich, G. N. (1963). *The Theory of Turbulent Jets*, English Translation published by M.I.T. Press, Massachussetts, 671 pp.

Alabaster, S., Lloyd, R. (1980). Finely divided solids. London. Water quality criteria for freshwater fish: 1-20.

Alam, S. (1999). "The influence and management of sediment at hydro projects." *Hydropower & Dams*, 3, 54-57.

Alam, S. (1999). "The influence and management of sediment at hydro projects." Hydropower & Dams 3: 54-57.

Albertson, M. L., Dai, Y.B.Jensen, R.A., Rousse, H. (1950). "Diffusion of submerged jets." *Trans. ASCE*, 115, 639-697.

Armenante, P. M., and Nagamine, E. U. (1998). "Effect of low off-bottom impeller clearance on the minimum agitation speed for complete suspension of solids in stirred tanks." *Chemical Engineering Science*, 53, 1757-1775.

Basson, G.R. and Rooseboom A. (1997), Dealing with Reservoir Sedimentation, Water Research Commission Report No. TT 91/97, Pretoria, 395 pp.

Basson, G.R. (2009). Management of siltation in existing and new reservoirs. General Report Q. 89, Proceedings (on CD) of the 23rd Congress of the Int. Commission on Large Dams CIGB-ICOLD, 25-29 May 2009, Brasilia, Volume II.

Batuca, D. G., Jordaan, J.M. (2000). *Silting and desilting of reservoirs*, A.A. Balkema, Rotterdam.

Bechteler, W. (2008). *Sediment Sources and Transport Processes*, Institut für Wasserwesen, Universität der Bundeswehr München, Germany.

Beyer Portner, N. (1998). *Erosion des basins versants alpines par ruissellement de surface*, PhD thesis, Communication 6, Laboratory of Hydraulic Constructions (LCH), Swiss Federal Institute of Technology, Lausanne, Switzerland.

Blevins, R. D. (1984). *Applied fluid dynamics handbook*, Reprint edition with corrections, Krieger Publishing Company, Malabar, Florida 32950.

Boes, R. (2010). "Kontinuierliche Messung von Schwebstoffkonzentration und –korngrössenverteilung im Triebwasser und Quantifizierung der Hydroabrasion an einer Peltonturbine", *wasser, energie, luft - eau, énergie, air*, 102. Jahrgang, Heft 2, p. 101-107.

Boillat, J.-L., Delley, P. (1992), "Transformation de la prise d'eau de Malvaglia, étude sur modèle et réalisation". "Wasser Energie Luft", 84. Jahrgang, Heft 7/8, p. 145 – 151.

Boillat, J.-L., Pougatsch, H. (2000), "State of the art of sediment management in Switzerland." *International Workshop and Symposium on Reservoir Sedimentation Management*, Tokyama, Japan.

Bouvard, M. (1984). *Barrages mobiles et ouvrages de dérivation: à partir des rivières transportant des matériaux solides*, Editions Eyrolles, Paris.

Broccard, A. (2010), personal communication.

Brooker, L. (1993). "Mixing with the jet set." *Chemical Engineer*, 30, p. 16.

Brown, C.B. (1943). *The control of reservoir silting*, U.S. Dept. of Agriculture. Miscellaneous publication no. 521, Washington, D.C.

Brown, C.B. (1950) *Sedimentation*. in *Proceedings of the Forth Hydraulics Conference. Iowa Institute of Hydraulic Research.*

Brown, P. P., Lawler, D. F. (2003). "Sphere Drag and Settling Velocity Revisited." *Journal of Environmental Engineering*, 129(3), 222-231.

Brune, G. M. (1953). "Trap efficiency of small reservoirs." *Transaction of the American Geophysical Union* 34(3), 407-418.

Bucher, R. (2002). "Feinsedimente in schweizerischen Fliessgewässern, Einfluss auf die Fischbestände". Fischnetz-Publikation, Projekt Fischrückgang Schweiz, Teilprojekt-Nr. 01/07, Eawag.

Busnaina, A. A., Lilley, D.G., Moretti, P.M. (1981). "Prediction of local destratification of lakes." *Journal of Hydraulic Division, ASCE*, 3, 259-272.

Chen, J., Zhao, K. (1992). "Sediment management in Nanqin Reservoir." *International Journal of Sediment Research*, 7(3), 71-84.

Churchill, M. A. (1948). "Discussion of analysis and use of reservoir sedimentation data." *Federal Interagency Sedimentation Conference*, Denver, Colorado, 139-140.

Coldrey, P. W. (1978). "Jet mixing." University of Bradford, Bradford, England.

Corrsin, S. (1946). "Investigation of flow in an axially symmetric heated jet of air." N.A.C. Wartime Report.

Davies, J. T. (1972). *Turbulence Phenomena*, Academic Press, New York.

De Cesare, G. (1998), *Alluvionnement des retenues par courants de turbidité*. phD thesis, Communication 7, Laboratory of Hydraulic Constructions (LCH), Swiss Federal Institute of Technology, Lausanne, Switzerland.

De Cesare, G. and Schleiss, A. (1999). "Turbidity current monitoring in a physical model flume using Ultrasonic Doppler method." Proc., 2nd Int. Symp. on Ultrasonic Doppler Method for Fluid Dyn. and Fluid Engrg., PSI, Villigen, Switherland.

Dietrich, W. E. (1982). "Settling velocity of natural particles." *Water Ressources Research*, 18(6), 1615-1626.

Donald, M. B., and Singer, H. (1959). "Entrainment in turbulent fluid jets." *Transactions of the Institution of Chemical Engineers*, 37, 255-267.

Das, D. (2005). "Prospects and problems in hydropower development in India." Script of LCH-Conference.

Fan, J. (1985). "Methods of preserving reservoir capacity, Methods of Computin Sedimentation in Lakes and Reservoirs: A Contribution to the International Hydrological Programme." IHP-II Project A. 2.6.1 Panel, e. S. Bruk, ed., Unesco, Paris, 65-164.

Fan, J., and Morris, G. L. (1992). "Reservoir sedimentation I, II." *Journal of Hydraulic Engineering*, 118(3), 354-369, 370-384.

Fanneloep, T. K., Hirschberg, S., Küffer, J. (1991). "Surface current and recirculating cells generated by bubble curtains and jets." *Journal of Fluid Mechanics*, 229, 629-657.

Fischer, H. B., List, J.B., Koh, R.C.Y., Imberger, J., Brooks, N.H. (1979). *Mixing in Inland and Coastal Waters*, Academic Press, New York.

Folsom, G., and Ferguson, C. K. (1949). *Tran. American. Soc. Mech. Eng.*, 71(73).

Fossett, H. and Prosser, L.E. (1949). The application of free jets to the mixing of fluids in bulk. *Proceedings of I Mechanical Engineering* 160, pp. 224–251.

Fossett, H., (1951). The action of free jets in the mixing of fluids. *Transactions of the Institution of Chemical Engineers* 29, pp. 322–332.

Fox, E.A. and Gex, V.E. (1956). Single-phase blending of fluids. *A.I.Ch.E. Journal* 2, pp. 539–544.

Giustolisti, O. and Savic, D.A. (2003). Evolutionary Polynomial Regression (EPR): Development and applications. Technical report, School of Engineering, Computer Science and Mathematics, Centre for Water System, University of Exeter.

Goertler, H. (1942). "Berechnung von Aufgaben der freien Turbulenz auf Grund eines neuen Näherungsansatzes." *Z.A.M.M.*, 22, 244-254.

Goossens, L.K. (1979). "Reservoir destratification with bubble columns". Thesis, Delft University Press.

Graf, R. (2009). "Evacuation des sédiments fins des retenues alpines par mise en suspension et turbinage – Cas d'étude Mauvoisin." Master thesis (unpublished), Laboratory of Hydraulic Constructions (LCH), Swiss Federal Institute of Technology, Lausanne, Switzerland.

Graf, W. H. (1984). "Storage losses in reservoirs." *International Water Power & Dams Construction*, 36(4), 37-40.

Grenville, R., Tilton, J.N. (1996). "A new theory improves the correlation of blend time date from turbulent jet mixed vessels." *Chemical Engineering Research and Design*, 74(3), 390-396.

Griffiths, W., and B. Walton., (1978). "The effects of sedimentation on the aquatic biota." Alberta Oil Sands Environmental Research Program, Report #35.

Hauenstein, W. (2005). "Vorstellung des Projektes ALPRESERV". Interreg IIIB-Projet Alpreserv, Conférence sur la problématique de la sédimentation dans les réservoirs, Gestion durable des sédiments dans les réservoirs alpins, Communication 22, Laboratoire de Constructions Hydrauliques (LCH), Ecole Polytechnique Fédérale de Lausanne (EPFL), Switzerland.

Hinze, J. O., Zijnen, B.G. Van der Hegge. (1949). "Transfer of heat and matter in the turbulent mixing zone of an axially symmetrical jet." *Journal of Appl. Sci. Res.*, A1, 435-461.

Hotchkiss, R. H., Huang, X. (1995). "Hydrosuction sediment-removal systems (HSRS): principles and field test." *Journal of Hydraulic Engineering*, 121(6), 479-489.

Huwyler, P. (2002). "Möglichkeiten zur Feststoffevakuation aus Stauseen durch die Treibwasserleitung", Technical report, Travail de diplôme postgrade EPFL-LCH, Zürich, Switzerland.

International Committee on Large Dams (ICOLD). Sedimentation control of reservoirs – Guidelines, Vol. 67 (1989).

Jacobsen, T. (1998). "New sediment removal techniques and their applications." *Hydropower & Dams*, 135-146.

Jacobsen, T. (1999) Sustainable reservoir development: The challenge of reservoir sedimentation, Conference Proceedings "Hydropower into the next century", Gmunden, Austria, pp. 719-728, 1999.

Jayanti, S. (2001). "Hydrodynamics of jet mixing in vessels." *Chemical Engineering Science*, 56(1), 193-210.

Jirka, G. (2004). "Integral Model for Turbulent Buoyant Jets in Unbounded Stratified Flows. Part I: Single Round Jet." *Environmental Fluid Mechanics*, V4(1), 1-56.

Jirka, G. H., Harlemann, D.R.F. (1979). "Stability and mixing of a vertical plane buoyant jet in confined depths." *Journal of Fluid Mechanics*, 94, 275-304.

Kantoush, S. (2008). *Experimental study on the influence of the geometry of shallow reservoirs on flow patterns and sedimentation by suspended sediments*. phD thesis, Communication

37, Laboratory of Hydraulic Constructions (LCH), Swiss Federal Institute of Technology, Lausanne, Switzerland.

Kaskas, A. A. (1970). "Schwarmgeschwindigkeiten in Mehrkornsuspensionen am Beispiel der Sedimentation", Diss. TH Berlin

Kereselidze, N. B., Kutavaya, V.I., Tsagareli, Y.A. (1986). "Silting and flushing mountain reservoirs, exemplified by the Rioni series of hydroelectric stations " *Hydrotechnical Construction*, 19(9), 514-520.

Knoblauch H., Hartmann S. und De Cesare G. (2005). Sedimentmanagement an alpinen Speichern - Das EU-INTERREG IIIB Projekt ALPRESERV, Österreichische Wasser- und Abfallwirtschaft, Nr. 57/ 11-12, 2005, ISSN 0945-358X, SpringerWienNewYork, Wien, Austria, pp. 185-190

Krause, M., Grein, H. (1993). "Abrasion, research and prevention." *Sulzer Technical Review*, 2, 30-36.

Lafitte, R., and De Cesare, G. "Quantified criteria for electricity generation systems" *Hydro 2005*, Villach, Austria., 1-12.

Lane, A. C. G., Rice, P. (1982). "An investigation of liquid jet mixing employing an inclined side entry jet." *Transactions of the Institution of Chemical Engineers*, 60, 171-176.

Lehrer, I. H. (1981). "New model for free turbulent jets of miscible fluids of different density and a jet mixing time criterion." *Transactions of the Institution of Chemical Engineers*, 59(4), 247-252.

Leitch, A.M., Baines, W.D. (1989). "Liquid volume flux in a weak bubble plume". *Journal of fluid mechanics*, 205, p. 77-98.

Mahmood, K. (1987). "Reservoir Sedimentation: Impact, Extent and Mitigation." 71, World Bank Technical Paper.

Maruyama, T. (1986). Jet mixing of fluids in vessels. In: N.P. Cheremesinoff, *Encyclopedia of fluid mechanics*, Houston, USA: Gulf Publishing Co. (Chapter 21).

Maruyama, T., Ban, Y. and Mizushina, T. (1982). Jet mixing of fluids in tanks. *Journal of Chemical Engineering Japan* 17, p. 120.

Maruyama, T., Kamishima, N. and Mizushina, T. (1984). "An investigation of bubble plume mixing by comparison with liquid jet mixing". *Journal of Chemical Engineering of Japan* 17(2), pp. 121-126.

McCabe, W. L., Smith, J.C., Harriott, P. (2005). *Unit Operations of Chemical Engineering*, McGraw-Hill, New York, USA.

Mewes, D., Renz, R. "Jet mixing of liquids in storage tanks." *7th European Conference on Mixing*, Kiav, Brugge, Belgium, 131-137.

Metflow (2005). Ultrasonic Velocity Profile Monitor, User's guide. Technical Report, Metflow.

Mobley, M., Tyson, W., Webb, J., and Brock, G. (1995). "Surface water pumps to improve dissolved oxygen content of hydropower releases." *WaterPower'95*, July, ASCE, New York, NY, 20-29.

Molino, B. (2006). "Esperienze sulla gestione dei sedimenti nell'ambito del Progetto PRIN", Alpreserv-Conference in Milan, Interreg III B.

Morillo, S., Imberger, J., Antenucci, J. P., and Copetti, D. (2009). "Using impellers to distribute local nutrient loadings in a stratified lake: Lake Como, Italy." *Journal of Hydraulic Engineering*, 135(7), 564-574.

Morris, G. L. (1995), "Reservoir Sedimentation and sustainable development in India: problem scope and remedial strategies. Sixth International Symposium on River Sedimentation, Management of Sediment: Philosophy, Aims, and Techniques, New Delhi, 7-11 November, Balkema, Rotterdam, pp. 53-61.

Morris, G.L. (1996), "Reservoirs and integrated management", Reservoir Sedimentation, Proceedings of the St Petersburg Workshop May 1994, S. Bruk and H. Zebidi, eds, IHP-V, Technical Documents in Hydrology no. 2, UNESCO, Paris, pp. 135-148.

Morris, G. L., Fan, J. (1997). *Reservoir Sedimentation Handbook: Design and Management of Dams, Reservoirs and Watersheds for Sustainable Use*, McGraw-Hill, New York.

Newcombe, C. P., MacDonald, D.D. (1991). "Effects of suspended sediments on aquatic ecosystems." *North Americal Journal of Fisheries Management*, 11, 72-82.

Newcombe, C. P., Jensen, J. (1996). "Channel suspended sediment and fisheries: a synthesis for quantitative assessment of risk impact." *North Americal Journal of Fisheries Management*, 16, 693-727.

Oehy, Ch.; De Cesare, G.; Schleiss, A. (2000). Einfluss von Trübeströmen auf die Verlandung von Staubecken. Symposium Betrieb und Überwachung wasserbaulicher Anlagen, 19.-21. Oktober 2000, Graz, Österreich, Mitteilung des Instituts für Wasserbau und Wasserwirtschaft Nr. 34, 2000; p. 413-422

Oehy, Ch. (2003), *Effects of obstacles and jets on reservoir sedimentation due to turbidity currents*, phD thesis, Communication 15, Laboratoire de constructions hydrauliques (LCH), Swiss Federal Institute of Technology (EPFL), Lausanne, Switzerland.

Office federal de l'environnement, des forêts et du paysage (OFEFP), 1994. Conséquences écologiques des curages de bassins de retenue, Cahier de l'environnement 219.

Okita, N., and Oyama, Y. (1963). "Mixing characteristics of jet mixing." *Kagaku Kogaku*, 27, 252-259.

Oliver, D. R. (1961). "The sedimentation suspension of closely-sized spherical particles." *Chemical Engineering Science*, 15, 230-242.

Oseen, C. W. (1927). *Hydrodynamik*, Akademische Verlagsgesellschaft, Leipzig, Germany.

Palmiere, A., Shah, F., and Dinar, A. (2001). "Economics of reservoir sedimentation and sustainable management of dams." *Journal of Environmental Management*, 61(2), 149-163.

Patwardhan, A. W. (2002). "CFD modelling of jet mixed tanks." *Chemical Engineering Science*, 57(8), 1307-1318.

Patwardhan, A. W., Gaikwad, S.G. (2003). "Mixing in tanks agitated by jets." *Chemical Engineering Research and Design*, 81(2), 211-220.

Patwardhan, A. W., Thatte, A.R. (2004). "Process design aspects of jet mixers." *Canadian Journal of Chemical Engineering*, 82, 198-205.

Perona, J. J., Hylton, T.D., Youngblood, E.L., Cummins, R.L. (1998). "Jet mixing of liquids in long horizontal cylindrical tanks." *Industrial and Engineering Chemistry Research*, 37(4), 1478-1482.

Rajaratnam, N. (1976). *Turbulent Jets*, Vol. 5, Elsevier, Amsterdam, Netherlands.

Ranade, V.V. (1996). Towards better mixing protocols by designing spatially periodic flows: The case of a jet mixer. *Chemical Engineering Science* 51(11), pp. 2637–2642.

Revill, B.K. (1992), in "Mixing in Process Industries", Harnby, J., Edwards, N.F., Nienow, A.W. (eds) 2nd edn chapter 9 (Butterworth-Heinemann, Oxford, UK), 159.

Ricou, F. P., Spalding, D.B. (1961). "Measurements of entrainment by axisymmetrical turbulent jets." *Journal of Fluid Mechanics*, 11, 21-32.

Riess, I. R., and Fannelop, T. K. (1998). "Recirculating Flow Generated by Line-Source Bubble Plumes." *Journal of Hydraulic Engineering*, 124(9), 932-940.

Robinson, K. M., Garton, J. E., and Punnett, R. E. (1982). "Localized destratification at Lake Texoma." *Journal of Environmental Engineering Division, ASCE*, 108(4).

Robinson, K. M. (1981). "Reservoir Release Water Quality Improvement by Localized Destratification." *PB81-203145*, Springfield, VA.

Ryan, P. (1991). "Environmental effects of sediment on New Zealand streams: a review." *New Zealand Journal of Marine and Freshwater Research*, 25, 207-221.

Ryan, P. (1991). "Environmental effects of sediment on New Zealand streams: a review." New Zealand Journal of Marine and Freshwater Research 25: 207-221.

Salih, E.-T.H.M. (1994), "The effects of Flushing on the Fish Communitiy in the Khashm el Girba Reservoir, Eastern Sudan", M. Sc. Thesis, Department of Fisheries and Marine Biology, University of Bergen, 72 pp.

Schaad, F. (1979). "Vorschläge zur Verminderung der Stauraumverlandung bei starker Schwebestoffzufuhr." *Wasser und Boden*, 31(12), 347-352.

Scheidegger, A., Stöckli, A., and Wüest, A. (1994). "Einfluss der internen Sanierungsmassnahmen auf den Sauerstoffhaushalt im Hallwilersee." *wasser, energie, luft - eau, énergie, air*, 86. Jahrgang, Heft 5/6, 126-131.

Scheuerlein, H. (1995), "Downstream effects of dam construction and reservoir operation". Sixth International Symposium on River Sedimentation, Management of Sediment:

Philosophy, Aims and Techniques, New Delhi, 7-11 November, Balkema, Rotterdam, pp. 1101-1108.

Schleiss, A. (2007), *Aménagements hydrauliques*, Cours polycopié EPFL

Schleiss, A., De Cesare, G., Jenzer Althaus, J. (2009). "Verlandung der Stauseen gefährdet die nachhaltige Nutzung der Wasserkraft". *wasser, energie, luft - eau, énergie, air*, 101. Jahrgang 2009, Heft 1, p. 31-40.

Schleiss, A., Feuz, B., Aemmer, M. and Zünd, B. (1996). Verlandungsprobleme im Stausee Mauvoisin. Ausmass, Auswirkungen und mögliche Massnahmen, Int. Symposium "Verlandung von Stauseen" – Mitteilungen VAW, No. 141, Teil 1, Zürich, Switzerland, pp. 37-58.

Schleiss, A., and Oehy, C. (2002). "Verlandung von Stauseen und Nachhaltigkeit." *Wasser, energie, luft – eau, énergie, air*, 94.Jahrgang 2002 (Heft 7/8), 227-234.

Schlichting, H. (1968). *Boundary layer theory*, McGraw-Hill, New York, USA.

Schneider, J., Badura, H., Troy, W., Knoblauch, H. (2007). "Determination of Parameters for Venting Turbiditiy Currents througha Reservoir", IAHR Congress, Venice, Italy, pp. 425.

Schoklitsch, A. (1935). *Stauraumverlandung und Kolkabwehr (The silting of reservoirs and scour protection)*, Springer, Wien.

Sharma, R. N., and Shaikh, A. A. (2003). "Solids suspension in stirred tanks with pitched blade turbines." *Chemical Engineering Science*, 58, 2123 - 2140.

Shen, H. W. and Lai, J.-S. (1996), "Sustain reservoir useful life by flushing sediment". *International Journal of Sediment Research*, Vol. 11(3), pp. 10-17.

Sherman, B. (2000). "Scoping options for mitigating cold water discharges from dams", Consultancy Report 00/21, Canberra.

Shresta, P.L., Kaluarachchi, I.D., Anid, P.J. (2001). "Cohesive sediment resuspension: Experimentation and Analysis", World Water Congress 2001.

Simon, M. and Fonade, C. (1993). "Experimental study of mixing performances using steady and unsteady jets", *Can. J. Chem. Eng.* 71(4), pp. 507–513.

Sinniger, R.O., and De Cesare, G. "Spülung von Grundablassstollen - Theorie und Modellversuche." *Internationales Symposium Verlandung von Stauseen und Stauhaltungen, Sedimentprobleme in Leitungen und Kanälen*, Mitteilungen der VAW Nr. 142, Teil 1, 93-110.

Sinniger, R., De Cesare, G. and Boillat, J.-L. (1999). "Propriétés des alluvions récentes dans les retenues alpines", *wasser, energie, luft – eau, énergie, air*, Heft 9/10, 92. Jahrgang, p. 255-258.

Sinniger R. O., De Cesare G. und Boillat J.-L. (2000). "Eigenschaften junger Sedimente in Speicherseen", *wasser, energie, luft – eau, énergie, air*, Jahrgang 92, Heft 1/2-2000, pp. 9-12.

Staub, E. (2000). "Effects of sediment flushing on fish and invertebrates in Swiss alpine rivers." Toyama, International Workshop and Symposium on reservoir sedimentation management 185-194.

Stefan, H.G., Gu, R. (1992). "Efficiency of jet-mixing of temperature-stratified water". *Journal of Environmental Engineering*, 118 (3), 363-379.

Stephens, R., and Imberger, J. (1993). "Reservoir destratification via mechanical mixers." *Journal of Hydraulic Engineering*, 119(4), 438-456.

Sumi, T. (2004). "Reservoir sedimentation management with bypass tunnels in Japan." Proceedings of the ninth international symposium on river sedimentation, Yichang, China, 1036-1043.

Suter, P. (1998). „Verlandung und Spülung des Rempenbeckens der AG Kraftwerk Wägital“, *wasser, energie, luft – eau, énergie, air*, 91. Jahrgang, Heft 5/6, p. 127-131.

Takeda, Y. (1995) Instantaneous velocity profile measurement by ultrasonic Doppler method. *Int. J. Japan. Soc. Mech. Eng., Series B*, 35, 8-16.

Tollmien, W. (1926). "Berechnung turbulenter Ausbreitungsvorgänge." *Z. angew. Math. Mech*., 6, 468-478.

U.S. Army Corps of Engineers (1995). "Sedimentation Investigations of Rivers and Reservoirs." *Engineer Manual EM 1110-2-4000, CECW-EH-Y*, Washington, DC 20314-1000.

Van Rijn, L. C. (1990). *Principles of Sediment Transport in Rivers, Estuaries and Coastal Sciences*, Aqua Publications, University of Utrecht.

Varma, C.V.J., Naidu, B.S.K., Rao, A.R.G. (2000). Silting problems in hydro power plants, International Conference on Silting problems in Hydro Power Plants, New Delhi.A. A. Balkema, Rotterdam

Vigl L., Pürer, E. (1996). “Speicher Bolgenach : Feststoffbewirtschaftsungskonzept und erforderliche Massnahmen,“ proc. of Internationales Symposium "Verlandung von Stauseen und Stauhaltungen, Sedimentprobleme in Leitungen und Kanälen", Mitteilungen der Versuchsanstalt für Wasserbau, Hydrologie und Glaziologie an der Eidgenössischen Technischen Hochschule Zürich, no 142, ISSN 0374-0056, pp. 223-230

Vischer, D.L., Hager, W.H., Casanova, C., Joos, B., Lier, P. and Martini, O., (1997). "Bypass tunnels to prevent reservoir sedimentation". 19th Congress ICOLD, Florence Q74 (R.37): 605-624

Wadell, H. (1932). "Volume, shape, and roundness of rock-particles." *J. Geol.*, 40, 443-451.

Walling, D. E. (1997). "The response of sediment yields to environmental change." *Human impact on erosion and sedimentation, IAHS*, Rabat, 245:77-89.

Wasewar, K. L. (2006). "A design of jet mixed tank." *Chemical and Biochemical Engineering Quarterly*, 20(1), 31-46.

Wüest, A., Brooks, N. H., Imboden, D. M. (1992). "Bubble Plume Modeling for Lake Restoration." *Water Resources Research*, 28(12), 3235 - 3250.

Zanke, U. (1982). *Grundlagen der Sedimentbewegung*, Springer Verlag, Berlin.

Zanke, U. C. E. (2002). *Hydromechanik der Gerinne und Küstengewässer*, Parey, Berlin.

Zughbi, H. D. (2006). "Numerical simulation of mixing in a jet agitated horizontal cylindrical tank." *International Journal of Computational Fluid Dynamics*, 20(2), 127-136.

Zughbi, H. D., Rakib, M.A. (2004). "Mixing in a fluid jet agitated tank: effects of jet angle and elevation and number of jets." *Chemical Engineering Science*, 59(4), 829-842.

Zughbi, H. D., Ahmad, I. (2005). "Mixing in liquid-jet-agitated tanks: effects of jet asymmetry." *Industrial and Engineering Chemistry Research*, 44(1052-1066).

Zwietering, T. N. (1958). "Suspending of solid particles in liquid by agitators." *Chemical Engineering Science*, 8, 244-253.

Acknowledgments

This thesis couldn't have been carried out without the support and guidance of my supervisor and thesis director Prof. Anton Schleiss. I would like to express my gratitude for the rich scientific discussions and for steadily being optimistic and flexible and respecting the young family induced working conditions during the course of the present work.

Special thanks go to the thesis Co-director Dr Giovanni De Cesare for his confidence in my abilities, his constant encouragement and his catching enthusiasm in research. I'm very grateful for the great many of interesting discussions and progressive advices.

Dr Jean-Louis Boillat deserves my high gratitude for supporting me with his ideas and the many fruitful discussions, his optimistic point of view and his profound experience in performing physical experiments.

This work was funded by the Swisselectric Research. My thanks are due to Dr. Paulus and Dr. Kauert for following this project and for their positive attitude and encouraging interest.

I'm indebted to Dr Johannes Bühler who has shared with me his remarkable knowledge about reservoir sedimentation and impressed me always with his quick perception and his very broad view on research. I appreciate also his help and advice in editing parts of the thesis report.

I gladly acknowledge my debt to Iván Parrá and Reto Graf, who thoroughly and conscientiously carried out a great part of the physical experiments during my second maternity leave. Moreover, I would like to thank the many spontaneous and reliable hands of the LCH and Raphaël Sprenger assisting the performance of the experiments.

I am very grateful for the relevant help of Dr Olivier Braun in the numerical simulations. Without his advice and knowledge the numerical simulations could not have been bearing fruits. My thanks also go to Dr Krishna Mohanarangam from CSIRO (Australia) who supervised my simulations in the final phase from the distance and lent me a hand via e-mail. I would also like to thank Cédric Bron for his assistance in software questions and Jean-Claude Leballeur for his reliable help to run the simulations on the new server Vega.

I would like to express my thanks to the talented mathematician Sahra Sinaei who assisted me developing a limit function.

High gratitude is dedicated to Louis Schneiter and his team, namely Michel Teuscher, Virgile Cavin and Eric Pantillon for their technical assistance and for always accomplishing modifications and improvements on the experimental set-up on time and with humor.

It's a pleasure to thank all the colleagues and friends from LCH for their help, their fruitful, fascinating and distractive discussions and the many hours we laughed together.

I wish to express my warmest thanks to my beloved family for the great support. Without the love and comprehension and the continuous encouragement and motivation from my dear husband Christian and the enormous patience of my children Nils and Sarina it would not have come to a thesis.

Last but not least I wish to express cordial thanks to my mother and my mother in law who lovingly took great care about the children and from whom I could adopt many precious emotional and educational boosts.

Appendix A

concentration		*ml/l*	*Vol.-%*	*mg/l*	*ppm*
1 ml/l	$\triangleq$	*1*	*0.1*	ρs	10^3
1 Vol.-%	$\triangleq$	*10*	*1*	$10 \rho s$	10^4
1 mg/l	$\triangleq$	$1/\rho s$	$0.1/\rho s$	*1*	$10^3/\rho s$
1 ppm	$\triangleq$	10^{-3}	10^{-4}	$10^{-3} \rho s$	*1*

Table A.1 Concentration conversion table

Appendix B

Flow patterns for circular jet arrangements with different discharges

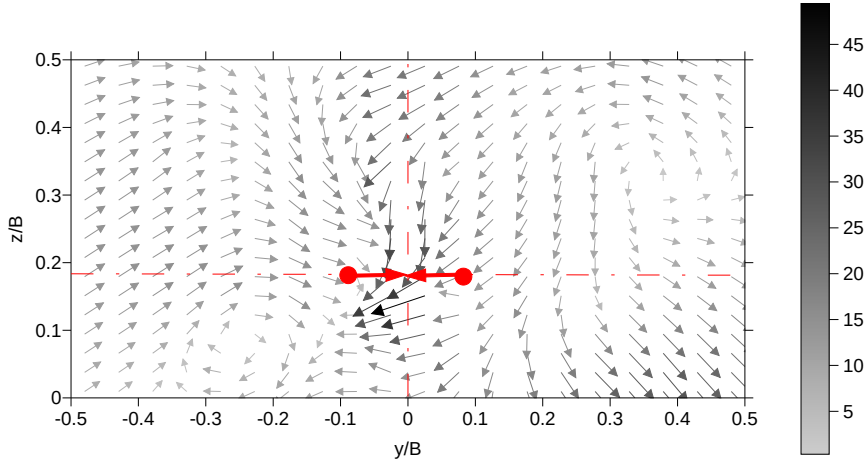

Figure B.1 *Velocity vectors [mm/s] in the transversal plane for off-bottom clearance C/B = 0.175, water intake height h_i/B = 0.25, distance between neighbouring jets l_j/B = 0.15, distance between jet circle centre and front wall d_{axis}/B = 0.525, water height h/B = 0.6, total jet discharge $\Sigma Q_j = Q_{out}$ = 570 l/h.*

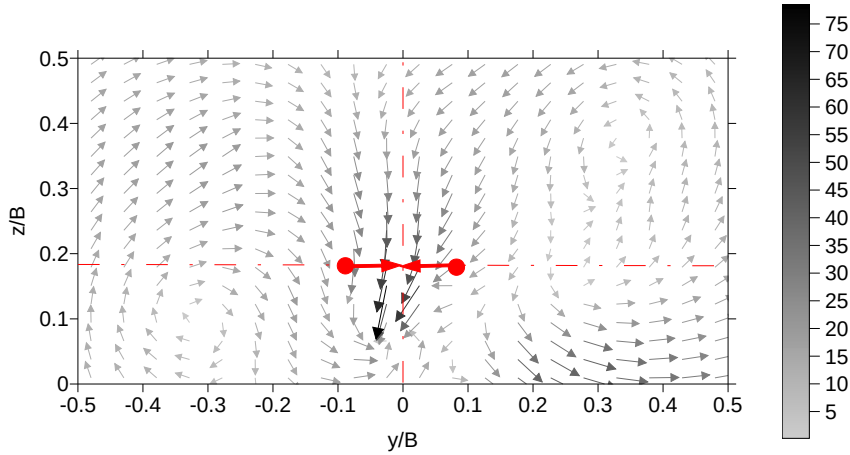

Figure B.2 *Velocity vectors [mm/s] in the transversal plane for off-bottom clearance C/B = 0.175, water intake height h_i/B = 0.25, distance between neighbouring jets l_j/B = 0.15, distance between jet circle centre and front wall d_{axis}/B = 0.525, water height h/B = 0.6, total jet discharge $\Sigma Q_j = Q_{out}$ = 760 l/h.*

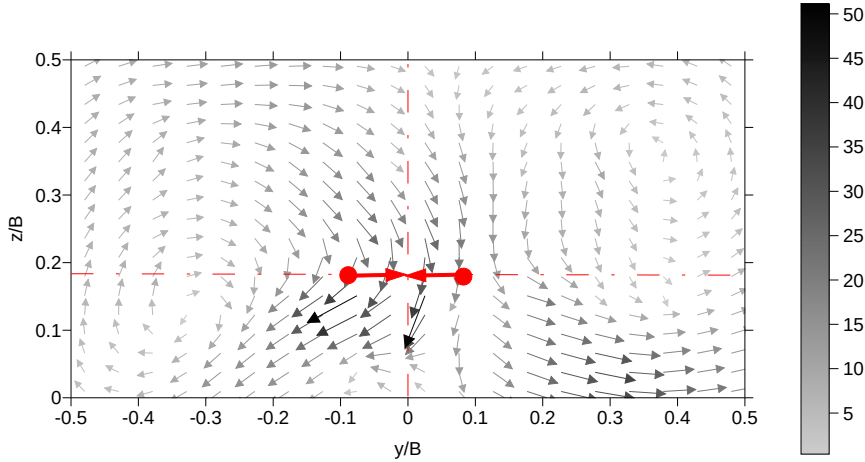

Figure B.3 *Velocity vectors [mm/s] in the transversal plane for off-bottom clearance C/B = 0.175, water intake height h_i/B = 0.25, distance between neighbouring jets l_j/B = 0.15, distance between jet circle centre and front wall d_{axis}/B = 0.525, water height h/B = 0.6, total jet discharge $\Sigma Q_j = Q_{out}$ = 1140 l/h.*

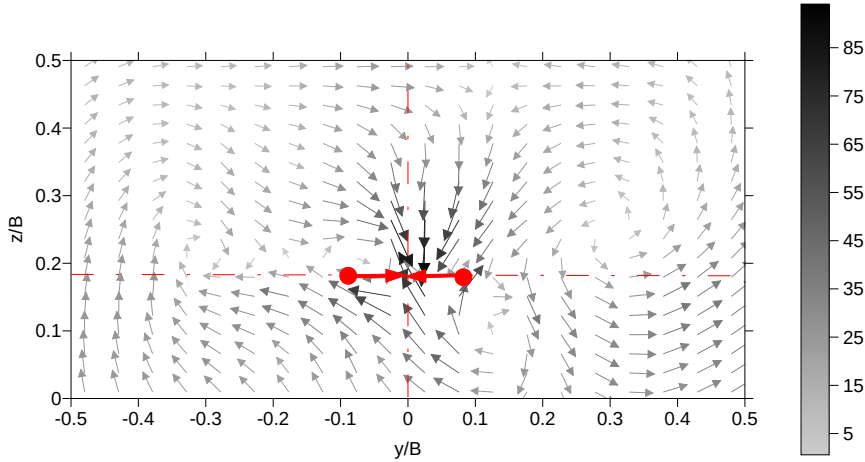

Figure B.4 *Velocity vectors [mm/s] in the transversal plane for off-bottom clearance C/B = 0.175, water intake height h_i/B = 0.25, distance between neighbouring jets l_j/B = 0.15, distance between jet circle centre and front wall d_{axis}/B = 0.525, water height h/B = 0.6, total jet discharge $\Sigma Q_j = Q_{out}$ = 3040 l/h.*

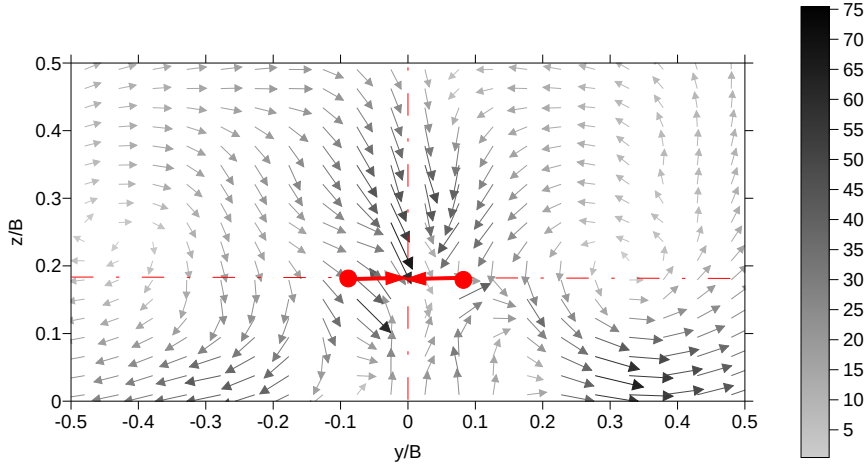

Figure B.5 *Velocity vectors [mm/s] in the transversal plane for off-bottom clearance C/B = 0.175, water intake height h_i/B = 0.25, distance between neighbouring jets l_j/B = 0.15, distance between jet circle centre and front wall d_{axis}/B = 0.525, water height h/B = 0.6, total jet discharge $\Sigma Q_j = Q_{out}$ = 4050 l/h.*

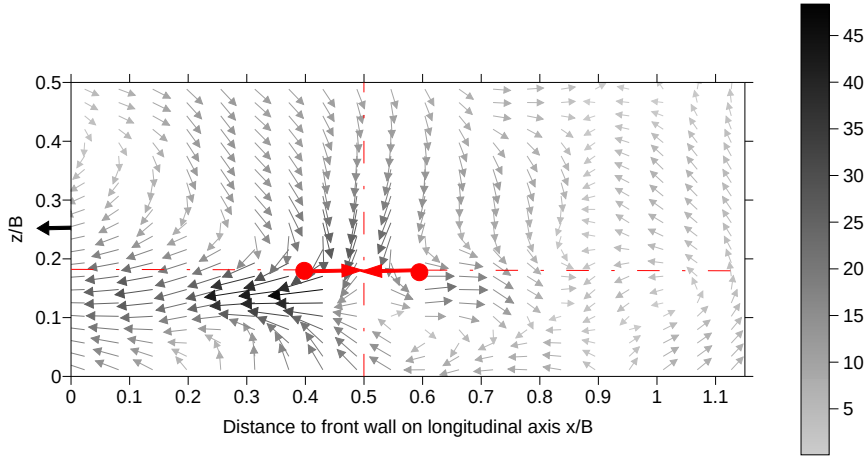

Figure B.6 *Velocity vectors [mm/s] in the longitudinal plane for off-bottom clearance C/B = 0.175, water intake height h_i/B = 0.25, distance between neighbouring jets l_j/B = 0.15, distance between jet circle centre and front wall d_{axis}/B = 0.525, water height h/B = 0.6, total jet discharge $\Sigma Q_j = Q_{out}$ = 570 l/h.*

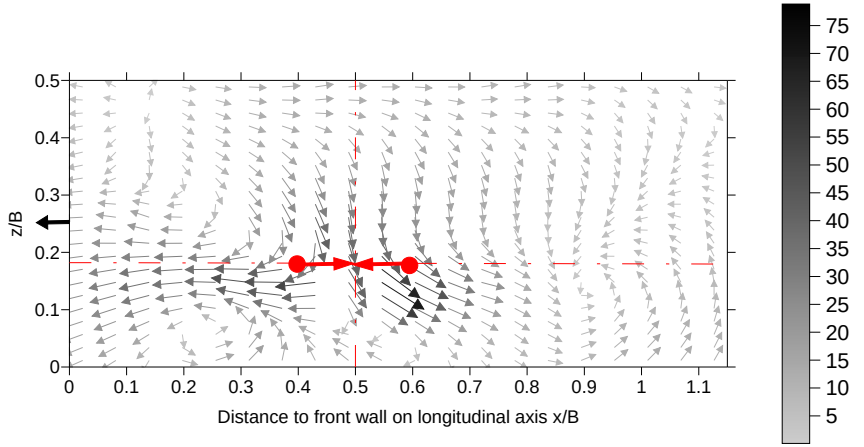

Figure B.7 *Velocity vectors [mm/s] in the longitudinal plane for off-bottom clearance C/B = 0.175, water intake height h_i/B = 0.25, distance between neighbouring jets l_j/B = 0.15, distance between jet circle centre and front wall d_{axis}/B = 0.525, water height h/B = 0.6, total jet discharge $\Sigma Q_j = Q_{out}$ = 760 l/h.*

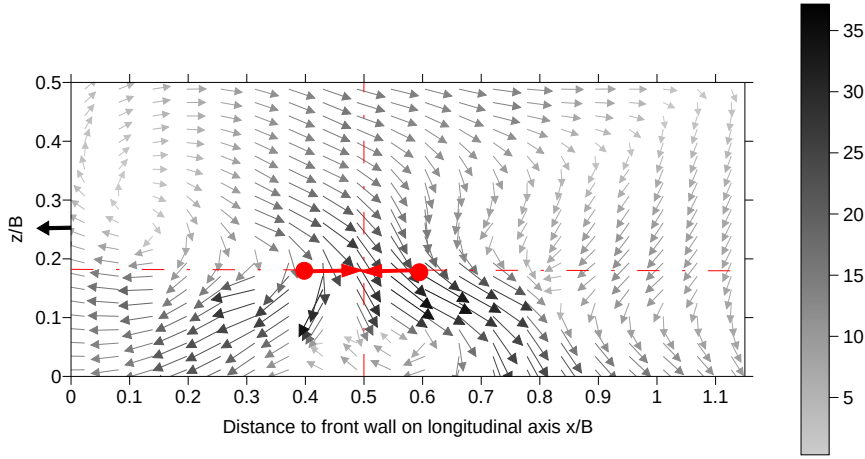

Figure B.8 *Velocity vectors [mm/s] in the longitudinal plane for off-bottom clearance C/B = 0.175, water intake height h_i/B = 0.25, distance between neighbouring jets l_j/B = 0.15, distance between jet circle centre and front wall d_{axis}/B = 0.525, water height h/B = 0.6, total jet discharge $\Sigma Q_j = Q_{out}$ = 1140 l/h.*

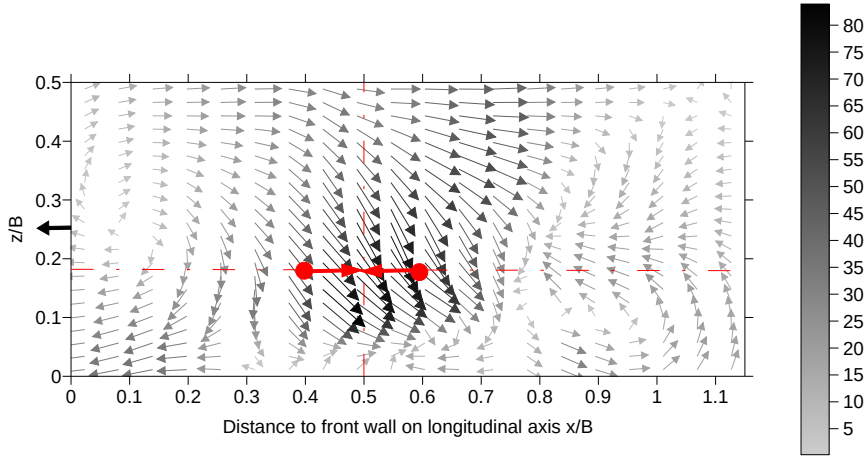

Figure B.9 *Velocity vectors [mm/s] in the longitudinal plane for off-bottom clearance C/B = 0.175, water intake height h_i/B = 0.25, distance between neighbouring jets l_j/B = 0.15, distance between jet circle centre and front wall d_{axis}/B = 0.525, water height h/B = 0.6, total jet discharge $\Sigma Q_j = Q_{out}$ = 3040 l/h.*

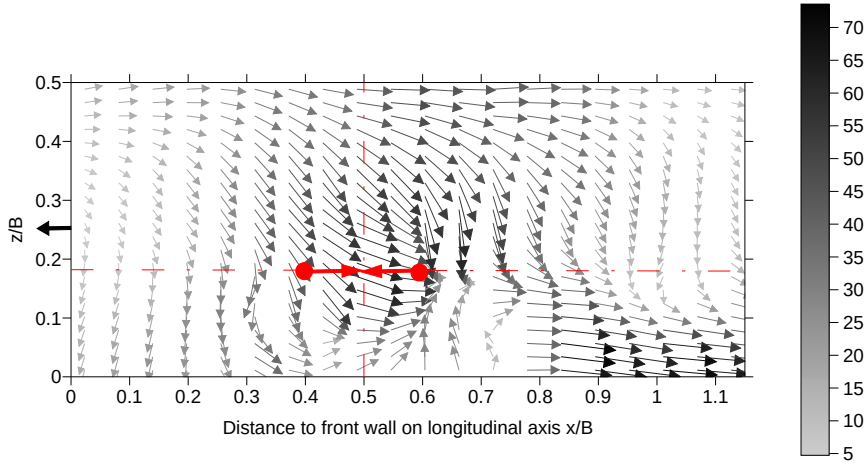

Figure B.10 *Velocity vectors [mm/s] in the longitudinal plane for total jet discharge ΣQ_j = Q_{out} = 4050 l/h, off-bottom clearance C/B = 0.175, water intake height h_i/B = 0.25, distance between neighbouring jets l_j/B = 0.15, distance between jet circle centre and front wall d_{axis}/B = 0.525, water height h/B = 0.6.*

Flow patterns for circular jet arrangements with different off-bottom clearance

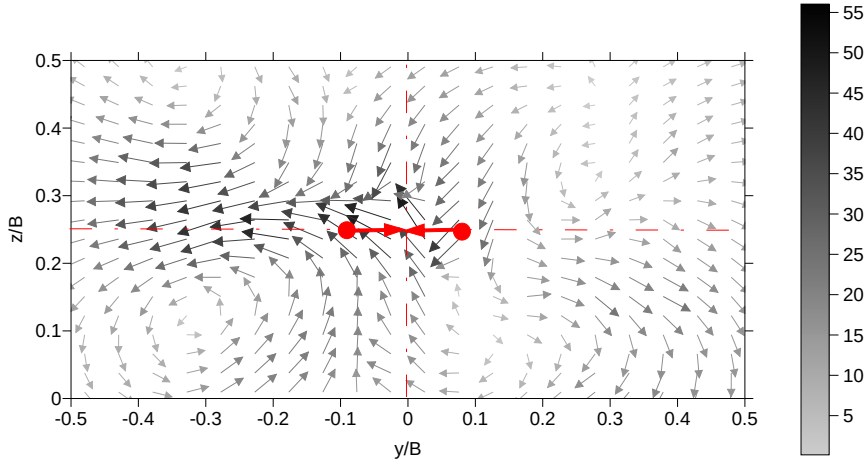

Figure B.11 *Velocity vectors [mm/s] in the transversal plane for off-bottom clearance C/B = 0.25, water intake height hi/B = 0.25, distance between neighbouring jets lj/B = 0.15, distance between jet circle centre and front wall daxis/B = 0.525, water height h/B = 0.6, total jet discharge Qj = Qout = 760 l/h.*

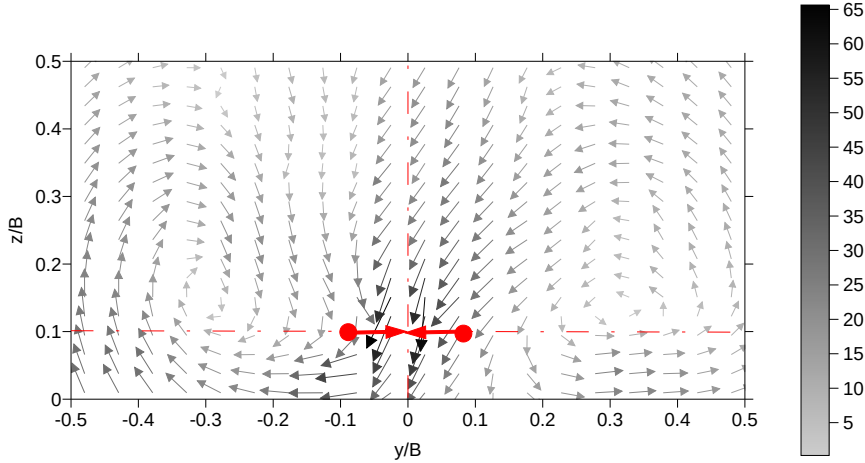

Figure B.12 *Velocity vectors [mm/s] in the transversal plane for off-bottom clearance C/B = 0.1, water intake height h_i/B = 0.25, distance between neighbouring jets l_j/B = 0.15, distance between jet circle centre and front wall d_{axis}/B = 0.525, water height h/B = 0.6, total jet discharge $\Sigma Q_j = Q_{out}$ = 760 l/h.*

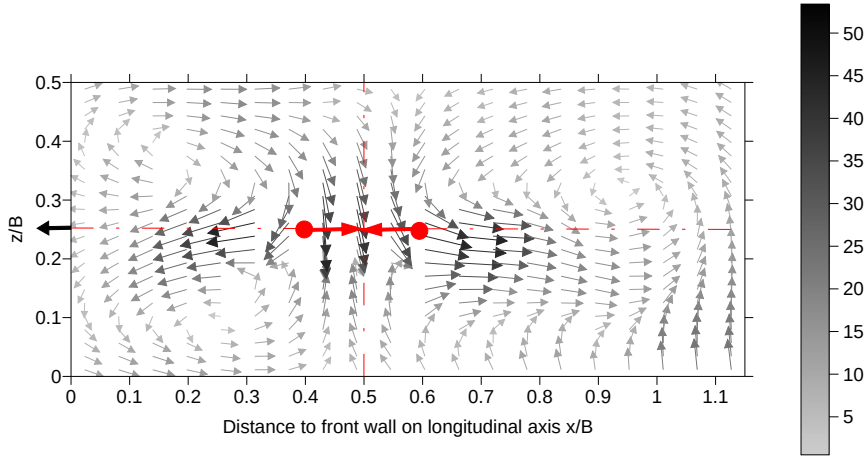

Figure B.13 *Velocity vectors [mm/s] in the longitudinal plane for off-bottom clearance C/B = 0.25, water intake height h_i/B = 0.25, distance between neighbouring jets l_j/B = 0.15, distance between jet circle centre and front wall d_{axis}/B = 0.525, water height h/B = 0.6, total jet discharge $\Sigma Q_j = Q_{out}$ = 760 l/h.*

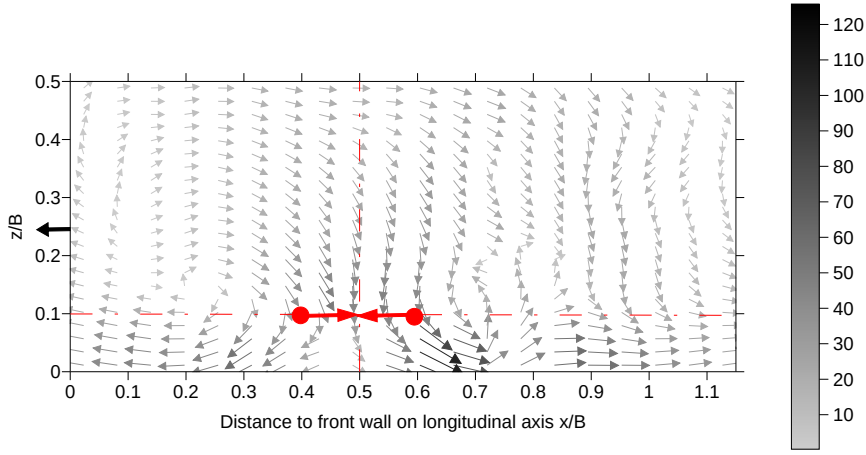

Figure B.14 *Velocity vectors [mm/s] in the longitudinal plane for off-bottom clearance C/B = 0.1, water intake height h_i/B = 0.25, distance between neighbouring jets l_j/B = 0.15, distance between jet circle centre and front wall d_{axis}/B = 0.525, water height h/B = 0.6, total jet discharge $\Sigma Q_j = Q_{out}$ = 760 l/h.*

Flow patterns for circular jet arrangements with different water intake heights

Off-bottom clearance C/B	*Water intake height h_i/B*	*Transversal plane*	*Longitudinal plane*
0.1	*0.125*	*Figure B.15*	*Figure B.21*
	0.25	*Figure 4.30*	*Figure 4.31*
		Figure B.12	*Figure B.14*
	0.375	*Figure B.16*	*Figure B.22*
0.175	*0.125*	*Figure B.17*	*Figure B.23*
	0.25	*Figure 4.22*	*Figure 4.23*
		Figure B.2	*Figure B.7*
	0.375	*Figure B.18*	*Figure B.24*
0.25	*0.125*	*Figure B.19*	*Figure B.25*
	0.25	*Figure 4.28*	*Figure 4.29*
		Figure B.11	*Figure B.13*
	0.375	*Figure B.20*	*Figure B.26*

Table B.1 Studied combinations of off-bottom clearance C/B of the circular jet arrangement and the water intake height above tank bottom. Results presented in the transversal and longitudinal plane: overview of figures.

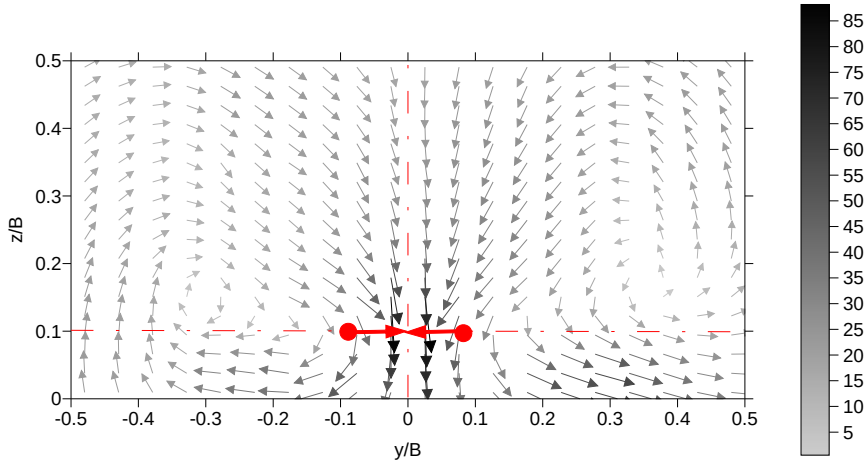

Figure B.15 Velocity vectors [mm/s] in the transversal plane for off-bottom clearance C/B = 0.1, water intake height h_i/B = 0.125, distance between neighbouring jets l_j/B = 0.15, distance between jet circle centre and front wall d_{axis}/B = 0.525, water height h/B = 0.6, total jet discharge $\Sigma Q_j = Q_{out}$ = 760 l/h.

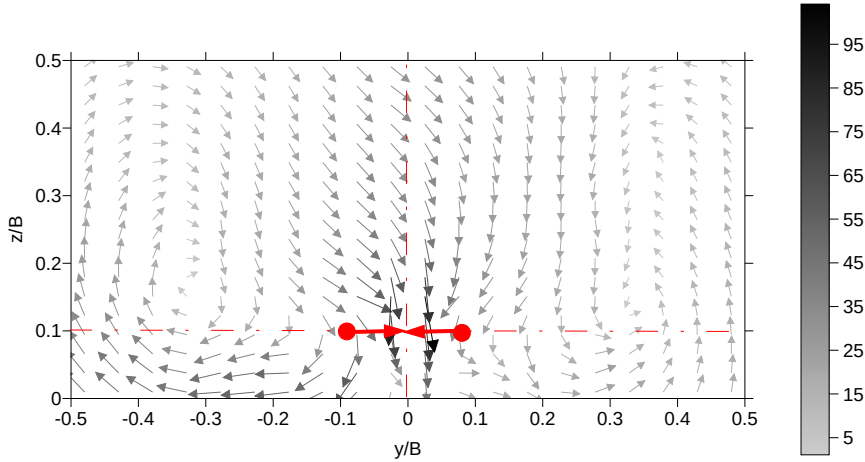

Figure B.16 Velocity vectors [mm/s] in the transversal plane for off-bottom clearance C/B = 0.1, water intake height h_i/B = 0.375, distance between neighbouring jets l_j/B = 0.15, distance between jet circle centre and front wall d_{axis}/B = 0.525, water height h/B = 0.6, total jet discharge $\Sigma Q_j = Q_{out}$ = 760 l/h.

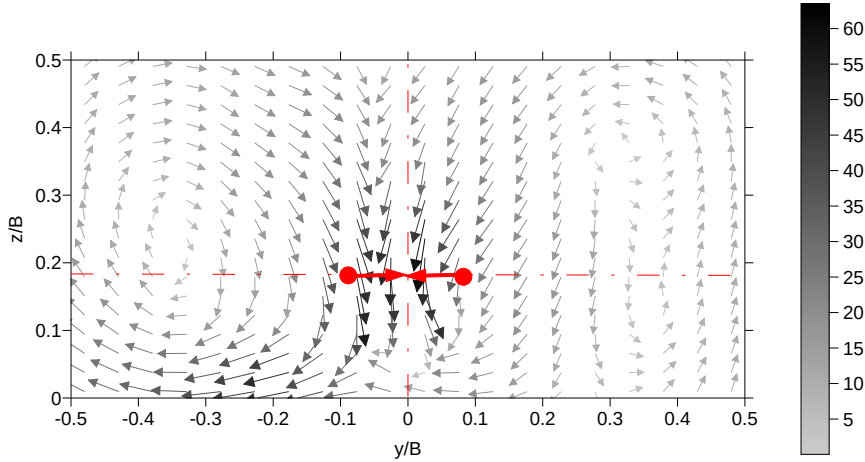

Figure B.17 Velocity vectors [mm/s] in the transversal plane for off-bottom clearance C/B = 0.175, water intake height h_i/B = 0.125, distance between neighbouring jets l_j/B = 0.15, distance between jet circle centre and front wall d_{axis}/B = 0.525, water height h/B = 0.6, total jet discharge $\Sigma Q_j = Q_{out}$ = 760 l/h.

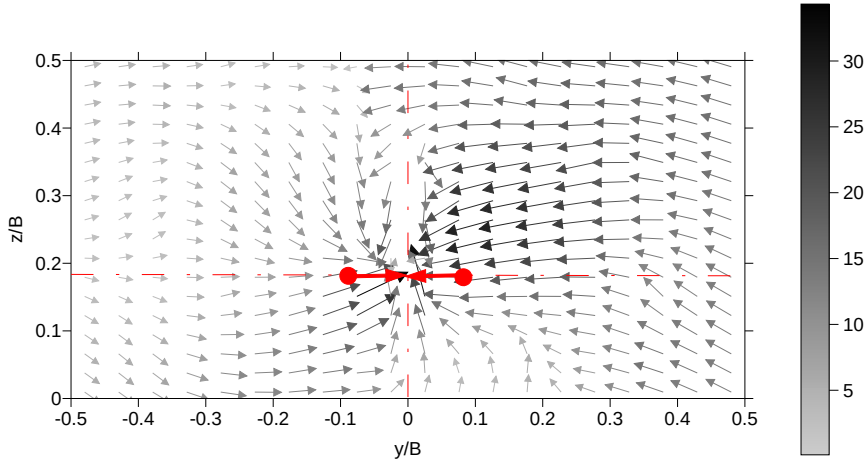

Figure B.18 Velocity vectors [mm/s] in the transversal plane for off-bottom clearance C/B = 0.175, water intake height h_i/B = 0.375, distance between neighbouring jets l_j/B = 0.15, distance between jet circle centre and front wall d_{axis}/B = 0.525, water height h/B = 0.6, total jet discharge $\Sigma Q_j = Q_{out}$ = 760 l/h.

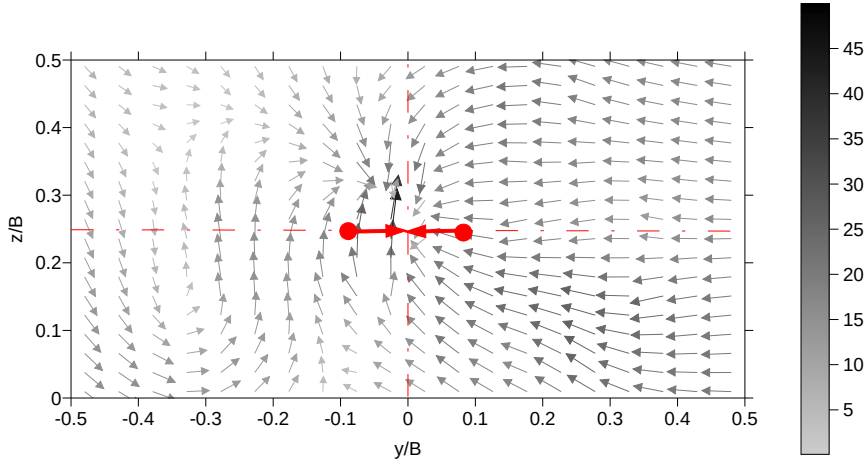

Figure B.19 Velocity vectors [mm/s] in the transversal plane for off-bottom clearance C/B = 0.25, water intake height h_i/B = 0.125, distance between neighbouring jets l_j/B = 0.15, distance between jet circle centre and front wall d_{axis}/B = 0.525, water height h/B = 0.6, total jet discharge $\Sigma Q_j = Q_{out}$ = 760 l/h.

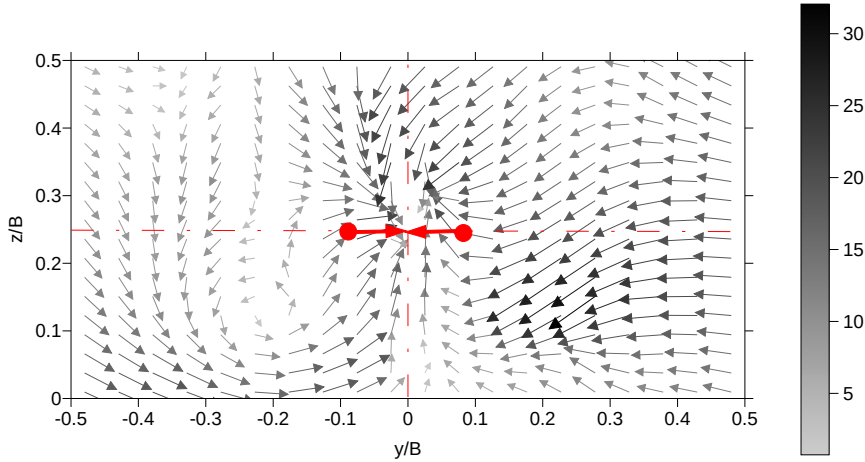

Figure B.20 *Velocity vectors [mm/s] in the transversal plane for off-bottom clearance C/B = 0.25, water intake height h_i/B = 0.375, distance between neighbouring jets l_j/B = 0.15, distance between jet circle centre and front wall d_{axis}/B = 0.525, water height h/B = 0.6, total jet discharge $\Sigma Q_j = Q_{out}$ = 760 l/h.*

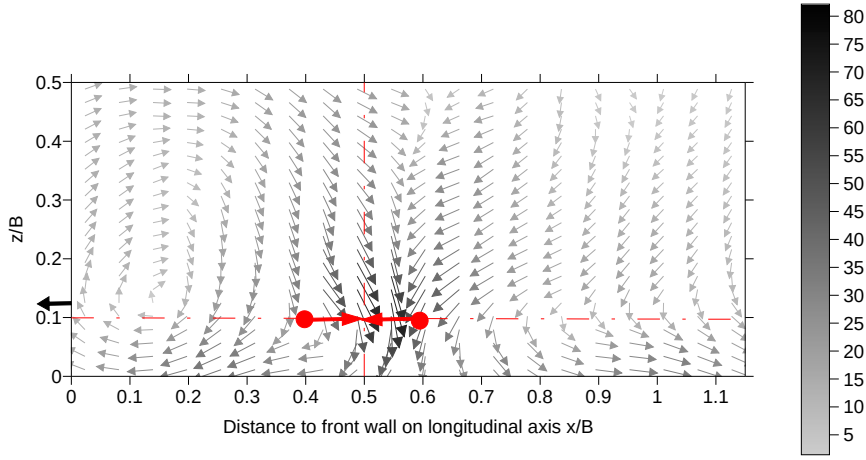

Figure B.21 *Velocity vectors [mm/s] in the transversal plane for off-bottom clearance C/B = 0.1, water intake height h_i/B = 0.125, distance between neighbouring jets l_j/B = 0.15, distance between jet circle centre and front wall d_{axis}/B = 0.525, water height h/B = 0.6, total jet discharge $\Sigma Q_j = Q_{out}$ = 760 l/h.*

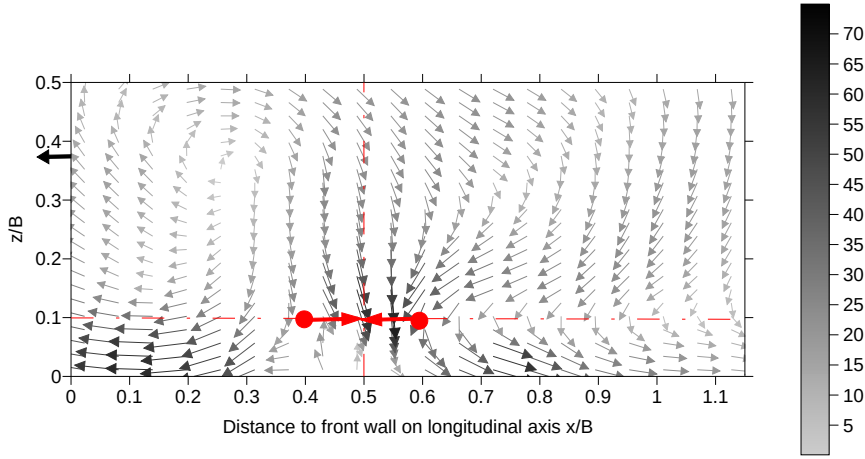

Figure B.22 Velocity vectors [mm/s] in the longitudinal plane for off-bottom clearance C/B = 0.1, water intake height h_i/B = 0.375, distance between neighbouring jets l_j/B = 0.15, distance between jet circle centre and front wall d_{axis}/B = 0.525, water height h/B = 0.6, total jet discharge $\Sigma Q_j = Q_{out}$ = 760 l/h.

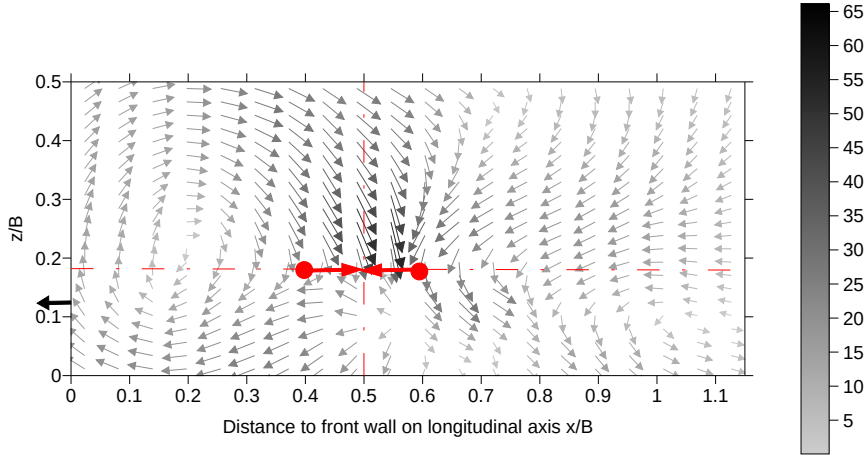

Figure B.23 Velocity vectors [mm/s] in the longitudinal plane for off-bottom clearance C/B = 0.175, water intake height h_i/B = 0.125, distance between neighbouring jets l_j/B = 0.15, distance between jet circle centre and front wall d_{axis}/B = 0.525, water height h/B = 0.6, total jet discharge $\Sigma Q_j = Q_{out}$ = 760 l/h.

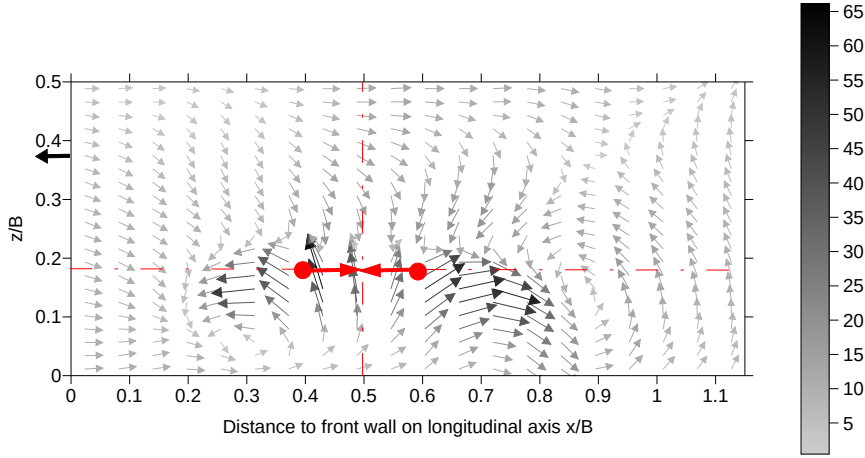

Figure B.24 *Velocity vectors [mm/s] in the longitudinal plane for off-bottom clearance C/B = 0.175, water intake height h_i/B = 0.375, distance between neighbouring jets l_j/B = 0.15, distance between jet circle centre and front wall d_{axis}/B = 0.525, water height h/B = 0.6, total jet discharge $\Sigma Q_j = Q_{out}$ = 760 l/h.*

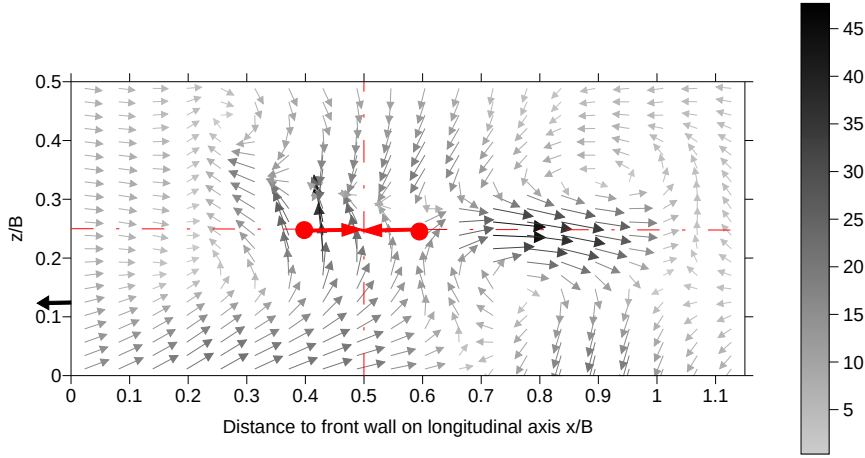

Figure B.25 *Velocity vectors [mm/s] in the longitudinal plane for off-bottom clearance C/B = 0.25, water intake height h_i/B = 0.125, distance between neighbouring jets l_j/B = 0.15, distance between jet circle centre and front wall d_{axis}/B = 0.525, water height h/B = 0.6, total jet discharge $\Sigma Q_j = Q_{out}$ = 760 l/h.*

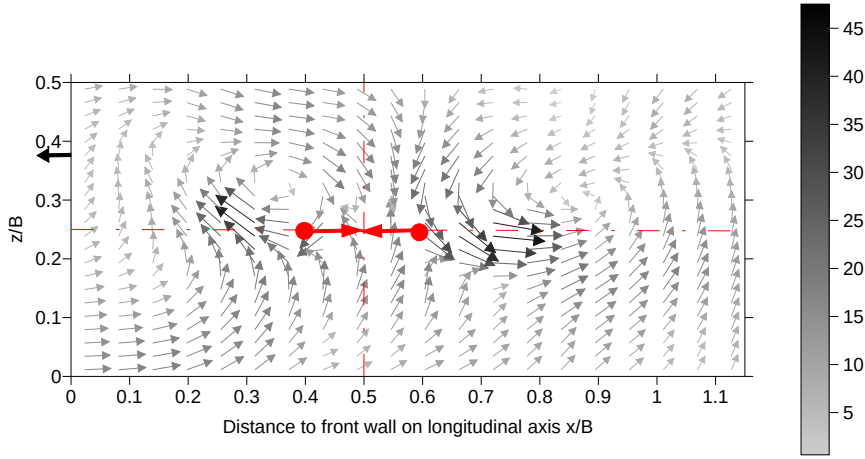

Figure B.26 Velocity vectors [mm/s] in the longitudinal plane for off-bottom clearance C/B = 0.25, water intake height h_i/B = 0.375, distance between neighbouring jets l_j/B = 0.15, distance between jet circle centre and front wall d_{axis}/B = 0.525, water height h/B = 0.6, total jet discharge $\Sigma Q_j = Q_{out}$ = 760 l/h.

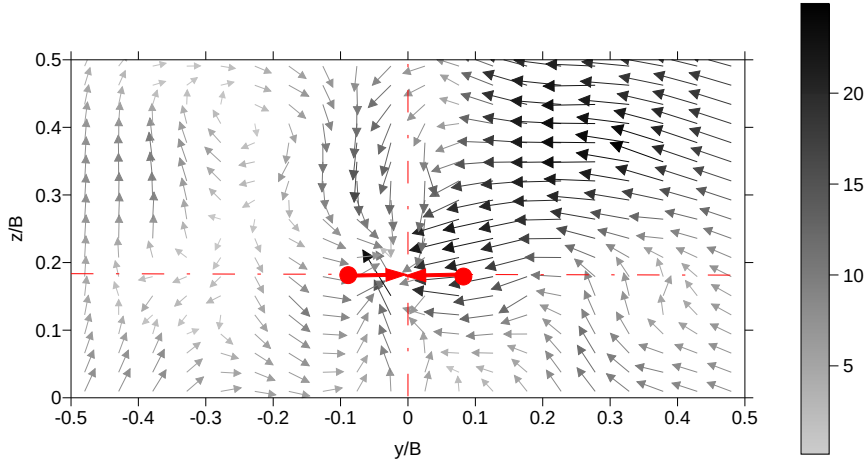

Figure B.27 Velocity vectors [mm/s] in the transversal plane for off-bottom clearance C/B = 0.175, water intake height h_i/B = 0.25, distance between neighbouring jets l_j/B = 0.15, distance between jet circle centre and front wall d_{axis}/B = 0.525, water height h/B = 0.65, total jet discharge $\Sigma Q_j = Q_{out}$ = 760 l/h.

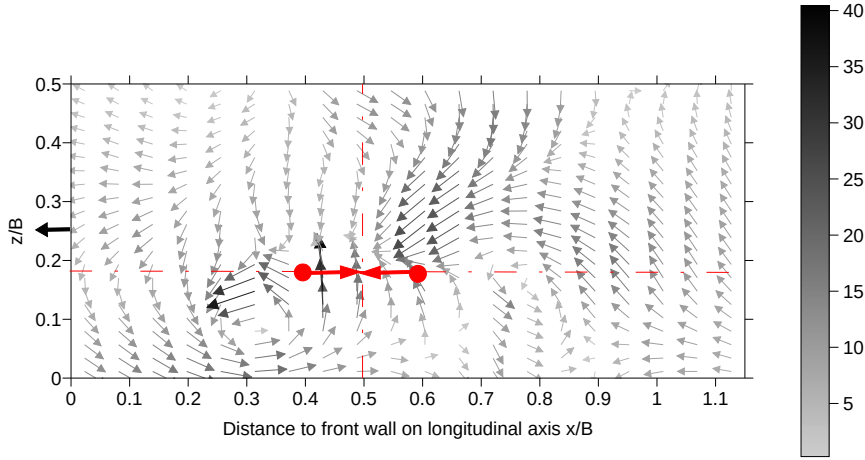

Figure B.28 Velocity vectors [mm/s] in the longitudinal plane for off-bottom clearance C/B = 0.175, water intake height h_i/B = 0.25, distance between neighbouring jets l_j/B = 0.15, distance between jet circle centre and front wall d_{axis}/B = 0.525, water height h/B = 0.65, total jet discharge $\Sigma Q_j = Q_{out}$ = 760 l/h.

Flow patterns for circular jet arrangements with different water heights in tank

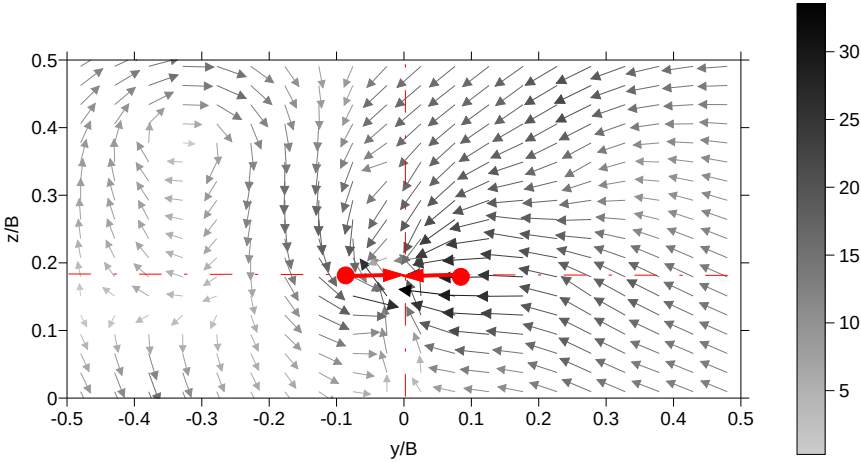

Figure B.29 *Velocity vectors [mm/s] in the transversal plane for off-bottom clearance C/B = 0.175, water intake height h_i/B = 0.25, distance between neighbouring jets l_j/B = 0.15, distance between jet circle centre and front wall d_{axis}/B = 0.525, water height h/B = 0. 5, total jet discharge $\Sigma Q_j = Q_{out}$ = 760 l/h.*

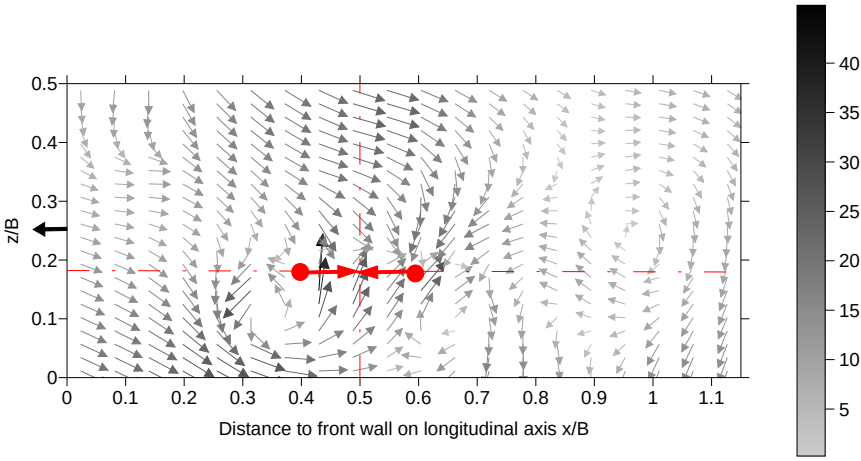

Figure B.30 *Velocity vectors [mm/s] in the longitudinal plane for off-bottom clearance C/B = 0.175, water intake height h_i/B = 0.25, distance between neighbouring jets l_j/B = 0.15, distance between jet circle centre and front wall d_{axis}/B = 0.525, water height h/B = 0.5, total jet discharge $\Sigma Q_j = Q_{out}$ = 760 l/h.*

Flow patterns for circular jet arrangements with different distances of jet arrangement to the front wall

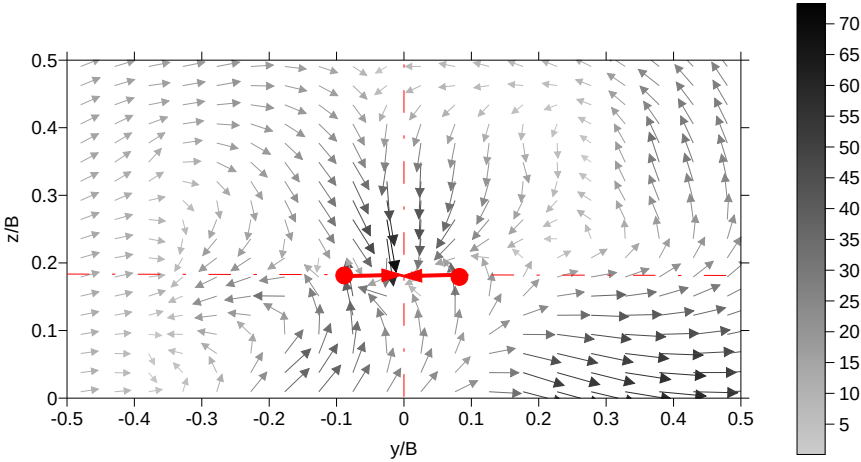

Figure B.31 *Velocity vectors [mm/s] in the transversal plane for off-bottom clearance C/B = 0.175, water intake height h_i/B = 0.25, distance between neighbouring jets l_j/B = 0.15, distance between jet circle centre and front wall d_{axis}/B = 0.3, water height h/B = 0.6, total jet discharge $\Sigma Q_j = Q_{out}$ = 4050 l/h.*

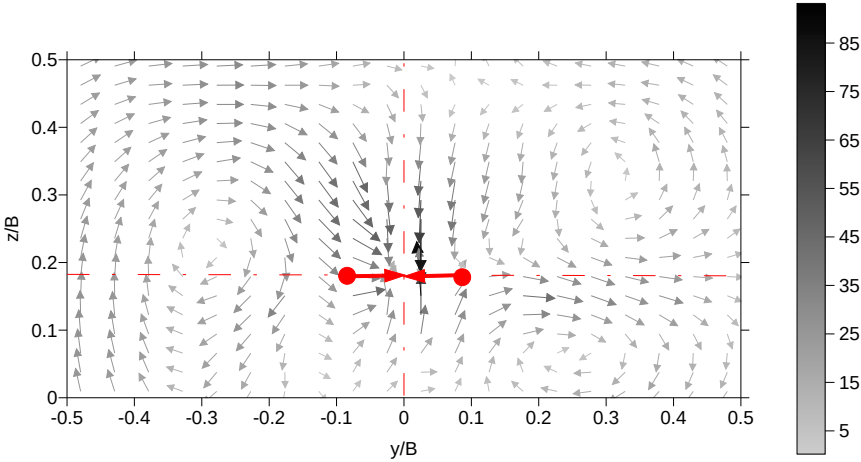

Figure B.32 *Velocity vectors [mm/s] in the transversal plane for off-bottom clearance C/B = 0.175, water intake height h_i/B = 0.25, distance between neighbouring jets l_j/B = 0.15, distance between jet circle centre and front wall d_{axis}/B = 0.4, water height h/B = 0.6, total jet discharge $\Sigma Q_j = Q_{out}$ = 4050 l/h.*

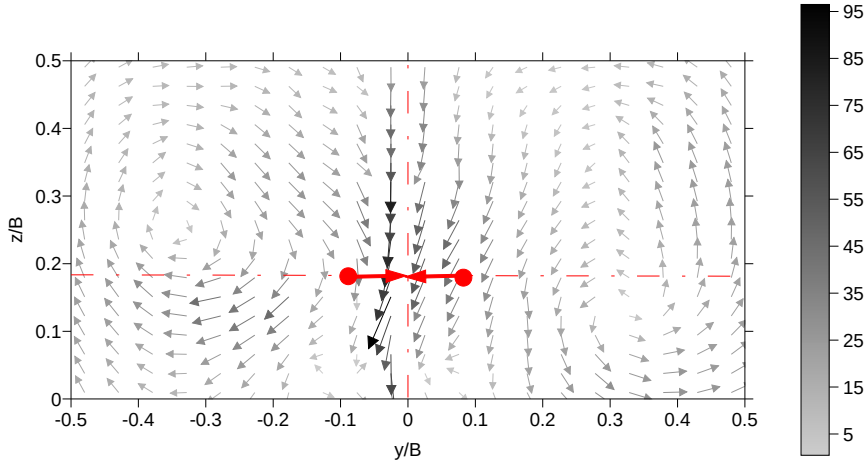

Figure B.33 *Velocity vectors [mm/s] in the transversal plane for off-bottom clearance C/B = 0.175, water intake height h_i/B = 0.25, distance between neighbouring jets l_j/B = 0.15, distance between jet circle centre and front wall d_{axis}/B = 0.4, water height h/B = 0.6, total jet discharge $\Sigma Q_j = Q_{out}$ = 760 l/h.*

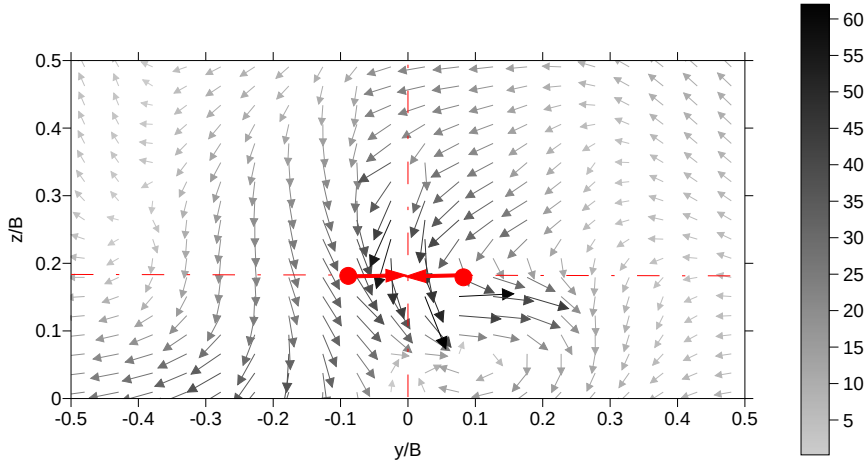

Figure B.34 *Velocity vectors [mm/s] in the transversal plane for off-bottom clearance C/B = 0.175, water intake height h_i/B = 0.25, distance between neighbouring jets l_j/B = 0.15, distance between jet circle centre and front wall d_{axis}/B = 0.65, water height h/B = 0.6, total jet discharge $\Sigma Q_j = Q_{out}$ = 760 l/h.*

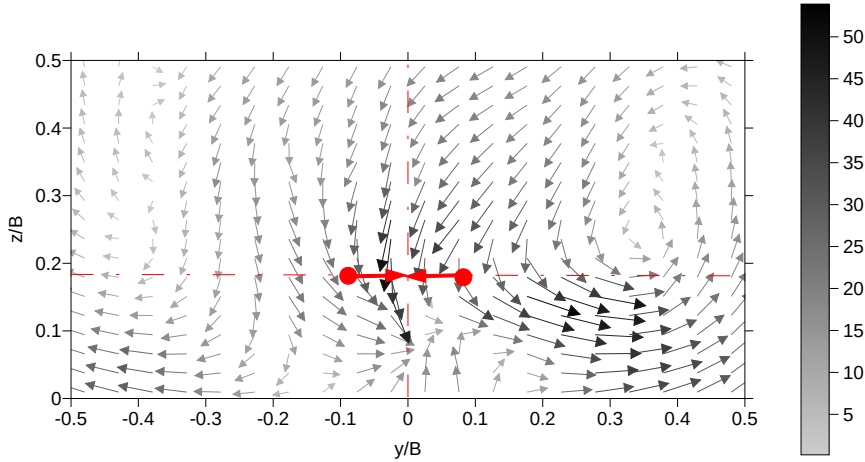

Figure B.35 Velocity vectors [mm/s] in the transversal plane for off-bottom clearance C/B = 0.175, water intake height h_i/B = 0.25, distance between neighbouring jets l_j/B = 0.15, distance between jet circle centre and front wall d_{axis}/B = 0.775, water height h/B = 0.6, total jet discharge $\Sigma Q_j = Q_{out}$ = 760 l/h.

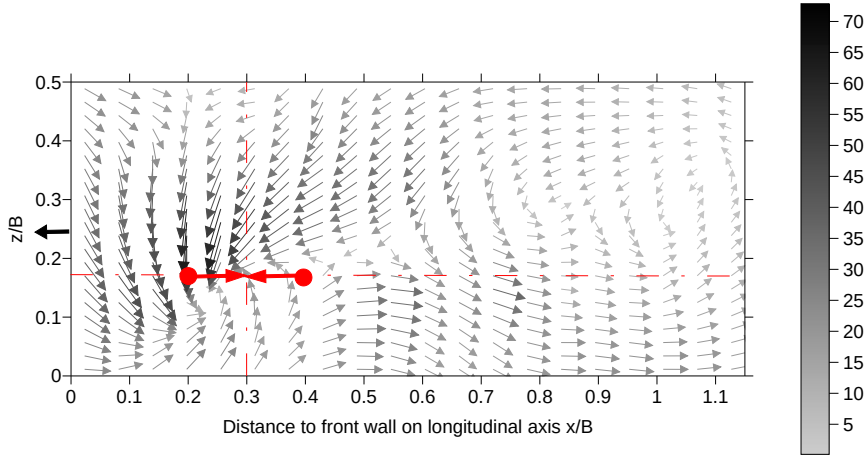

Figure B.36 Velocity vectors [mm/s] in the longitudinal plane for off-bottom clearance C/B = 0.175, water intake height h_i/B = 0.25, distance between neighbouring jets l_j/B = 0.15, distance between jet circle centre and front wall d_{axis}/B = 0.3, water height h/B = 0.6, total jet discharge $\Sigma Q_j = Q_{out}$ = 4050 l/h.

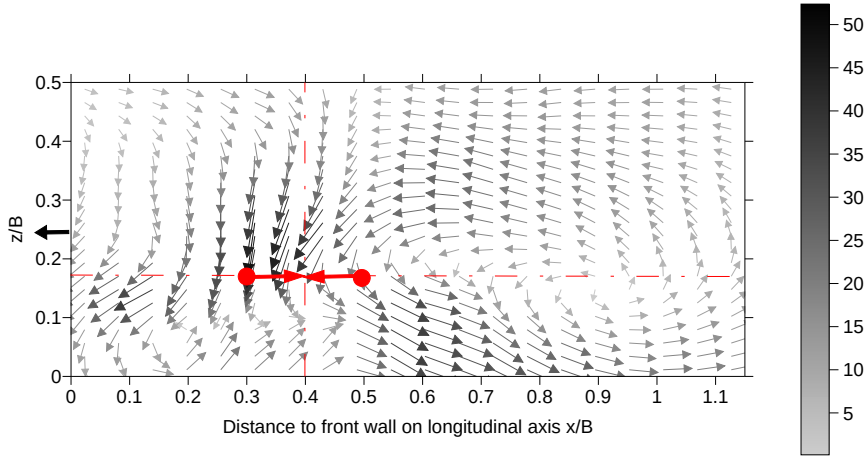

Figure B.37 Velocity vectors [mm/s] in the longitudinal plane for off-bottom clearance C/B = 0.175, water intake height h_i/B = 0.25, distance between neighbouring jets l_j/B = 0.15, distance between jet circle centre and front wall d_{axis}/B = 0.4, water height h/B = 0.6, total jet discharge $\Sigma Q_j = Q_{out}$ = 760 l/h.

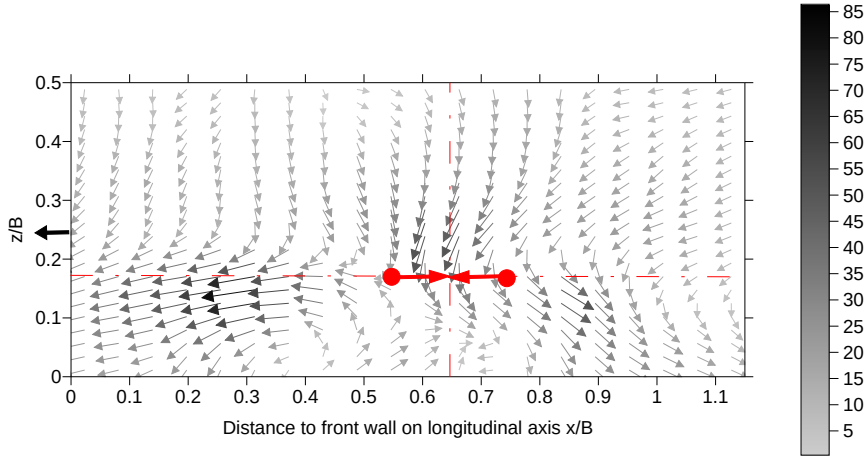

Figure B.38 Velocity vectors [mm/s] in the longitudinal plane for off-bottom clearance C/B = 0.175, water intake height h_i/B = 0.25, distance between neighbouring jets l_j/B = 0.15, distance between jet circle centre and front wall d_{axis}/B = 0.65, water height h/B = 0.6, total jet discharge $\Sigma Q_j = Q_{out}$ = 760 l/h.

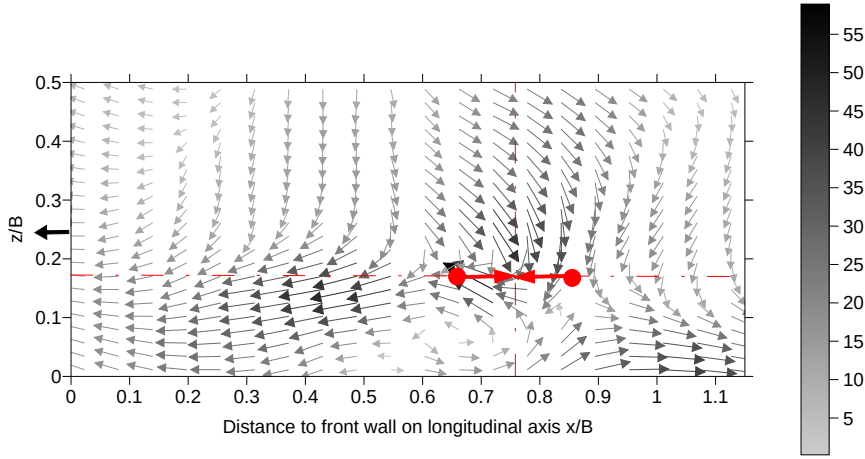

Figure B.39 Velocity vectors [mm/s] in the longitudinal plane for off-bottom clearance C/B = 0.175, water intake height h_i/B = 0.25, distance between neighbouring jets l_j/B = 0.15, distance between jet circle centre and front wall d_{axis}/B = 0.775, water height h/B = 0.6, total jet discharge $\Sigma Q_j = Q_{out}$ = 760 l/h.

Flow patterns for circular jet arrangements with different distances between neighboring jets

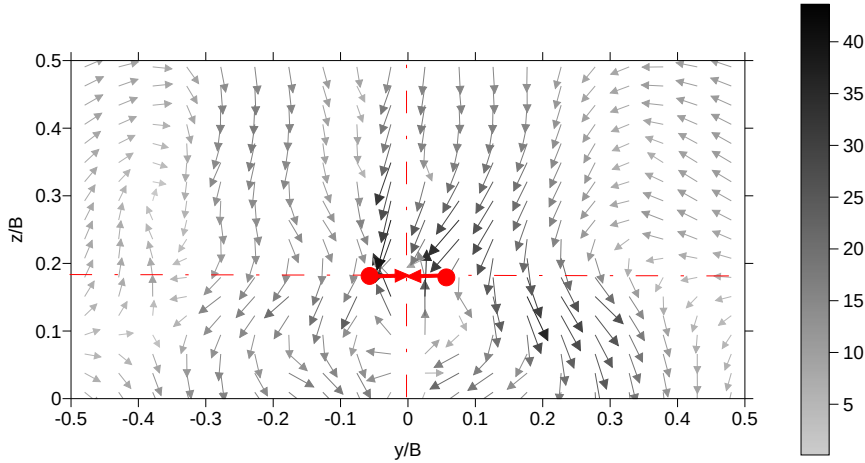

Figure B.40 Velocity vectors [mm/s] in the transversal plane for off-bottom clearance C/B = 0.175, water intake height h_i/B = 0.25, distance between neighbouring jets l_j/B = 0.1, distance between jet circle centre and front wall d_{axis}/B = 0.525, water height h/B = 0.6, total jet discharge $\Sigma Q_j = Q_{out}$ = 760 l/h.

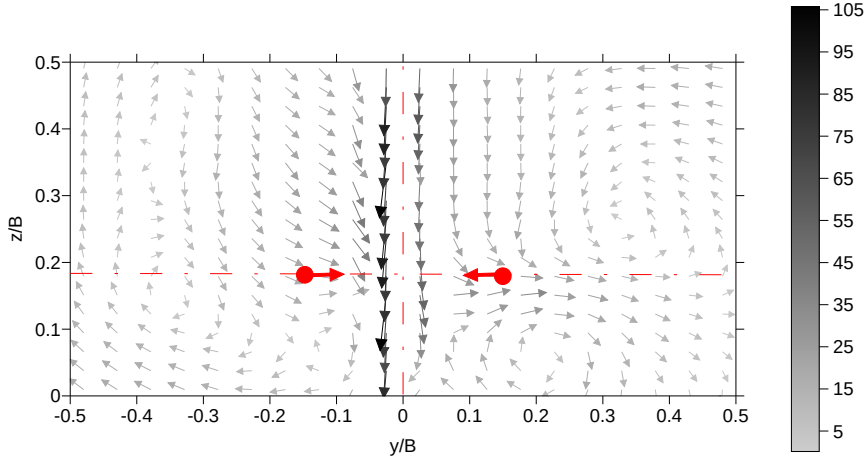

Figure B.41 *Velocity vectors [mm/s] in the transversal plane for off-bottom clearance C/B = 0.175, water intake height h_i/B = 0.25, distance between neighbouring jets l_j/B = 0.225, distance between jet circle centre and front wall d_{axis}/B = 0.525, water height h/B = 0.6, total jet discharge $\Sigma Q_j = Q_{out}$ = 760 l/h.*

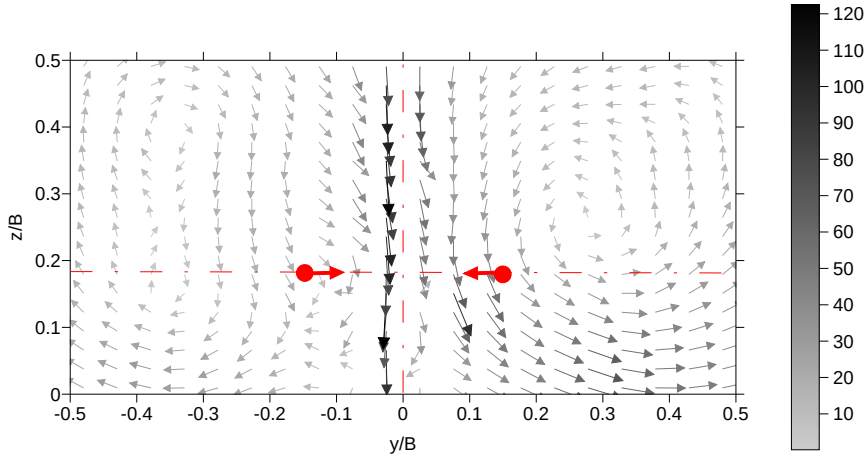

Figure B.42 *Velocity vectors [mm/s] in the transversal plane for off-bottom clearance C/B = 0.175, water intake height h_i/B = 0.25, distance between neighbouring jets l_j/B = 0.225, distance between jet circle centre and front wall d_{axis}/B = 0.525, water height h/B = 0.6, total jet discharge $\Sigma Q_j = Q_{out}$ = 760 l/h.*

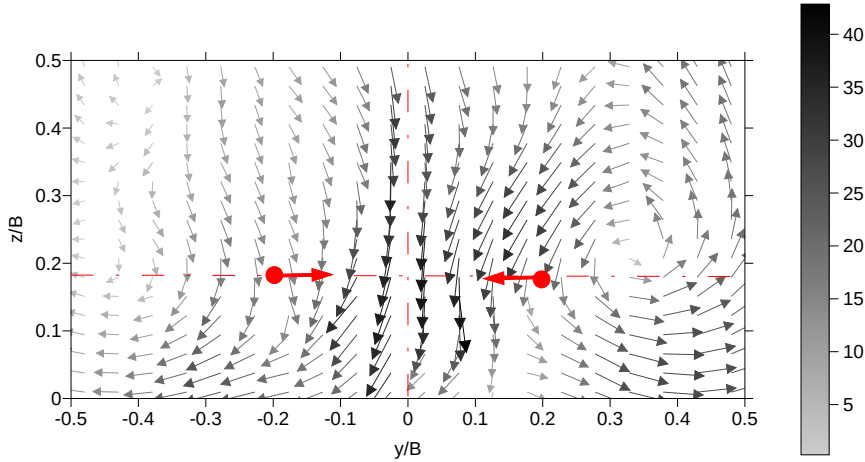

Figure B.43 *Velocity vectors [mm/s] in the transversal plane for off-bottom clearance C/B = 0.175, water intake height h_i/B = 0.25, distance between neighbouring jets l_j/B = 0.3, distance between jet circle centre and front wall d_{axis}/B = 0.525, water height h/B = 0.6, total jet discharge $\Sigma Q_j = Q_{out}$ = 760 l/h.*

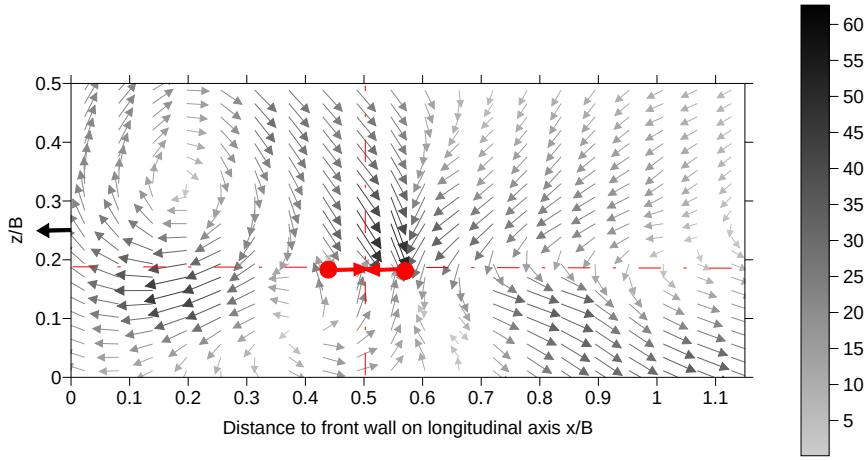

Figure B.44 *Velocity vectors [mm/s] in the longitudinal plane for off-bottom clearance C/B = 0.175, water intake height h_i/B = 0.25, distance between neighbouring jets l_j/B = 0.1, distance between jet circle centre and front wall d_{axis}/B = 0.525, water height h/B = 0.6, total jet discharge $\Sigma Q_j = Q_{out}$ = 760 l/h.*

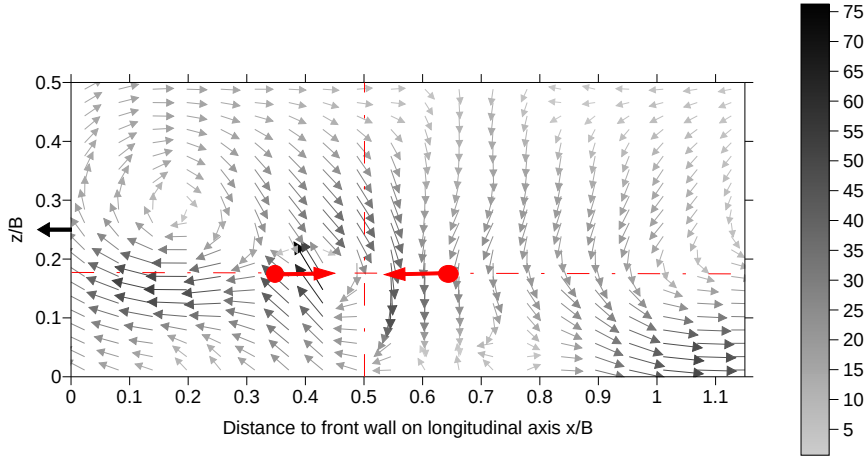

Figure B.45 Velocity vectors [mm/s] in the longitudinal plane for off-bottom clearance C/B = 0.175, water intake height h_i/B = 0.25, distance between neighbouring jets l_j/B = 0.225, distance between jet circle centre and front wall d_{axis}/B = 0.525, water height h/B = 0.6, total jet discharge $\Sigma Q_j = Q_{out}$ = 760 l/h.

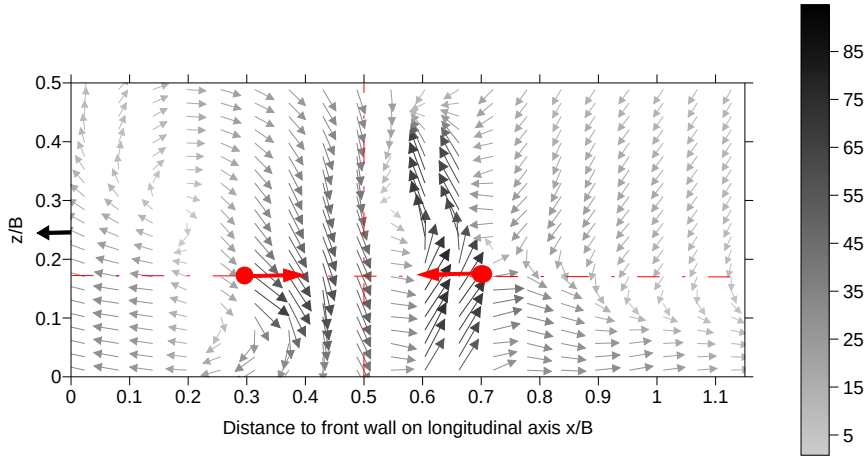

Figure B.46 Velocity vectors [mm/s] in the longitudinal plane for off-bottom clearance C/B = 0.175, water intake height h_i/B = 0.25, distance between neighbouring jets l_j/B = 0.3, distance between jet circle centre and front wall d_{axis}/B = 0.525, water height h/B = 0.6, total jet discharge $\Sigma Q_j = Q_{out}$ = 760 l/h.

Flow patterns for circular jet arrangements with a jet inclination angle of 45°

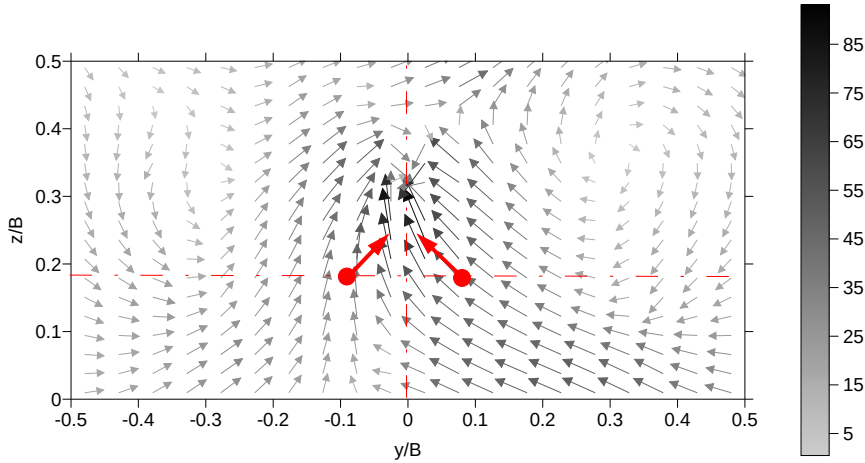

Figure B.47 *Velocity vectors [mm/s] in the transversal plane for off-bottom clearance C/B = 0.175, water intake height h_i/B = 0.25, distance between neighbouring jets l_j/B = 0.15, distance between jet circle centre and front wall d_{axis}/B = 0.525, water height h/B = 0.6, angle θ = 45°, total jet discharge $\Sigma Q_j = Q_{out}$ = 760 l/h.*

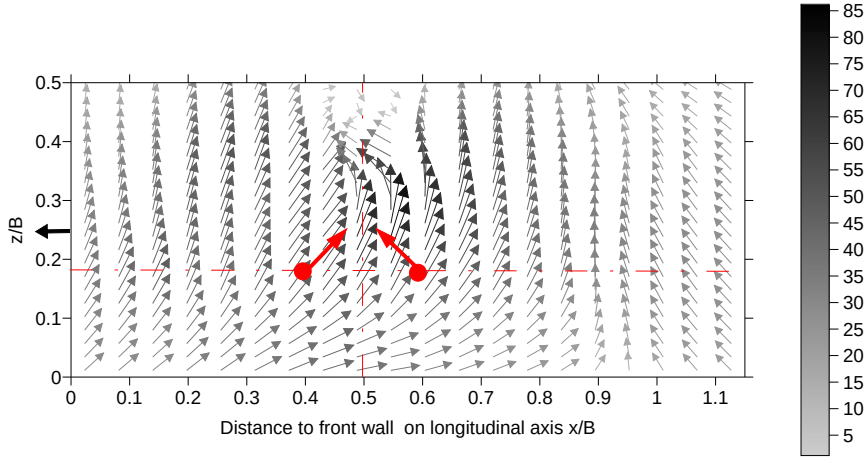

Figure B.48 *Velocity vectors [mm/s] in the longitudinal plane for off-bottom clearance C/B = 0.175, water intake height h_i/B = 0.25, distance between neighbouring jets l_j/B = 0.15, distance between jet circle centre and front wall d_{axis}/B = 0.525, water height h/B = 0.6, angle θ = 45°, total jet discharge $\Sigma Q_j = Q_{out}$ = 760 l/h.*

Flow patterns for linear jet arrangement

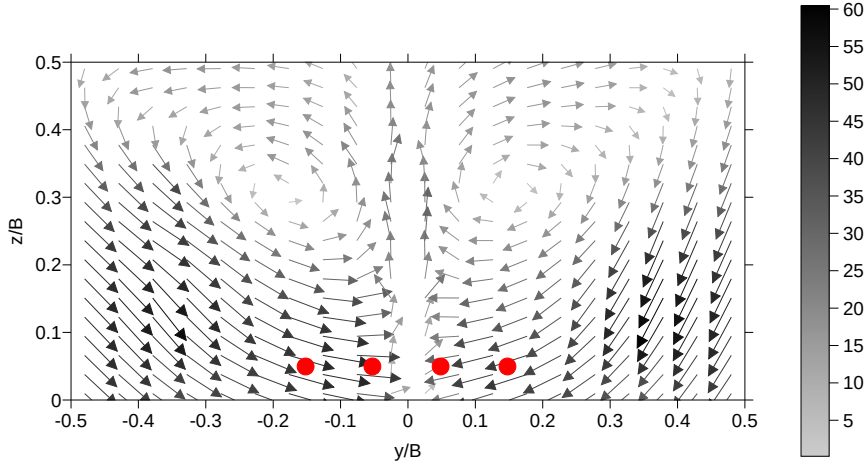

Figure B.49 Velocity vectors [mm/s] in the transversal plane for off-bottom clearance C/B = 0.05, distance of jet line to front wall d_{line} /B = 0.2, water height h/B = 0.6, angle θ = 45°, total jet discharge $\Sigma Q_j = Q_{out}$ = 4050 l/h.

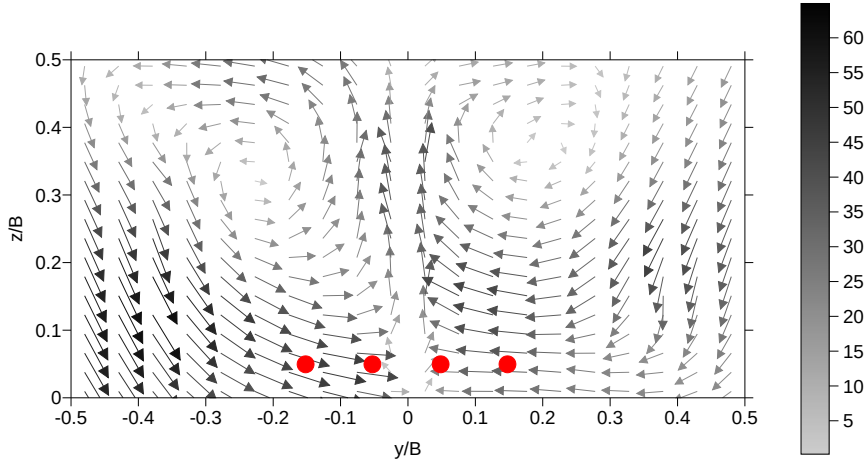

Figure B.50 Velocity vectors [mm/s] in the transversal plane for off-bottom clearance C/B = 0.05, distance of jet line to front wall d_{line} /B = 0.3, water height h/B = 0.6, angle θ = 45°, total jet discharge $\Sigma Q_j = Q_{out}$ = 4050 l/h.

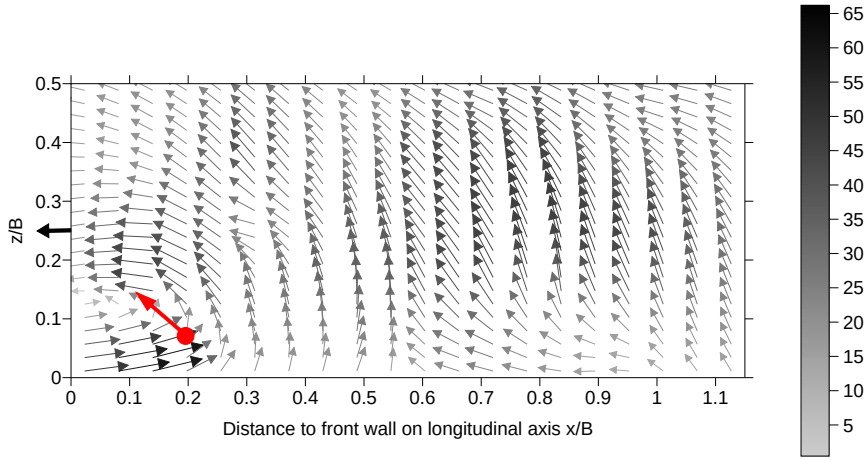

Figure B.51 Velocity vectors [mm/s] in the longitudinal plane for off-bottom clearance C/B = 0.05, distance of jet line to front wall d_{line} /B = 0.2, water height h/B = 0.6, angle θ = 45°, total jet discharge $\Sigma Q_j = Q_{out}$ = 4050 l/h.

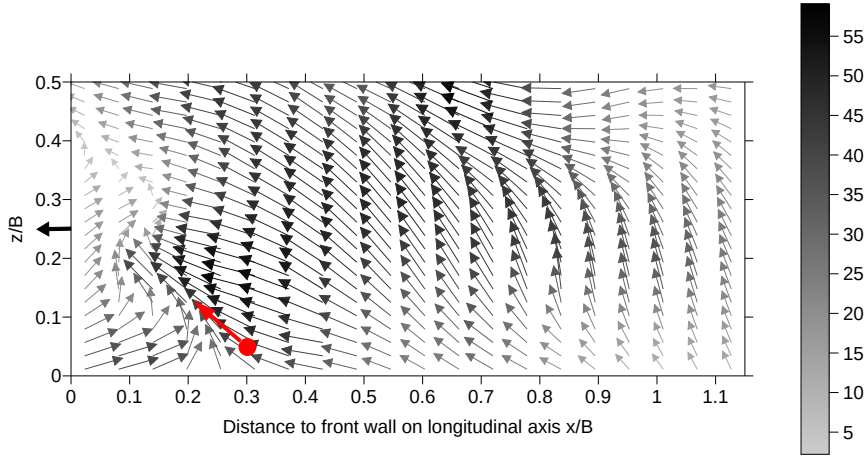

Figure B.52 Velocity vectors [mm/s] in the longitudinal plane for off-bottom clearance C/B = 0.05, distance of jet line to front wall d_{line} /B = 0.3, water height h/B = 0.6, angle θ = 45°, total jet discharge $\Sigma Q_j = Q_{out}$ = 4050 l/h.

Appendix C

Numerical simulation N1

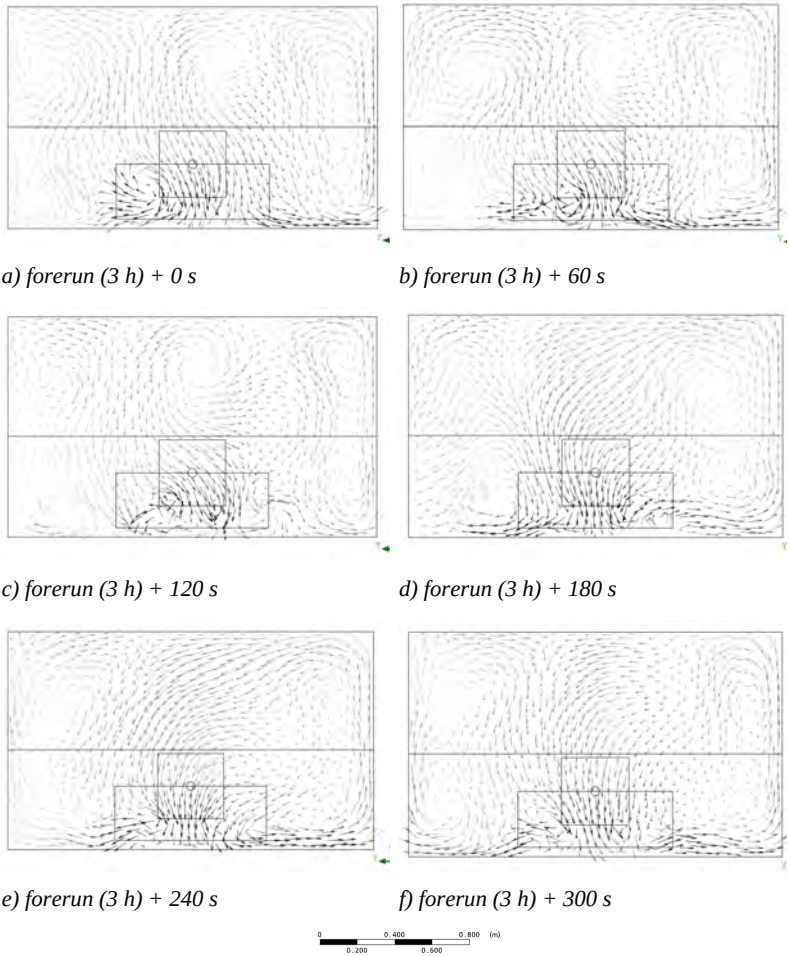

a) forerun (3 h) + 0 s

b) forerun (3 h) + 60 s

c) forerun (3 h) + 120 s

d) forerun (3 h) + 180 s

e) forerun (3 h) + 240 s

f) forerun (3 h) + 300 s

Figure C.1 Time sequence of transversal flow patterns of the numerical simulation N1 (C/B = 0.1, h_i/B = 0.175). From a) to f): forerun of 3 h + 0 s, 60 s, 120 s, 180 s, 240 s, 300 s, respectively. The level of the water intake is indicated by a circle.

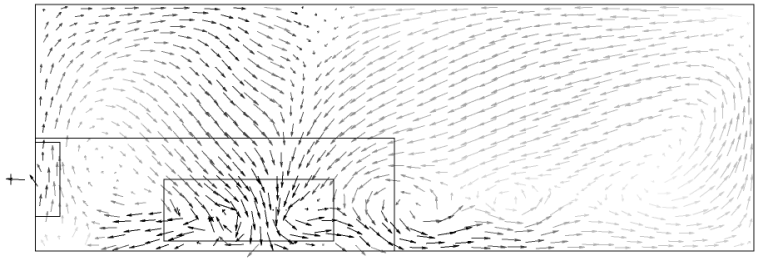

a) forerun (3 h) + 0 s

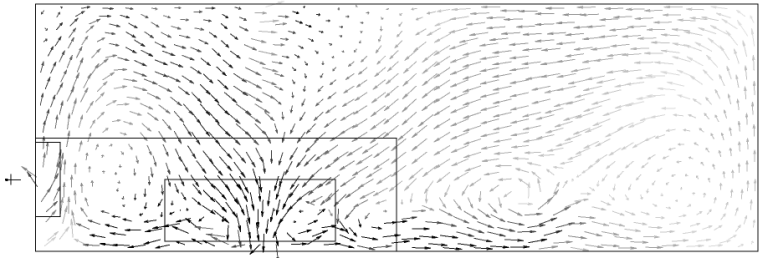

b) forerun (3 h) + 60 s

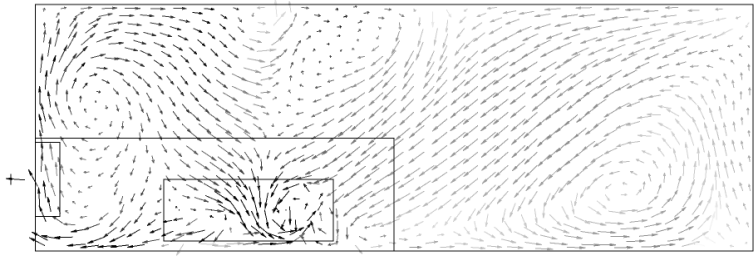

c) forerun (3 h) + 120 s

Figure C.2 Time sequence of longitudinal flow patterns of the numerical simulation N1 (C/B = 0.1, h_i/B = 0.175). From a) to c): forerun of 3 h + 0 s, 60 s, 120 s. The water intake is on the left indicated by a cross outside of the tank perimeter.

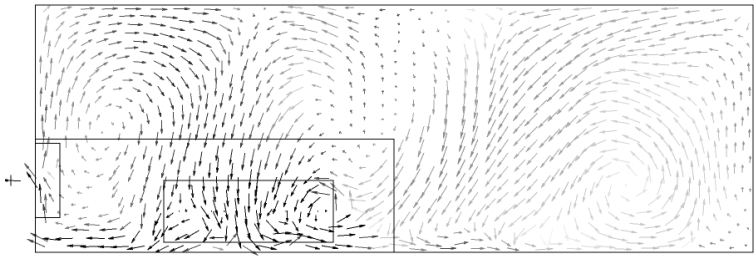

d) forerun (3 h) + 180 s

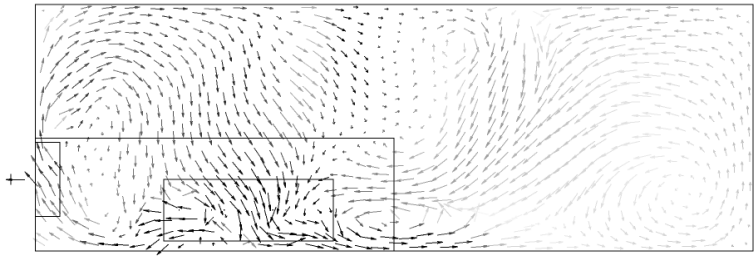

e) forerun (3 h) + 240 s

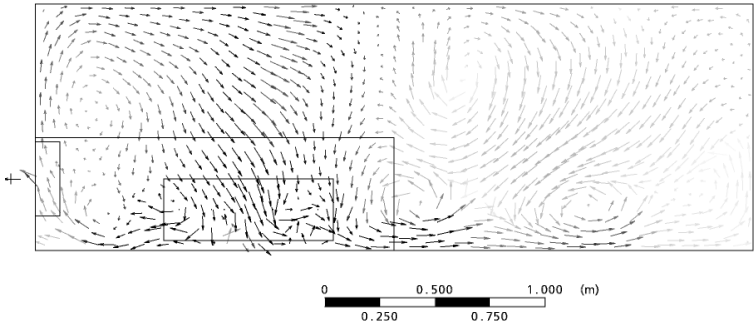

f) forerun (3 h) + 300 s

Figure C.3 Time sequence of longitudinal flow patterns of the numerical simulation N1 (C/B = 0.1, hi/B = 0.175). From d) to f): forerun of 3 h + 180 s, 240 s, 300 s. The water intake is on the left indicated by a cross outside of the tank perimeter.

Numercial Simulation N2

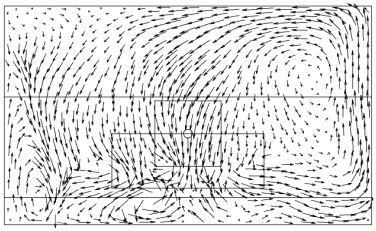

a) forerun (1.5 h) + 0 s

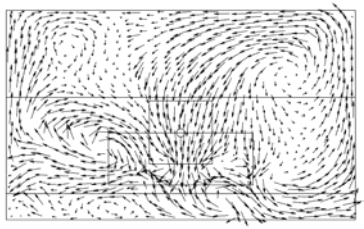

b) forerun (1.5 h) + 60 s

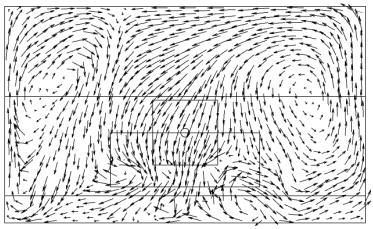

c) forerun (1.5 h) + 120 s

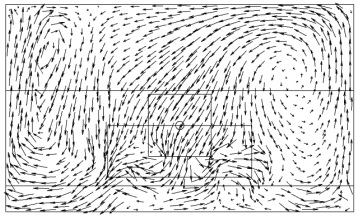

d) forerun (1.5 h) + 180 s

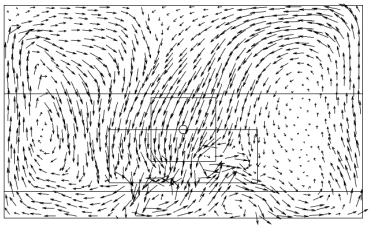

e) forerun (1.5 h) + 240 s

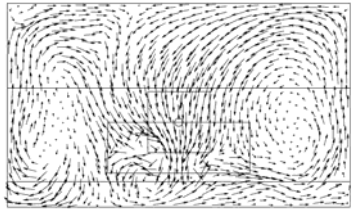

f) forerun (1.5 h) + 300 s

Figure C.4 Time sequence of transversal flow patterns of the numerical simulation N2 (C/B = 0.175, hi/B = 0.25). From a) to f): forerun (1.5 h) + 0 s, 60 s, 120 s, 180 s, 240 s, 300 s. The level of the water intake is indicated by the circle.

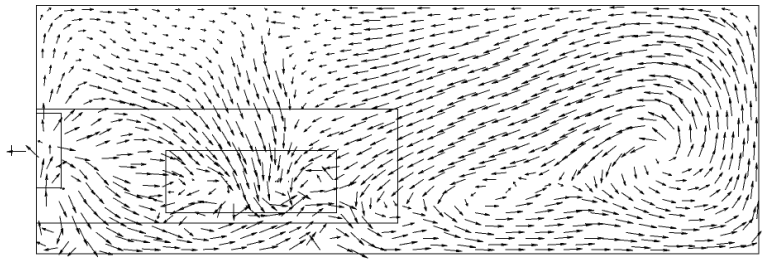

a) forerun (1.5 h) + 0 s

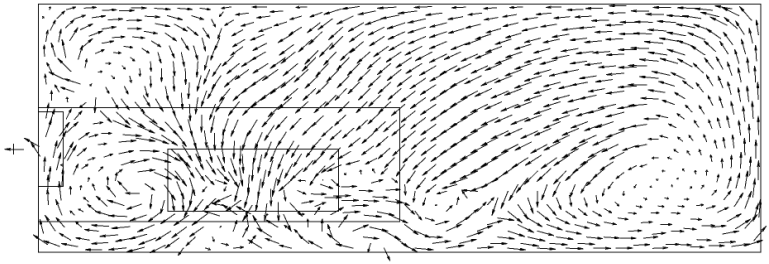

b) forerun (1.5 h) + 60 s

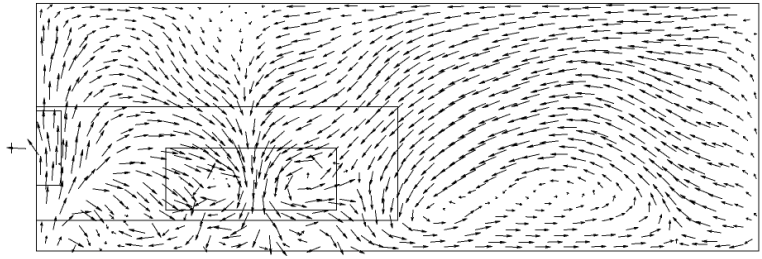

c) forerun (1.5 h) + 120 s

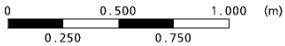

Figure C.5 Time sequence of longitudinal flow patterns of the numerical simulation N2 (C/B = 0.175, h_i/B = 0.25). From a) to c): forerun (1.5 h) + 0 s, 60 s, 120 s. The water intake is on the left indicated by a cross outside of the tank perimeter.

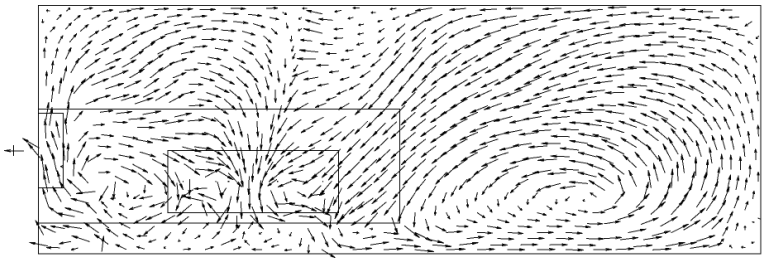

d) forerun (1.5 h) + 180 s

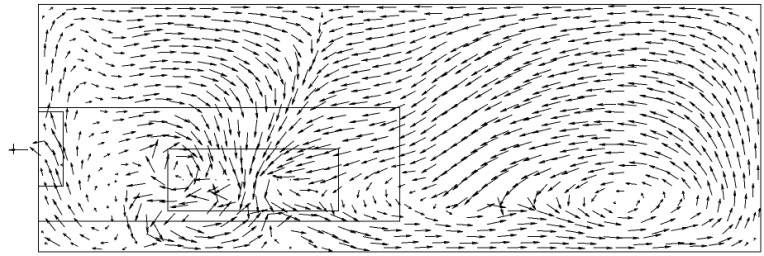

e) forerun (1.5 h) + 240 s

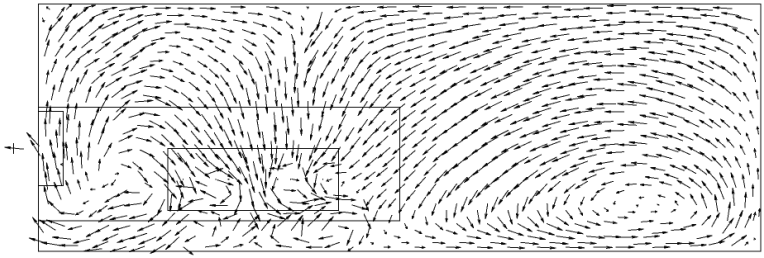

f) forerun (1.5 h) + 300 s

Figure C.6 Time sequence of longitudinal flow patterns of the numerical simulation N2 (C/B = 0.175, h_i/B = 0.25). From d) to f): forerun (1.5 h) + 180 s, 240 s, 300 s. The water intake is on the left indicated by a cross outside of the tank perimeter.

Numerical simulation N3

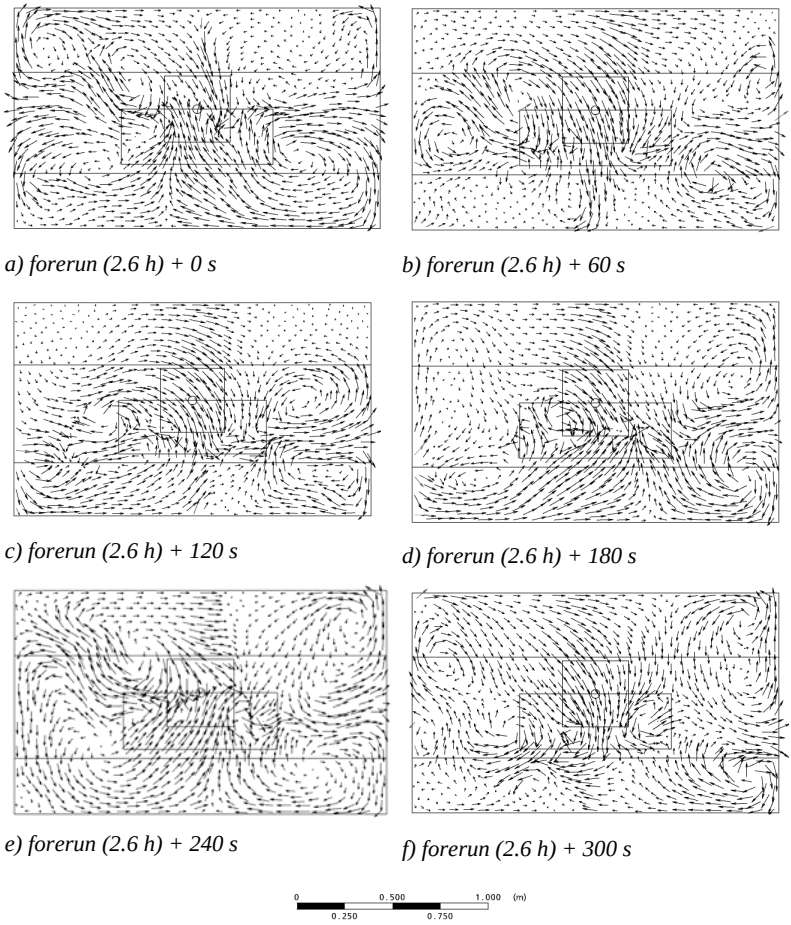

a) forerun (2.6 h) + 0 s

b) forerun (2.6 h) + 60 s

c) forerun (2.6 h) + 120 s

d) forerun (2.6 h) + 180 s

e) forerun (2.6 h) + 240 s

f) forerun (2.6 h) + 300 s

Figure C.7 Time sequence of transversal flow patterns of the numerical simulation N3 (C/B = 0.25, h_i/B = 0.325). From a) to f): forerun (2.6 h) + 0 s, 60 s, 120 s, 180 s, 240 s, 300 s. The level of the water intake is indicated by the circle.

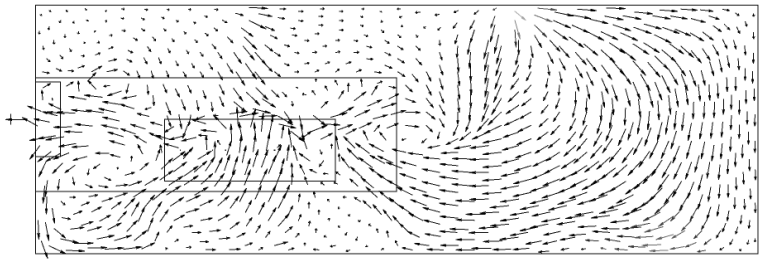

a) forerun (2.6 h) + 0 s

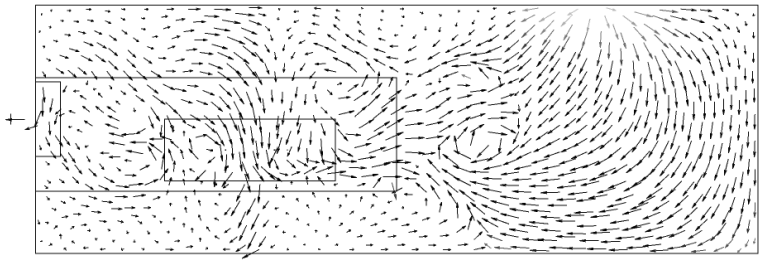

b) forerun (2.6 h) + 60 s

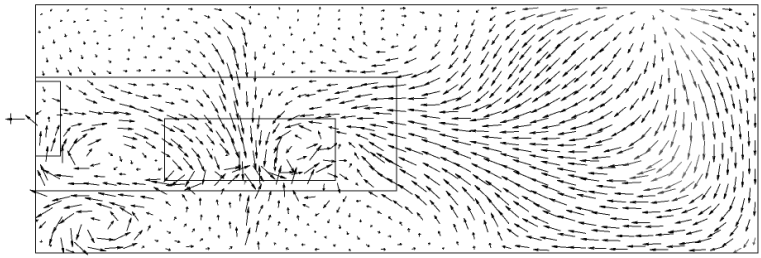

c) forerun (2.6 h) + 120 s

Figure C.8 *Time sequence of longitudinal flow patterns of the numerical simulation N3 (C/B = 0.25, h_i/B = 0.325). From a) to c): forerun (2.6 h) + 0 s, 60 s, 120 s. The water intake is on the left indicated by a cross outside of the tank perimeter.*

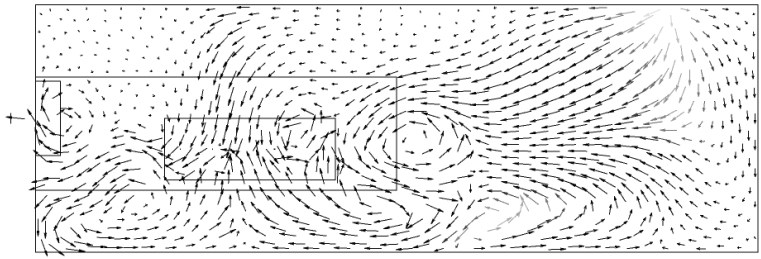

d) forerun (2.6 h) + 180 s

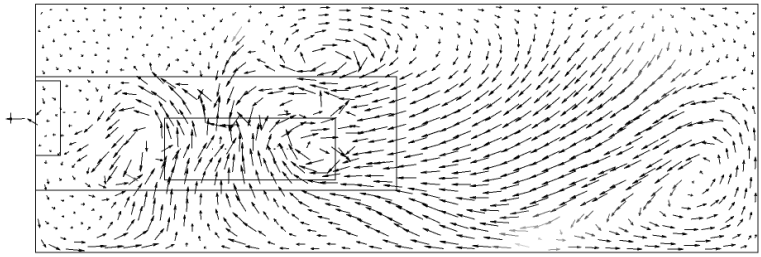

e) forerun (2.6 h) + 240 s

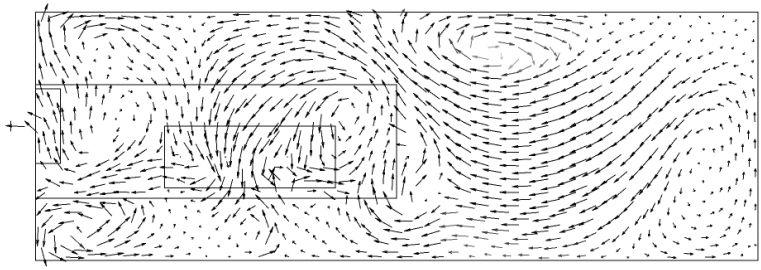

f) forerun (2.6 h) + 300 s

Figure C.9 Time sequence of longitudinal flow patterns of the numerical simulation N3 (C/B = 0.25, h_i/B = 0.325). From d) to f): forerun (2.6 h) + 180 s, 240 s, 300 s. The water intake is on the left indicated by a cross outside of the tank perimeter.

Numerical simulation N4

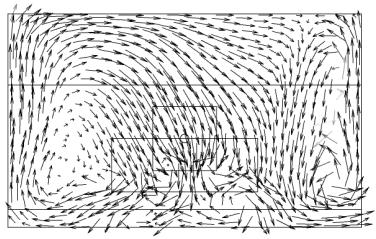

a) forerun (33 min) + 0 s

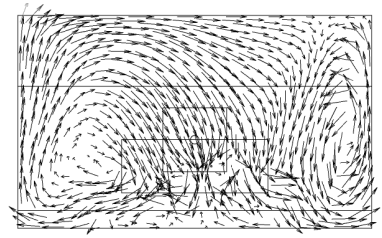

b) forerun (33 min) + 60 s

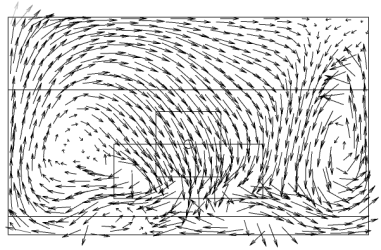

c) forerun (33 min) + 120 s

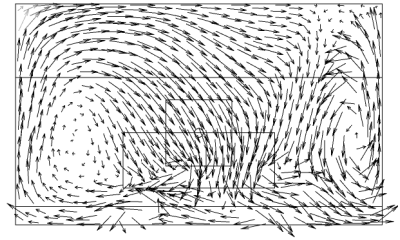

d) forerun (33 min) + 180 s

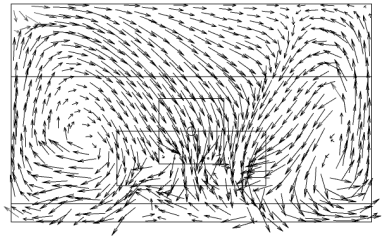

e) forerun (33 min) + 240 s

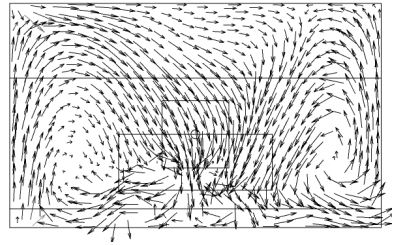

f) forerun (33 min) + 300 s

Figure C.10 Time sequence of transversal flow patterns of the numerical simulation N4 (C/B = 0.175, h_i/B = 0.25). From a) to f): forerun (33 min) + 0 s, 60 s, 120 s, 180 s, 240 s, 300 s. The level of the water intake is indicated by the circle.

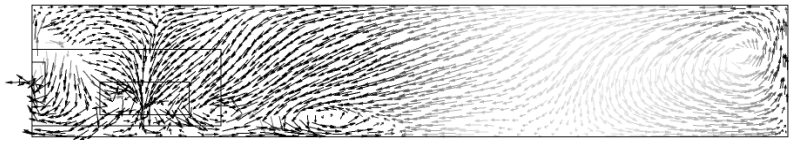

a) forerun (33 min) + 0 s

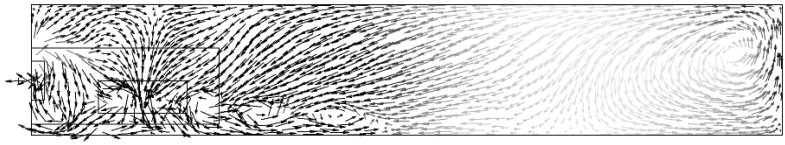

b) forerun (33 min) + 60 s

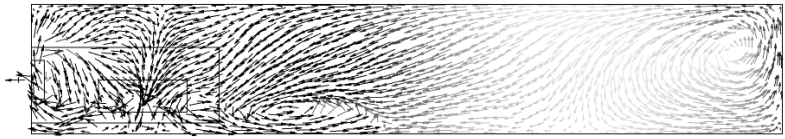

c) forerun (33 min) + 120 s

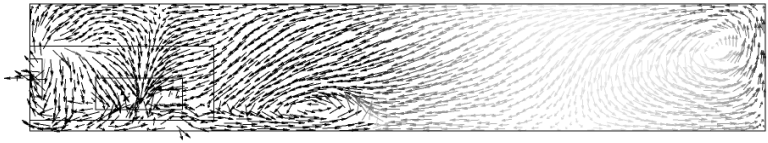

d) forerun (33 min) + 180 s

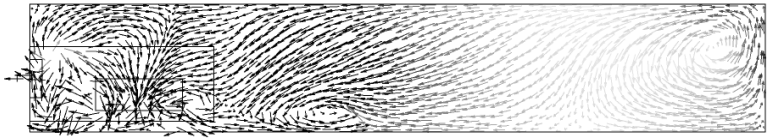

e) forerun (33 min) + 240 s

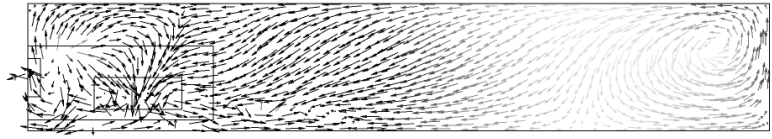

f) forerun (33 min) + 300 s

Figure C.11 Time sequence of longitudinal flow patterns of the numerical simulation N4 (C/B = 0.175, hi/B = 0.25). From a) to f): 33 min + 0 s…300 s. The water intake is on the left indicated by a cross outside of the tank perimeter.

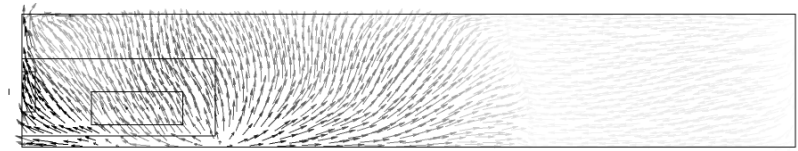

y/B = 0.45

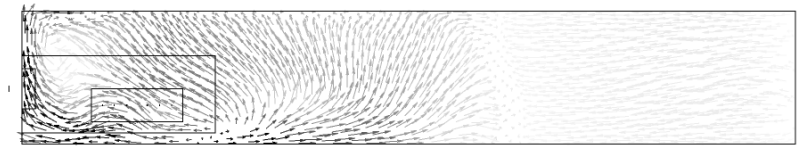

y/B = 0.4

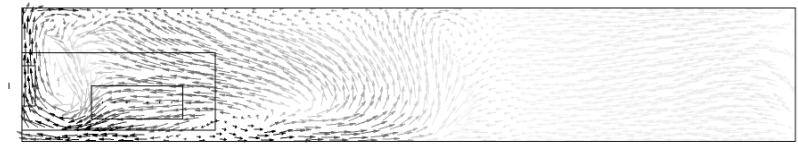

y/B = 0.35

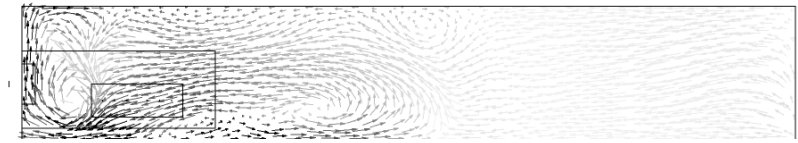

y/B = 0.3

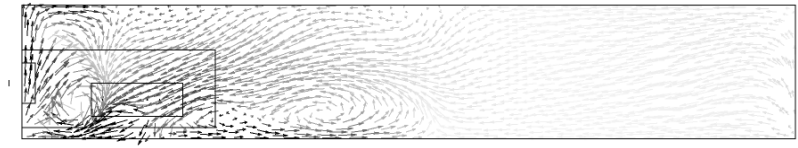

y/B = 0.25

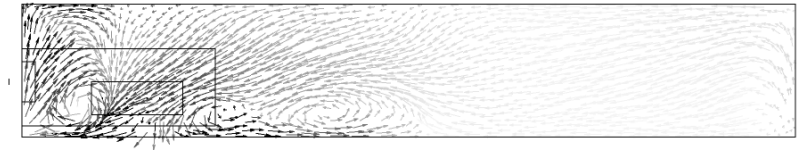

y/B = 0.2

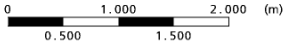

Figure C.12 Flow pattern in the longitudinal plane, where the plane was shifted in parallel to the side walls (y/B between 0.45 and 0.2).

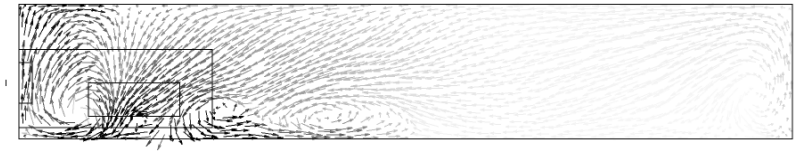

y/B = 0.15

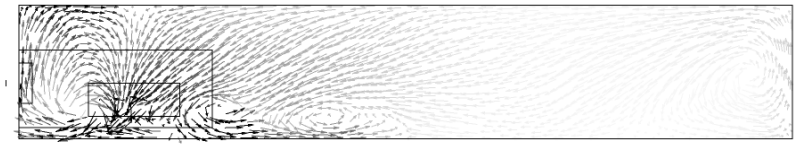

y/B = 0.1

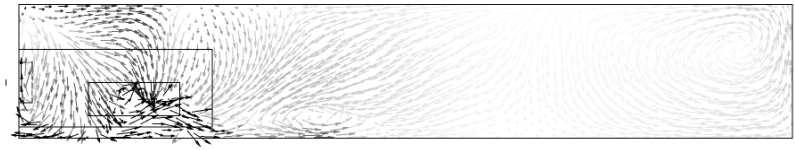

y/B = -0.1

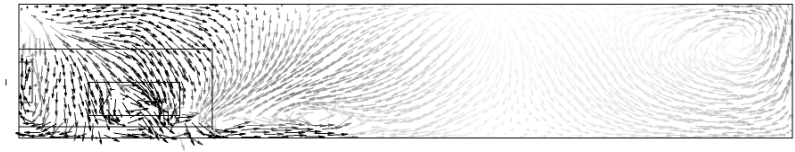

y/B = -0.15

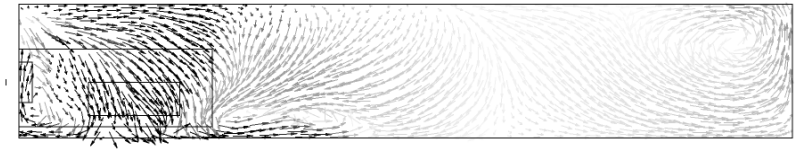

y/B = -0.2

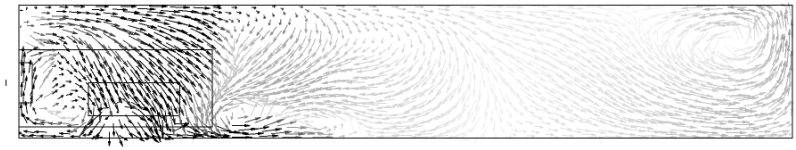

y/B = -0.25

Figure C.13 Flow pattern in the longitudinal plane, where the plane was shifted in parallel to the side walls (y/B between 0.15 and -0.25).

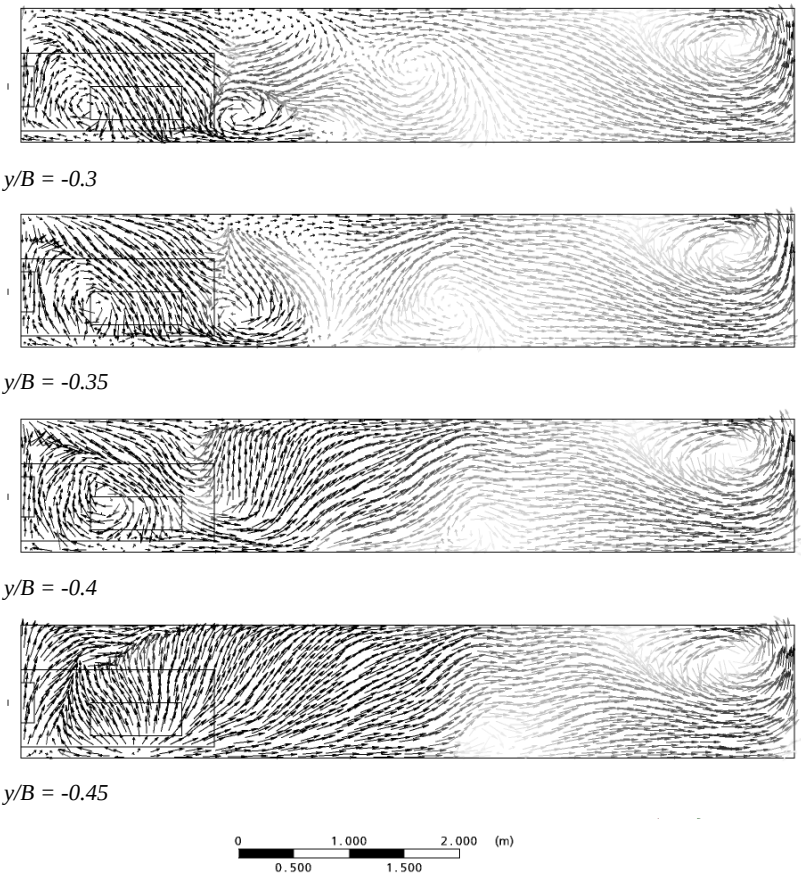

Figure C.14 Flow pattern in the longitudinal plane, where the plane was shifted in parallel to the side walls (y/B between -0.3 and -0.45).

Communications du Laboratoire de Constructions Hydrauliques ISSN 1661-1179
Ecole Polytechnique Fédérale de Lausanne
Editeur: Prof. Dr A. Schleiss

ISSN 1661-1179

Prof. Dr A. Schleiss
Laboratoire de constructions hydrauliques - LCH
EPFL, Bât. GC, Station 18, CH-1015 Lausanne
http://lch.epfl.ch
e-mail: secretariat.lch@epfl.ch